

The basal ganglia and action selection: a computational study at
multiple levels of description

Author: Mark Daniel Humphries

Submitted for: PhD

Department of Psychology, University of Sheffield
Sheffield, S10 2TP UK

Date of submission: July 2002

Abstract

An action selection problem arises whenever stimuli (external or internal) requiring behavioural responses co-occur or overlap in time. It has been proposed that the basal ganglia, a collection of nuclei predominantly located in the forebrain, are a crucial part of the neural substrate of the action selection process. The work presented here builds on a previous computational model of intrinsic basal ganglia processing (Gurney et al. 2001a, 2001b) which demonstrated that its function was consistent with a selection mechanism. Two groups of extensions to this original model are described. First, structural extensions, comprising the addition of new internal connections or of structures extrinsic to the basal ganglia. Second, the instantiation of the extended model at a lower level of abstraction through the use of spiking model neurons. Results from the former group showed that the selection and switching capabilities of the basal ganglia were maintained following all biologically-constrained additions and demonstrated the existence of other action selection mechanisms in the brain instantiated outside of, but in contact with, the basal ganglia. These results support the hypothesis that the basal ganglia play a crucial role in action selection. Modelling at a lower level of detail provided four main results. First, selection and switching were maintained. Second, inputs which represented equally urgent actions caused oscillations in basal ganglia output which were consistent with rapid alternations of selected actions. Third, neural noise was required for selection of low-level inputs and, paradoxically, for ensuring that a model neuron's output was a coherent representation of its input. Fourth, the successful simulation of the results from an *in vitro* study of a basal ganglia sub-circuit provided evidence for a channel-based architecture within the basal ganglia. These results emphasise the utility of modelling the same neural circuit at different levels of abstraction.

Acknowledgements

There are many people to thank for helping me complete this complex and frustrating work. I am heavily indebted to my supervisor, Dr. Kevin Gurney, for his tireless and meticulous devotion to improving the quality of my scientific prose and, more importantly, for his seemingly effortless ability to hand me a new, fruitful lead whenever I couldn't see a way out of my research dead-ends. One day I will return his books.

It is my good fortune to be part of a wonderful loving and caring family: my love and thanks to Mum and Dad for their many words of wisdom on work and life, and for seeing me all the way through to the end. And of course to my brothers Andy and Tim, who keep my feet on the ground and make sure I can still get my head through the door: they've surprisingly turned out to be fine young men despite having me as an elder brother.

Of the many others who deserve credit, I only have space to name a few, lest this be longer than the introduction. So, I must also thank: my friends and colleagues from the department, current and departed, especially Richard Cooke for his tireless ability to look interested while I complain and Nick Davis for his enthusiasm for everything except work; my band for providing fun and friction in equal doses, but primarily for providing an opportunity to de-stress by playing guitar real loud; and my many good friends, especially Kit Barker, Chris Box, Bella Davies, Angela Hornby, Liza Jones, Andy Washbrook, Iain Westacott, and Michael Williams, all of whom made a telling contribution to the completion of this thesis, whether they knew it or not.

Finally, I give my deepest thanks and love to my girlfriend Nic, who looked after the bills while I pursued science, and looked after my head when science pursued me. Without her support and love, this work may never have been finished.

Contents

1 The basal ganglia and action selection	8
1.1 The action selection problem	8
1.2 Potential solutions	10
1.3 Neuroanatomy of the basal ganglia	13
1.3.1 Striatum	15
1.3.2 Subthalamic nucleus	17
1.3.3 Globus pallidus	18
1.3.4 Output nuclei	19
1.3.5 The basal ganglia fulfill the criteria for a central switch	20
1.4 Modelling the basal ganglia	21
1.4.1 Previous models of the basal ganglia	22
1.4.2 A new functional anatomy of the basal ganglia	24
1.5 Modelling issues	31
1.6 Summary	34
2 The role of the thalamic complex in action selection	36
2.1 Introduction	36
2.2 Thalamocortical interactions	37
2.2.1 The motor thalamocortical loop	37
2.2.2 The thalamic reticular nucleus	40
2.2.3 The requirements of a switching mechanism	43
2.2.4 Aims	45

2.3	Quantitative modelling	45
2.3.1	The model neuron	45
2.3.2	Motor cortex	45
2.3.3	Thalamic reticular nucleus	46
2.3.4	Ventrolateral thalamus	46
2.3.5	Striatum	47
2.3.6	STN	48
2.3.7	GP and EP	48
2.3.8	Parameter details	49
2.4	Simulation Results	50
2.4.1	Example outputs	50
2.4.2	Quantifying selection properties	53
2.4.3	Improving EP output contrast	56
2.4.4	Transient suppression	58
2.4.5	Closely matched saliences	60
2.4.6	Dopaminergic modulation of selection	61
2.4.7	The significance of basal ganglia to TRN projections	65
2.4.8	TRN design alternatives	67
2.5	Discussion	68
2.5.1	Thalamocortical loop	69
2.5.2	A functional role for the thalamic reticular nucleus	70
2.5.3	The action of dopamine	71
2.5.4	Modelling issues and further work	72
2.5.5	Conclusions	73
3	Robustness of the basal ganglia model	75
3.1	Introduction	75
3.2	GP to striatum connectivity	77
3.3	Striatal interneurons	80

3.4	Axon collaterals in STN	82
3.5	A feedback loop formed by GP and EP	86
3.6	Combinations	87
3.6.1	Striatal interneurons form a compensatory pathway to the EP-GP pathway	87
3.6.2	Pallidostriatal connections to projection- and inter-neurons	89
3.7	Summary	93
4	Spiking models of the basal ganglia	96
4.1	Introduction	96
4.2	Methods	99
4.2.1	The model neuron	99
4.2.2	Dopamine	101
4.2.3	Network design	101
4.2.4	Implementation details	103
4.3	Results	107
4.3.1	The extended model	107
4.3.2	Dopamine level changes	122
4.3.3	The role of noise	125
4.4	Discussion	127
4.4.1	Behavioural consequences	130
4.4.2	Methodological considerations	131
4.4.3	Conclusions	132
5	STN-GP loop bursting	134
5.1	Introduction	134
5.2	Method	136
5.2.1	Extending the model neuron	136
5.2.2	Network design	141
5.2.3	Analysis of simulation data	143

5.2.4	Implementation details	146
5.3	Results	146
5.3.1	STN neuron-like bursting is not possible without the Ca^{2+} mechanism . .	146
5.3.2	The role of noise	150
5.3.3	Simulation of the basal ganglia pacemaker	154
5.3.4	Burst detection methods	165
5.3.5	De-channelising the model	168
5.4	Discussion	170
5.4.1	Ca^{2+} mechanism is essential for bursting in simulation	170
5.4.2	The effects of noise	172
5.4.3	Quasi-compartmental modelling	173
5.4.4	The factors determining bursting frequency	176
5.4.5	What is a ‘burst’?	177
5.4.6	The channel constraint	180
5.4.7	Conclusions	181
6	General Discussion	183
6.1	Thematic conclusions	183
6.1.1	Action selection	183
6.1.2	The effects of noise and dopamine	188
6.1.3	Levels of modelling	190
6.2	Issues and Directions	193
6.2.1	The trouble with dopamine	193
6.2.2	The lack of learning	194
6.2.3	Phenomenological modelling	195
6.2.4	Conclusion	196

Chapter 1

The basal ganglia and action selection

1.1 The action selection problem

We shall begin by considering an illustrative example of this problem. An antelope, whilst grazing due to hunger (an internal stimulus), sees what could be a lioness, an external stimulus that causes fear. It is faced with a choice: to stay and graze or to flee from a potential predator. It cannot do both actions as they require the same motor resource, namely the leg muscles. To graze the animal must maintain a stable rigid posture while it lowers its neck to feed; to flee requires the leg muscles to be used in locomotion. Furthermore, the imminent danger presented by a potential predator should take precedence over hunger. Thus, a decision must be taken between competing actions that require the same motor resource or that are dangerous in combination.

So how does it decide which action to execute next? At any given moment in time, the antelope's external senses are continuously assimilating environmental information, its memory may be prompting it with long-term goals, and its brain is receiving constant proprioceptive information to help determine what it is physically capable of doing. A reasonable assumption would be that the decision making process makes use of this information - but how and in what form? These key questions are explored later in this chapter.

Of course, the selection process does not end with the decision to execute a particular action based on a snapshot of the world at any given moment. The animal's environment and body

state would constantly change as other living things move around it, as the light levels fluctuate or the weather changes, as the animal itself moves around its environment, and so on. These factors would change the information the decision process was receiving, and it may become crucial to interrupt an ongoing selected action if, based on the newly received information, it becomes inappropriate or if another becomes more urgent. So, to continue the example, if the antelope initially ‘decided’ to remain grazing, and the lioness moved more clearly into view, then the grazing should be interrupted in favour of fleeing.

If the action is successfully completed without interruption then it should be de-selected and a new selection competition begun to determine the subsequent action. For example, this would occur if the antelope had continued grazing and become sated: it would then need to decide what to do next. Thus, through the processes of selection and de-selection, the resolution of competition between actions at each juncture generates sequences of behaviour. It should be stressed that throughout this work no assumptions are made about the level of complexity of the actions in each selection competition - they may be anything between simple individual movements, such as “bend the knee”, to complex goal-driven events, such as “go to the bank”. Whatever level of action is considered, the parts of the selection process considered thus far are valid.

A major constraint on action selection, which was highlighted by the opening example, is that there is a limited set of motor resources available with which to execute the selected action(s). For each single resource, possibly a limb or a group of muscles, the competition must be resolved in favour of one action at most. More importantly, the selection of actions across multiple resources must result in mutually compatible selections (e.g. walking and chewing). Preferably, from the perspective of the animal’s long-term survival, the selections would result in useful, safe behaviours. Thus, this limited-resource constraint also forms a core part of the selection process, as it limits the set of actions which can compete for selection.

The preceding discussion can be encapsulated into a simple declaration of the “action selection problem”: how does an animal decide which action to select next, given the information and potential actions that are available to it?

The work presented here is part of a research programme that has at its core the study of how the action selection problem has been solved in the vertebrate brain. For ease of conception, the problem is considered separate from any long-term aims or planned sequences. The intention is to study the moment-to-moment selection process of how the competition between actions is resolved. Below I discuss how prior research explored the properties a neural substrate would need to solve the action selection problem and identified candidate structures, building on previous ethology and robotics studies of action selection (Kupfermann and Weiss, 2001; Blumberg, 1994; Humphrys, 1996; Matarić, 1998; Prescott, 2001).

1.2 Potential solutions

There have been previous computational models of action selection (e.g. Blumberg, 1994; Houston and Sumida, 1985) , but they have not been constrained by biological plausibility or consideration of the underlying neural mechanism. The first task was, therefore, to establish the functional form that an action selector should take, from which candidate neural structures can be identified. The foregoing section follows the work presented in Prescott, Redgrave, and Gurney (1999) and Redgrave, Prescott, and Gurney (1999a).

The concept of action selection as an emergent feature of a control system which has multiple interconnected simple components is prevalent in the robotics literature. In an emergent scheme there can be no single locus of action selection, and so it would be futile to attempt to determine a specific neural substrate for such a system. A common feature of emergent systems is the use of reciprocal inhibition between components such that every functional unit has an inhibitory connection with every other unit: an illustrative circuit diagram is shown in Figure 1.1. This creates a winner-takes-all network because the unit which is most activated suppresses the activation of the other units. Thus, if in such a system each unit represented an action, the competition would be resolved across the entire network in favour of a single action.

While such a distributed system may be involved at some point during action selection in the vertebrate brain (see section 1.3), it is probably not the core component (Prescott et al., 1999). The need for every unit to connect to all other units ensures a massive ‘wiring’ cost

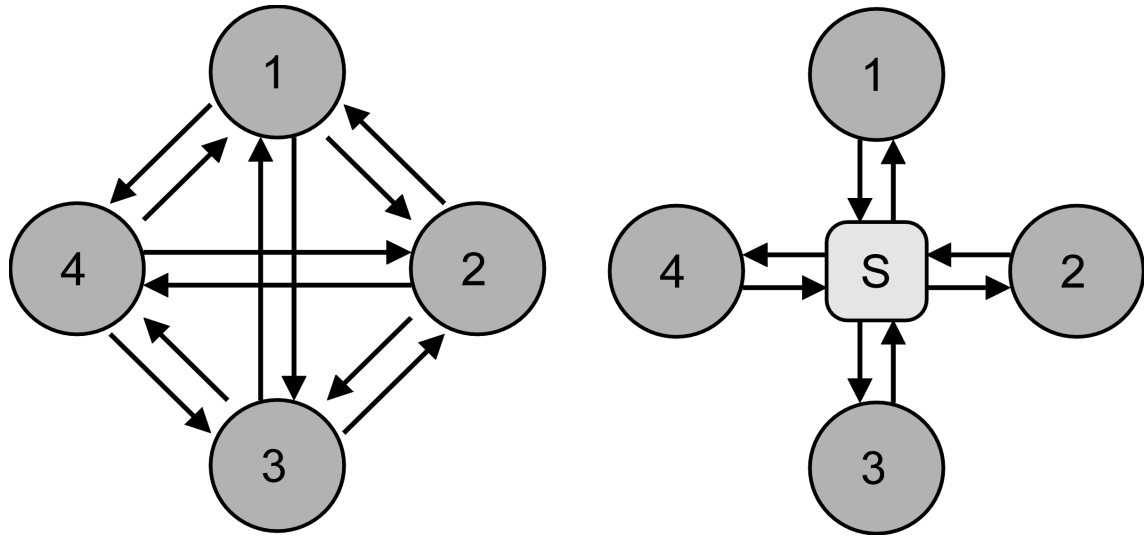


Figure 1.1: Alternative forms of connections within a network of nodes. Left: A fully interconnected network has reciprocal inhibitory connections between every unit. Right: By utilising a central switch (S) to connect units, the number of connections is significantly reduced.

whenever it is necessary to add new units. Furthermore, as brains increase in volume, long-range connections between neurons decrease in proportion to the volume. As a result, fully connected neural networks within the brain become increasingly localised, making it unlikely that emergent action selection could be sustained. Thus, an emergent system is probably too complex and costly to have evolved as the major action selector.

The alternative to an emergent scheme is a central selection mechanism which takes input from all sources and reciprocally projects to them (see Figure 1.1 for an example circuit). This reduces the cost of adding new sources by an order of magnitude, thus facilitating their introduction over time via evolutionary processes. More importantly, the connection scheme is much simplified, and can easily scale up with increases in brain volume as it is not dependent on multiple long-range connections. Therefore, it has been argued that the vertebrate brain uses a central switching mechanism to resolve the competition between actions (Prescott et al., 1999).

If a central switch is the most likely candidate for the action selection mechanism then a neural substrate for such a mechanism needs to be identified. Numerous authors have argued

that the basal ganglia play a crucial role in action selection (Redgrave et al., 1999a; Kropotov and Etlinger, 1999; Mink and Thach, 1993). Moreover, some authors have argued that the basal ganglia's functional design suggests that they operate as a central switching mechanism (Prescott et al., 1999; Redgrave et al., 1999a). To illustrate why these researchers have reached this consensus, the following discussion highlights three of the strong criteria which should be fulfilled by the neural substrate of a central switching mechanism involved in action selection in the vertebrate brain.

First, as discussed in the previous section, the action selection process may be based on all the available extero- and interoceptive information. This ties in neatly with the idea of a central switch: all of the input sources send the information required for the decision to the switching mechanism. Therefore, the neural substrate would ideally receive input from as many known sources of extero- and interoceptive information as possible.

Second, the substrate of the central switching mechanism should ideally exist across the whole of the vertebrate subphylum. This implies that the substrate must have existed in some common ancestor and is, therefore, likely to be ancient (Prescott, 2001). Further, within the subphylum there are classes, such as amphibians, whose member species do not have any significant development of neo-cortex (Marin, Smeets, and González, 1998). Moreover, action selection and execution is relatively normal in decorticate rats and cats (Whishaw, 1990; Grillner et al., 1997). Thus, if a common neural substrate existed across all vertebrates then it would be sub-cortical.

Third, as the explicit concern here is with the the selection of actions which lead to motor responses, the neural substrate must have a means of expressing the selected action in the motor pathways. Thus, the final criterion is that the substrate's designated output would directly contact neural structures that are known to be involved in the expression or control of motor behaviours.

Below, I detail the anatomy and connectivity of the basal ganglia, identifying how each of the three criteria for the neural substrate are met.

1.3 Neuroanatomy of the basal ganglia

The term ‘basal ganglia’ is the collective noun for a group of brain structures that are predominantly located in the forebrain. Its core composition has remained fixed for a significant period. Denny-Brown (1962) defined these core structures, in terminology used by the neurologist, as the caudate nucleus, putamen, globus pallidus, subthalamic nucleus, and substantia nigra. However, he also considered for inclusion structures as diverse as the amygdala, the claustrum, and the zona incerta. None of these are any longer considered candidates for inclusion under the basal ganglia umbrella. For example, the recent research on the amygdala’s role in fear conditioning, conducted and inspired by Joseph LeDoux and colleagues (see LeDoux, 1995a, 1995b), has clearly delineated the amygdala as a functional unit distinct from the basal ganglia. Recent authors, for example Greenberg (2001), have identified André Parent’s 1986 book “Comparative neurobiology of the neostriatum” as the first major work to state the current widely accepted form of the basal ganglia, even though it was in good agreement with the core structures identified by Denny-Brown.

The composition and connection scheme used throughout this work is illustrated in Figure 1.2 and is based primarily on the rat basal ganglia. This is comprised of the striatum, the subthalamic nucleus (STN), the entopeduncular nucleus (EP), the globus pallidus (GP), and the two sub-divisions of the substantia nigra: pars reticulata (SNr), and pars compacta (SNC). Homologous nuclei exist within other species. For example, the EP is equivalent to the globus pallidus internal segment (GPi) in primates; and the GP is the globus pallidus external segment (GPe) in primates.

It should be noted that there are other structures which exist within the basal ganglia, but which do not have an obvious role in motor behaviour. The striatum, as I have used the term, signifies the dorsal part of the striatal complex, which comprises the caudate nucleus and the putamen. The ventral striatum primarily consists of the nucleus accumbens, a structure normally associated with the ‘limbic’ system; within the basal ganglia, this system also incorporates the ventral pallidum (Joel and Weiner, 1997).

There is a growing consensus that the basic plan of basal ganglia anatomy and connectivity

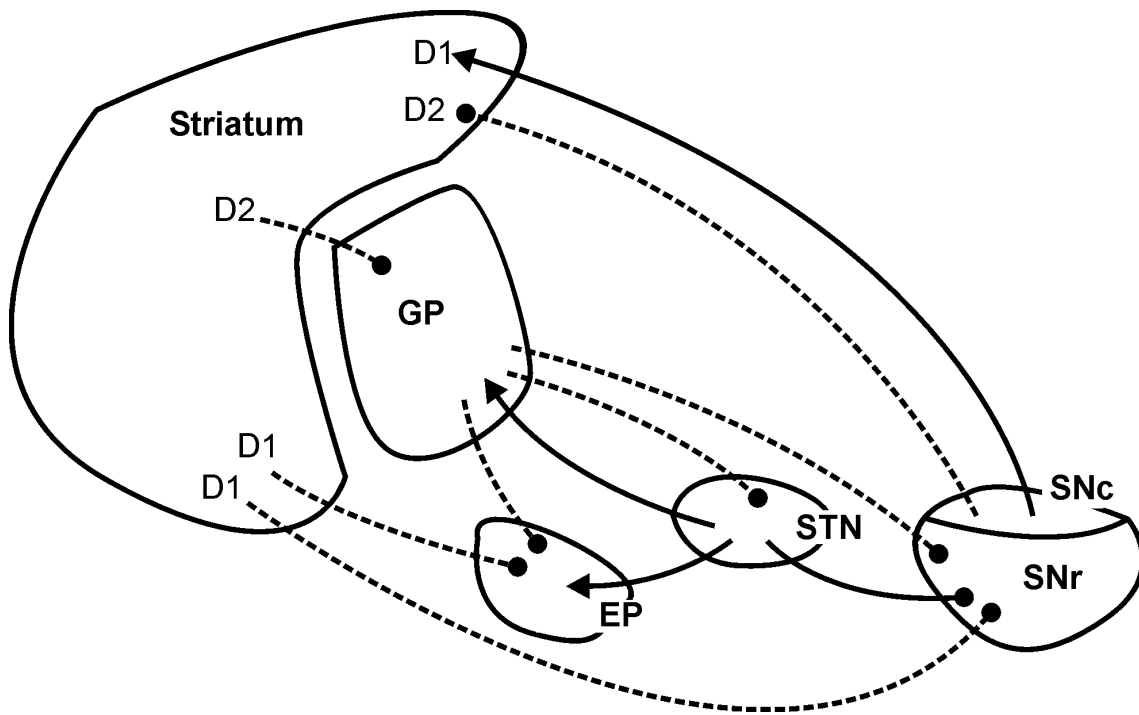


Figure 1.2: The connectivity, relative position, and relative size of the nuclei that comprise the rat basal ganglia. Note the separate projection targets of the D1 receptor and D2 receptor striatal neurons. Excitatory pathway: solid line; inhibitory pathway: dashed line . GP: globus pallidus. STN: subthalamic nucleus. SNC: substantia nigra pars compacta. SNr: substantia nigra pars reticulata. EP: entopeduncular nucleus.

is maintained in all vertebrates (Prescott et al., 1999). A recent comparative review, incorporating new evidence from amphibian studies, made a convincing case that the basal ganglia were an integral part of the tetrapod (four-legged vertebrate) phenotype (Marin et al., 1998). The authors concluded that the basic organisation of basal ganglia was conserved across extant tetrapods and this gave strong evidence for a common ancestor with basal ganglia-like structures. Another recent comprehensive review concluded that a fully formed basal ganglia could be seen in ‘lower-order’ vertebrate classes including lobe-finned, ray-finned, and bony fish (e.g. sharks) (Reiner, Medina, and Veenman, 1998). Thus, the conservation of the basal ganglia throughout the vast majority of vertebrate species implies that the basal ganglia is an ancient structure: it therefore meets the second criterion for the neural substrate.

1.3.1 Striatum

The striatum receives massive excitatory input from all of cortex (Gerfen and Wilson, 1996), from intralaminar thalamic nuclei (Jones, 1985; Price, 1995), and from the amygdala and hippocampal formation (Kelley, Domesick, and Nauta, 1982). It is this disparate set of input structures which identified the basal ganglia as being a potential neural substrate of the action selection mechanism because it allows striatum to receive sensory, motor, contextual, and proprioceptive information. The vast majority of afferent projections synapse upon the medium spiny projection neurons of the striatum, which comprise approximately 95 percent of the cells in this nucleus (Gerfen and Wilson, 1996). Cortical input also synapses upon the four different classes of interneurons (see below).

Striatum also receives dopaminergic input from the SNC (Poirier and Sourkes, 1965; Gerfen and Wilson, 1996), the effect of which is determined by the receptor type on the post-synaptic projection neuron. Dopamine has a predominantly excitatory effect on neurons with D1-type receptors *in vitro* (Umekiya and Raymond, 1997) and *in vivo* (Hernández-López, Bargas, Surmeier, Reyes, and Galarraga, 1997; Gonon, 1997). Conversely, dopamine has been observed to have an inhibitory effect on D2-type receptor neurons (Harsing and Zigmond, 1997; Morari, Marti, Sbrenna, Fuxé, Bianchi, and Beani, 1998). The mechanism via which dopamine is able to have opposite effects on projection neuron output is not clear, although both post- and pre-synaptic factors have been implicated (Hsu, Huang, Yang, and Gean, 1995).

Other dopamine receptor types exist in the central nervous system. The D3 and D4 receptors have the same post-synaptic mechanism as the D2 receptor type and are therefore considered to be functionally equivalent; similarly, D5 receptors are considered equivalent to the D1 receptor type (Missale, Nash, Robinson, Jaber, and Caron, 1998).

Dopamine is crucial to the normal functioning of the basal ganglia. In the early 1960s the work of the three groups led by Carlson, Hornykiewicz, and Sourkes determined, respectively, that dopamine was a neurotransmitter and not a precursor to some other neurochemical; that dopamine levels were depleted in brain slices of recently deceased Parkinson's Disease patients; and that administering L-DOPA (dopamine's immediate precursor) to Parkinson's patients

alleviated some symptoms (for review see Roe, 1999; Sourkes, 2000) . These lines of evidence again implicated the basal ganglia in motor function, for Parkinson's Disease is most clearly shown through motor deficits such as rigidity and limb tremor.

Output from striatal projections neurons is GABAergic and phasically active and, therefore, provides inhibitory inputs to their targets within the basal ganglia. The distinction between D1 and D2 type receptor neurons is further reinforced by their projection targets: D1 neurons project predominantly to SNr and EP while D2 neurons project predominantly to GP (Gerfen, Engber, Mahan, Susel, Chase, Monsma, and Sibley, 1990). It is this distinction between the projection targets that has led to the prevalence of dual-pathway models of basal ganglia function (see section 1.4).

A feature of medium spiny projection neurons, which may be crucial to action selection, is that they are silent in the absence of afferent input (DOWN-state). In this state, the neuron's membrane potential is far below the firing threshold, and is very stable. Massive co-ordinated input from cortex and other afferent connections is required to push the neuron into its firing-ready UP-state. Therefore, striatal cells can act as filters that prevent low-level signals from reaching downstream nuclei of the basal ganglia.

The final aspect of striatal neuroanatomy considered here that may be crucial in action selection, is the possible intra-nucleus communication between projection neurons which may be facilitated by axon collaterals or interneurons. There is an inhibition of projection neurons following stimulation of afferent neurons in cortex and thalamus. *Prima facie*, this inhibition would seem to be facilitated by the GABAergic axon collaterals of the projection neurons (Wilson, Chang, and Kitai, 1983; Mink and Thach, 1993). However, recent studies have reported diametrically opposed results: research utilising dual-recording of projection neurons provided evidence that the axon collaterals play no role in the inhibition (Jaeger, Hitoshi, and Wilson, 1994) and that the generation of an action potential can illicit an IPSP in a nearby projection neuron (Tunstall, Oorschot, Kean, and Wickens, 2002).

The inhibition of projection neurons by the set of interneurons which use GABA as a neurotransmitter is not controversial. Koós and Tepper (1999) demonstrated that the extensive

axonal arborisation of a single GABAergic interneuron allows it to contact over one hundred projection neurons, and that a single action potential from the interneuron can interrupt the ongoing firing of its target. Therefore, despite the relative paucity of the GABAergic interneurons, they have a wide-ranging, powerful influence on the output of the striatum.

If the interneurons are responsible for the inhibition seen in projection neurons then this would cause problems for standard models of striatal function (Mink and Thach, 1993). Many models presumed that the axon collaterals under-pinned feedback lateral inhibition within striatum, which allowed a form of winner-takes-all competition to take place. However, lateral inhibition via interneurons is necessarily feedforward because they receive the majority of their input, and certainly all their excitatory input, from cortex and thalamus (Kawaguchi, Wilson, Augood, and Emson, 1995; Centonze, Gubellini, Bernardi, and Calabresi, 1999). Thus, local circuit competition between inputs does not occur via a single layer winner-takes-all network, but rather the competition is effectively decided by the strength of afferent input to the interneurons (see Figure 1.3 for explanation).

1.3.2 Subthalamic nucleus

The STN neurons receive widespread excitatory cortical input, in addition to excitatory input from intralaminar thalamic nuclei (Bevan, Francis, and Bolam, 1995). They utilise glutamate as a neurotransmitter and, therefore, their output is excitatory. STN neurons are also tonically active, with a spontaneous firing rate of between 10 and 30 Hz (Fujimoto and Kita, 1993; Wichmann, Bergman, and DeLong, 1994). Thus, the STN is the major source of excitation within the basal ganglia, driving neurons in the GP, EP and SNr. There is some evidence for extensive axon collateralisation within STN (Fujimoto and Kita, 1993) which may allow the majority of the neurons to fire in rough synchrony following a sufficiently powerful excitatory input (see sections 3.4 and 5.2.2 for more details).

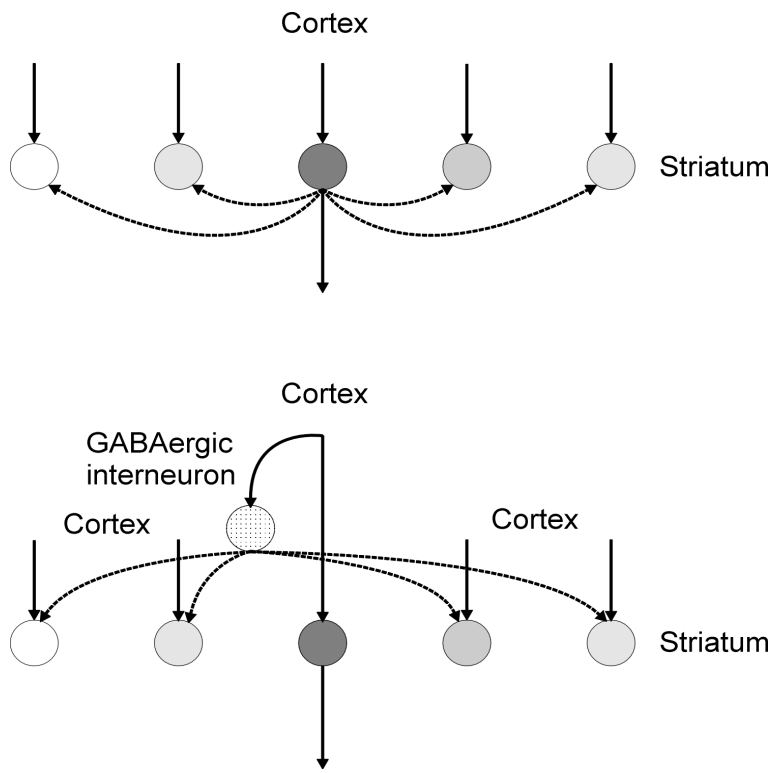


Figure 1.3: Top: standard models of striatum presume that the GABAergic axon collaterals underlie a single layer lateral inhibition feedback circuit which allows winner-takes-all functionality. Bottom: recent research has demonstrated that GABAergic interneurons are the source of the inhibition observed in striatal projection neurons after afferent stimulation. Thus, the local circuits within striatum have feedforward inhibition, radically altering their function. Excitatory pathway: solid line; inhibitory pathway: dashed line

1.3.3 Globus pallidus

GP neurons are GABAergic and reciprocally project to the STN, forming a negative feedback loop. Besides the excitatory input from STN, the GP also receives inhibitory input from D2-type striatal neurons (see section 1.3.1). The globus pallidus neurons also project to the SNr and EP. Because these projections form the majority of GP output, it is often considered to be just an intrinsic nucleus of the basal ganglia (Mink, 1996) and it is assigned a relatively minor role by the prevailing model of basal ganglia function (see section 1.4.1).

However, recent studies have shown that the GP is in a position to heavily influence the

input (Rajakumar, Elisevich, and Flumerfelt, 1994; Bevan et al., 1995) as well as the output of the basal ganglia (Bevan, Clarke, and Bolam, 1997) and that there is a significant external projection from the GP to the thalamic reticular nucleus (Hazrati and Parent, 1991). The influence of the GP over the output structures was incorporated into the original computational model of the basal ganglia, which is covered in section 1.4.2 below. The recently discovered GP to striatum pathway(s) are studied in models presented in chapter 3. There we see that GP input to projection neurons or to both projection and inter-neurons can have a significant impact on EP output. Furthermore, the effects are dependent on the projection neuron dopamine-receptor sub-population that the GP input reaches. By contrast, the results in section 2.4.7 show that modelling the GP to thalamic reticular nucleus projection does not affect basal ganglia output.

1.3.4 Output nuclei

The EP and SNr are the output nuclei of the basal ganglia, each composed of a single neuron type which utilises GABA as a neurotransmitter. They tonically inhibit their thalamic and hindbrain targets, in part because they are driven by the tonic excitatory input from STN. Output from these nuclei to thalamus and, indirectly, to cortex is segregated into separate, discrete channels (Hoover and Strick, 1999; Hoover and Strick, 1993) which have clearly delineated targets.

The anatomical channels found in projections from the output nuclei appear to be maintained throughout the basal ganglia (Gerfen and Wilson, 1996). Striatal and subthalamic nucleus afferents converge on single GP and SNr neurons (Hazrati and Parent, 1992a). Furthermore, a clear somatotopic organisation is maintained throughout the basal ganglia, again suggestive of the existence of a discrete channel architecture (Hoover and Strick, 1999; Brown and Sharp, 1995; Brown, Smith, and Goldbloom, 1998).

The brainstem targets of the EP are predominantly motor-related nuclei, including the motor trigeminal nucleus, the parabrachial area, and the parvicellular reticular nucleus (Takada, Tokuno, Ikai, and Mizuno, 1994). There is also a dense projection to the ventrolateral thalamus

(Kha, Finkelstein, Pow, Lawrence, and Horne, 2000) which is considered the principal motor relay nucleus (see section 2.2.1).

The SNr also projects densely to the thalamus, principally to the ventromedial nucleus (Mink, 1996). In addition, there is a significant projection to the superior colliculus: work by Hikosaka and colleagues has elucidated the role the SNr plays in saccadic eye movements (Hikosaka and Wurtz, 1989).

To simplify the basal ganglia models (described below) the EP is used as the representative of the basal ganglia output structures (Gurney, Prescott, and Redgrave, 1998b, 2001a, 2001b). A functional equivalence between the SNr and EP was assumed, based on their neurons' identical afferent inputs, electrical properties, and tonic inhibitory output. The distinctions between the outputs of the SNr and the EP were not important in the initial development of the computational models as these did not contain any target structures of the basal ganglia. However, the models described in chapters 2, 3, and 4 all contained extrinsic structures, but continued to use the EP as the representative output nucleus to maintain consistency with the existing models. Thus, the distinction between the SNr and EP targets constrained the structures that could be included in these models.

1.3.5 The basal ganglia fulfill the criteria for a central switch

While much is known about the anatomy and physiology of the basal ganglia researchers have had difficulty clearly defining its functional role. The basal ganglia has been implicated in numerous computational processes, including procedural/behavioural sequencing (Hikosaka, Nakahara, Rand, Sakai, Lu, Nakamura, Miyachi, and Doya, 1999; Berns and Sejnowski, 1995), learning and conditioning (Beiser and Houk, 1998; Brown, Bullock, and Grossberg, 1999; Spanagel and Weiss, 1999), memory (Floresco, Braaksma, and Phillips, 1999), attention (Brown and Marsden, 1998), and many aspects of executive motor function (Marsden and Obeso, 1994). The hypothesis that the basal ganglia acts as a central switching mechanism unifies this disparate set of functions because it would play a role in all of them.

In the previous sections we have seen how the basal ganglia fulfilled three strong criteria

for the neural substrate of a switching mechanism. First, the striatum and STN both receive extensive projections from all parts of cortex and from the thalamus. This could indicate that the basal ganglia is in a position to receive wide ranging information, as laid out in the first criterion. Second, the conservation of the basic plan of basal ganglia structures in the brains of vertebrate species points to an ancient instantiation of the selection mechanism; and one, moreover, which cannot depend on cortex for its function. Third, the motor-related brainstem and thalamic targets of the SNr and EP could make possible the expression of the selected action(s).

However, the identification of the basal ganglia as the neural substrate is not unequivocal. There is strong evidence that the basal ganglia are not directly involved in generating motor actions: “The traditional clinical view that the striatal complex is primarily ‘motor’ in function is not supported by findings that large, uni- or bilateral lesions of its various parts may result in no obvious disability” (MacLean, 1978 p.176) .

I would argue that casting the basal ganglia as an action selector neatly solves this conundrum of an obvious motor-related structure (from its output connections) having no impact on limited behaviours; it is only in the sequencing and selection of actions that an impairment would be found.

1.4 Modelling the basal ganglia

The preceding review of anatomy and connectivity has highlighted numerous lines of evidence which support the hypothesis that the basal ganglia are a central component of the brain’s action selection mechanism. However, a crucial test of this hypothesis was to create a working quantitative model of the system and show that it was capable of action selection. Numerous computational models of the basal ganglia exist, but most omit key structures or connections: some of the major models are briefly reviewed below.

1.4.1 Previous models of the basal ganglia

The direct-indirect pathway model

The dominant qualitative model of basal ganglia functional anatomy, illustrated in Figure 1.4a, was proposed by Albin, Young, and Penney (1989). They split the internal connections of the basal ganglia into two pathways: the direct pathway containing the D1-type striatal cells and the output nuclei, and the indirect pathway containing the D2-type striatal cells, the STN and the GP. The direct pathway expressed the output of the basal ganglia through the inhibition of the EP/SNr and, therefore, the disinhibition of their target structures; the indirect pathway had a modulatory influence on the direct pathway.

This ‘direct-indirect’ pathway model briefly became the prevailing model of basal ganglia function, despite never being quantitatively simulated. However, this model was criticised by its own authors within six years of its publication, who looked forward to “...the destruction of the model, and its resurrection in a more realistic form...” (Albin, Young, and Penney, 1995, p. 64) . Parent & Cicchetti’s criticism was more scathing: “...this model has failed to integrate new pieces of essential information about the anatomic and functional organization of the basal ganglia and has thus become obsolete.” (1998, p. 199) . In a more recent paper, Parent and colleagues again called for the abandonment of the ‘direct-indirect’ model, and have argued that any dual pathway model does not adequately capture the functions of the basal ganglia (Parent, Lévesque, and Parent, 2001). However, the success of the ‘direct-indirect’ model in accounting for some aspects of basal ganglia related disorders has maintained its usage as a framework for some current research (Onla-or and Winstein, 2001; Ni, Bouali-Benazzouz, Gao, Benabid, and Bennazzouz, 2001).

Computational models

Strangely, although the majority of recent basal ganglia research has been informed by the central role they play in motor behaviour, most computational models are concerned with its role in cognitive processes or in learning during conditioning. Most models are roughly based on the ‘direct-indirect’ pathway scheme just outlined. The information processing models of Amos

(2000) and Beiser & Houk (1998) use only the direct pathway (cortex-striatum-GPi); Berns & Sejnowski's (1995) model of basal ganglia decision-making uses the full scheme (though omitting the D1/D2 type neuron distinction and the GP to EP pathway). Interestingly, the latter model includes segregated information processing channels within its GPi and thalamus, similar to the channel-based architecture proposed for the basal ganglia (see section 1.4.2).

The models concerned with learning and memory do not follow a consistent functional architecture. Brown et al's (1999) model of SNc cell responses during conditioning simulates the 'limbic' basal ganglia, namely the ventral striatum and ventral pallidum, and their links to extrinsic structures. However, this model completely omits the STN. Less biologically-constrained models of the basal ganglia's memory-related role by Taylor & Taylor (2000) and Suri & Schultz (1998) are too abstract to be considered useful guides to intrinsic basal ganglia function. For example, the former model contains a single basal ganglia unit type, which receives inhibitory somatosensory feedback to limit its activity; the neural source of this feedback is not specified.

As far as I am aware, there is a single existing basal ganglia model primarily concerned with motor tasks (Contreras-Vidal and Stelmach, 1995). A potential problem with this model lies in its presumption of lateral inhibition between D1 and D2 type striatal neurons (see section 1.3.1). More importantly, however, the model's GPi units have positive feedback connections with themselves. This implies that the authors are modelling either excitatory axon collaterals or interneurons within the GPi, for which there is no anatomical or physiological data. In its favour, this model contains a connection from GPi to GPe which was missing from the initial model on which my work is based (see below), but for which there is some evidence (Hazrati et al., 1990). The implementation of this pathway is described in chapter 3.

Most of these models were designed to fulfill a specific simulation task. Thus, their accuracy in modelling the structures and connections of the basal ganglia was limited by the minimum number of components required to achieve a successful simulation. In doing so all these models omitted major pathways or added non-existent sources of input. In contrast to the goal-oriented design of these models, the computational model of Gurney et al. was expressly designed

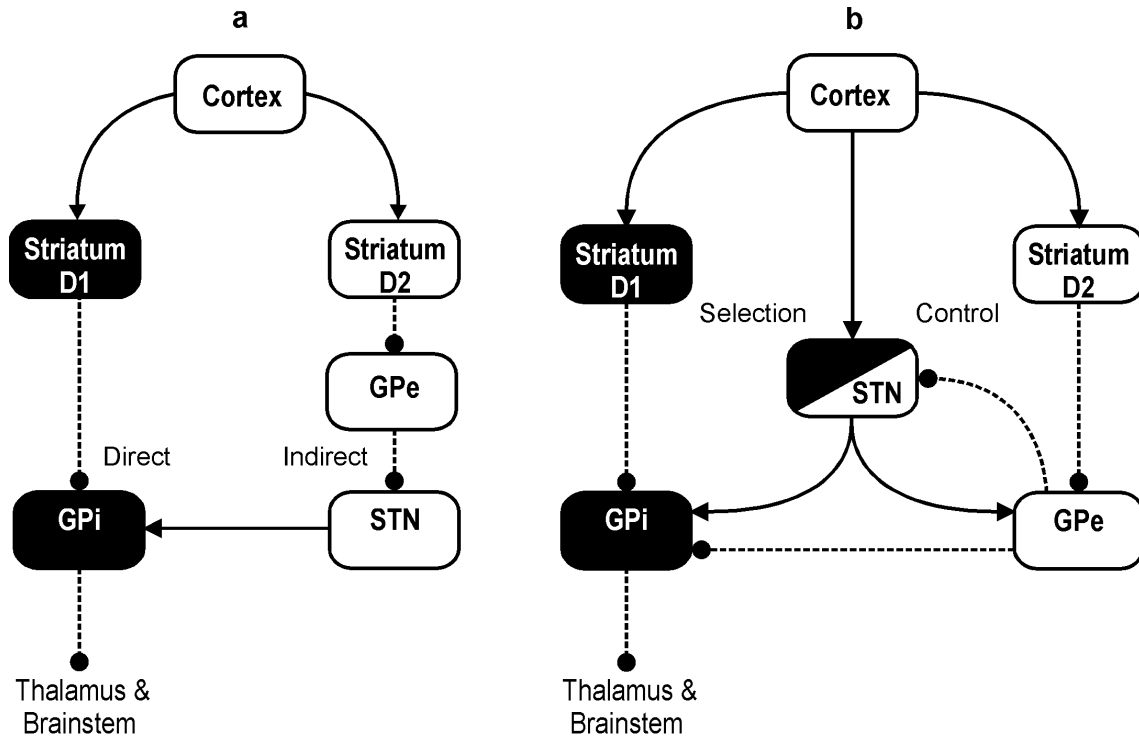


Figure 1.4: **a** The direct and indirect pathway model of basal ganglia anatomy proposed by Albin et al. (1989). **b** The proposed new functional anatomy of the basal ganglia, from Gurney et al. (2001a). The selection pathway (shaded boxes) causes the disinhibition of the basal ganglia's projection targets. One of the actions of the control pathway is to scale the level of activity in the selection pathway. The subthalamic nucleus is half-shaded as it plays a role in both pathways. Excitatory: solid line . Inhibitory: dashed line .

to incorporate all the major structures and pathways of the basal ganglia into a realistic, biologically constrained system. To this end, it was first necessary to construct a qualitative model of basal ganglia functional anatomy.

1.4.2 A new functional anatomy of the basal ganglia

Gurney, Prescott, and Redgrave (2001a) proposed a new functional anatomy (see Figure 1.4b) based on the unifying hypothesis that the basal ganglia play a crucial role in action selection, and which took into account various pathways missing from the 'direct-indirect' model. The selection hypothesis implied that the basal ganglia component structures should be described

in terms of their ability to form neural circuits for selecting signal inputs. In the new model the ‘selection’ pathway (which performs selection per se) and ‘control’ pathway (which has a modulatory influence on the selection pathway) supersede the ‘direct’ and ‘indirect’ pathways of Albin et al’s model. I go on now to outline how the basal ganglia operates as an action selector, based on this functional anatomy.

It should be stressed that I am discussing the competition between actions for the limited motor resources as the computational operation of the basal ganglia: the actions themselves were not necessarily incompatible. The competition for the incompatible use of a single motor resource, such as a limb, is assumed to be resolved at local circuit level in the striatum through its inhibitory networks (Gurney et al., 2001a). Thus, the distributed network solution discussed in section 1.2 could be utilised to provide a single action per potential muscle or effector group to the competition; it was not crucial which form of inhibitory circuit (feedback or feedforward) was used to resolve the local action competition.

In the model, every possible appropriate action is represented in a separate channel. The evidence for the existence of anatomical channels, based on tracing studies, has been detailed previously (section 1.3.4). There are further lines of evidence from lesion and behavioural studies for the existence of an action-based channel segregation in the basal ganglia output nuclei. For example, a study using squirrel monkeys showed that specific lesions in the GPi caused the attenuation or disruption of a species-typical display (used for greeting, aggression, and courtship), but did not impair normal movement (MacLean, 1978); rat-based studies that used electrode-recording in freely moving rats have shown reductions in firing rate in small sets of SNr neurons during specific movements (Gulley, Kuwajima, Mayhill, and Rebec, 1999). Thus, while I have been careful to leave the exact nature of a ‘channel’ unspecified, it would be perfectly consistent with what follows to consider each channel as representing a single set of effectors.

The level of neural activity input to a channel represents the urgency attached to that action, or the *salience* of that action. Salience levels are calculated in the striatum from sensory, proprioceptive, and contextual information. The striatum’s extensive afferent connections,

described above, make it ideally placed to perform this function. The salience level provides the basis for action selection: the action(s) with the highest salience are selected and executed.

Within the selection pathway, the more salient an action is, the more the D1 striatal neurons inhibit the output nuclei neurons of the same channel. The tonic inhibitory output of each channel in the EP/SNr, therefore, decreases with increasing inhibition provided by the striatum (and, by definition, with increases in the salience level). With a sufficiently high level of salience the output channel can effectively be turned ‘off’, removing its tonic inhibition. This causes a complete disinhibition of the targets of that channel (a subset of cells in the basal ganglia target nuclei and/or a subset of those nuclei). Any subsequent excitatory input reaching these targets, such as a motor command from cortex, can then cause the target cells to fire. This mechanism of selection has been termed ‘selective disinhibition’ (Chevalier and Deniau, 1990).

The diffuse projections of STN neurons to the EP and SNr across multiple channels allows STN to increase the output level of non-selected channels, therefore emphasising the difference between the outputs of the selected and non-selected channels. Thus, the combination of striatal and STN input forms an off-centre on-surround network in the basal ganglia output nuclei. Mink and Thach (1993) had already proposed that just this network could plausibly underlie the gating of motor programs by the output of the basal ganglia. Gurney et al. (2001a) have further proposed that a second, identically structured, off-centre on-surround network exists within the GP, formed by the diffuse excitatory input from STN and focused inhibitory input from the striatal D2 cell population. As already noted, the striatum to GP pathway is termed the *control* pathway, in part due to its influence over the output nuclei, and in part due to the reciprocal connection from the GP to STN which allows the GP to influence its own input.

Figures 1.5-1.7 illustrate how the above described selection and switching mechanism is hypothesised to work in a three channel version of Gurney et al.’s proposed functional anatomy. They describe in sequence the three functions of action suppression, action selection, and action switching. Action suppression occurs in the default or ‘resting’ state of the basal ganglia (Figure 1.5) due to the tonic output of EP on all channels. Action selection then occurs when a single action of medium salience becomes available to the selection competition (Figure 1.6), and EP

output on its channel is turned off. Action switching then occurs when a second action of a higher salience is made available to the selection competition (Figure 1.7) and EP output on its channel is turned off while EP output on the first action's channel restarts.

Analysis and simulation of a quantitative model of the functional anatomy described above (henceforth the *intrinsic* model) showed that the basal ganglia were capable of outputting signals consistent with action selection (Gurney et al., 2001b) (the model used a single leaky-integrator artificial neuron per channel in each basal ganglia structure, which continuously outputs a scalar value - this neuron is described in the next chapter). Further, the ability of the model to perform action selection was critically dependent on the level of dopamine. When dopamine levels were too high, multiple channels were selected too easily corresponding to many actions being executed, which is possibly consistent with behavioural states associated with attention deficit hyperactivity disorder (ADHD) (Swanson, Castellanos, Murias, LaHoste, and Kennedy, 1998). Very low levels of dopamine resulted in no selection occurring which may correspond to immobility and the inability to initiate actions, as observed in Parkinson's Disease patients. Thus, direct parallels could be drawn between the model's behaviour under abnormal dopamine conditions and disorders known to be caused by dysfunction of the basal ganglia.

Gurney et al. (2001b) showed that the control pathway has several functions, one of which is to automatically limit, via the GP-STN negative feedback loop, the overall level of excitatory input EP receives from STN (see also Gurney et al., 1998b). The limit is kept roughly constant as the basal ganglia recruits more channels so that the selection process can continue properly.

The findings from the intrinsic model generated two hypotheses. First, that the GP is a source of control signals for the rest of the basal ganglia. The role of the GP as the basal ganglia's central control structure is further explored in chapter 3, where I look at how recent data indicating that GP innervates striatum (Bevan, Booth, Eaton, and Bolam, 1998; Rajakumar et al., 1994) further supports this hypothesis as GP could potentially influence every structure in the basal ganglia. Second, that dopamine acts synergistically in both control and selection pathways to regulate the ease of selection; increased dopamine promotes 'promiscuous' selection

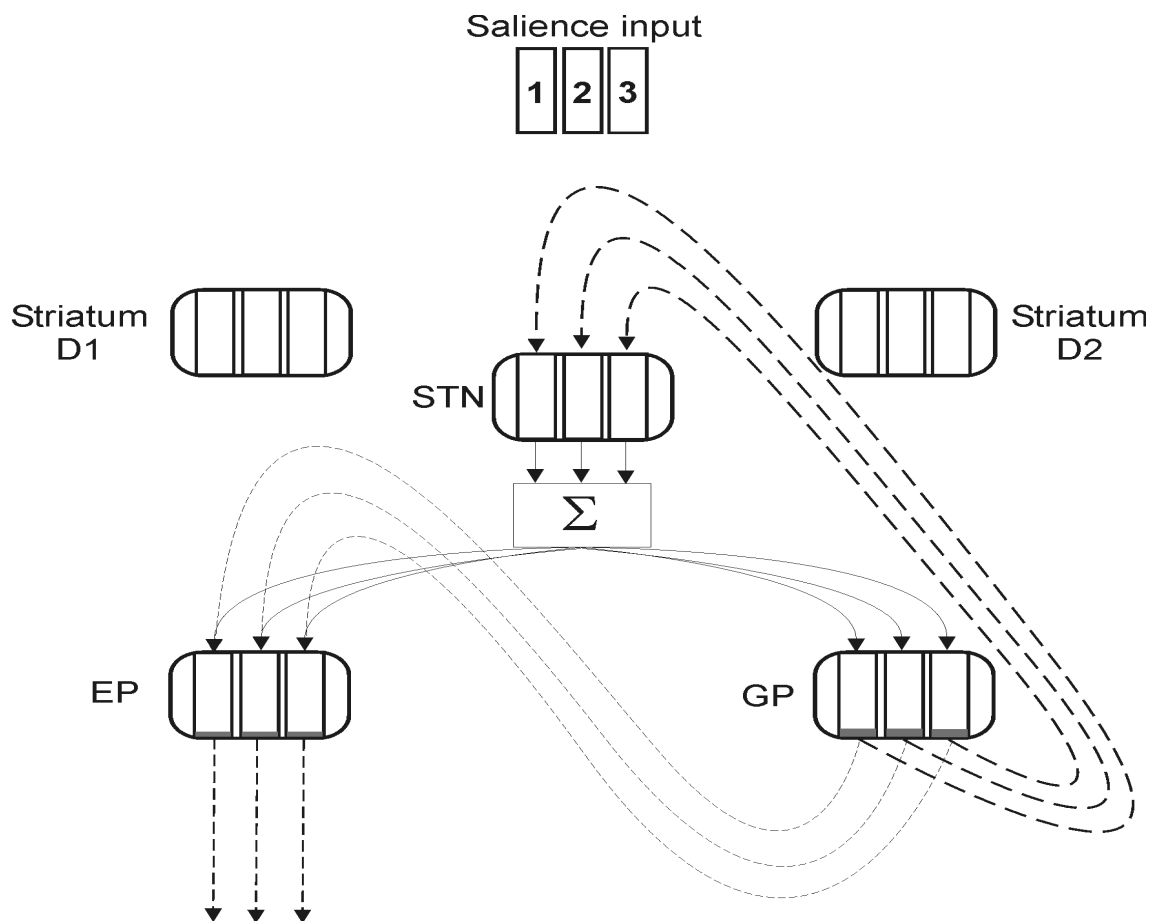


Figure 1.5: The resting state of the proposed basal ganglia switching mechanism. The grey shading represents the activity level of that channel (3 channels are shown) and a connecting line's width indicates the weighted output of that channel. Diffuse output from STN is modelled by summing (the Σ box) over all its outputs. With no salience input, all three channels in both striatal sub-populations are silent. Tonic output from EP provides constant inhibition to its efferent targets and is modified by low-level input from GP and STN. Excitatory: solid line. Inhibitory: dashed line.

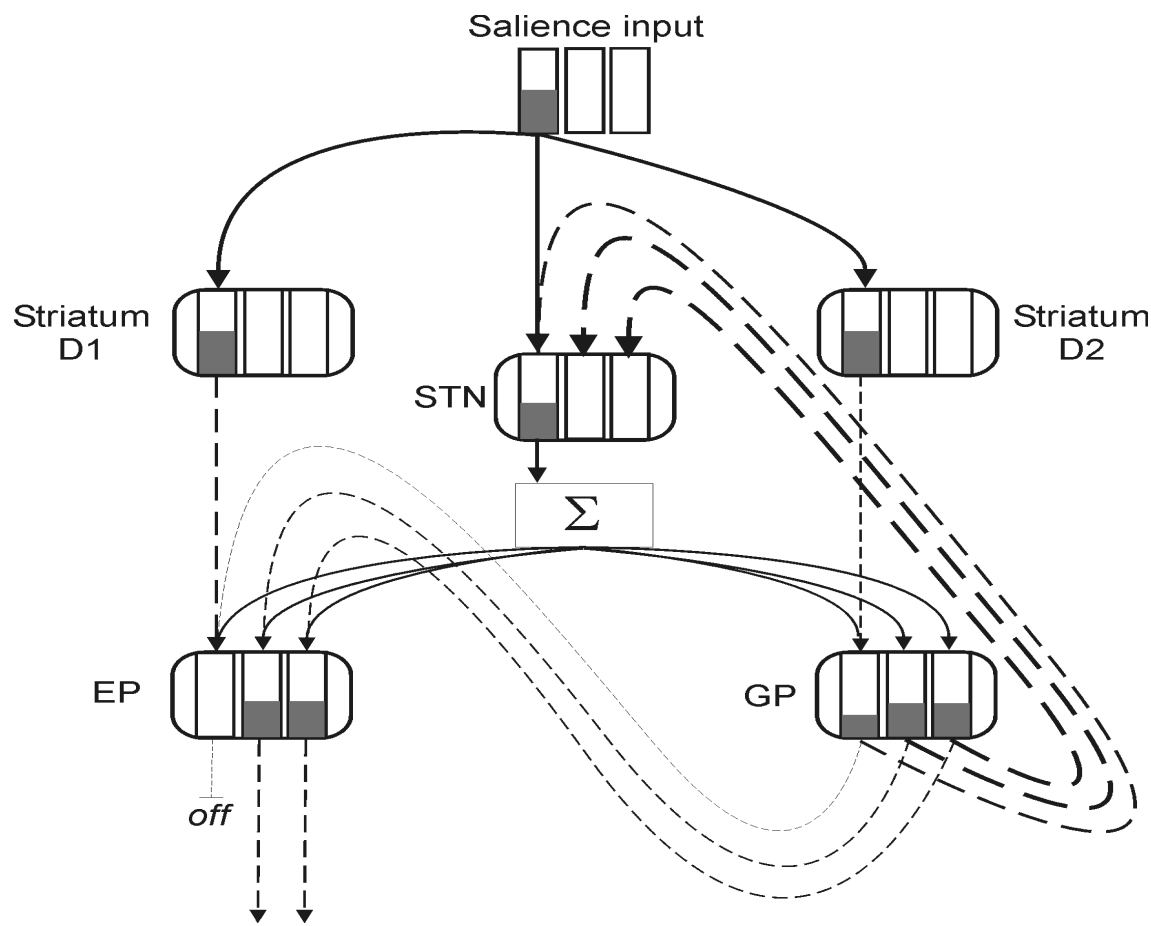


Figure 1.6: Action selection by the proposed basal ganglia switching mechanism. The grey shading represents the activity level of that channel (3 channels are shown) and a connecting line's width indicates the weighted output of that channel. Input to channel 1 represents an action of medium salience. This generates inhibitory output from both striatal populations. In the selection pathway, this output prevents activation of the corresponding EP channel, thus turning off the EP channel 1's output. In the control pathway, striatal D2 output on channel 1 reduces GP activation and output in the same channel, compared to the other channels in GP. Reduced GP inhibition allows STN output on channel 1 to increase, in combination with its direct input from salience. Due to the diffuse output of STN, this results in increased activation and output of EP channel's 2 and 3, thus clearly differentiating the selected and non-selected channels. Excitatory: solid line. Inhibitory: dashed line.

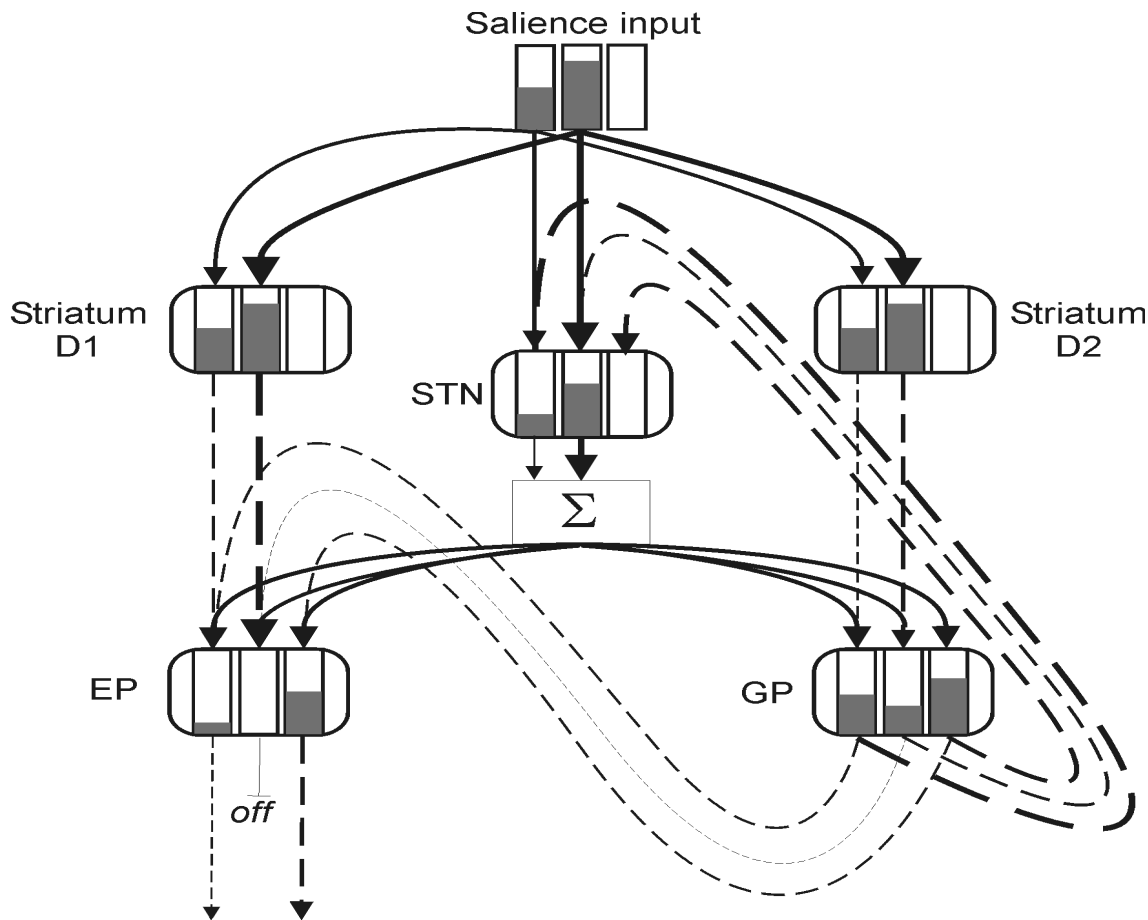


Figure 1.7: Action switching by the proposed basal ganglia switching mechanism. The grey shading represents the activity level of that channel (3 channels are shown) and a connecting line's width indicates the weighted output of that channel. After channel 1 has been selected, an input to channel 2 commences which represents an action of high salience. The input to channel 2 generates inhibitory output from both striatal populations which exceeds that on channel 1. In the selection pathway, this output prevents activation of the EP channel 2, turning off the EP channel 2's output. Thus, the higher salience action becomes selected. The increased level of diffuse STN output, due to the extra direct excitatory input of salience and concomitant reduction in GP inhibition of STN on channel 2, results in increased activation and output of EP channel's 1 and 3 (compared to the single input case). Thus channel 1 becomes de-selected and a successful switch has occurred. Excitatory: solid line. Inhibitory: dashed line.

in which channels are more easily disinhibited, whilst reduced dopamine results in a ‘stiffer’ competition in which there are fewer winners and higher levels of basal ganglia target inhibition.

The primary aim of this thesis is to expand on the intrinsic model by incorporating it into a fuller neural circuit that includes basal ganglia targets such as thalamus, which will allow me to further elucidate the relationship between basal ganglia output and behaviour. Moreover, I can identify which extrinsic structures may be crucial to action selection, and what functional roles these structures play.

1.5 Modelling issues

As noted in section 1.3, the gross anatomy and connectivity of the basal ganglia has been established for at least four decades. However, the details of basal ganglia microcircuitry - the intra-nucleus axon collaterals, the interneuron types, the functions of receptor sub-types, and so on - are constantly being updated. Much of the work described in section 1.3, such as the studies of striatal interneurons, has been published in the past three years.

These changes in the agreed composition of basal ganglia microcircuitry may rapidly invalidate any detailed functional model. As already noted, the relatively high-level direct-indirect pathway model of basal ganglia function was criticised for its inadequacies by its own authors soon after publication. The possibility of new data invalidating a model is generally true of any attempt to create detailed models of a neural system. Thus, it would be prudent to also explore the properties of the models which are not specific to the system under study: properties of biologically-constrained and plausible computational models which have wider applications to neural circuits and to modelling techniques.

To address this issue in the present work, I have concentrated particularly on the usefulness of analysing a neural circuit model at multiple levels of detail. The intrinsic model of basal ganglia processing may be termed a ‘systems’ level model, as the number of functional units within it are minimised (there is just one ‘neuron’ per channel) and the simplest possible artificial neuron model was used. A computational model at this level allows exploration of the gross phenomena of a complex neural circuit in a simple simulation environment. Further, the

computing load is minimised so that comparatively complex circuits can be built and simulated with ease. This facilitates thorough analysis and testing of the model's properties by reducing the computing time necessary to achieve the required results. The utility of the systems-level approach is demonstrated in the next two chapters through extensions of the intrinsic model that include thalamocortical loops and additional intrinsic pathways of the basal ganglia.

However, the scalar valued, continuous output of the systems-level model units requires careful interpretation. It is often convenient to characterise such outputs as representing the mean firing rate of either a single neuron averaged over a suitably long time window or an ensemble of neurons, averaged over a short time window. In either case, the actual nature of the underlying train(s) of action potentials is obscured, since irregular and regular tonic, oscillatory, and burst firing would all be possible but mutually incompatible interpretations of a given mean firing rate. Thus, lower level phenomena may be obscured in these models, phenomena which can only be studied using more complex artificial neuron models.

The first, obvious, step would be to construct an artificial neuron model which outputs a binary spike train where, using a sufficiently small time bin, a 1 codes an action potential, and 0 codes the absence of a potential. In doing so the computational operations performed by a network of these neurons is altered: the input arriving at the systems-level model units is a continuous scalar value and the input to a spiking artificial neuron is stochastic - the timing of spike arrival becomes important to the output of the unit as it will dictate the level of activation.

While such a spiking model is an advance on the continuous output models, this extra level of realism at the output stage is not maintained throughout the model. Ideally, a complete model would fully capture the intracellular operations which occur between the arrival of action potentials at the pre-synaptic membrane and the output of an action potential from the axon hillock of the post-synaptic neurons. In order to do this it is necessary to build multi-compartmental model neurons (Segev, Fleshman, and Burke, 1989; Softky and Koch, 1995) in which each compartment is a separate electrical circuit which mimics the changes in current caused by the opening and closing of ion channels in a neuron's membrane. Multiple compart-

ments also capture the attenuation of a current as it moves across space. A full compartmental model requires separate circuits for each ion channel modelled in every physical compartment of the modelled neuron’s soma and dendrites, which means that a complete model can become prohibitively complex to simulate. Even if the complexity of the neuron model is reduced, a full network of relatively simple compartmental units may require prohibitive amounts of computing power to simulate. Further, the parameter space may become very large, thereby hindering effective exploration of even a simple network because of the number of variables within a compartmental model. Moreover, the contribution that each parametrised mechanism makes to a neural circuit’s behaviour becomes increasingly difficult to evaluate.

To overcome the problems of limited computing power and a large parameter space I sought a modelling paradigm which could capture the complexities of interacting ion-channels and the effect of space while retaining something of the simplicity of the continuous-output models. To this end the phenomenological modelling approach was adopted, in which a spiking model neuron mimics the effects of current changes *phenomenologically*, that is, just the change they ultimately have on the membrane potential of the neuron (Maass, 1997). The use of this form of artificial neuron model in networks and their development to incorporate new forms of current changes are investigated in chapters 4 and 5. Thus, the secondary aim of this thesis can now be stated: to explore the different levels of modelling available to the computational neuroscientist and to assess their relative usefulness.

A central component of the phenomenological modelling approach (and, indeed, most models which output spikes) is the addition of noise to the model neuron’s membrane potential. This is done to mimic the many forms of noise present in a real neuron which may affect the timing of the action potential output (see section 4.2.1 for further details). In the networks presented in chapters 4 and 5, numerous phenomena were observed that were directly dependent on the presence and level of noise within the model neurons. Thus, the third aim of this work is to draw general conclusions about how neural noise affects the behaviour of networks.

1.6 Summary

To recap, within the vertebrate nervous system there is a selection problem whenever significant stimuli (whether external or internal) that require actioned responses co-occur or overlap in time. At this juncture a decision must be made about which stimulus to respond to, and some neural substrate must be implicated in making that decision. Prior research identified a central switching mechanism as the most elegant solution to the action selection problem, at least in the vertebrate brain, and that the basal ganglia are the prime candidate for this role (Redgrave et al., 1999a; Prescott et al., 1999). A computational model of the intrinsic basal ganglia showed that it could output signals consistent with action selection (Gurney et al., 2001a; Gurney et al., 2001b). The present work will extend this research by expanding the scope of the investigation, in terms of both the anatomical extent and computational detail of the models. Thus, the three main aims of this thesis can be stated as:

- to incorporate the existing intrinsic basal ganglia model into a neural circuit which includes thalamus and cortex, determine the changes this causes in the basal ganglia's output, and interpret the behavioural impact of these outputs.
- to assess the utility of different levels of modelling detail in functional models of neural circuitry
- to draw general conclusions on how the presence and level of neural noise may affect a network's behaviour

In the next chapter, I introduce the ‘extended’ or ‘TRN’ model which incorporates the intrinsic model into a biologically-constrained motor thalamocortical loop. The goal of this model was to show that the selection and switching capabilities of the basal ganglia could be maintained when it was embedded in a more complete neural circuit, and to investigate the role of extrinsic structures in action selection (specifically the thalamic reticular nucleus).

Having established the form of the extended model, additions to the intrinsic structure of the basal ganglia are explored in chapter 3. The model’s responses to these additions, in terms of changes to the action selection ability, illustrate how robust the model is to changes in its

connectivity and weights. This, in turn, highlights the relative ease with which the effects of changes to systems-level models can be understood and interpreted.

The extended model used the same artificial neuron type as the intrinsic model. To explore the theme of developing models of neural circuits at multiple levels of description, chapter 4 details the effect of using more detailed spiking artificial neurons in the extended model. In particular, this more detailed model is used to investigate the effect of closely matched inputs to the basal ganglia, in an attempt to reveal low-level phenomena such as oscillations and bursting in the basal ganglia output which could not be captured at the systems-level.

To further explore the differences in levels of detail in computational modelling, chapter 5 introduces new methods of expanding the spiking artificial neuron model to incorporate ion channel dynamics without recourse to an overly complex model. The new methods are used to explore the STN-GP subloop of the basal ganglia, and the results of a recent culture-based study of this circuit (Plenz and Kitai, 1999) are successfully simulated.

Chapter 2

The role of the thalamic complex in action selection

2.1 Introduction*

As outlined in Chapter 1, Redgrave and colleagues' analysis of internal circuitry and external connectivity led them to propose that the basal ganglia played a crucial role in solving the action selection problem (Redgrave et al., 1999a; Prescott et al., 1999). This led to the development of a computational model of intrinsic basal ganglia processing (Gurney et al., 2001a; Gurney et al., 2001b). The primary aim of this chapter is to determine the changes to the action selection capabilities of this model caused by its extension to structures extrinsic to the basal ganglia. By embedding the intrinsic model into a neural circuit which is able to implement the output of the action selection process it is hoped that its signal selection ability is maintained and that new features of the selection process are revealed through the additional connections. As the explicit focus of the original model was on the selection of actions, the external structures should subserve motor functions. Further, because the focus is on how the signal selection output of the basal ganglia may be modified, and not in the specifics of how the output affects the downstream motor plant, the external circuit need only contain feedback to the basal ganglia input structures. Thus, the intrinsic model was embedded in a model of the thalamocortical

*This chapter is based on material previously presented in Humphries and Gurney (2002).

loop which subserves motor functions.

The plan of this chapter is as follows: the motor thalamocortical loop is introduced, along with an explanation for the maintenance of the channel-based architecture in structures extrinsic to the basal ganglia. This is followed by a detailed description of the thalamic reticular nucleus and arguments for the specific design adopted for it in the model presented here. To enable successful comparison of the results of the three models described in this chapter, I go on to discuss the primary characteristics of a switching mechanism which have been previously identified (Redgrave et al., 1999a). The simulations which tested for the presence of these characteristics in the original intrinsic model and two versions of the extended model are reported.

2.2 Thalamocortical interactions

2.2.1 The motor thalamocortical loop

To extend the intrinsic model, it was embedded into a thalamocortical loop comprising the ventrolateral (VL) thalamus, the motor cortex, and the thalamic reticular nucleus (TRN). The resulting extended model is shown in Figure 2.1.

The VL thalamus is normally considered to be the principal motor thalamic nucleus (Price, 1995; Jones, 1985). EP/GPi neurons project densely to the VL thalamus in all vertebrates (Uno, Ozawa, and Yoshida, 1978; Kha et al., 2000) and the VL thalamic neurons predominantly project in turn to the primary motor cortex, primarily arborising in layer V (Zarzecki, 1991; Jacobson and Trojanowski, 1975). Completing the loop, primary motor cortex neurons in layer V project to the striatum and STN (Lévesque, Charara, Gagnon, Parent, and Deschênes, 1996; Turner and DeLong, 2000; Gerfen and Wilson, 1996) and those in layers V and VI project reciprocally to the VL thalamus (Jacobson and Trojanowski, 1975): all of these cortical neurons have dendritic fields which extend up to layer IV. Thus, there is a monosynaptic connection between the thalamic input to cortex, and the cortical neurons which project to the target structures (White, 1989). Collaterals from the corticothalamic and thalamocortical

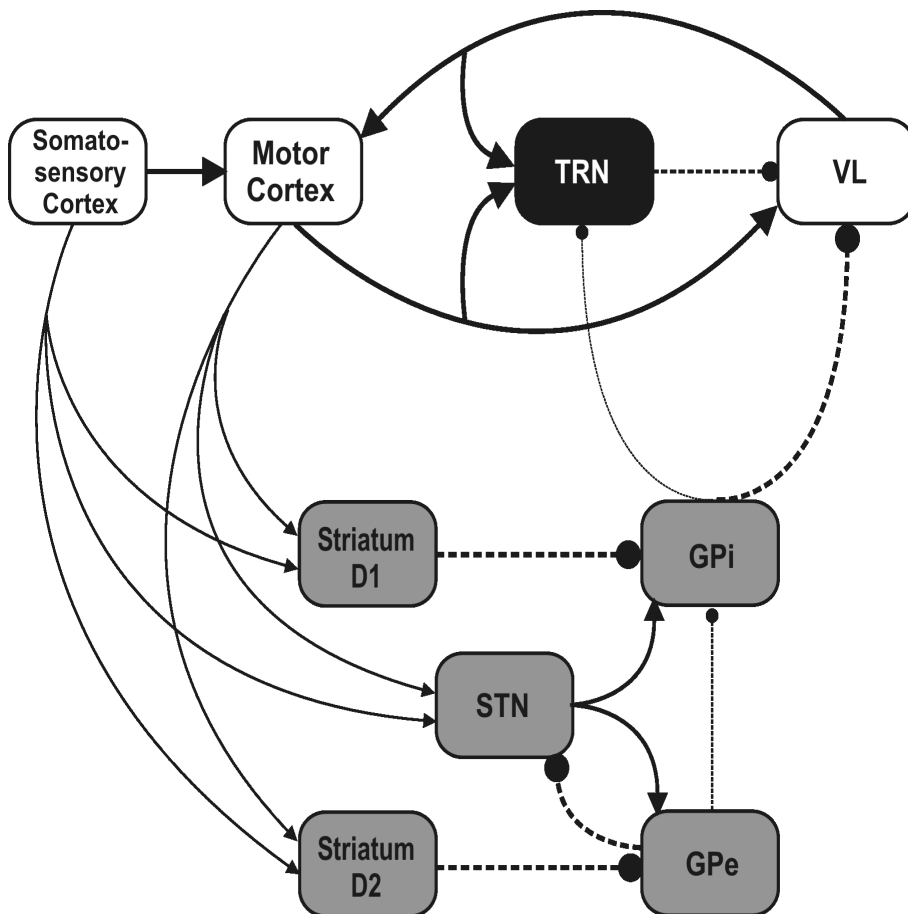


Figure 2.1: The connection scheme of the extended computational model: the original intrinsic model (grey-shaded boxes) is embedded into a thalamocortical loop comprising the motor cortex, ventrolateral (VL) thalamus, and the thalamic reticular nucleus (TRN). Sensory signal levels are input to the model from the somatosensory cortex, and copies are sent to the motor cortex, subthalamic nucleus (STN) and the striatal D1 and D2 receptor neuron populations. The thickness of each line denotes the relative strength of that connection. Solid line: excitatory connection; broken line: inhibitory connection.

projections converge on neurons in the anterior pole of the TRN (Cicirata, Angaut, Serapide, and Panto, 1990) which, in turn, send inhibitory connections back to the VL thalamus (Ilinsky, Ambardekar, and Kultas-Ilinsky, 1999). Thus there are three loops in operation: the extended motor cortex-basal ganglia-VL thalamus-motor cortex loop; the positive feedback loop formed by the motor cortex and VL thalamus; and the negative feedback loop formed by the TRN and VL thalamus which is modulated by cortical input.

The channel-based architecture of the intrinsic functional model was retained in the extrinsic structures of the extended model as there is a wealth of evidence for the existence of channels outside the basal ganglia. The basal ganglia output nuclei send somatotopically organised projections to their targets, in particular the thalamic nuclei (Hoover and Strick, 1993). Further, all cortically projecting thalamic nuclei contain topographic maps which are maintained in the projections to the cortical areas (Adams, Lozsádi, and Guillery, 1997) and there is evidence that the somatotopic projections from the GPi are maintained in the VL thalamus projections (Hoover and Strick, 1999). The region of primary motor cortex which receives input from VL thalamus contains a well defined somatotopic map, with separate areas for vibrissae, eyes, tongue, lips, and so on (Hall and Lindholm, 1974). Finally, the projection from primary motor cortex to striatum and STN is also somatotopically organised (Brown et al., 1998; Brown and Sharp, 1995; Joel and Weiner, 1997). Thus, there is substantial evidence that discrete channels are maintained outside the basal ganglia, at least at the level of separate body parts.

Input to the extended model comes from somatosensory cortex and represents pre-processed sensory data. A copy of the input is sent to the motor cortex via the extensive intra-cortical connections (Farkas, Kis, Toldi, and Wolff, 1999; Izraeli and Porter, 1995; Miyashita, Keller, and Asanuma, 1994). The original input signal and the copy (via motor cortex) are summed in the striatum and the STN, forming the salience level. This operation is achieved via the overlapping projection targets of somatosensory and motor cortex neurons in the striatum and STN (Flaherty and Graybiel, 1994; Bevan et al., 1995).

2.2.2 The thalamic reticular nucleus

The thalamic reticular nucleus (TRN) has been attributed a variety of roles related to attention. For example, there is evidence that it has a specific role to play in covert attention: lesioning the TRN in rats disrupts their ability to orient towards a visual cue (Weese, Phillips, and Brown, 1999). Some authors have suggested that the TRN could conceivably control all forms of attention in humans (Crick, 1984; Guillory, Feig, and Lozsádi, 1998) or, more generally, that it is a ‘gateway’ to consciousness (Newman, Baars, and Cho, 1997).

The functional design of the TRN used in the current model did not explicitly address attentional processing, instead it followed from anatomical data on the TRN interpreted in the channel-based scheme. The design’s basic form is shown in Figure 2.2 for three channels. The TRN can be divided into multiple sensory, motor and ‘association’ *sectors* defined by their input-output connections (Guillory et al., 1998; Lozsádi, 1994). Each sector receives input from the appropriate thalamic nuclei and cortical areas; this input is derived from collaterals of the reciprocal projections between the thalamus and cortex (Jones, 1985). In turn, the neurons in a TRN sector project back solely to the appropriate thalamic nucleus: the work of Ilinsky and colleagues (Tai, Yi, Ilinsky, and Kultas-Ilinsky, 1995; Kultas-Ilinsky, Yi, and Ilinsky, 1995; Ilinsky et al., 1999) has demonstrated that well preserved projections exist from the appropriate subdivisions of the TRN to the mediodorsal, anterior, and motor (ventrolateral and ventroanterior) thalamus in monkeys. They also reported that projections from TRN neurons synapse both on thalamocortical projection neurons and local circuit neurons (interneurons) in all thalamic nuclei. However, as I am explicitly modelling the basal ganglia and external circuitry based on the gross anatomy and physiology of the rat brain, interneuron synapses may be ignored for the proposed model of TRN-VL connections as there are no interneurons in the rat VL thalamus (Sawyer, Martone, and Groves, 1991; Ilinsky, Toga, and Kultas-Ilinsky, 1993).

The level of topographic organisation within the TRN allows each sector and its associated thalamocortical loop to be regarded as a distinct circuit. For example, in the rat, the vibrissal somatosensory sector of the TRN receives input from the ‘barrel’ cortex (Hoogland, Welker, and

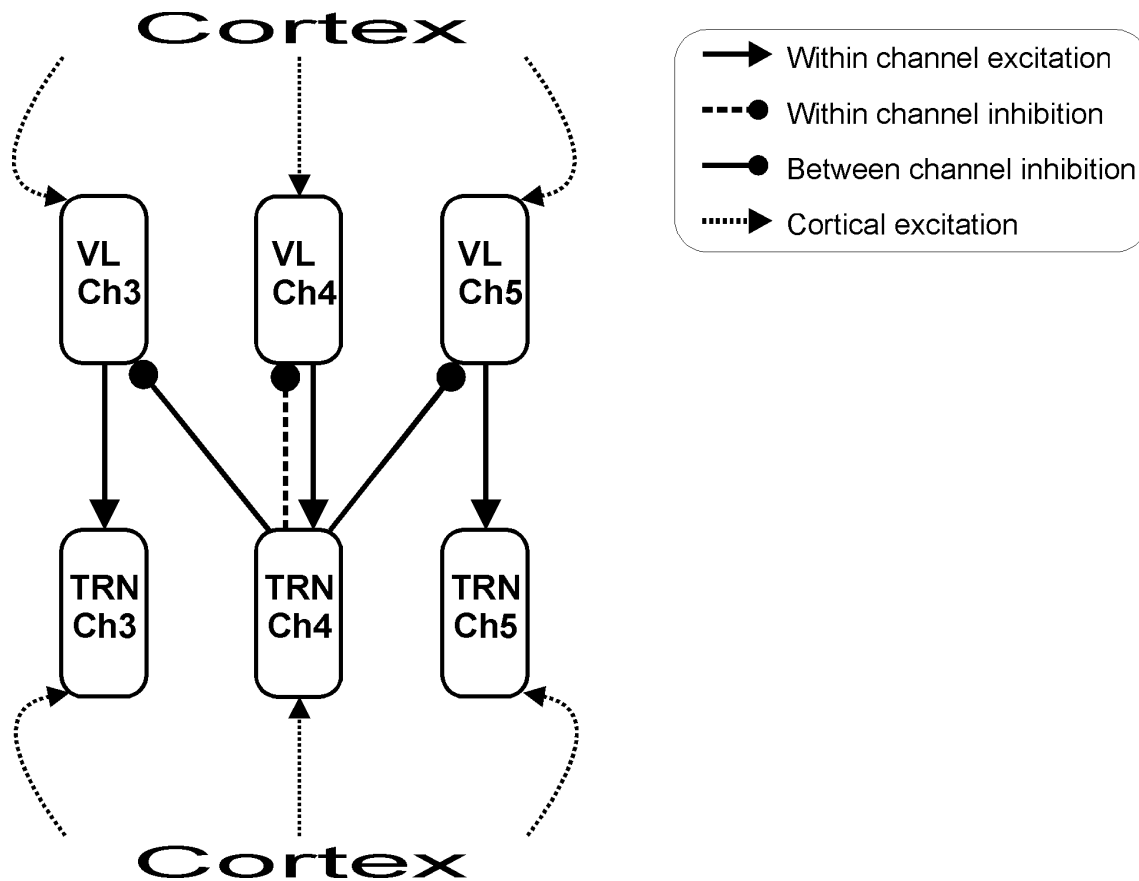


Figure 2.2: The functional design used in the extended model for the interconnectivity of the ventrolateral thalamus (VL) and the thalamic reticular nucleus (TRN). Full connections are only shown for channel 4. Basal ganglia inputs are omitted for clarity.

Van der Loos, 1987) and ventrobasal thalamus, and projects back to the ventrobasal thalamus (Shosaku, Kayama, and Sumitomo, 1984), thus creating a self-contained ‘whisker’ processing circuit. Because of this level of separation between thalamocortical circuits, the self-contained circuit formed by the motor cortex, VL thalamus, and the anterior pole of the TRN need only be considered for the model.

An important factor for the design of the TRN-VL thalamus interconnections is that TRN neurons rarely project back to the thalamic neurons from which they receive synaptic contact. This implies that when a thalamocortical neuron is driven by excitatory input, the TRN neuron(s) it synapses on are driven to inhibit other thalamocortical neurons in the same nucleus. Thus, the output of one thalamocortical neuron causes the inhibition of surrounding thalamo-

cortical neurons, which can be characterised as a distal lateral inhibition mechanism (Pinault and Deschênes, 1998).

I have interpreted this functional organisation within the channel architecture. The thalamocortical neurons in a channel project only to the TRN neurons in the same channel; these TRN neurons then project predominantly back to VL thalamus neurons in other channels. However, a weak inhibitory input from the TRN channel back to the corresponding channel in the VL has been included to model the minority of TRN neurons which *do* synapse back on to the VL thalamus neurons that project to them (Kim and McCormick, 1998). Thus, the TRN-VL thalamus interconnection design adopted here has both within- and between-channel inhibition in VL thalamus, but only within-channel excitation in the TRN (see Figure 2.2).

While this channel-based interpretation of the TRN-dorsal thalamus connectivity remains to be confirmed anatomically in the motor pathway, there is evidence for it in other pathways. The ascending sensory pathway of the rat vibrissal system contains discrete cell groups in every structure. In the ventrobasal thalamus, these discrete cell groups (barreloids) respond maximally to the stimulation of a specific whisker; and they are arranged in a topographic map of the whiskers on the contralateral side of the face (Diamond, 1995; Friedberg, Lee, and Ebner, 1999). Thalamocortical neurons in one barreloid all project to the same area of TRN, forming a corresponding discrete cell cluster of maximally responsive neurons in the TRN (Sumitomo and Iwama, 1987). Sumitomo and Iwama also found that stimulation of a single whisker activated the cells in the corresponding barreloid and, as expected, these excited the corresponding area of the TRN. However, the activity in other barreloids was inhibited. Hence, these TRN neurons appeared to project back to thalamocortical neurons in other barreloids. The channel-based scheme is, therefore, consistent with mechanisms of between-channel inhibition in place in the TRN-dorsal thalamus complex.

Finally, there is evidence for a sparse inhibitory input from the basal ganglia output nuclei to the TRN. Projections from the SNr synapse in TRN sectors which project to VL and VM thalamus (Kolmac and Mitrofanis, 1998; Cornwall, Cooper, and Phillipson, 1990; Gandia, De Las Heras, Garcia, and Giménez-Amaya, 1993; Paré, Hazrati, Parent, and Steridæ, 1990). In

the extended model, this input has been assumed to be channel specific. This connection will be discussed in more detail in section 2.4.7.

2.2.3 The requirements of a switching mechanism

Integral to the basal ganglia's postulated role as the vertebrate brain's primary action selection mechanism is the ability to switch between actions after an initial action has been selected. For this role, Redgrave et al. (1999) laid out two computational requirements and three desirable characteristics that a central switching mechanism must fulfill, following the work of Snaith and Holland (1990). The first computational requirement has been outlined, namely that selection depends on the relative salience levels of the competing actions. Therefore, the action(s) with the highest salience(s) is (are) selected and expressed, with the caveat that the level of EP/SNr output must be below some selection threshold to allow sufficient disinhibition of the target structures.

The second computational requirement covered the criteria for terminating an action. Termination may occur, in a normally functioning basal ganglia, when an action is interrupted by a competing action with a higher salience. This condition ensures that the animal progresses smoothly from one action to another without a conflicting use of motor resources occurring. It was previously shown that the intrinsic model was able to fulfill both of these computational requirements (Gurney et al., 2001b).

They also set out the desirable characteristics to define how an ideal switching mechanism should operate and the behavioural effects this would have. The primary characteristic was *clean switching*: the competition between actions should be resolved rapidly and decisively. If this did not occur then an animal would be forced into lengthy periods of quiescence after the termination of an action while the next one is being selected. This would leave an animal vulnerable to predators and natural hazards. Moreover, the switching between actions should occur without significant concurrent periods of selection so that incompatible actions are not simultaneously attempted. The latter feature is demonstrated in chapter 4.

Once an action has been successfully selected, it is undesirable that its expression be ham-

pered or temporarily interrupted by losing competitors. The second desirable characteristic, therefore, was that there should be an *absence of distortion*. Any losing competitor should be sufficiently suppressed so that it can not interfere with the selected action. Furthermore, short-term increases in salience on a non-selected channel should also be suppressed, unless the increase is of a sufficient magnitude to warrant selection.

When the competition for selection is between actions with almost equal saliences then it is essential that the selected action continues after its salience has dropped below the level of its immediate competitors. We may call this desirable characteristic *persistence* and, to illustrate its utility, consider the case in which an animal is almost equally hungry and thirsty. One of these, say thirst, is slightly more salient and so the action of drinking is selected. However, after a brief period of drinking, the salience level of thirst drops below that of hunger, so the animal begins to eat. Again, after a brief period of eating, the salience level of hunger would drop below that of thirst, and the animal would return to drinking. This could continue *ad infinitum* as neither sensation is properly sated, with the animal constantly oscillating between two behaviours: a phenomenon known as ‘dithering’ (Houston and Sumida, 1985). Hence, the ability for an action to persist until it has been satisfactorily completed is desirable for normal function.

One feature of salience input which is pertinent to the arguments above concerning persistence is the possibility of transient increases in salience level. The suppression of transient decreases in basal ganglia output resulting from transient salience increases on non-selected channels would allow the selected action to be successfully completed. However, in reality, there must be a trade-off between persistence and the criteria for switching as the highest salience action cannot both be selected and suppressed in favour of an ongoing action. An action which has a consistently and sufficiently high salience should be selected in favour of a lower salience persistent (on-going) action, so that the animal is not forced to ignore potentially important events.

2.2.4 Aims

While the output signals from the intrinsic model were consistent with action selection, it remains to be determined that the model works effectively when embedded in a wider anatomical context; hence I constructed a model which includes the thalamus and cortex. There were two aims for this extended model. First, to show that the selection and switching capabilities of the intrinsic model could be maintained. Second, to ascertain whether the extended model could fulfill the desirable characteristics of a switching mechanism laid out in the previous section.

2.3 Quantitative modelling

2.3.1 The model neuron

The extended model uses leaky-integrator artificial neurons, just as were used in the intrinsic model (Gurney et al., 2001b). Let u be the total afferent input and k be the constant determining the rate of activation decay. The activation a of a leaky integrator is then

$$\dot{a} = -k(a - u) \quad (2.1)$$

where $\dot{a} \equiv da/dt$. In all that follows, the activation at equilibrium \tilde{a} (where $\dot{a} = u$) is described.

The output y of the neuron, corresponding to the mean firing rate, is bounded below by 0 and above by 1. In simulation, this is achieved by using a piecewise linear output function. However, as has been previously demonstrated (Gurney et al., 2001b), in simulation y never exceeds 1 so that the output relation can be written as

$$y = m(a - \epsilon)H(a - \epsilon) \quad (2.2)$$

where ϵ is a threshold for the activation (below which the output is zero), $H()$ is the Heaviside step function, and m is the linearly increasing part of the output function.

2.3.2 Motor cortex

Motor cortex receives sensory input S_i from somatosensory cortex, and input from VL thalamus y_i^v , where i is the channel index. The strength of the synaptic connections from VL thalamus

and somatosensory cortex are denoted by w_{vl} and w_s , respectively (weights are assumed to be given as absolute magnitudes throughout this section). If \tilde{a}_i^m is the equilibrium activation of channel i in motor cortex then

$$\tilde{a}_i^m = w_{vl}y_i^v + w_sS_i. \quad (2.3)$$

Then, if ϵ_m is the output relation threshold term (see equation 2.2) the output y_i^m of motor cortex is given by

$$y_i^m = m(\tilde{a}_i^m - \epsilon_m)H(\tilde{a}_i^m - \epsilon_m). \quad (2.4)$$

2.3.3 Thalamic reticular nucleus

The TRN receives input from three sources: motor cortex y_i^m , VL thalamus y_i^v , and the basal ganglia output nuclei, y_i^b . Let the synaptic strengths from the three sources be w_m , w_v , and w_{bg} , respectively, and let \tilde{a}_i^t be the activation at equilibrium of the i th channel of TRN, then

$$\tilde{a}_i^t = w_vy_i^v + w_my_i^m - w_{bg}y_i^b. \quad (2.5)$$

Thus, if ϵ_t is the output relation threshold term, then the output y_i^t of TRN is given by

$$y_i^t = m(\tilde{a}_i^t - \epsilon_t)H(\tilde{a}_i^t - \epsilon_t). \quad (2.6)$$

2.3.4 Ventrolateral thalamus

VL thalamus receives input from motor cortex y_i^m , the basal ganglia output nuclei y_i^b , and the TRN y_i^t . The inhibitory input from the TRN has two distinct components, as discussed in section 2.2.2. Within-channel input is assigned the weight w_T^* . The between-channel input contacts all channels in VL thalamus except the corresponding channel i . Hence, the total between-channel output Y_i^t of the TRN is given by

$$Y_i^t = m \sum_{j \neq i}^n (\tilde{a}_j^t - \epsilon_t)H(\tilde{a}_j^t - \epsilon_t), \quad (2.7)$$

where n is the total number of channels. Let the strength of the between channel connection be w_b , the motor cortical input be w_x , and the basal ganglia input be w_o . Then the activation

at equilibrium of the i th channel in VL thalamus is

$$\tilde{a}_i^v = w_x y_i^m - (w_o y_i^b + w_T^* y_i^t + w_b Y_i^t). \quad (2.8)$$

Then, if ϵ_v is the output relation threshold term, the output y_i^v of VL thalamus becomes

$$y_i^v = m(\tilde{a}_i^v - \epsilon_v)H(\tilde{a}_i^v - \epsilon_v). \quad (2.9)$$

2.3.5 Striatum

Input to the striatum is a combination of sensory input (from somatosensory cortex) and motor cortical input, which are denoted by S_i and y_i^m , respectively. The strength of the synaptic connections from somatosensory and motor cortex are w_{sc} and w_{mc} . Thus, the salience level c input to the i th striatal channel is given by

$$c_i = w_{sc}S_i + w_{mc}y_i^m. \quad (2.10)$$

The disparate action of dopamine on the selection and control pathways is retained by using a multiplicative factor on the appropriate synaptic weight. Thus, let λ_g and λ_e parameterise the tonic level of dopamine in the control and selection pathways respectively, where $0 \leq \lambda_e, \lambda_g \leq 1$. Then the action of dopamine in the control pathway can be characterised as a modification to the synaptic weights: $(1 - \lambda_g)w_{sc}$ and $(1 - \lambda_g)w_{mc}$. Similarly, for the selection pathway: $(1 + \lambda_e)w_{sc}$ and $(1 + \lambda_e)w_{mc}$. The activation functions for D1 and D2 striatal neurons, respectively, are then

$$\tilde{a}_i^e = c_i(1 + \lambda_e), \quad (2.11)$$

$$\tilde{a}_i^g = c_i(1 - \lambda_g).$$

The output relation for neurons in the selection pathway is

$$y_i^e = m(\tilde{a}_i^e - \epsilon)H^\uparrow(\lambda_e), \quad (2.12)$$

where $H^\uparrow(\lambda_e) = H(\tilde{a}_i^e - \epsilon)$. The up-arrow emphasises that the value of ϵ indicates the difficulty of the UP-state/DOWN-state transition: if ϵ is given a positive value, then the unit must

receive input of at least this level to have a non-zero output. Similarly, the control pathway's output relation is

$$y_i^g = m(\tilde{a}_i^g - \epsilon)H^\uparrow(\lambda_g). \quad (2.13)$$

2.3.6 STN

Similar to the previous section on striatum, the equations describing STN activation and output have to be rewritten to accommodate the split input from somatosensory cortex S_i and motor cortex y_i^m , which replaces the original single salience input. Let the strength of the synaptic connections from somatosensory and motor cortex be w_{st} and w_{mt} . Then the equilibrium activation \tilde{a}_i^+ of the i th STN channel is given by

$$\tilde{a}_i^+ = w_{st}S_i + w_{mt}y_i^m - w_g y_i^p, \quad (2.14)$$

where w_g is the weight of the GP-STN pathway and y_i^p is the output of GP. If ϵ' is the output relation threshold term, the output y_i^+ of STN remains

$$y_i^+ = m(\tilde{a}_i^+ - \epsilon')H(\tilde{a}_i^+ - \epsilon'), \quad (2.15)$$

where ϵ' is given a moderate negative value to simulate the tonic output of STN. However, as STN output is diffuse across all channels in its target structures we need to consider the total STN output Y^+ , which is given by

$$Y^+ = m \sum_{i=1}^n (\tilde{a}_i^+ - \epsilon')H(\tilde{a}_i^+ - \epsilon'), \quad (2.16)$$

where n is the number of channels.

2.3.7 GP and EP

The equations for the activation and output of the GPe and GPi from Gurney et al. (2001b) are briefly recapped here. A GP channel receives input from the corresponding striatal D2 population channel y_i^g . It also receives input from all the STN channels Y^+ . Let the striatum D2 to GP connection strength be w_{gp} and that of the STN to GP connection be w_{sp} . Then the

activation at equilibrium \tilde{a}_i^p of the i th GP channel is given by

$$\tilde{a}_i^p = w_{sp}Y^+ - w_{gp}y_i^g. \quad (2.17)$$

If ϵ_p is the output threshold term, then the output y_i^p of i th GP channel is

$$y_i^p = m(\tilde{a}_i^p - \epsilon_p)H(\tilde{a}_i^p - \epsilon_p). \quad (2.18)$$

An EP channel receives input from three sources: the corresponding striatal D1 population y_i^e and GP channel y_i^p , and diffuse STN input Y^+ . The strength of the synaptic connections from striatum D2, GP, and STN are given by w_{eb} , w_{pb} , and w_{sb} , respectively. The equilibrium activation of the i th EP channel \tilde{a}_i^b is thus given by

$$\tilde{a}_i^b = w_{sb}Y^+ - w_{pb}y_i^p - w_{eb}y_i^e. \quad (2.19)$$

Letting ϵ_b be the output threshold term, the output y_i^b of an EP channel is

$$y_i^b = m(\tilde{a}_i^b - \epsilon_b)H(\tilde{a}_i^b - \epsilon_b). \quad (2.20)$$

2.3.8 Parameter details

All simulations were conducted using a six channel model, to be consistent with the previously published model and because the extra channels contribute to the tonic output of the STN, GP, and EP. Most parameter settings from the original model were maintained, thus w_{eb} , w_{gp} , and w_g were set to 1, w_{sp} and w_{sb} were 0.8, and w_{pb} was 0.4 (see Gurney et al. 2001b for details). The slope parameter m was set to 1 throughout.

The dopamine parameters, λ_e and λ_g , were set to 0.2, as they were for a ‘normally’ operating intrinsic model. To model the difficulty of forcing striatal neurons in to their UP-state, the offset ϵ was set to 0.2, so that a significant level of excitatory input would be required before a striatal neuron gave a non-zero output. Finally, to ensure that STN, GP, and EP units give tonic output in the absence of input, the offset values ϵ' , ϵ_p , and ϵ_b were set to -0.25, -0.2, and -0.2, respectively.

For the new parameters, the weights w_v , w_s , w_x , w_m , w_o , and w_{vl} were also set to 1. Weights w_{sc} , w_{mc} , w_{st} , and w_{mt} were set to 0.5, to model the roughly equal level of somatosensory and

motor cortex input to striatum and STN, and to limit the total excitatory input to a possible maximum of 1 (in line with the synaptic strength of the direct salience connection in the intrinsic model). To model the very sparse nature of closed loop connections between VL thalamus and the TRN, w_T^* was set to 0.1. The open-loop (between channel) connection weight w_b was set to 0.7, because TRN input to VL thalamus is significantly smaller than cortical feedback (Price, 1995). Finally, w_{bg} was set to 0.2 to model the sparse nature of the connection between the basal ganglia output nuclei and the TRN. The offset (threshold) values ϵ_m , ϵ_t , and ϵ_v were set to 0.

2.4 Simulation Results

2.4.1 Example outputs

I first describe example outputs from a single simulation which serve to illustrate the features analysed in the subsequent sections. Three models were tested. First, the original intrinsic model, for comparison purposes with the new models. Second, a model with the thalamocortical loop but no TRN (the ThalamoCortical or TC model) obtained by setting the weights w_T^* and w_b to 0. This allowed a study of the effect of the positive feedback loop formed by motor cortex and VL thalamus on its own. Third, the full extended model, shown in Figure 2.1, which is termed the TRN model. Figure 2.3 shows the outputs of the EP and motor cortex (where applicable), and the sensory input, on three channels for all three models. In each simulation, the input on channel 1 (0.4) started at $t = 1$, and the input on channel 2 (0.6) started at $t = 2$. A transient event on channel 1 began at $t = 3$ and terminated at $t = 4$. The transient was 0.2 in amplitude so that the sensory inputs on both channels temporarily became equal.

A channel i was considered selected if the EP output y_i^b of that channel fell below the selection threshold θ_s , which was set to 0.05. This was chosen to indicate that the tonic inhibition from the EP had decreased sufficiently to allow its targets to fire. Although a zero output would demonstrate unequivocal selection, it is unrealistic to suppose that neurons have to be held in a completely silent state for a behaviourally meaningful period to indicate selection.

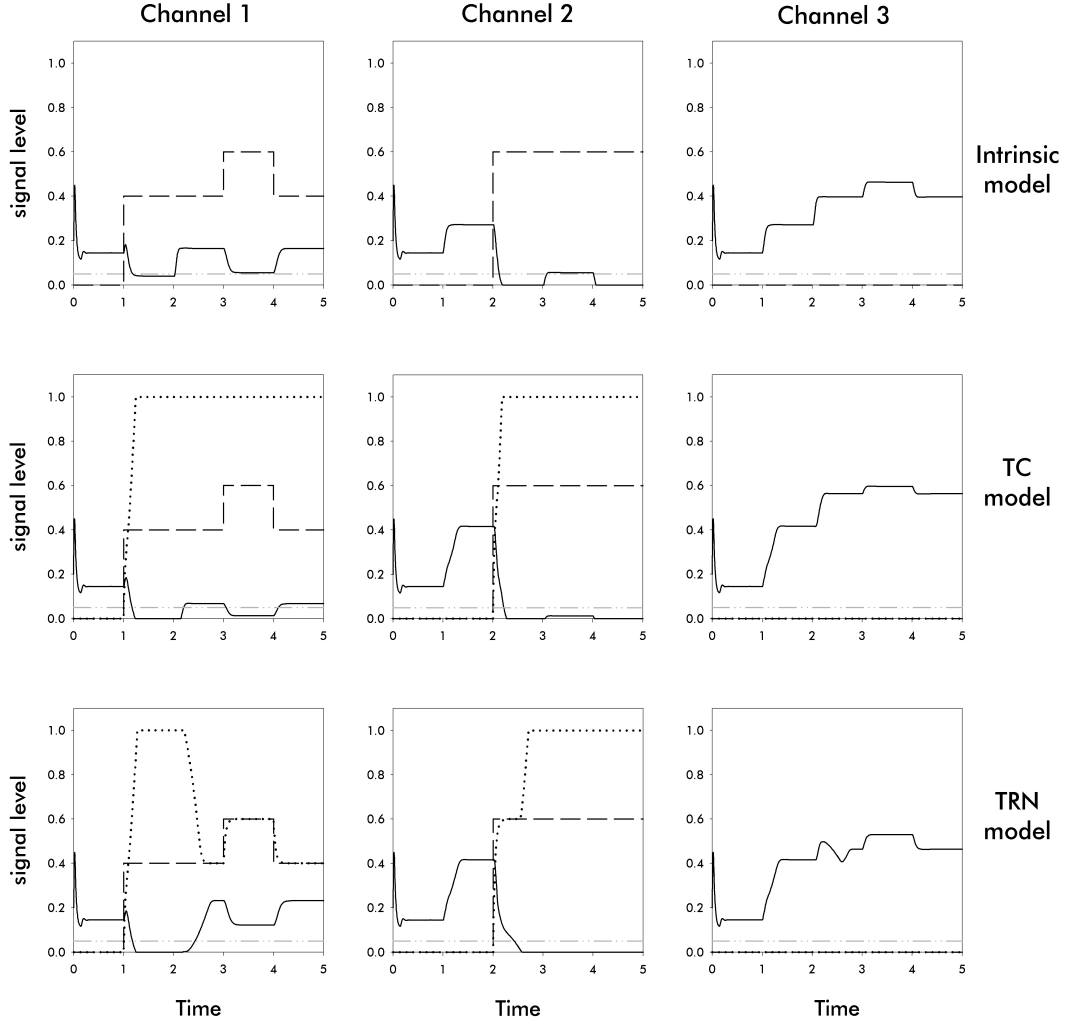


Figure 2.3: Example outputs from the intrinsic model (top), TC model (middle), and TRN model (bottom). They show the selection (at $t=1$) and switching (at $t=2$) capabilities of all three models. Note the varying levels of inter-channel differences between the EP outputs across the three models after the onset of channel 2 salience. Only the TRN model showed successful suppression of the transient event at $t=3$. The third column illustrates the EP output changes in a non-active channel in response to changes in input levels on active channels. EP: solid line. Motor cortex: dotted line. Sensory input: dashed line. Selection threshold θ_s : dash-dot line (light grey).

Therefore, θ_s is given a non-zero value to allow for low level firing that may occur in real basal ganglia output neurons while under inhibition from D1 striatal neurons. Furthermore, this value for the selection threshold is used for consistency with the spiking model version of the TRN model presented in chapter 4 - see section 4.3.1 for explanation of its selection threshold value.

The successful switching between actions is dependent on the selection of the newly winning competitor and the deselection of the losing competitor (the desirable characteristic of absence of distortion - see Section 2.2.3). In model terms, a successful switch occurred when channel 2's EP output fell below θ_s and channel 1's EP output exceeded θ_s after the onset of channel 2's input.

Inspection of the left-hand column of graphs in Figure 2.3 shows that after the onset of sensory input on channel 1 the EP output fell below θ_s in all models and, therefore, the channel became selected. After the onset of sensory input on channel 2, this channel also became selected (centre column). Simultaneously, the EP output on channel 1 rose above the selection threshold, thereby deselecting the channel. Thus, with this input pair, successful selection of both channels, and switching between them, could take place. Of particular note is the different levels of channel 1 EP output equilibrium reached after deselection: the TRN and intrinsic models shows a considerable contrast between the outputs of channels 1 and 2 at time $t \approx 2.7$, whereas the TC model shows a much smaller difference.

The transient event on channel 1 illustrates the abilities of the three models to maintain an ongoing action in the face of possible disruption. During the transient, the EP output of channel 1 in both the intrinsic and TC models was equal to the EP output of channel 2. As both outputs were below θ_s there is the possibility that the two actions would be expressed simultaneously or that some amalgam of the two action would occur. In the TRN model, the EP output on channel 1 was prevented from falling below θ_s , while EP output on channel 2 was held constant. Thus, the transient event did not adversely affect the ongoing behaviour in the TRN model, but had the potential to do so in the other models.

The right-hand column of graphs shows the EP output on a third, inactive, channel in each of

the three models (Figure 2.3). They illustrate how the onset of sensory inputs to other channels caused a corresponding rise in the EP output level of the inactive channels in all models. This rise in output level served to strengthen the contrast between active and non-active channels, ensuring that there was no interference with the ongoing action selection competition.

For the TC and TRN models, the output of motor cortex is also plotted for all channels. Obviously, with no sensory input, there was nothing to drive motor cortex and so it stayed silent. When there was sensory input, the models responded differently. The onset of input to a TC model channel caused the motor cortex output to rapidly reach saturation and to remain there constantly, regardless of sensory events in the same or other channels. However, the motor cortex output in the TRN model became saturated in the selected channel only. When that channel was deselected, the motor cortical output fell to the level of the sensory input. Note that, in channel 1, motor cortex output in the TRN model did not increase beyond the sensory input level during the transient event but was suppressed.

2.4.2 Quantifying selection properties

The single trial simulation experiments in the previous section provide useful qualitative insights into the behaviour of the different models. In particular, they show the phenomena that occur in the basal ganglia output of active and non-active channels. I go on now to look at how the selection properties of the models may be quantified.

It was first necessary to establish that the introduction of the thalamocortical loop and the TRN did not cause the loss of the basal ganglia's selection and switching abilities, as reported in Gurney et al. 2001b. To test this, 121 simulations were run on each model, consisting of the sensory input pairs (S_1, S_2) where S_1 and S_2 range from 0 to 1 in steps of 0.1. The input to channel 1 began at time $t = 1$; the input to channel 2 began at $t = 2$. This gives us two time intervals in which EP output on any channel may change: $I_1 = [1 \leq t \leq 2]$ and $I_2 = [t > 2]$.

In the previous section, selection of channel i occurred when $y_i^b \leq \theta_s$, where y_i^b is the basal ganglia output (from EP) of the i th channel. Using this definition, and given the onset times of the sensory input, the outcome of a simulation could be characterised by one of four states:

- First, *no selection*, where y_1^b and $y_2^b > \theta_s$ for all t . Neither active channel becomes selected during the time course of the simulation.
- Second, *selection*, where $y_1^b \leq \theta_s$ in I_1 and $y_2^b > \theta_s$ in I_2 ; or $y_1^b > \theta_s$ for all t and $y_2^b \leq \theta_s$ in I_2 . A single channel is selected at some point in the duration of the simulation: either channel 1 becomes selected in the first interval or channel 2 becomes selected in the second interval.
- Third, *no switching*, where y_1^b and $y_2^b \leq \theta_s$ in I_2 . Concurrent channel selection occurs in the second interval (channel 1 must be selected in the first interval to remain selected in the second interval; but note that selection in the first interval does not mean automatic selection in the second interval).
- Fourth, *switching*, where $y_1^b \leq \theta_s$ in I_1 and $y_1^b > \theta_s$ in I_2 and $y_2^b \leq \theta_s$ in I_2 . A clean switch between channels: channel 1 is selected in the first interval, then becomes de-selected as channel 2 becomes selected in the second interval.

The sets of input pairs which caused these four output states in each of the three models are illustrated in Figure 2.4. The results are summarised in the histogram in the bottom right-hand corner. It is clear from the plots that all three models showed successful selection across a wide range of input pairs and, furthermore, that they were capable of successful switching. A comparison of the three models shows that the introduction of the thalamocortical loop (TC model) allowed lower-level sensory inputs to become selected: the minimum input needed was 0.2, compared with the intrinsic model's minimum of 0.4. However, there was a large increase in the number of instances for which there was no switching in the TC model compared to the intrinsic model. Thus, there was a trade-off between low input selection capability and the ability to successfully switch over a wide range of pairs.

After the introduction of the TRN the low input selection capability gained by the thalamocortical loop was maintained. Furthermore, the TRN model was able to successfully switch between actions over a much greater range of pairs than the TC model, and returned switching performance to that of the intrinsic model. Thus, both the TRN and intrinsic models were able

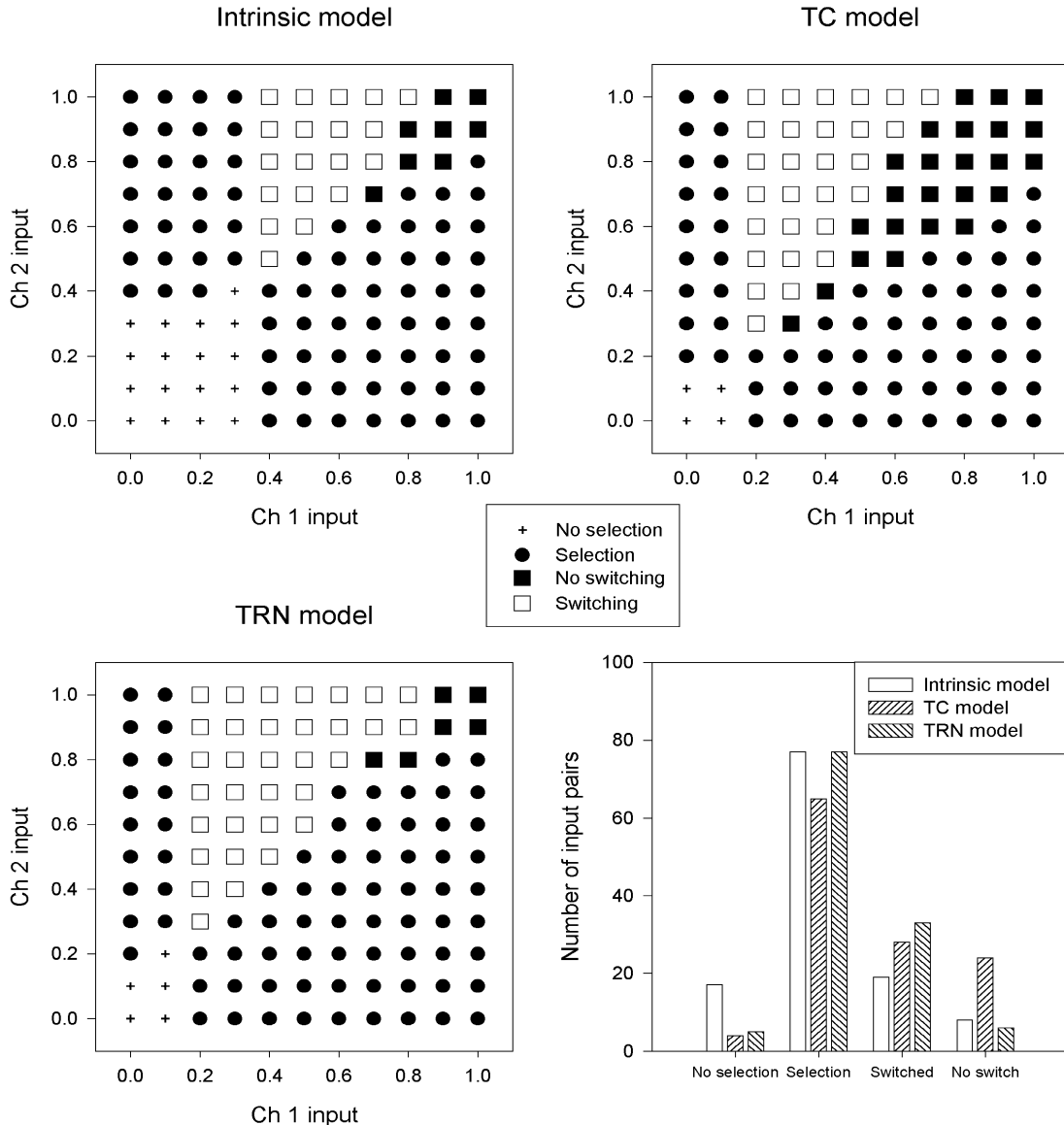


Figure 2.4: Selection and switching abilities of the intrinsic, TC, and TRN models, in response to the input sequences described in the text. The histogram shows the number of input pairs that cause each of the four output states. The addition of the thalamocortical loop allowed channel selection with low level inputs. Adding the TRN maintained low level selection while also improving the switching capability.

to perform one aspect of clean switching in that most sensory input pair competitions were resolved decisively.

2.4.3 Improving EP output contrast

Having established the basic selection properties of the three models, the investigation turned to how the thalamocortical loop and TRN affected the differentiation of EP outputs. This is an important aspect of maintaining an absence of distortion, for the EP outputs of the selected and non-selected channels should be sufficiently different so that the non-selected channels' outputs cannot interrupt the ongoing action. This requirement exists because, although the model neuron outputs are interpreted as a mean firing rate, the output of real neurons is noisy, and so the firing rates in a non-selected channel may temporarily fall below that of the selected channel if they are not sufficiently differentiated. The potential for distortion is determined by simply measuring the difference between the EP outputs on channels 1 and 2 when they have reached equilibrium after the onset of input on both channels.

There are two possible ways in which output contrast could be compromised. First, through the disruption of the selected channel by another channel becoming active with a low-level competitor (i.e. channel 2 after channel 1 has been selected). Second, if the switching is not clean enough, due to a high input level on the deselected channel, then the output is not sufficiently differentiated when switching is completed (i.e. high-level input on channel 1 after channel 2 has been selected). Therefore, the absolute difference δ_y^b between the EP outputs is used so that both possibilities could be taken into account.

Mesh plots of δ_y^b for every simulation run on the three models (as detailed in the preceding section) are shown in Figure 2.5. The intrinsic model showed small δ_y^b for low-level input pairs, and zero differences for equal input pairs. The TC model, while showing large δ_y^b for low-level pairs, showed small differences for all medium-to-high level pairs. By contrast, the TRN model showed relatively large δ_y^b for all medium-level pairs and also had large differences for equal-level pairs. The histogram of total δ_y^b for each model (in Figure 2.5) quantifies the improvement in EP output contrast which is gained with the TRN model. The intrinsic and TC models were

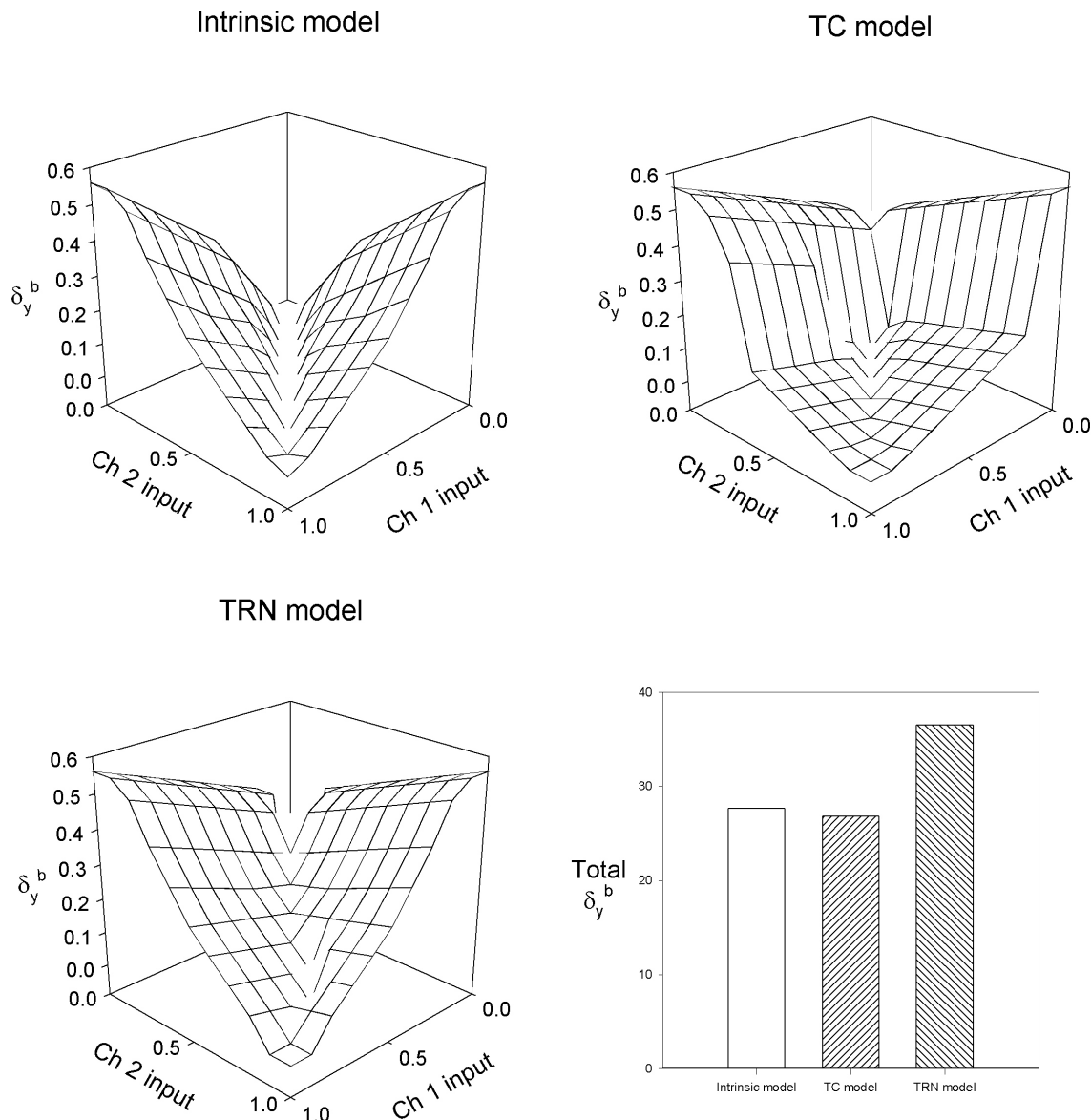


Figure 2.5: The changes in difference in EP output (δ_y^b) between channels 1 and 2 after the onset of input to both channels (at equilibrium after $t = 2$). The TRN model had a greater or closely matched difference to the other models with almost any input pair combination. The histogram highlights the enhanced EP output contrast of the TRN model, in comparison to the intrinsic and TC models.

very similar with totals of 27.65 and 26.77, respectively, but the TRN model's total was 36.5.

2.4.4 Transient suppression

It was noted in section 2.2.3 that short-term increases in salience on a non-selected channel should be suppressed so that the ongoing action was not hampered or interrupted. To test the ability to suppress transient salience increases in non-selected channels, 55 simulations were run on each model, one for each pair in which $S_2 > S_1$ (in the TC and TRN models, a transient salience increase is caused by an increase in sensory input). Three levels of transient increase were used: $0.5\Delta S$, ΔS , and $1.5\Delta S$, where $\Delta S = S_2 - S_1$ (giving a total of 165 simulations per model). These levels correspond to transients that are less than, equal to, and greater than the level of sensory input on channel 2, respectively (an example of a ΔS size transient salience increase is shown in Figure 2.3). The transient occurred on channel 1 at $t=3$, and lasted for 1 time unit. Successful suppression required that $y_1^b > \theta_s$ ($t > 3$) and that, if $y_2^b \leq \theta_s$ ($t = 3$), then $y_2^b \leq \theta_s$ ($t > 3$).

The results of the simulations are shown in the bubble plots in Figure 2.6. Only the top left diagonal of the plots is of interest, as the effect of the salience increase on channel 1 was only tested for $S_2 > S_1$. The histogram shows the number of input pairs in each suppression category (no suppression, suppression up to $0.5\Delta S$, suppression up to ΔS , and suppression up to $1.5\Delta S$). The intrinsic model was capable of suppressing transients on channel 1 which were below the level of S_2 (i.e. $0.5\Delta S$) over the majority of input pairs (40/55). However, there was only one case ($S_1 = 0.6, S_2 = 1.0$) where an equal-level transient was suppressed, and no transients greater than the input on channel 2 were suppressed.

The TC model could suppress $0.5\Delta S$ transients at a lower level of input than the intrinsic model. It also showed a couple more cases of suppression with equal-level transients, and one case ($S_1 = 0.1, S_2 = 0.2$) of suppression of a $1.5\Delta S$ transient. However, the suppression abilities at low input levels cannot be directly compared to the intrinsic model as the intrinsic model was incapable of selection at these levels (see section 2.4.2). Furthermore, the TC model was capable of suppressing transients in the smallest number of cases (33) of all three models.

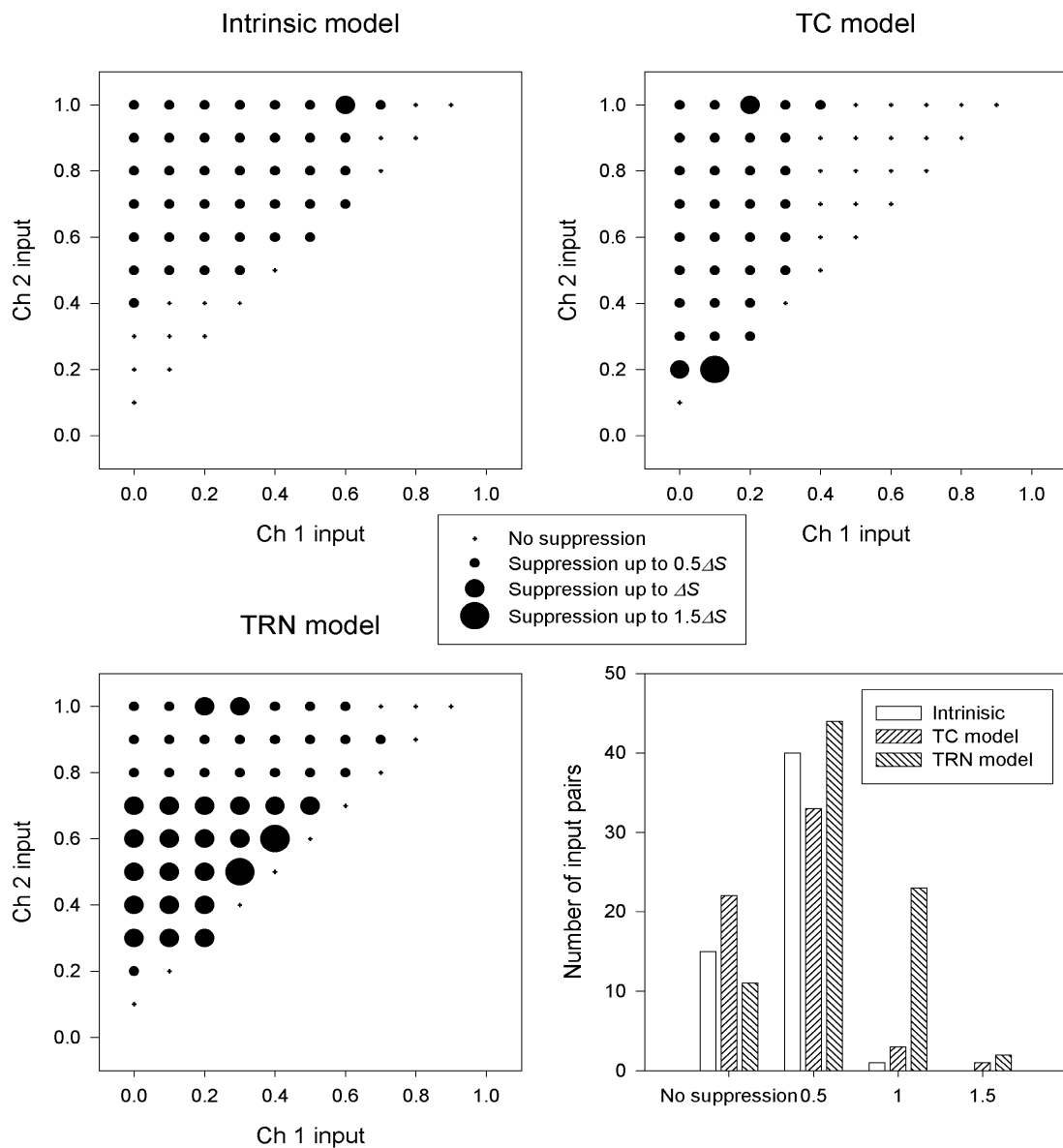


Figure 2.6: Transient suppression ability of the intrinsic, TC, and TRN models. The intrinsic model could suppress transients in channel 1 which were lower than the channel 2 salience level for most values that were tested. The TRN model expanded on this capability by suppressing many transients which were equal to the salience input on channel 2.

The TRN model could suppress transients over the greatest number of input pairs (44), but this was partly due to its ability to do so with low-level inputs which are not comparable to the intrinsic model. More pertinently, the TRN model was able to suppress equal-level transients over a much greater range of input pairs (21) than the other two models. This indicates that the addition of the TRN prevented transient events from disrupting the ongoing action when the transient was equally as important as the current action. Furthermore, it should be noted that the input pairs which did not show suppression of equal transients had very high sensory input levels on channel 2. This may be a useful feature as it makes sense for a transient competitor to be able to interrupt the selected action if it is very urgent.

2.4.5 Closely matched saliences

A further aspect of persistence (discussed in section 2.2.3 with reference to the behavioural phenomenon of dithering) is that a selected action should not be interrupted by a closely matched competing action. That is, the ongoing action should persist. To test the ability of the models to perform this function, simulations were run using closely matched sensory input pairs.

The inputs consisted of ten levels of channel 1 input ($S_1 = 0, 0.1, \dots, 0.9$). Each level was matched with eleven levels of input on channel 2 that were equal to or larger than the channel 1 input. Thus, if $\Delta S_2 = S_2 - S_1$, then ΔS_2 had the values 0, 0.01, ..., 0.1. Input to channel 1 began at $t = 1$; channel 2 salience input began at $t = 2$. Persistence of selection occurred if $y_1^b \leq \theta_s$ and $y_2^b > \theta_s (t > 2)$.

The plots in Figure 2.7 show the responses of the three models (in terms of the four output states detailed in section 2.4.2) to each of the input pairs: persistence is, therefore, indicated by single-channel selection (*selection* as defined in section 2.4.2). The intrinsic model showed continued selection of channel 1 with greater levels of channel 2 input at $S_1 = 0.4, 0.5$. Similarly, the TC model only showed persistence of selection for two levels of S_1 (0.1 and 0.2). For most selection-capable values of S_1 the TC model showed dual channel selection for all values of ΔS_2 . By contrast, the TRN model showed continued selection of channel 1 after channel 2 onset for

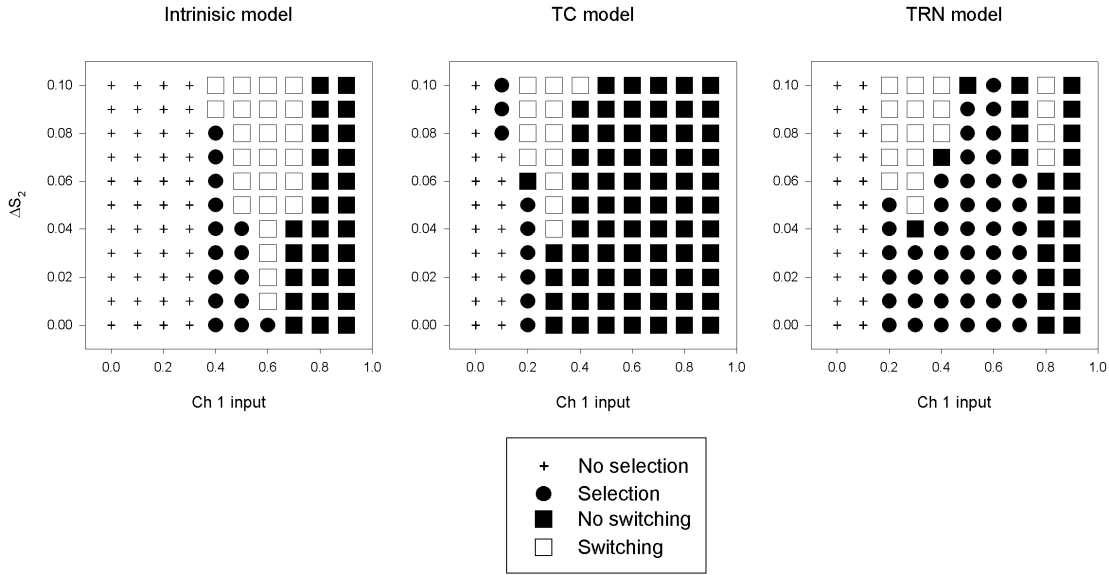


Figure 2.7: The relative ability of the the intrinsic, TC, and TRN models to maintain the selection of channel 1 after the onset of a closely matched salience on channel 2. The TRN model was able to maintain the selection of channel 1 for six levels of salience input.

six levels of S_1 . This suggests that the TRN model was able to prevent the ongoing action from being interrupted by a closely matched competing action under most selectable input values. It should be noted that, for the TRN model, there was not a monotonic relationship between S_1 and the level of ΔS_2 at which selection of channel 1 ceases, even though there was a suggestion of such a relationship in the intrinsic model.

2.4.6 Dopaminergic modulation of selection

Changing the dopamine level affected the selection and switching capabilities of the intrinsic model (Gurney et al., 2001b) and, as outlined in section 1.4.2, the behaviour of the model showed clear parallels with basal ganglia related dysfunctions. Here I report the effects of dopamine level changes in the TC and TRN models.

Figure 2.8 shows the selection and switching properties of the three models under different dopamine conditions. The central column of plots shows the results for the three models with normal dopamine levels, as previously shown in Figure 2.4. The same simulations were used

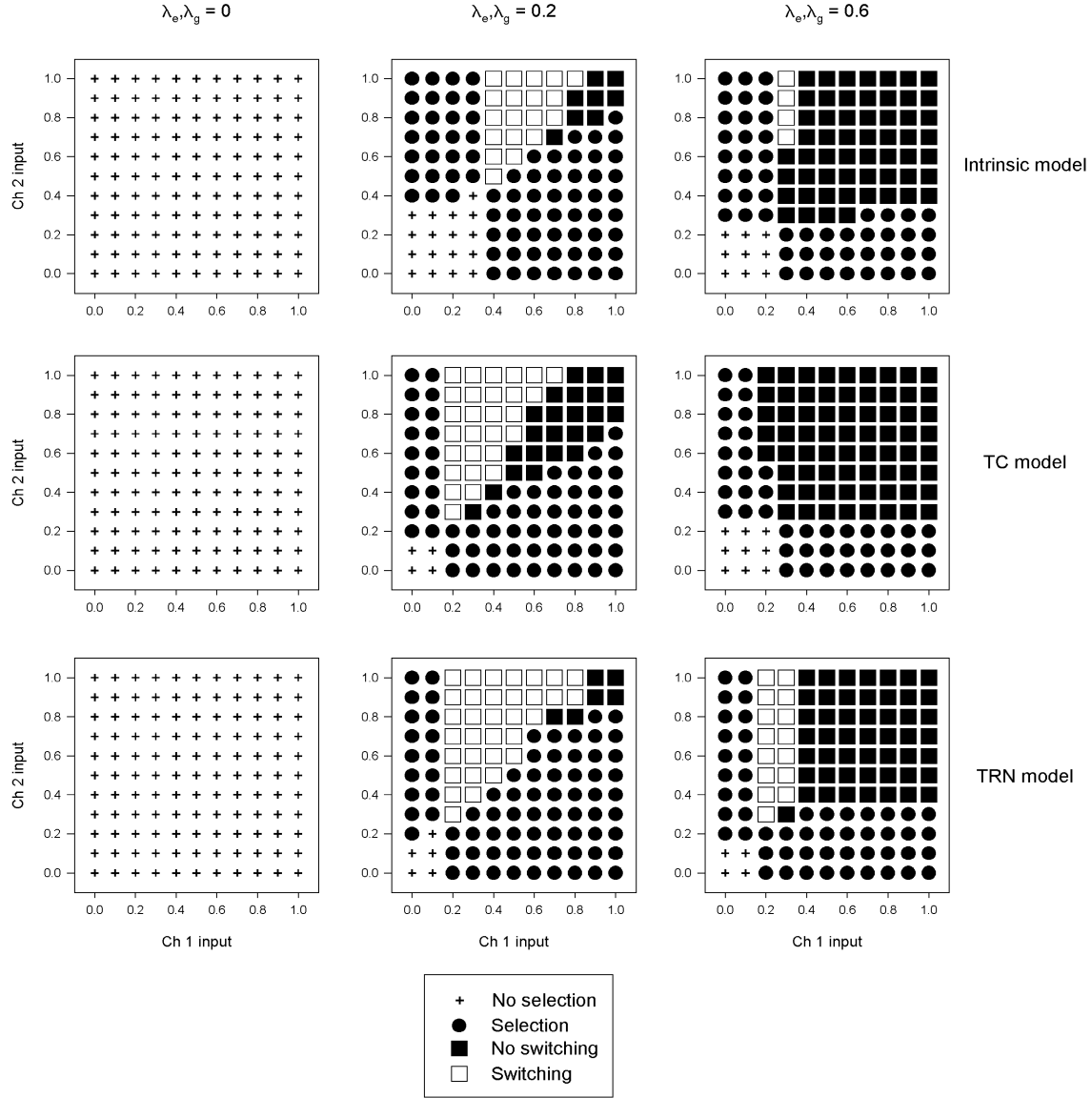


Figure 2.8: The alteration of the selection and switching abilities of the three models due to changes in the tonic dopamine level. The centre column shows the normal responses, as illustrated in Figure 2.4. Removing dopamine (left-hand column) resulted in no selection at any salience level in all three models. With high levels of dopamine the majority of salience inputs caused simultaneous channel selection. The TRN model was the most robust as it maintained the highest number of successful switching cases with increased dopamine.

to generate equivalent results for each model using two different levels of dopamine: $\lambda_e, \lambda_g = 0$ (no dopamine) and $\lambda_e, \lambda_g = 0.6$ (excess dopamine).

With no tonic dopamine (left-hand column of plots), all the models showed no selection or switching capability. High levels of tonic dopamine (right-hand column of plots) resulted in increased dual channel selection (*no switching*) and a reduction in switching. This was particularly prevalent in the TC model which completely lost its switching ability. The TRN model showed the most robust response to high dopamine levels as it retained the greatest number of successful switches.

So far I have looked at the effects of changing the level of simulated dopamine affecting both D1 and D2 receptors simultaneously (which simulates the neurotransmitter levels found following SNc cell death in Parkinson's disease or following stimulation of dopamine release by amphetamines). However, there are disorders which affect just one dopamine receptor type and which can be simulated by altering the level of dopamine in the pathway corresponding to that receptor. Of particular interest here is the dopamine hypothesis of schizophrenia, which states that numerous symptoms of schizophrenia may be due to an overactive dopamine pathway. This is based on the elevated level of D2 receptors found during post-mortem examination of schizophrenic patients' brains, and on the D2-receptor blocking action of anti-psychotic drugs (Seeman, 1987; Seeman, Ulpian, Bergeron, Riederer, Jellinger, Gabriel, Reynolds, and Tourtellotte, 1984). Thus, changes in basal ganglia output behaviour under simplified 'schizophrenic' conditions can be examined by increasing the level of dopamine λ_e in the striatum control pathway (where the D2 receptors are found) to 0.6. By doing this, the assumption is made that the increased number of receptors can be replicated by increasing the efficacy of dopamine in this pathway. The full batch of 121 input-pair simulations (as detailed in section 2.4.2) was run on the TRN model and, to further elucidate the possible effects of increasing D2 dopamine, the transient suppression simulations (outlined in section 2.4.4) were also conducted on the TRN model.

Figure 2.9 shows the resulting output state and transient suppression level bubble plots for the elevated D2 level TRN model. There was an increase in the instances of dual channel

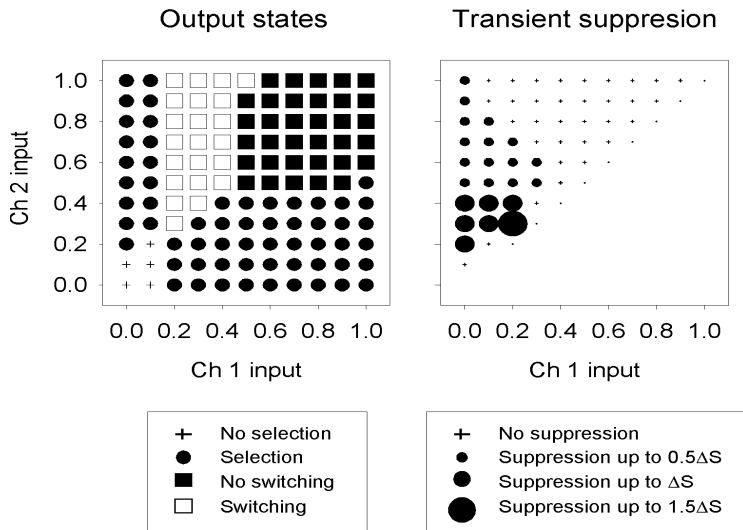


Figure 2.9: Increasing the control pathway dopamine level increased dual channel selection, similar to the effect of increasing overall dopamine levels, but retained more successful switches (left). Transient suppression was markedly reduced compared to the normal TRN model (see Figure 2.6, with no suppression occurring for high channel 2 input levels (right).

selection compared to the normal TRN model, but this was not as substantial an increase as was seen when dopamine levels were elevated in both pathways. Thus, normal responses to inputs were maintained except when inputs to both channels were medium or high.

The ability of the basal ganglia to suppress large transients (to maintain selection of channel 2 and prevent selection of the channel 1) at low input levels was retained from the normal dopamine level TRN model. However, the increase in control pathway dopamine prevented suppression from occurring for the majority of input pairs - particularly all medium-to-high level input pairs. This indicates a striking breakdown in the ability of the basal ganglia to suppress the influence of transient salience increases on a non-selected channel. This is consistent with the lack of suppression of random actions/behaviours and speech patterns that are symptoms of schizophrenia.

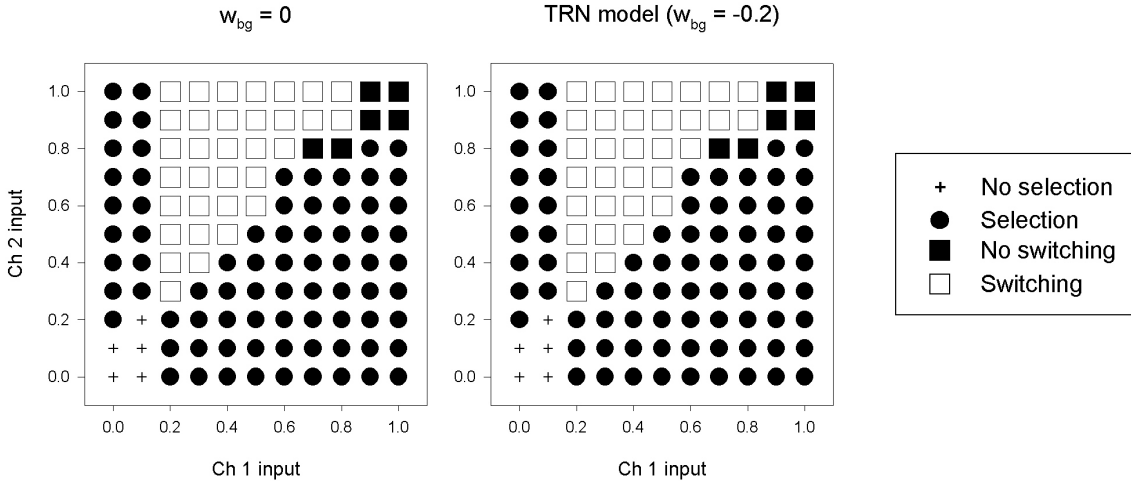


Figure 2.10: The selection and switching abilities of the TRN model with (right) and without (left) the EP to TRN connection (the simulations used to generate these results were the same as those described in section 2.4.2). No difference was observed between the two versions of the model.

2.4.7 The significance of basal ganglia to TRN projections

So far, the use of the EP as the sole example of the basal ganglia output nuclei has been maintained for consistency with our previous papers (Gurney et al., 2001a; Gurney et al., 2001b). Although there is good evidence for a projection from SNr to the TRN (see section 2.2.2), there is little evidence for an EP to TRN projection. Numerous tracing studies which have looked at EP or GPi nucleus targets failed to report a projection to TRN (Kha et al., 2000; Mengual, De Las Heras, Erro, Lanciego, and Giménez-Amaya). Thus, the EP to TRN connection only exists in the model because of the underlying assumption of the functional equivalence of the output nuclei (see section 1.3.4). However, as illustrated in Figure 2.10, the removal of the EP to TRN connection (by setting $w_{bg} = 0$) made no difference to the behaviour of the TRN model.

Further, there is also good evidence for a GP to TRN connection (Hazrati and Parent, 1991; Gandia et al., 1993; Asanuma, 1994), although it is not clear which TRN sectors this projection reaches. However, the addition of this connection to the TRN model in place of the EP to TRN connection, and with the same weight (0.2), did not change the behaviour of the model.

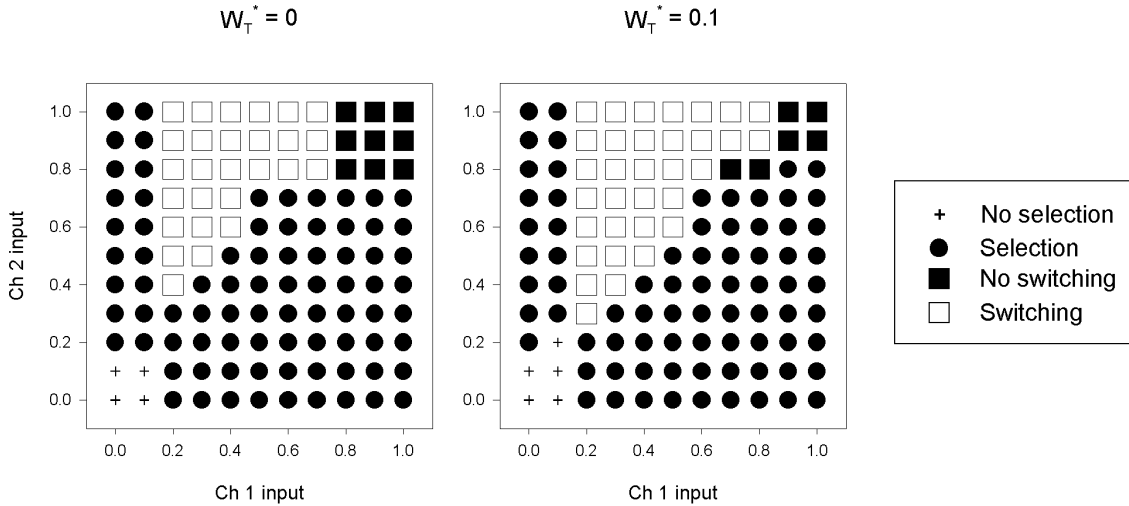


Figure 2.11: A comparison of the selection and switching abilities of the TRN model with (right) and without (left) the within-channel TRN-to-VL thalamus connection. The removal of the TRN within-channel inhibition of VL thalamus caused minor changes in the switching and selection patterns. This illustrates that this pathway has a discernible effect on the model’s behaviour, even though it has a very low magnitude weight.

The ineffectiveness of the EP-TRN and GP-TRN pathways cannot necessarily be attributed simply to their low weight as there are other weak connections in the model which alter the model’s behaviour if their weight is changed. For example, Figure 2.11 shows the change in the selection and switching abilities of the TRN model when the within-channel TRN inhibitory connection to VL thalamus is removed ($w_T^* = 0$). Even though the normal strength of this connection is only 0.1, its removal substantially affected switching: there were 6 fewer successful switches, and 3 more cases of dual channel selection (no switching).

Thus, given that changing the within-channel TRN connection could affect basal ganglia output, I speculate that the ineffectiveness of both basal ganglia-to-TRN pathways on the output of active EP channels had two related causes which were not solely based on the low weights of the pathways. First, in a selected channel, the large excitatory input from motor cortex and VL thalamus to the TRN would have overwhelmed the small inhibitory input from the basal ganglia to the TRN. Second, in a non-selected channel, the TRN output would have no impact on the corresponding channel in VL thalamus, because that channel is already inhibited

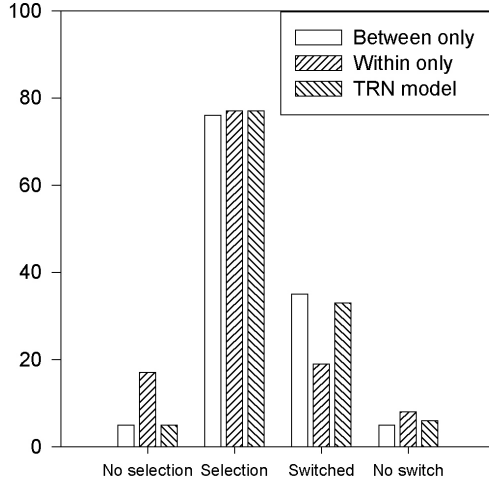


Figure 2.12: Summary histogram of the frequency of each of the four output states (described in section 2.4.2) for the TRN, Between-only, and Within-only models. It shows that using a single connection type between TRN and VL thalamus altered the selection and switching capability of the TRN model.

by EP output.

2.4.8 TRN design alternatives

In the previous section, it was shown that the removal of the weak, within-channel pathway slightly degraded the TRN model's switching capability. To further illustrate the effect of varying the connection strengths in the mixed connection TRN-VL thalamus design, the results of two alternative models are considered here. In the Within-only model, the between-channel connection was removed by setting $w_b = 0$ and the within-channel connection weight was increased to compensate (thus $w_T^* = 1$). In the Between-only model, the within-channel connection was removed by setting $w_T^* = 0$ and the between-channel connection weight was increased to compensate (thus $w_b = 1$).

The full set of 121 input-pair simulations (see section 2.4.2) was run on each model: their relative selection and switching abilities, as compared to the normal TRN model, are summarised in Figure 2.12. Compensating for the removal of the within-channel connection by

setting $w_b = 1$ in the Between-only model ensured that its outputs showed the same pattern of the four output states as the normal TRN model. By contrast, the Within-only model had substantially more input pairs for which selection did not occur (all at low levels, thus giving equivalent performance to the intrinsic model) and fewer cases of successful switching. These results illustrate the necessity of the between-channel connection in the TRN model for its improvement in action selection capability over the intrinsic and TC models. Moreover, in combination with the observations of the previous section, we see that in the TRN model the within-channel connection, while not necessary for the model's improvements, does not degrade performance relative to the Between-only model. However, because the loss of some switching and selection capability observed following the removal of the within-channel pathway connection (previous section), that pathway appears to compensate for any reduction in the strength of the between-channel pathway.

2.5 Discussion

The addition of a thalamocortical loop and appropriately designed TRN to a computational model of the basal ganglia has enhanced its action selection capabilities. Furthermore, these additions to the model gave five main results which are desirable in behavioural terms: low sensory inputs (i.e. low salience actions) can become selected; the range of input values for which switching can take place has increased; responses to large transient events on a non-selected channel are suppressed; actions which are closely matched to the current action are also suppressed; and the EP output contrast between the selected and non-selected channels is enhanced. Finally, the TRN model possesses all of the desirable characteristics of a switching mechanism that were outlined in the introduction. These features are discussed in greater detail below.

Although substantial use of the three different models was made in this chapter, the intention was not to use the intrinsic or TC models as ‘straw men’ against which the improved abilities of the TRN model could be compared. Rather, the overriding aim was to use the three different models to show how the addition of new, anatomically constrained, connections

and structures could add new abilities while maintaining existing selection and switching abilities. Decomposing the circuit additions into two phases facilitated the determination of which additional component was responsible for which ability.

2.5.1 Thalamocortical loop

Analysis and simulation of the intrinsic model had already shown that the intrinsic connectivity of the basal ganglia could produce output signals (from EP) which were consistent with action selection. It has been shown here that, with the addition of a thalamocortical loop, low-level sensory inputs (representing low salience actions) now also result in output signals which are consistent with the selection of an action. Low salience selection may be behaviourally important because, when an animal is faced with numerous relatively unimportant choices of subsequent action, it must be able to pick and execute one of them. The alternative is to remain in a quiescent state until an event of sufficiently large salience occurs. However, there is a minimum sensory input level required for selection (0.2) in the TC and TRN models which seems to be limited by the threshold for inducing an UP-state transition in a striatal neuron. Thus, very low-level inputs may be filtered out by the striatum (as suggested in section 1.3.1), which could prevent signals that are indistinguishable from noise affecting action selection. As previously noted, the ability of the TRN model to successfully resolve competitions over a wide range of sensory input values shows that it has the decisive aspect of clean switching.

The low input selection can be attributed to the positive feedback loop formed by VL thalamus and motor cortex. Amplification of the sensory input in this loop means that the striatum receives a greater input than just two identical copies of the sensory signal. However, this thalamocortical feedback is also responsible for the simultaneous channel selection seen at many input levels in the TC model. The positive feedback loop causes motor cortex output to saturate and, when added to the sensory input in striatum, the combined total forces the basal ganglia to select both actions. Clean switching was recovered by the introduction of the TRN.

2.5.2 A functional role for the thalamic reticular nucleus

Besides clean switching, the TRN model also had the desirable characteristics of persistence and absence of distortion. It was able to prevent interruption of an ongoing action by a closely matched competitor, to suppress a wide range of transient salience events, and to enhance EP output contrast. These abilities can be all attributed to the presence of the TRN, as they were not as evident in the other two models. In addition, while introducing these improvements, the low-level input selection capability of the TC model was maintained.

The most probable explanation for these abilities centres on the role of the between-channel inhibition. Losing competing actions are suppressed because the between-channel inhibition prevents their representative channels from increasing their activity through the positive feedback loop formed by VL thalamus and motor cortex. This could account for the TRN model's switching and persistence abilities. The same mechanism would also prevent transients and closely matched competing actions from causing an increase in activity on their corresponding channels. Therefore, the input to striatum on the transient's/competitor's channel would remain at a lower level than on the currently selected channel. This would be facilitated by the TRN reducing the level of activity in the thalamocortical loop of the deselected channel (e.g. the reduction of motor cortex output; see Figure 2.3). The crucial role of the between-channel connection was highlighted in section 2.4.8 as the low-level selection and improved switching abilities were maintained following the removal of the within-channel connections and a corresponding increase in the between-channel weight

However, the within-channel inhibition may also have influenced the switching ability, as removing this connection without a corresponding increase in between-channel weight reduced the number of successful switching cases. Thus, the within-channel inhibition acts to compensate for the reduction in between-channel weight, making the thalamocortical circuit more robust to damage. Further, although an argument can be made that the performance of the Between-only model was marginally superior to the TRN model in terms of preventing dual channel selection, it must be remembered that the anatomical data does not support such a design. Thus, the TRN-to-VL thalamus connection design instantiated in the TRN model in-

corporates all the known anatomical features and gives superior switching performance to the only viable alternative (the Within-only model).

Thalamocortical feedback and the between-channel inhibition can also account for the improved EP output contrast. The higher levels of input to striatum (when compared to the intrinsic model) from the combined somatosensory and motor cortex input drive the STN to excite EP, leading to elevated EP output levels. On the winning channel, the high levels of cortical input specific to that channel enables the striatal inhibition to exceed this massive excitatory drive and cause the channel to become selected. The prevention of feedback in the thalamocortical loop by the action of the TRN ensures that the other channels in EP receive no major inhibitory input, leading to enhanced contrast between the selected and non-selected channels.

The preceding discussion highlights two functional roles for the TRN, which can be encapsulated as follows. First, the TRN acts as a gain control and effectively sets a ceiling level of total activation in the thalamocortical loop. Second, the TRN acts to ‘clean-up’ basal ganglia output, allowing the selection of, and the switching between, a wider variety of salient actions. Thus, the TRN acts as *another* selection mechanism whose action is complementary to that of the basal ganglia.

Finally, it should be noted that though the functional design of the TRN and VL thalamus inter-connections did not address the TRN’s hypothesised role in attentional processing, the findings presented here are consistent with Crick’s (1984) searchlight hypothesis, as the action of the TRN on focusing selection could be interpreted as the focusing of attention on that channel.

2.5.3 The action of dopamine

Changing the level of tonic dopamine to extreme high or low values was detrimental to the selection and switching abilities of all three models. The removal of dopamine completely prevented selection of an action, which is consistent with the difficulty of initiating voluntary movement in Parkinsonian patients. Excess dopamine increased the ‘promiscuity’ of selection,

as all three models showed simultaneous channel selection with the majority of inputs. The TRN model was the more robust (with high dopamine values) as it was capable of successful switching in a substantial number of cases and also maintained its low-level input selection capability.

The simulation of a condition consistent with the DA dysfunction known to occur in schizophrenia (obtained by increasing the level of dopamine in the control pathway) produced results that could be interpreted as consistent with schizophrenic behavioural symptoms. Of particular interest was the loss of ability to suppress any level of transient increase in salience for medium-to-high urgency actions. The inactive channel became selected briefly during the transient, which could lead to brief selection of that action before returning to the previously selected action. If a competition involving multiple actions is considered, then it is clear that this response to a transient salience increase on an unselected (losing) channel could lead to rapid, brief alternations between the currently designated ‘selected’ channel. Thus, the sudden, seemingly disordered behaviour and speech changes seen in schizophrenic patients (Jahanshahi and Frith, 1998) could conceivably be due to an over-activity of dopamine in the control pathway. I stress that, although this provides some support for the dopamine hypothesis of schizophrenia, the complexities of the disorder (or, indeed, disorders) prevent this from being anything other than a tentative interpretation.

2.5.4 Modelling issues and further work

There are two major issues specific to the modelling work presented in this paper that need to be addressed. First, the VL thalamus is modelled identically to all other nuclei in the circuit, and its output is continuous in the range (0,1). This fails to capture the well known two-state output of thalamocortical neurons: tonic firing mode (which is effectively what is modelled here), and burst firing mode (Sherman, 2001). It has been recently demonstrated that burst firing in thalamocortical neurons can take place *in vivo* in awake animals (Swadlow and Gusev, 2001). Hitherto, burst firing in thalamocortical neurons had been mostly observed *in vitro* (Kim, Sanchez-Vives, and McCormick, 1997; Kim and McCormick, 1998). The functional

significance of this mode of firing is unclear, although it is possibly a robust ‘wake-up’ signal to the cortex. To study how two-state firing in the thalamus would affect the behaviour of the TRN model, it would be necessary to construct a lower level model which made explicit use of membrane properties. Initial work on developing such a model has been carried out, and it has been tested in a detailed model of the STN-GP loop - the results of that study are reported in chapter 5 (see also Humphries & Gurney, 2001).

The second major issue is that the model is primarily constrained by data from rat based studies. For example, as noted in section 2.2.2, there are no interneurons modelled in the VL thalamus because the rat motor thalamus is devoid of them (Sawyer et al., 1991). However, the primate motor thalamus has an extensive network of interneurons that have a strong influence on the output of cortically projecting neurons and that receive input from TRN neurons (Ando et al., 1995; Ilinsky et al., 1999; Jones, 1985). The rat-oriented nature of the model was intentional for two reasons. First, the data available on the rat basal ganglia and thalamocortical connections is extensive and, second, the TRN model has been adapted for use in a *Khepera* mobile robot which is explicitly designed to mimic behaviour patterns specific to the rat (Montes-Gonzalez, Prescott, Gurney, Humphries, and Redgrave, 2001).

2.5.5 Conclusions

The models presented here have shown that the addition of anatomically constrained extrinsic pathways to a computational model of the basal ganglia improves the previously demonstrated selection abilities and brings new features. The positive feedback loop formed by the motor cortex and VL thalamus allowed low salience actions to be selected. The addition of the TRN made the model capable of fulfilling the desirable characteristics of a switching mechanism. Moreover the instantiation of the TRN, VL thalamus, and motor cortex consistently improved the selection and switching capabilities of the intrinsic model in every measure used. Therefore, I conclude that our models provide evidence that the TRN-dorsal thalamic complex and the thalamocortical loop have a functional role in action selection. Thus, because of its success within the family of models explored in this chapter, the TRN model was used as the basis

for many subsequent studies. We will meet it again in the following two chapters in different guises.

The findings presented in this chapter also require comment in the context of the issue of modelling levels. The TRN model is a systems-level model - it does, after all, use identical components to the intrinsic model. This mean firing rate model is sufficient to capture the gross phenomena - the selection and switching improvements, the response to transients, and so on - and to elucidate a detailed explanation of how these phenomena occurred, based on the adopted design of the thalamocortical loop and TRN-to-VL thalamus connections. As we will see in chapter 4, an immediate instantiation of the full TRN model using more complex model neurons may have obscured the basic selection and switching results reported here and would have made analysis of the underlying causes more complex. But, having obtained the results from the systems-level model, the construction of the more complex model could be constrained by the need to first replicate the results of the simple model (as detailed in this chapter) before considering the unique features of the more detailed model outputs.

Chapter 3

Robustness of the basal ganglia model

3.1 Introduction

In this chapter I detail extensions to the research described in the previous chapter which address the problems that rapid knowledge assimilation cause for the development of functional models (as discussed in section 1.5). Since the development of the original action selection hypothesis and of the basal ganglia functional anatomy (Gurney et al., 1998a; Gurney et al., 1998b) numerous studies have come to light or have been published which add new pathways to the model or suggest reinterpretations of the existing connections. As the core focus of our action selection hypothesis was on the role of the basal ganglia, all of the studies described here concern changes to the basal ganglia intrinsic structure within the context of the full TRN model. Figure 3.1 summarises the additions made to the basal ganglia part of the the TRN model in each study presented here. Note that each study will be dealt with individually to maintain the coherence of the chapter, as they are mostly unrelated, but the general conclusions are contained in the Summary at the end of the chapter. I begin by looking at the effect of explicitly instantiating a feedback pathway from GP to striatum.

Motor and somatosensory cortex

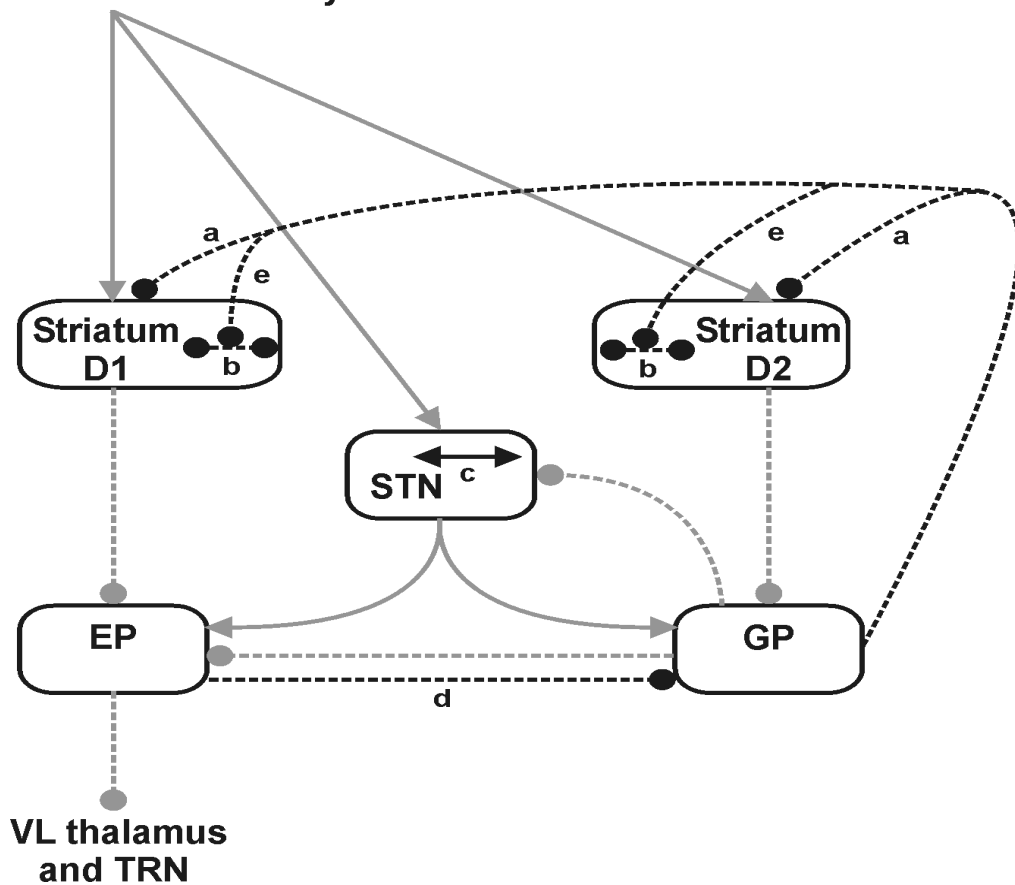


Figure 3.1: A summary of all the additions to the intrinsic basal ganglia connectivity made in this chapter. The original connections, as found in the TRN model, are shown in grey. Each of the additions was made individually, except where described in the text. **a** Pallidostriatal connections, contacting D1 and D2 receptor-type projection neurons, described in section 3.2. **b** GABAergic striatal interneurons, presumed to connect channels. Described in section 3.3. **c** Local axon collaterals in STN, again assumed to connect channels. Described in section 3.4. **d** Reciprocal connection between EP and GP, described in section 3.5. **e** Pallidostriatal connections contacting both D1 and D2-type projection neurons and striatal interneurons, described in section 3.6.2. The other study reported in this chapter contained striatal interneurons (**a**) and the reciprocal EP to GP connection (**d**). Solid line: excitatory connection. Dashed line: inhibitory connection.

3.2 GP to striatum connectivity

Recent research has demonstrated that there is a substantial projection from GP to striatum in monkeys and rats (Kita, Tokuno, and Nambu, 1999; Rajakumar et al., 1994; Bevan et al., 1998). Further, this projection is known to contact both striatal projection neurons and interneurons. However, to date there is no convincing data which shows what proportion of GP neurons project to each neuron type or whether the projections from GP follow the D1/D2 split in striatal output and synapse only on striatal neurons in the control pathway. The latter question is explored in this section, namely, how does instantiating a GP to striatum projection which is predominantly within the control pathway affect selection and switching? Can any suggestions be made regarding the likely division of GP output based on our simulation results?

To simplify the modelling task, the possibility of explicitly modelling GP synapses on striatal interneurons is ignored for now (the simulation of the interneurons at this level of modelling is explored in section 3.3). Instead it is assumed that, as each channel in striatum represents a local circuit containing projection neurons and interneurons, the projection from GP will be contacting an interneuron population. Further, because both GP neurons and the predominant striatal interneurons utilise GABA as a neurotransmitter, the net effect of GP stimulation of the interneurons would be disinhibition of the projection neurons. Thus, the assumption is made that each GP projection in the model effectively synapses on the striatal projection neuron in the corresponding channel.

A further assumption is that GP input to projection neurons is denser than that to interneurons, with net result that GP input inhibits striatal output. This is based on the observation that GP collaterals predominantly synapse on a subset of striatal projection neurons in the rat (Rajakumar et al., 1994). It is not clear whether this is also the case for primates as studies to date have reported GP neuron synapses on a subset of striatal interneurons (Bevan et al., 1998) but have provided no clear evidence of significant contact with projection neurons (Kita et al., 1999). However, as stated in section 1.3, the Gurney et al. (2001a) functional model of the basal ganglia is primarily based on rat neuroanatomy. Therefore, a small negative weight modelling the GP input to the striatal projection neuron is added to equation 2.11 so that the

activation level \tilde{a} in the i th striatal channel is now given by

$$\tilde{a}_i^e = (c_i - (w_{pe}y_i^p))(1 + \lambda_e) \quad (3.1)$$

$$\tilde{a}_i^g = (c_i - (w_{pg}y_i^p))(1 - \lambda_g)$$

where w_{pe} is the weight of the GP to striatum D1 connection, w_{pg} is similarly the weight to D2, and y_i^p is GP output. The output relation and salience c equations remain unchanged from those given in section 2.3.5.

Two versions of the GP-striatum model are considered here. The first follows the assignment of the GP to the control pathway in the original intrinsic model and, therefore, the GP input to striatum is predominantly to the D2 sub-population. Thus, $w_{pe} = 0.1$ and $w_{pg} = 0.4$: this is termed the GP-Str Control model. The second model, GP-Str Equal, presumes that the density of the GP projection to the striatal output pathways is equal (though still channel-specific) and so $w_{pe} = w_{pg} = 0.4$. Beside simulating the balance between inhibition and disinhibition of a striatal channel by GP input, low weights are also used because the input is assumed to be much less dense than the massive input from cortex to striatum.

The full set of 121 simulations described in section 2.4.2 were run on both models: the bubble plots for each model and the summary histogram are shown in Figure 3.2. The GP-Str Control model showed a degradation in selection and switching performance when compared to the TRN model, as there were more unselected inputs and more unsuccessful switches (no switching). By contrast, the GP-Str Equal model surprisingly showed a new pattern of output behaviour as there were no cases of unsuccessful switches at all. Instead, in the top right diagonal on the bubble plot, where both S_1 and S_2 had relatively high input levels, there was only selection of channel 1 where, for the other models described in the previous chapter, there was simultaneous selection of both channels (after the onset of input on channel 2).

Common to both GP-Str models was the increase in the minimum level of input required for selection to occur from 0.2 for the TRN model to 0.3. They also had fewer successful switching cases in comparison to the TRN model. For the GP-Str Control model, this was because there was an increase in unsuccessful switching cases, similar to the TC model (see section 2.4.2). As we've already seen, for the GP-Str Equal model the decrease in switching corresponded to an

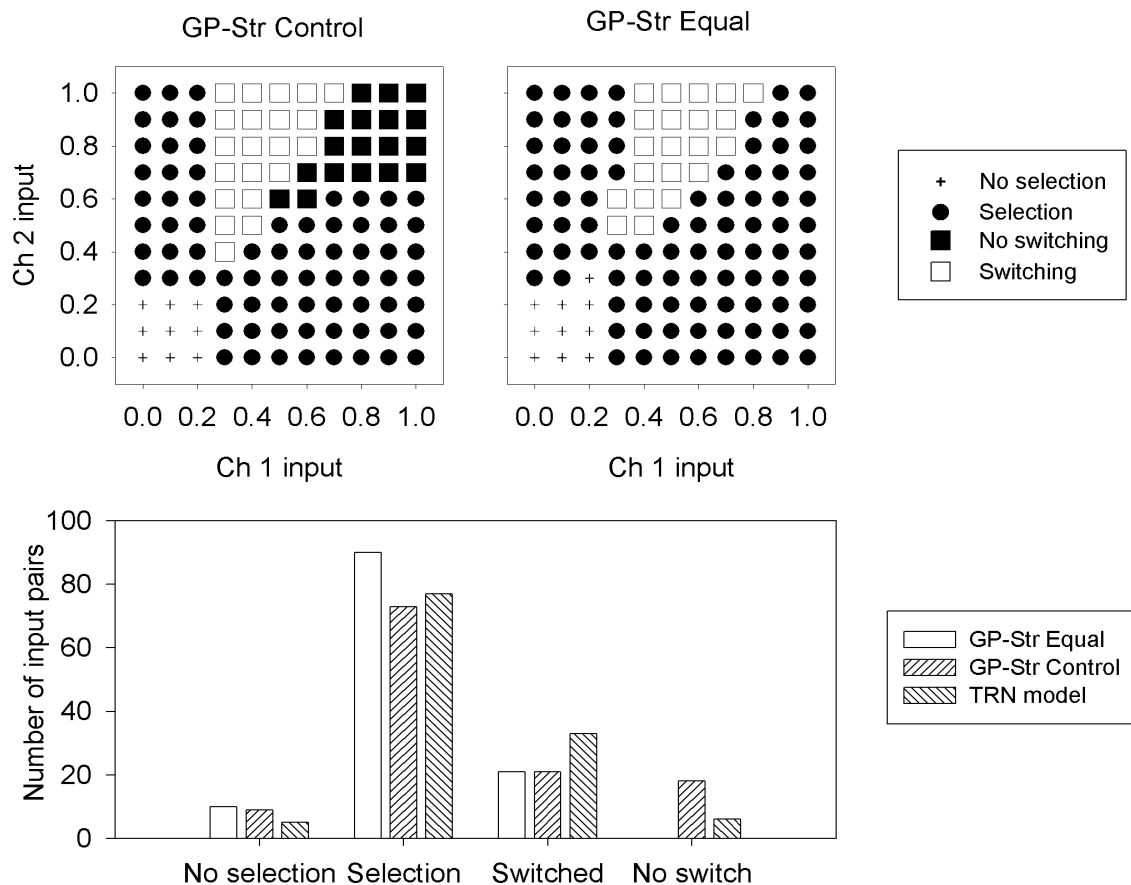


Figure 3.2: The effects of incorporating a pallidostriatal pathway into the TRN model. If the GP projection was predominantly to the striatal D2 neuron sub-population (in the control pathway) then the selection and switching performance degraded (GP-Str Control). However, equalising the pathway weights resulted in a new pattern of behaviour - there were no unsuccessful switches observed at any input level (GP-Str Equal). These results are emphasised by their comparison to the TRN model's output states (bottom).

increase in selection cases.

To answer the questions raised at the beginning of this section, the instantiation of a GP to striatum projection confined to the control pathway degraded the TRN model's selection and switching performance. However, the instantiation of equally weighted GP to striatum connections in the control and selection pathways prevented any unsuccessful switches from occurring. Thus, although this result raises questions about which output state is preferable from a behavioural viewpoint (discussed in section 3.7), it may be tentatively concluded that the maintenance of successful action selection was dependent on there being an equal split in GP output to striatum. An exploration of explicitly instantiating striatal interneurons in the two GP-to-striatum models is presented in section 3.6.2.

3.3 Striatal interneurons

There is a sparse interneuron population in striatum which may have a disproportionately large effect on projection neuron output, as outlined in section 1.3.1. As stated above, it was previously assumed that local circuit competition in striatum, mediated via axon collaterals or interneurons, was restricted to a single channel (Gurney et al., 1998b; Gurney et al., 2001a). However, tracing studies have shown that the extensive reach of interneuron axons may be incompatible with the assumption that interneurons are wholly contained in their corresponding channel (Koós and Tepper, 1999; Kawaguchi et al., 1995). Thus, the effect of explicitly modelling cross-channel interneuron communication is reported in this section.

To simplify the model, I follow the philosophy of the original intrinsic model and represent the interneuron population by the smallest possible ensemble - a single interneuron unit per channel. This unit contacts all other channels in the striatum other than its own so that the subsumption of the local circuit interneuron action in each channel is maintained. Further, as we've seen in chapter 1, the interneurons form a feedforward inhibitory layer, receiving their driving input from cortex. Within the model, the interneurons thus receive input from both somatosensory and motor cortex in a similar fashion to the projection neurons. Finally, any action of dopamine on the interneurons is ignored to maintain the simplicity of the model. A

recent study has demonstrated that interneurons with D2 receptors are inhibited by dopamine release, which has the net effect of disinhibiting the projection neurons (Delgado, Sierra, Querjeta, Valdiosera, and Aceves, 2000). However, there is no data on whether the D2 receptor interneurons are also restricted to the control pathway or whether there are D1 receptor interneurons. Thus, dopamines effect on the interneurons has been omitted from the model due to the lack of concrete data.

For this Interneuron model, there are two units which need describing. First, the interneuron unit itself needs defining. Input to interneuron l is a combination of sensory input (from somatosensory cortex) and motor cortical input, which are denoted by S_i and y_i^m , respectively. The strength of the synaptic connections from somatosensory and motor cortex are w_{sl} and w_{ml} . Thus, the equilibrium activation level \tilde{a}_i^l of the i th striatal interneuron is

$$\tilde{a}_i^l = w_{sl}S_i + w_{ml}y_i^m, \quad (3.2)$$

Then, if ϵ_l is the output relation threshold term (see equation 2.2) the output y_i^l of a striatal interneuron is given by

$$y_i^l = m(\tilde{a}_i^l - \epsilon_l)H(\tilde{a}_i^l - \epsilon_l). \quad (3.3)$$

Second, the basic striatal channel equations must be re-written to accommodate the interneuron connections. As the i th interneuron output contacts all channels other than its own, the total between-channel interneuron output Y_i^l becomes

$$Y_i^l = m \sum_{j \neq i}^n (\tilde{a}_j^l - \epsilon_l)H(\tilde{a}_j^l - \epsilon_l), \quad (3.4)$$

where n is the total number of channels. Then, letting w_{lc} be the weight of the interneuron to projection neuron connection, equation 2.11 is modified so that the activation level \tilde{a} in the i th striatal channel is now given by

$$\begin{aligned} \tilde{a}_i^g &= (c_i - (w_{lc}Y_i^l))(1 - \lambda_g) \\ \tilde{a}_i^e &= (c_i - (w_{lc}Y_i^l))(1 + \lambda_e), \end{aligned} \quad (3.5)$$

for the control and selection pathways respectively. The output relation and salience c equations remain unchanged from those given in section 2.3.5.

Two complete sets of the 121 simulations were run on the Interneuron model to determine the effects of different interneuron connection strengths: one set used $w_{lc} = 0.1$, the other used $w_{lc} = 0.5$.

The output states from each of the two sets are shown in the bubble plots and histogram of Figure 3.3. For both connection weights tested, the Interneuron model retained identical low input selection performance to the TRN model. In the low weight simulations, the reduction in the occurrences of dual channel selection did not correspond to a decrease in the occurrence of switches. With an increase in interneuron connection strength, an output state similar to that shown by the GP-Str Equal model resulted, where the absence of dual channel selection corresponded to a large increase in single channel selection and a reduction in switching. Thus, instantiating cross-channel interneurons in the striatum with a small weight slightly improved the switching performance of the TRN model; increasing that weight led to a second pattern of output behaviour which favoured single channel selection.

3.4 Axon collaterals in STN

Following on from the previous section, the effects of instantiating STN intra-nucleus connections are considered here. In the original intrinsic model, the output from STN was diffuse across all channels in its contact with EP and GP, which modelled the wide reaching arborisation of the STN neuron's axons in their target structures (Hazrati and Parent, 1992a; Hazrati and Parent, 1992b). This was termed the 'discrete' model of STN, as the channel boundaries were maintained within STN (Gurney et al., 1998b; Gurney et al., 2001b). An alternative 'homogeneous' model of STN, where all of the channels were represented by a single population of cells, was also tested and found to be functionally equivalent to the 'discrete' model (Gurney et al., 1998b; Gurney et al., 2001b). The 'homogeneous' model accounted for the possibility of dense axon collateralisation within the STN (Fujimoto and Kita, 1993). Recent in vitro and modelling studies have provided more evidence for the existence of the collaterals and information on their possible functional effect (Atherton, Gillies, and Arbuthnott, 2000; Gillies, Atherton, Arbuthnott, and Willshaw, 2000; Gillies and Willshaw, 1998). Thus, the aim of the

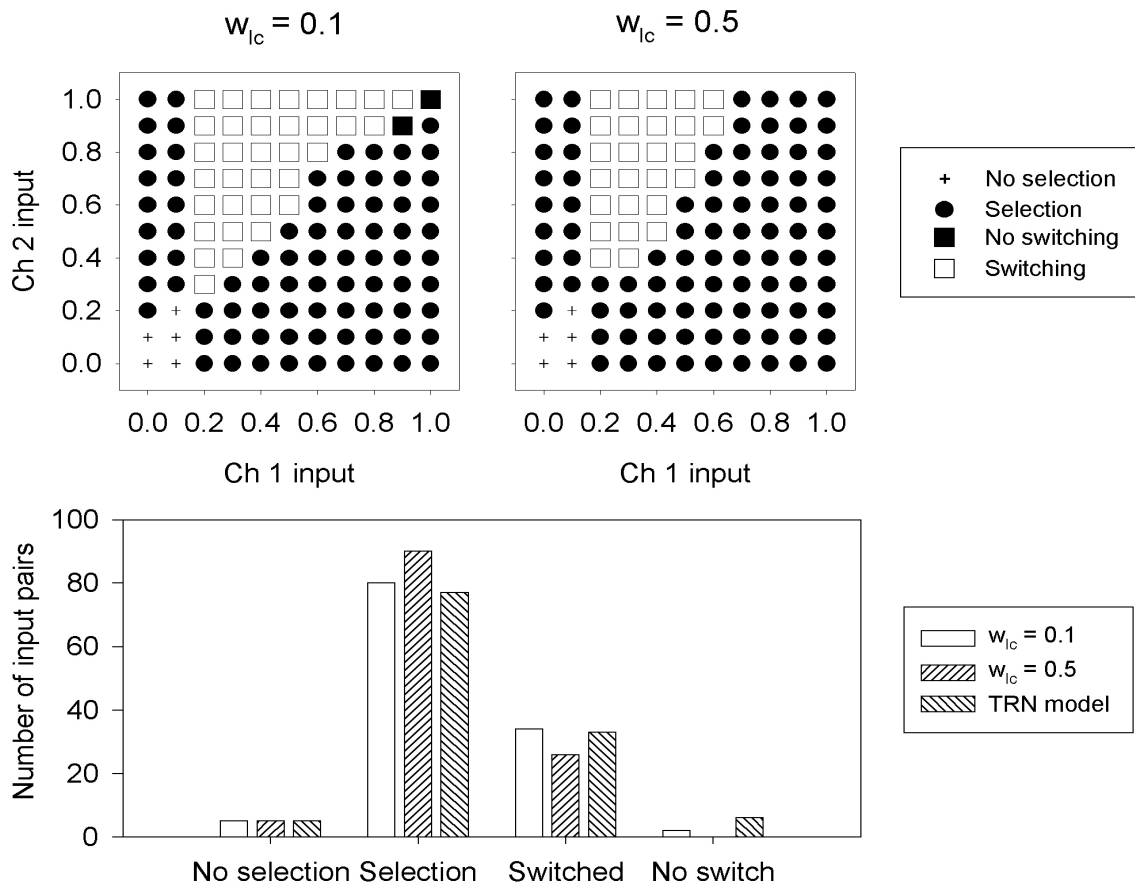


Figure 3.3: Plots showing how changing the connection strength of striatal interneurons affects EP output. The instantiation of low-strength cross-channel inhibitory interneurons in the striatum reduced the number of unsuccessful switches, while maintaining the low salience selection capability (left). Using a larger weight $w_{lc} = 0.5$ substantially reduced the number of switching cases (right). The number of occurrences of the four output states are summarised and compared to the TRN model (bottom).

study reported in this section was to investigate how the instantiation of explicit STN axon collaterals altered the output of the TRN model.

To implement the widespread axon collaterals, the input of each STN channel is augmented with the summed output of all STN channels (suitably weighted). The total STN output X^+ is given by,

$$X^+ = m \sum_{i=1}^n (\tilde{a}_i^t - \epsilon') H(\tilde{a}_i^t - \epsilon'), \quad (3.6)$$

where \tilde{a}_i^t is the activation in the i th STN channel (see equation 2.14). Simply adding this total output into the activation equation for an STN channel gives:

$$\tilde{a}_i^+ = w_{ss} X^+ + w_{sc} S_i + w_{mc} y_i^m - w_g y_i^e, \quad (3.7)$$

where w_{ss} is the axon collateral weight. The resulting model is termed the ‘STN model’.

Recent modelling work (Gillies et al., 2000) has indicated that an excitatory post-synaptic potential (EPSP) elicited by a single STN neuron contacting another is likely to be small. Thus, low connection weights of $w_{ss} = 0.1$ and $w_{ss} = 0.4$ were used for two sets of 121 simulations of the STN model. The bubble plots showing the resulting output states from the two sets of simulations and the comparative histogram are in Figure 3.4. With the lowest weight axon collateral connection, the STN model retained the low input selection capability and decreased the number of dual channel selections, compared to the TRN model. However, the occurrence of successful switches also decreased. The stronger axon collateral connection weight caused a pattern of output similar to that seen in section 3.2 for the GP-Str Equal model, in that no dual channel selection occurred at all. Also similar was the marked reduction in switching and corresponding increase in single channel selection. Further, low salience selection was slightly impaired, compared to the TRN model.

It can be concluded that the presence of STN axon collaterals, given a very small connection strength, did not markedly impair the selection performance of the TRN model. Increasing the connection strength resulted in a second pattern of output in which dual channel selection had been abolished at the expense of markedly increasing single channel selection at high salience levels.

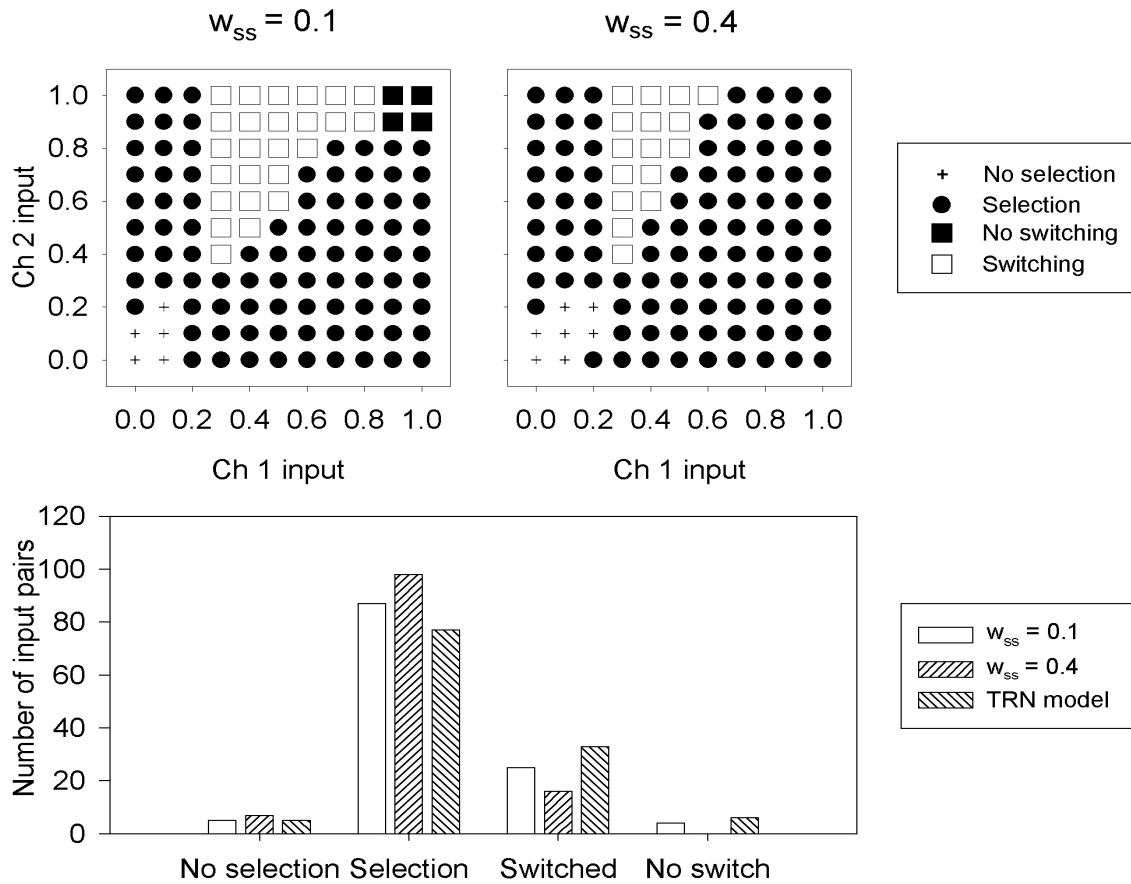


Figure 3.4: Plots showing the effects of altering the STN axon collateral weight in the STN model. Left: Introducing very low weight axon collateral connections ($w_{ss} = 0.1$) into the STN slightly increased the number of selected input pairs and reduced the number of unsuccessful switches, compared to the TRN model. Right: Increasing w_{ss} resulted in minor loss of low selection ability and greatly reduced the number of successful switches. Bottom: summary histogram of the STN model's results and the results from the TRN model.

3.5 A feedback loop formed by GP and EP

The short review of previous basal ganglia computational models in section 1.4.1 noted that the only model which was concerned solely with a motor-related role of the basal ganglia (Contreras-Vidal and Stelmach, 1995) contained an EP-to-GP connection which was omitted from our original functional anatomy. There is some independent evidence for the existence of this connection in the literature. Hazrati et al. (1990) reported the existence of GPi axon terminals in the GPe of primate basal ganglia following injections of an anterograde tracer; unfortunately there is no published data on the existence of this pathway in the rat basal ganglia, on which our functional anatomy is based. However, if consistency in the connectivity of the basal ganglia across mammals is assumed, as has been demonstrated for most extant basal ganglia pathways, it would be wise to explore what effect this pathway may have on basal ganglia output. Therefore, the addition of an EP-to-GP connection to the TRN model was simulated and the results are reported in this section.

A further assumption is that the projection to GP is made by collaterals of EP neurons which project outside of the basal ganglia as there is no evidence for any other class of neurons within EP/GPi (based on projection targets). As the synaptic contacts the EP neurons make with their thalamic and brainstem targets are known to use GABA as neurotransmitter (Gerfen and Wilson, 1996) it is reasonable to assume that the collaterals of the same neurons also use GABA at their synapses with GP neurons. Thus, the pathway between EP and GP is inhibitory, which forms a symmetric feedback loop between EP and GP.

To integrate the EP-to-GP pathway into the model basal ganglia and maintain the channel architecture it was presumed, in the absence of contrary data, that the connection is channel specific. Then, if the EP output is y_i^b , and letting the connection weight be w_{bp} , the equilibrium activation \tilde{a}_i^p of GP becomes

$$\tilde{a}_i^p = w_{sp}Y^+ - w_{bp}y_i^b - w_{gp}y_i^g, \quad (3.8)$$

where w_{sp} and w_{gp} are the weights of the connections from the STN and striatal D2 channel and Y^+ and y_i^g are the outputs of those structures. The output relation remains as given in

equation 2.18. Taking into account the possible sparseness of the EP-to-GP connection, as an explanation for its absence from the literature, w_{bp} was set to 0.4.

The bubble plot on the left-hand side of Figure 3.5 shows the proportion of the four output states that resulted from running the standard 121 simulation set on this EP-GP model.

Compared to the TRN model, some low salience selection was lost and the occurrences of both dual channel selection and switching were reduced. Therefore, the simple instantiation of a EP-to-GP feedback pathway led to the degradation of the model’s performance - the basal ganglia is, after all, being posited as a biological switching mechanism.

3.6 Combinations

The previous sections have reported the effects of instantiating single new pathways into the basal ganglia of the TRN model, with varying degrees of success in maintaining or improving the TRN model’s selection and switching performance. Here two models are briefly explored in which the functional influence of a previously-studied individual pathway is altered by the addition of a second pathway. In both cases the addition of the second pathway is made in an attempt to compensate for the degradation in the TRN model’s performance caused by the original addition of the first pathway.

Note that the combination of two new model pathways is not necessarily due to the need to compensate for a “negative” performance pathway with a “positive” performance counterpart. Two new pathways may instead act synergistically, such that they are ineffective when added individually but affect the function of the model when added in combination. Whether such pairs of pathways exist in the basal ganglia is unknown, and is the subject of future work.

3.6.1 Striatal interneurons form a compensatory pathway to the EP-GP pathway

In section 3.5 we saw that the addition of an EP-to-GP pathway to the basal ganglia markedly decreased switching performance, compared to the TRN model. Thus, as our major hypothesis

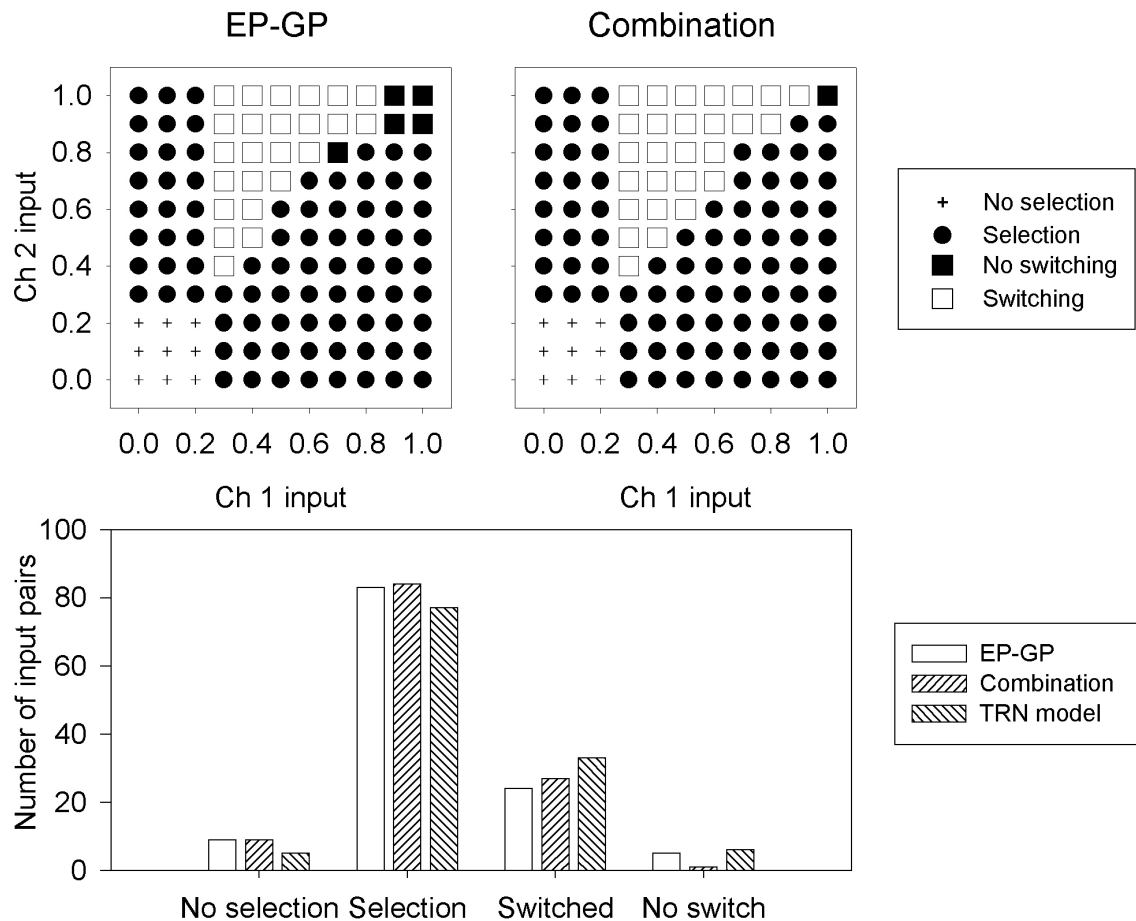


Figure 3.5: The effect of instantiating the EP-to-GP pathway (left) and then adding striatal interneurons (right - see section 3.6.1). Left: bubble plot of the EP-GP model output states, showing a reduction in low salience input selection and a decrease in dual channel selection. Right: adding the interneurons into striatum, with a small connection weight, further reduced the dual channel selection and increased the occurrence of switches, compared to the EP-GP model. Bottom: summary histogram, comparing the two models' performance with that of the TRN model.

is that the basal ganglia acts as a switching mechanism, it would be prudent to investigate whether the addition of a further pathway to the EP-GP model can improve its switching capability.

Through surveying the models already studied, it was noted that the addition of striatal interneurons resulted in the clearest improvement in switching ability beyond that achieved by the TRN model. More specifically, this improvement only occurred when the weight of the connection between the modelled interneurons and projection neurons was very low. Therefore, striatal interneurons, as described in section 3.3, were added to the EP-GP model, with $w_{lc} = 0.1$. It was hypothesised that the improvement in switching caused by the addition of interneurons would compensate for the degradation in performance caused by the EP-to-GP pathway.

The right bubble plot in Figure 3.5 shows the output states that resulted from 121 simulations of this combined pathway model. The consequent improvement in switching performance over the EP-GP model was immediately evident as the number of switching cases increased. Also of interest is that dual channel selection (no switching) only occurred following maximum input to both channels. This illustrates the synergistic action of the two pathways: both individually caused some reduction in dual channel selection and then when combined the dual channel selection was further reduced.

3.6.2 Pallidostriatal connections to projection- and inter-neurons

In section 3.2, which introduced the GP feedback pathway to striatum, evidence for synaptic contact on the GABAergic interneurons in the striatum by GP axon terminals was noted. The interneurons were initially assumed to be confined to each channel, and the net effect of GP input to the interneurons and projection neurons was assumed to be inhibition of the projection neurons. However, as a simplified model of striatal interneurons has been developed a second combined model, the GP-Int model, was constructed which contained channel-specific GP input to the interneuron population. Thus, the behaviour of the more complete circuit could be explored. Furthermore, in keeping with the theme of this section, it could be ascertained

whether the addition of interneurons could compensate for the switching deficit seen in the GP-Str models (as compared to the TRN model) or not.

The equilibrium activation of striatal projection neurons was given by equation 3.5 which included a term Y_i^l for the (combined) interneuron input. However, GP input y_i^p had to be accounted for in the equation for equilibrium activation of the interneuron \tilde{a}_i^l . In addition, the possible splits in GP output between the selection and control pathways need to be accounted for and so it was assumed that the GP-to-interneuron weight is the same as the GP-to-projection neuron weights w_{pe} and w_{pg} in the selection and control pathways, respectively. So, from equation 3.2, if the equilibrium activations of interneurons in the selection and control pathways are \tilde{a}_i^1 and \tilde{a}_i^2 , respectively, then

$$\begin{aligned}\tilde{a}_i^1 &= w_{sl}S_i + w_{ml}y_i^m - w_{pe}y_i^p, \\ \tilde{a}_i^2 &= w_{sl}S_i + w_{ml}y_i^m - w_{pg}y_i^p,\end{aligned}\tag{3.9}$$

where y_i^p is GP output. Further, the striatal channel activation equations need to be rewritten to account for the interneuron differentiation. First, the total between-channel interneuron outputs for the selection pathway Y_i^1 and control pathway Y_i^2 are

$$\begin{aligned}Y_i^1 &= m \sum_{j \neq i}^n (\tilde{a}_j^1 - \epsilon_l) H(\tilde{a}_j^1 - \epsilon_l), \\ Y_i^2 &= m \sum_{j \neq i}^n (\tilde{a}_j^2 - \epsilon_l) H(\tilde{a}_j^2 - \epsilon_l),\end{aligned}\tag{3.10}$$

where n is the total number of channels. Second, adding the total interneuron output and GP input to the striatal activation equations 2.11 gives,

$$\begin{aligned}\tilde{a}_i^e &= (c_i - (w_{pe}y_i^p + w_{lc}Y_i^1))(1 + \lambda_e) \\ \tilde{a}_i^g &= (c_i - (w_{pg}y_i^p + w_{lc}Y_i^2))(1 - \lambda_g),\end{aligned}\tag{3.11}$$

where w_{lc} is the weight from the combined interneuron output in that pathway. The output relation and salience c equations remain unchanged from those given in section 2.3.5.

The complete set of 121 simulations were run twice using the GP-Int model, once with $w_{pe} = 0.1$ and $w_{pg} = 0.4$ (GP-Int Control), the other with $w_{pe} = w_{pg} = 0.4$ (GP-Int Equal),

identical to the two sets run in section 3.2. Again the interneuron weight $w_{lc} = 0.1$ was used for both combined models.

Bubble plots and summary histogram of the resulting output states for the two models are shown in Figure 3.6. The GP-Int Equal model had an almost identical set of output states to the GP-Str Equal model (just one less case of switching). By contrast, a comparison of the GP-Int Control and GP-Str Control models' outputs shows that the instantiation of interneurons halved the number of input pairs resulting in dual channel selection and, moreover, increased the number of successful switches. Some features of both GP-Int model's output states are identical to their equivalent GP-Str model outputs: the low salience selection pattern and the minimum salience pair required for switching to occur particularly stand out. Further, a comparison between the two GP-Int models and the equivalent Interneuron model (left plot in Figure 3.3) shows that the addition of the GP-to-interneuron/projection neuron pathways greatly reduced the number of successful switches.

Comparing the results of the combination and GP-Str models shows that interneurons in the striatum only have a significant modulatory effect when the GP projection is weighted in favour of the control pathway. Similar to the results observed in the previous section, the instantiation of interneurons in the GP-Str Control model improved its switching performance. Thus, the interneurons again acted to compensate in part for the “negative” performance which resulted from the addition of a single new pathway.

In the initial study of the GP-to-striatum projection neuron models (section 3.2) it was tentatively concluded that the GP-Str Equal model was preferable to the GP-Str Control model because of the former's lack of dual channel selection. However, as seen here, the addition of interneurons improved switching performance only in the GP-Str Control model. Thus, it has become less obvious which weighting of GP output to striatal projection neurons and interneurons in the selection and control pathways is favoured. However, it may be concluded that if striatal interneurons are weakly connected to projection neurons then they will have their greatest effect on basal ganglia output if the GP-to-striatum connection (to projection neurons and interneurons) is weighted in favour of the control pathway.

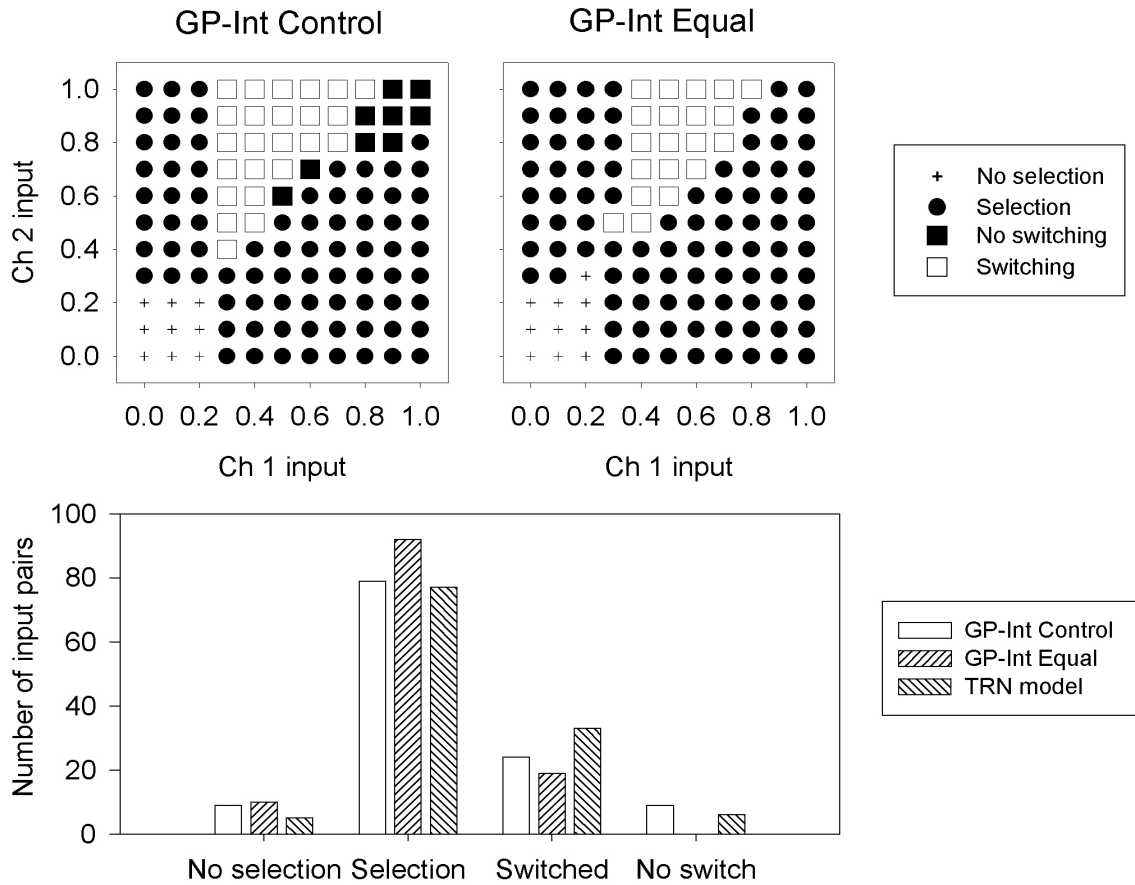


Figure 3.6: The effect on the EP outputs of instantiating both striatal interneurons and inhibitory connections from GP to projection neurons and interneurons in striatum. Left: if the GP-to-striatum control pathway had the greater connection strength then the lowest level input required for selection and switching increased; otherwise the outputs were very similar to those of the TRN model. Right: giving the GP-to-striatum pathways equal weights resulted in a similar increase in the lowest level input necessary for selection and switching. In addition, dual channel selection was abolished, with a corresponding increase in single channel selection. Bottom: histogram summarising the number of input pairs which resulted in each of the four states for the GP-Int Control, GP-Int Equal, and TRN models.

3.7 Summary

This chapter was not intended as an exhaustive survey of the basal ganglia's intrinsic connections and neuron types, nor did it attempt to report the effects of all combinations of the newly incorporated pathways. What has been reported here are short studies of computational models which illustrate two main points. First, the basal ganglia functional anatomy which underpins the design of the intrinsic model is robust in that the addition of new pathways does not alter the basic ability of the basal ganglia to act as a selection and switching mechanism. The significance of this achievement can be emphasised if we consider that there is no *a priori* reason for expecting that the addition of these pathways would not result in a complete breakdown in selection and switching; just this result would be seen if, for example, the GP-to-STN pathway was removed (Gurney et al., 2001b). Some parameter sets resulted in a second pattern of output behaviour which was not observed in the TRN model, in which dual channel selection was prevented and single channel selection was greatly increased - the behavioural implications of this second pattern are discussed below.

Second, the two combined models that were investigated showed how pathways which individually adversely affect the model's performance can be compensated for by the addition of a further "balancing" pathway. It seems, then, that there may be pairs of pathways in basal ganglia which must co-exist to prevent action selection from breaking down - the most basic of these pairs is obviously the selection/control pathway split, where the action of GP on STN limits EP activation. Here we have seen how striatal interneurons can compensate in part for the reduction in switching caused by the individual addition of either the EP-to-GP or the GP-to-striatum pathways. An example of how pairs of pathways may act synergistically to cause output states that neither can achieve when instantiated individually was also noted¹.

An important question remains unanswered: if the selection and switching ability of the basal ganglia was essentially retained regardless of which new pathways were added, what is the purpose of these other, seemingly non-crucial, pathways? Some pathways, such as the striatal interneurons, refine the ability of the basal ganglia to act as a switching mechanism through decreasing the dual channel selection while maintaining or improving the switching

ability. Other connections, when given moderate or strong connection weights (such as the STN neuron axon collaterals) detracted from the basal ganglia's ability to act as switching mechanism as they caused a large increase in single channel selection. The purpose of these latter pathways with low connection strengths may be to regulate the actions of the basal ganglia in system states that have not been explored here, such as those resulting from changes in dopamine levels, such that the response of the basal ganglia is robust in these states.

The changed pattern of behaviour in the GP-Str Equal model and others raises an important behavioural question: given two (or more) very urgent but possibly incompatible actions is it preferable for them to be simultaneously selected (as occurs in the TRN model) or for no action to be selected after the second (or last) action has become available (as occurs, for example, with the GP-Str Equal model)? It is possible that both of these modes of action selection could be expressed. To draw parallels with real behaviours, the former mode, 'promiscuous' selection, may be expressed by quick alternation between the selected actions or by simultaneous execution of two compatible actions. Either is possible as the interpretation of a model neuron's output as a mean firing rate does not allow one to determine the form of the underlying spike train. This issue is addressed in the next chapter, where it is demonstrated that the simultaneous selection of two channels in the intrinsic model and all its derivatives is likely to signify rapid alternation of selection.

In the second mode of action selection observed there was no selection of any channel when both channels were active with high saliences. It could be suggested that in such a case, a lower-level or 'automatic' behaviour would be expressed. Thus the animal would perform a displacement activity, which are often observed in ethological studies of conflict situations (that is, situations in which two or more equally salient actions are available) (Hinde, 1966).

This second pattern of output behaviour only occurred in some of the models, and then only when the new pathway had a moderate to high valued weight. Increasing the STN axon collateral, striatum interneuron, and GP to striatum weight all resulted in prevention of dual channel selection. Thus, the weight of the basal ganglia's intrinsic connections determines which of the two output patterns is observed. The analogies drawn between the pattern of output

and behaviour can be developed further: the resulting behaviour is directly dependent on how strong certain pathways within the basal ganglia are, and this may in turn be dependent on the animal's previous experiences. This idea is explored further in the concluding chapter.

Chapter 4

Spiking models of the basal ganglia

4.1 Introduction

Having investigated the systems-level model of the basal ganglia and associated thalamocortical structures in the previous two chapters, I turn now to the study of how the behaviour of the same computational model is affected when it is instantiated at a lower level of description.

The choices for the appropriate level of description were outlined in chapter 1. There it was noted that the level of computing power necessary to simulate a network of multi-compartmental units for a significant period of simulated real-time is prohibitive, and that the parameter space is too large for effective exploration. The alternative was to use the class of recently developed pulsed or spiking model neurons (Maass, 1997; Gerstner, 1999). These attempt to mimic *phenomenologically* the dynamics of the membrane potential u by combining a series of function kernels that model different mechanistic components of u . The development of spiking neuron models invites an intriguing question: is it possible, using this family of models, to simulate some of the complex dynamics shown by real neurons (and which is certainly within the grasp of the potentially more powerful models based explicitly on membrane compartments)? The main objective of this and the subsequent chapter is to show that, at least for some neural circuits, this question has an affirmative answer.

The current chapter's main aim is to address the problem of elucidating a detailed interpretation of the outputs from the systems-level models explored in the two previous chapters.

Because of their use of leaky-integrator units (which leads to us characterising them as *continuous time* models) their output had to be interpreted as a mean-firing rate, either across a substantial period of time for a single neuron, or across a group of neurons. This approach, while allowing the outputs to be interpreted in terms of their gross behavioural consequences, obscures the nature of the spike trains underlying the firing rates. The use of more detailed spiking model neurons in these basal ganglia models would allow the observation of a wider variety of unit output patterns (regular, irregular, bursting, oscillatory), all of which may be consistent with a given mean firing rate. Furthermore, it is likely that the form of spike train pattern from the basal ganglia output nuclei would influence the behavioural response of the animal.

One way of viewing the EP output of the continuous time models, and one which becomes important in this chapter, is that they encode an ON/OFF signal. The tonic output of EP is a continual OFF signal to its target structures, ensuring that they do not fire. Once selection has occurred, EP output on that channel (or channels) is an ON signal, indicating by its absence that the target structures can fire if sufficient afferent input is received. In the systems-level model this interpretation is somewhat trivial due to the continuous output of the model neurons and the use of only one model neuron per channel. However, as multiple units are used in each channel in the spiking model, the encoding of the ON/OFF signal becomes non-trivial as it is dependent on the outputs of all the units. The example results described in section 4.3.1 show how the output of multiple spiking units in the EP can encode the ON/OFF signal of a channel.

As a tool for studying the problem of interpreting continuous outputs, I constructed a version of the TRN model (see chapter 2) using spiking model neurons. To simplify the naming of models, this will be termed the extended model throughout to distinguish it from the continuous time TRN model. There is a further motivation for the construction and testing of this model: near-simultaneous, closely matched salience inputs to the continuous time TRN model result in equal level basal ganglia outputs (see Figure 4.1) which can be interpreted as either both actions being selected or both being non-selected. As this has major implications for behaviour, the

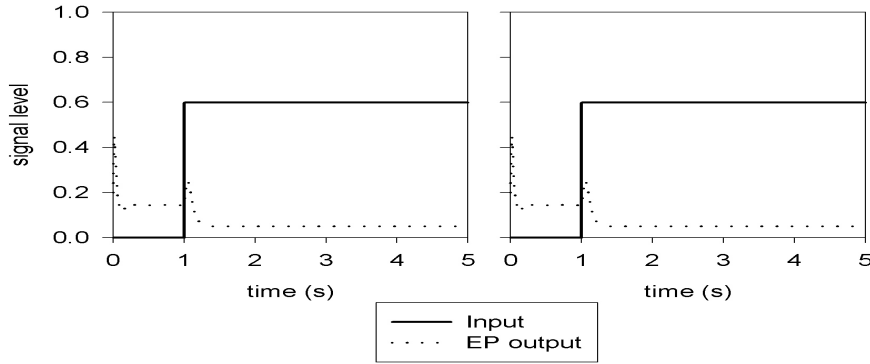


Figure 4.1: Example outputs from the continuous time (TRN) model showing the response to closely matched simultaneous inputs - the outputs on both channels are equal.

spiking version of the extended model will be used to investigate the firing patterns underlying this output. Specifically, I make the hypothesis that the basal ganglia output (from EP) will not consist of tonic spike trains due to the complex interactions of the feedback circuits extant in the extended model. Of course, it first needs to demonstrated that the spiking version of the extended model can successfully replicate the selection and switching behaviours of the original continuous time TRN model (see section 4.3.1).

It should also be noted that the spiking model neuron work described in this chapter was conducted in parallel with the work in chapter 3. Thus, the starting point of the work presented in this chapter was the TRN model described in chapter 2, and no use was made of any of the derivative models from chapter 3. This also maintained consistency in design across the continuous-time and spiking models which facilitated comparisons of the models across the different modelling levels.

4.2 Methods

4.2.1 The model neuron

The model neuron is based on the integrate-and-fire neuron described by Gerstner (1999). The total membrane current $I(t)$ is given by the sum of capacitive and resistive components

$$I(t) = \frac{u(t)}{R} + C \frac{du}{dt} \quad (4.1)$$

where C is the membrane capacitance, R its resistance, and u the membrane potential. The product $\tau_m = RC$ has dimensions of time and determines a characteristic time scale (the *membrane time constant*) for signals to change in the membrane. Using the definition of τ_m in equation (4.1) gives

$$\tau_m \frac{du}{dt} = -u(t) + RI(t). \quad (4.2)$$

Note that, with no input current, the equilibrium value of u is zero.

The model neuron ‘fires’ if u reaches a threshold θ from below; that is, $u = \theta$ and $du/d\theta \equiv u' > 0$. The set of firing times of the neuron is denoted by F where $F = \{t^{(1)}, t^{(2)}, \dots, t^{(n)}\}$. After firing, the membrane potential is reset to a value $u - (\theta - u_r)$, a process which models the neuron’s relative refractory period after firing. For the models described in this and the subsequent chapter, u_r is set to zero so that the membrane potential goes to zero after firing. However, it is possible that the membrane is being driven (by synaptic input or injection current) so hard that it rapidly reaches θ again. To counter this, a neuron also has a fixed time, the absolute refractory period τ_{abs} , during which it may not fire a spike regardless of the strength of input. This is modelled by stopping the solution of equation (4.2) for τ_{abs} and forcing the membrane potential to zero for this time. The combination of τ_{abs} and the resetting of the membrane potential gives the total refractory period.

The current $I(t)$ is constituted from three main sources. First, $I(t)$ contains a contribution $I_{syn}(t)$ from synaptic input. Let Γ be the set of afferents to the neuron under consideration (any index for this neuron is dropped to simplify notation). Let w_j represent the strength of connection (the ‘weight’) from afferent j and suppose that each current pulse is shaped

according to some kernel function $\alpha(s)$. Then, assuming that post-synaptic potentials (PSPs) combine additively

$$I_{syn}(t) = \sum_{j \in \Gamma} w_j \sum_{t_j^{(f)} \in F^j} \alpha(t - t_j^{(f)}) \quad (4.3)$$

Usually $\alpha(s)$ is taken to be a step followed by exponential decay

$$\alpha(s) = \frac{1}{\tau_s} e^{-s/\tau_s} H(s) \quad (4.4)$$

where $H(s)$ is the Heaviside step function which is zero for $s \leq 0$ and is one otherwise.

Second, it is possible to model the post-firing reset condition (and thereby the relative refractory period) using a current I_{ref} that consists of a series of Dirac δ pulses.

$$I_{ref} = -C(\theta - u_r) \sum_{t_i^{(f)} \in F_i} \delta(t - t_i^{(f)}) \quad (4.5)$$

In addition to the post-synaptic current (caused by pre-synaptic spike arrival) affecting a neuron's membrane potential, there is the effect of noise. The variability in the inter-spike intervals of a neuron's output following a constant current injection must occur through the existence of membrane noise (Calvin and Stevens, 1967). Three main sources of membrane noise have been identified (Manwani and Koch, 1999). First, the agitation of electrical charges in a conductor (here the membrane) is dependent on the temperature: this is termed thermal noise. Second, ion channels open and close randomly throughout the membrane, and this fluctuation in the number of active/open channels constitutes channel noise. Third, random synaptic activity, caused by the binding of neurotransmitter molecules from non-local sources, forms synaptic noise. All of these sources are encapsulated in a single noise component I_{noise} which is sufficient to model the many random processes occurring in the cell membrane (Gerstner, 1999). Ultimately, the I_{noise} current ensures that membrane potentials of different units with identical inputs and parameters are not the same. Thus, equation (4.2) becomes

$$\tau_m \frac{du}{dt} = -u(t) + R[I_{syn}(t) + I_{ref}(t) + I_{noise}(t)] \quad (4.6)$$

As a further addition to the calculation of I_t , a component I_{spon} is added which models the causal factors underlying spontaneous firing in some neuron types. Where necessary, I_{spon} is

given a constant low-level current value so that it can generate output for the model neuron in the absence of any synaptic input. For neuron types which are silent *in vivo* with no afferent input, this component is given the value zero. Thus, equation (4.6) becomes

$$\tau_m \frac{du}{dt} = -u(t) + R[I_{syn}(t) + I_{ref}(t) + I_{noise}(t) + I_{spon}(t)] \quad (4.7)$$

4.2.2 Dopamine

As there is no SNC within the basal ganglia model, the dopaminergic input to striatum was modelled as a single parameter representing the tonic level of dopamine. To maintain the distinction between the D1 and D2 receptor neurons, and their different target structures, the dopamine parameter is λ_e for striatal D1 neurons and λ_g for striatal D2 neurons. In line with its effect in the continuous time models, dopamine gated the input to the striatum. To do this, λ_e and λ_g were used as multiplicative factors on the appropriate input weights. To account for the dopamine parameter I_{syn} is rewritten so, where I_{syn}^e is the synaptic current due to inputs to D1 striatal neurons (selection pathway) and I_{syn}^g is due to D2 neurons (control pathway):

$$I_{syn}^e(t) = \sum_{j \in \Gamma} w_j (1 + \lambda_e) \sum_{t_j^{(f)} \in F^j} \alpha(t - t_j^{(f)}) \quad (4.8)$$

$$I_{syn}^g(t) = \sum_{j \in \Gamma} w_j (1 - \lambda_g) \sum_{t_j^{(f)} \in F^j} \alpha(t - t_j^{(f)}). \quad (4.9)$$

4.2.3 Network design

I now turn to the determination of the number of neurons in each channel. In real neural tissue each neuron is contacted by up to several thousand axon terminals. Clearly this is difficult to replicate in a network which uses relatively detailed models, and so it was necessary to establish what degree of connectivity could be built into the network while maintaining realistic units outputs. In general it may appear that if the number of afferents is halved but the synaptic weight of each afferent is doubled then no loss in realism ensues. However, because the afferent spike trains exert a noisy and discontinuous influence, their combined effect is non-linear. To determine the smallest usable number of afferents, without significant loss in the

Mean input rate (spikes/s)	Number of inputs (c)						
	2 (96)	8 (24)	16 (12)	32 (6)	64 (3)	128 (1.5)	192 (1)
2	1	0	0	0	0	0	0
8	5	3	2	2	2	2	2
16	16	15	14	14	14	14	14
32	32	32	34	34	35	35	35
64	63	64	67	68	68	69	69
128	86	116	123	123	124	124	124

Table 4.1: Changes in output frequency of a single model neuron with differing number of inputs and mean input frequency. The control case is shown in the final column for 192 inputs. c is the scaling factor on the connection weight

transfer characteristics of the model neuron, a series of experiments were run with different numbers of inputs N into a single model neuron described by equation (4.6). Every input was a spike train generated using a binomial distribution. The results are shown in Table 4.1.

Each column indicates, for each value of N , the output (in spikes/s) of the neuron in response to different mean firing rates of the input spike trains. The final column shows the control case with 192 inputs and a scaling factor c of 1 (see below for weight details). The outputs of this neuron were used as the target values for all subsequent experiments with smaller N values to determine if the corresponding increase in weight then led to a significant difference in output. It is clear from these results that small numbers of inputs (with correspondingly large weights) incur a loss in faithful reproduction of the control neuron's output which is especially severe at low input firing rates. On the other hand, no gain in accuracy was found above $N = 16$ inputs and so 16 units per channel were used.

Every simulated model contained three channels, and each channel contained 16 units described by equation (4.7), except striatum D1 and D2 units which were described by equations (4.8) and (4.9), respectively. Each unit in a channel received input from the corresponding 16 units in the afferent structure(s). In turn, each unit projected to all 16 units in the ef-

ferent structure(s). Therefore, the discrete nature of the channel architecture was maintained throughout the models, except the projections from the STN and TRN which are detailed below.

All EP and GP units received input from all STN units, regardless of their nominal channel membership. This modelled the diffuse projections from STN to its afferent targets (Hazrati and Parent, 1992a; Hazrati and Parent, 1992b). Reciprocal GP input to STN maintained the discrete channel projections.

For the TRN to VL thalamus projections, the within-channel projection from a TRN unit to all 16 units in the corresponding VL thalamus channel was given a small inhibitory weight to model its sparseness. In addition, each unit in a TRN channel sent a large weight inhibitory connection to all units in VL thalamus channels other than its own (see section 2.2.2 for more details on the TRN-VL connection design).

Model inputs

Sensory input to the model S_i (where i is the channel index), from the somatosensory cortex, consisted of 16 spike trains per channel. The interspike intervals for each spike train of x spikes/s were sampled from an exponential distribution with a mean of $1/x$ so that the trains followed a Poisson process (Press et al., 1989). To maintain biological plausibility, a refractory period for the spike trains was created by discarding any interspike interval of less than 2ms and the spike train was then constructed by recording a one at each interval with zeros in between. Every unit in a channel contacted by the input received all 16 spike trains.

4.2.4 Implementation details

Every simulation was of 60 seconds duration, and the inputs were started at $t = 1$ second to allow the model units to reach equilibrium states of tonic firing. Two of the three channels received input: the third channel received no input as it was intended that this channel be reserved for observing how sensory input level changes affect a non-active channel. The inputs to the active channels had two variables: the minimum level of input S_{min} and the ratio ϕS

ϕS	S_{min}			
	20	35	50	65
1.0	20/20	35/35	50/50	65/65
1.05	20/21	35/36.75	50/52.5	65/68.25
1.1	20/22	35/38.5	50/55	65/71.5
1.15	20/23	35/40.25	50/57.5	65/74.75

Table 4.2: The experiment matrix - each cell is a pair of salience inputs (in spikes/s) to the spiking extended model, in the form S_1/S_2 .

between the two inputs $S_1 : S_2$. The variables both had four levels, giving an experiment matrix of 16 simulations which is detailed in Table 4.2. The first row of the matrix contains simulations of exactly equal inputs (i.e where $\phi S = 0$) and the subsequent rows contain simulations of closely-matched inputs.

All simulations were written in Matlab v5.2 (Mathworks), and the model equations were solved in discrete time. Each time-step of a simulation was 0.1ms in duration, which was the minimum value commensurate with accurate solutions of the equations.

Spontaneous output values

At rest, *in vivo*, an STN neuron has a tonic firing rate of 10-30 spikes/s (Fujimoto and Kita, 1993; Wichmann et al., 1994). Similarly, EP and GP have high tonic output rates at rest. These were modelled by setting the STN I_{spont}^s value to $3\mu A$ and the EP I_{spont}^b value to $1.1\mu A$. This provided enough excitation to EP and GP for their mean output rates to be approximately 30 spikes/s, as well as maintaining an STN output level of approximately 20 spikes/s.

Striatal projection neurons, both D1 and D2 types, are silent *in vivo*. This DOWN-state is highly stable, and the membrane potential is far below the neuron's firing threshold. Shifting the neuron into its firing-ready UP-state requires massive co-ordinated input from cortex and other afferent structures (Gerfen and Wilson, 1996). To model the difficulty of forcing this change, the I_{spont} value for D1 and D2 striatal neurons was set to $-1\mu A$. Thus, large value

inputs were required before the striatal neurons could fire any spikes. For all other structures I_{spont} was set to zero.

Parameter values

All the neurons in every structure had identical parameter values, except for I_{spont} (see previous section) and the weights w_{ji} (where j is the structure of the afferent unit and i is the structure containing the unit in question). Capacitance C was set to $2 \mu F$. The synaptic and membrane time constants (τ_s and τ_m) were set to 3ms and 70ms, respectively. The firing threshold was set to 30mV. At each time-step of the simulation, the I_{noise} component was sampled from a Gaussian distribution ($\bar{x} = 0, \sigma^2 = 5$). Finally, the dopamine parameters λ_e and λ_g were both set to 0.2 in ‘normal’ simulations. The effects of dopamine level changes are reported in section 4.3.2.

The maximum size of the post-synaptic potential V_{max} was set at 5mV. To use this as a basis for deriving the weight of a connection, this has to be converted to give the maximum post-synaptic potential current I_{psc} . Thus, remembering that $\tau_m = RC$, and given Ohm’s law $R = V/i$ (where V is voltage, and i is current), then resistance can be given as $R = \tau_m C$. Substituting for τ_m gives

$$I_{psc} = \frac{V_{max}C}{\tau_m}. \quad (4.10)$$

Each connection has a scaling value (c_{ji}) in the range (0,1) which scales the I_{psc} value according to the relative strength and sign of the connection. Further, the connection weight is scaled by the the number of afferents n that each connection is nominally representing (for the simulations detailed here $n = 12$: see section 4.2.3). Finally, the resulting value is then scaled by τ_s . Thus, the weight w_{ji} of the connection between any two units is given by

$$w_{ji} = c_{ji} * n * I_{psc} * \tau_s. \quad (4.11)$$

The scaling values c used in the model are given in Table 4.3.

Connection	Parameter Name	Value
Input-Striatum D1	c_{SD1}	0.5
Input-Striatum D2	c_{SD2}	0.5
Input-STN	c_{Sn}	0.5
Input-Motor cortex	c_{Sm}	1
Motor cortex-Striatum D1	c_{mD1}	0.5
Motor cortex-Striatum D2	c_{mD2}	0.5
Motor cortex-STN	c_{mn}	0.5
Motor cortex-VL	c_{mv}	1
Motor cortex-TRN	c_{mt}	1
Striatum D1-EP	c_{D1i}	-1
Striatum D2-GP	c_{D2e}	-1
STN-GP	c_{ne}	0.8
STN-EP	c_{ni}	0.8
GP-STN	c_{en}	-1
GP-EP	c_{ei}	-0.4
EP-VL	c_{iv}	-1
EP-TRN	c_{it}	-0.2
VL-Motor cortex	c_{vm}	1
VL-TRN	c_{vt}	1
TRN-VL (within channel)	c_w	-0.1
TRN-VL (between channel)	c_b	-0.7

Table 4.3: Scaling values c_{ji} for all of the connections in the extended model.

4.3 Results

4.3.1 The extended model

Example outputs

Four complete sets of the simulations from the experimental matrix were conducted using the extended model. An example of one channel's EP output from the first set of simulations is described to exemplify the typical behaviour observed and the analysis methods employed before summarising the results from the entire matrix.

A snapshot of 5 seconds from the spike trains of all sixteen EP units in channel 1 is shown in Figure 4.2 for the simulation with inputs $S_1 = 50, S_2 = 50$ (where $S_{min} = 50$ spikes/s and $\phi S = 1.0$). The spike trains show long common periods of alternating sparse firing, more rapid firing, and silence. To quantify this output, the reciprocal of each interspike interval between adjacent spikes is taken to determine the instantaneous firing rate for each spike train at any given moment (in analysing data from a full simulation, the first second of tonic firing is removed to ensure that only the response to the input stimuli are considered). These values are binned at intervals of 100ms to smooth the data and, ultimately, to allow the observation of low frequency phenomena as this helps remove any high frequency noise. The result is the mean instantaneous firing rate plot for each unit. The mean of these plots is then taken to abstract the signal encoded by the entire channel's output: as the principal interest here is in the impact that EP output has on its downstream targets in brainstem and thalamus, the output of the entire channel is of most relevance. This *mean* mean instantaneous firing rate plot (henceforth termed the instantaneous rate plot $F(t)$ in deference to brevity) for the example simulation is shown in Figure 4.2b. The oscillations in firing rate of the individual spike trains are clearly captured by the mean firing plot for the entire channel.

To determine the selection behaviour of a channel two thresholds for $F(t)$ were set. First, a selection threshold θ_S of 5 spikes/s (illustrated by the bottom broken line): any time that the signal fell below this level the channel was considered to be selected. The value chosen was arbitrary within the basic limits that the selection threshold should be below the tonic

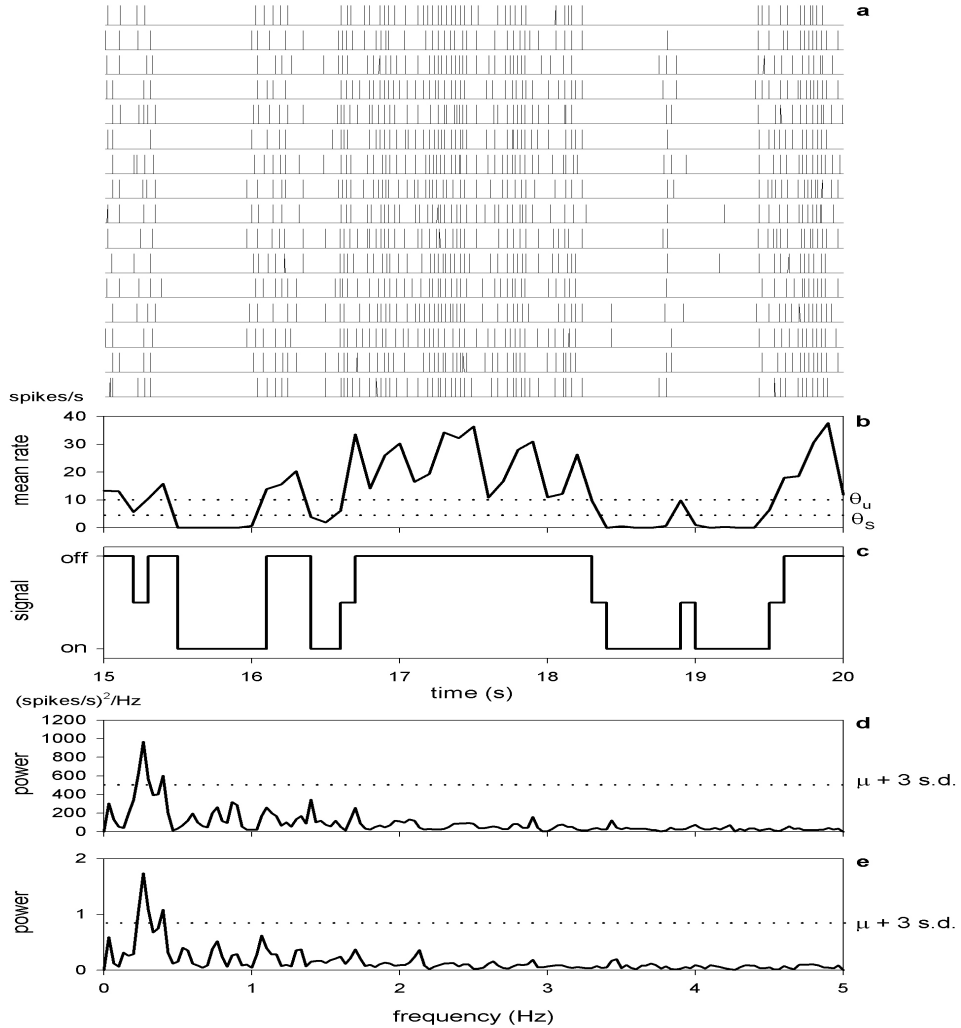


Figure 4.2: Analysis stages for an EP channel from an example simulation of the extended model. **a** 5 seconds of spike train output from each of the 16 units in EP channel 1. Note the common periods of similar firing patterns. **b** The instantaneous rate plot $F(t)$ shows clear oscillatory activity, often falling below the selection threshold θ_S (bottom dotted line). **c** The rectangular wave plot $R(t)$ is derived from $F(t)$ (see text for details). Here it shows how the ON/OFF signal is encoded within the channel output. **d** The power spectrum of $F(t)$, showing a major peak above the confidence limit. **e** the power spectrum of $R(t)$ showing the highest matching peak at 0.3Hz.

output level of the EP (as this is the continuous OFF signal sent to the motor structures) and that there was no *a priori* reason for presuming that only an output of zero spikes/s could indicate selection. Although the case of zero output would undoubtedly indicate unequivocal channel selection, allowances need to be made for the combined effects of noise and spontaneous currents on the output of a unit such that a single spike during a 100ms bin should not preclude that unit from being considered selected. The use of the selection threshold is elaborated in the Discussion.

The use of such a single fixed division between selected and non-selected inputs is probably unrealistic: it is conceivable that EP output levels just above θ_S often result in selection and that those just below would be disrupted by noise (Gurney et al., 2001a). Thus we implemented a second threshold, the “unsure” threshold θ_U set at 10 spikes/s (illustrated by the top broken line) to create a ‘fuzzy’ boundary between selected and non-selected outputs. Any output falling between θ_U and θ_S therefore indicated a potentially selected input. Thus, the addition of this second threshold implemented a stronger test of the basal ganglia’s action selection ability as it was more difficult to achieve a clear dichotomy between selected and non-selected inputs.

As indicated in the Introduction, the output of an EP channel can be thought of as encoding an ON/OFF signal, which can now be explicitly defined in terms of θ_S and θ_U such that any signal below the selection threshold is ON, any above the “unsure” threshold is OFF, and any between the two is undecided. This can be shown through the plotting of a rectangular wave form $R(t)$ generated from $F(t)$ by:

$$R(t)_i = \begin{cases} 0, & \text{if } F(t)_i < \theta_S; \\ 0.5, & \text{if } F(t)_i > \theta_S \text{ and } F(t)_i < \theta_U; \\ 1, & \text{if } F(t)_i > \theta_U \end{cases} \quad (4.12)$$

where i is the sample bin index. Figure 4.2c plots $R(t)$ for the example simulation; the ON/OFF encoding in the EP output is clearly shown.

The analysis of $F(t)$ is further refined by the calculation of its power spectrum to ascertain the dominant frequencies of oscillation. Following Kaneoke & Vitek (1996), we suppose that the presence of oscillations in a unit’s output are shown by a peak or peaks in the power spectrum

that are above some confidence limit. To ensure a minimum number of peaks are selected by this criterion, the confidence limit was set at 99% so that the peak should be greater than the mean μ of the power spectrum plus 3 standard deviations, as illustrated by the broken line in the example power spectrum in Figure 4.2d. As is clear from the example power spectra shown by Kaneoke & Vitek (1996), who used a 95% confidence limit, this method does not necessarily identify a single peak. Moreover, the power spectrum of $F(t)$ may be detecting high frequency oscillations in firing rate during non-selection periods, and sub-selection threshold oscillations during selection. These factors ensure that one cannot distinguish between oscillations in the output firing rate and the oscillations due to selection per se simply by identifying significant peaks in the $F(t)$ power spectrum. Thus, more work is needed to separate, where necessary, the frequency of the output and selection period oscillations and to show that the output is showing behaviour of interest.

A comparison of the power spectra of the rectangular waveform and the corresponding $F(t)$ can be made to elucidate the frequency of selection, as illustrated in Figure 4.2. The power spectrum of $R(t)$ was derived and the peak above the 99% confidence limit noted. This peak is compared with all of the significant points from the power spectrum of $F(t)$, and highest matching peak is taken as the frequency of selection: this is done to take account of sampling inaccuracies which may cause the peaks in the power spectra to not match exactly. For the example simulation results under consideration here, the significant peak in the power spectrum of $R(t)$ matched with the peak of the $F(t)$ power spectrum at 0.3Hz: therefore this was the *periodicity of selection*. This is not to be confused with the *output oscillation frequency* which is just the frequency as determined by the highest significant peak in the power spectrum of $F(t)$.

To emphasise that some novel phenomenon is occurring in the basal ganglia outputs following closely-matched inputs, the spike train response to the ‘control’ case of EP tonic firing alone can be compared. The $F(t)$ plots and power spectra for EP channels 1 and 2 in a simulation of 60 seconds with no inputs are shown in Figure 4.3. For both channels, the mean firing rate was approximately 30 spikes/s and the oscillations in firing rate had small amplitude (Figure 4.3a),

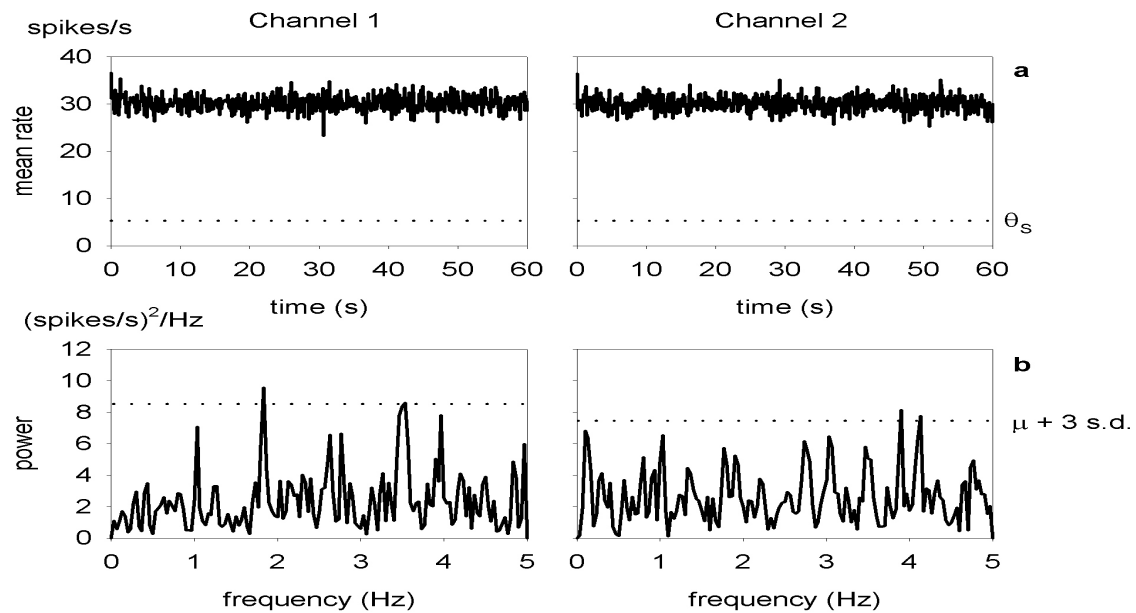


Figure 4.3: **a** Instantaneous rate plots of EP output from a 60 second simulation of the spiking extended model with no inputs. The tonic firing rate of approximately 30 spikes/s was maintained throughout, with no selection occurring. **b** The corresponding power spectra with a wide spread of power across the frequency range and low value peaks indicating that there was no single significant oscillation frequency.

ensuring that no selection occurred - emphasising that the tonic output is the OFF signal to basal ganglia target structures. The lack of any dominant oscillations in the output caused a spread of power in the power spectra, resulting in a wide range of similar height peaks. Thus, while there were significant peaks in the power spectra of $F(t)$ for channels 1 and 2, these peaks did not correspond to the periodicity of selection because no selection occurred.

Selection and switching

The signal $F(t)$ from the example simulation has shown that there is an effect of closely-matched inputs on EP output which is not captured by the systems-level continuous time model. To show that the comparison is valid, it needs to be established that the spiking version of the extended model has similar selection and switching properties to the corresponding continuous time model (the TRN model from chapter 2). Moreover, as noted at the end of chapter 2, this is an essential first step in using the spiking model neuron, as the need to replicate the continuous time model's results has constrained the changes made to the extended model to accommodate the spiking model neuron. Thus, the spiking model was simulated with an equivalent of the simulation set used in chapters 2 and 3 to establish the general selection and switching properties.

Given that θ_S has been set to 5 spikes/s here, and the equivalent value for the continuous time model was 0.05, this 1:100 ratio of firing rate:signal input level was retained for the simulation inputs. Therefore, 121 simulations were run on the spiking extended model, consisting of the sensory input pairs (S_1, S_2) where S_1 and S_2 range from 0 to 100 spikes/s in steps of 10 spikes/s. Simulations were 5 seconds long. The input to channel 1 began at time $t = 1$ second; the input to channel 2 began at $t = 2$. The $F(t)$ for each channel was constructed from the spike trains as detailed in the previous section. For consistency with the analysis of the continuous time models' outputs just θ_S was used as the threshold for selection. Therefore, the characterisation of the four output states (no selection, selection, no switching, switching) was identical to that given in section 2.4.2.

An example of the outputs from the continuous-time and spiking TRN models are shown

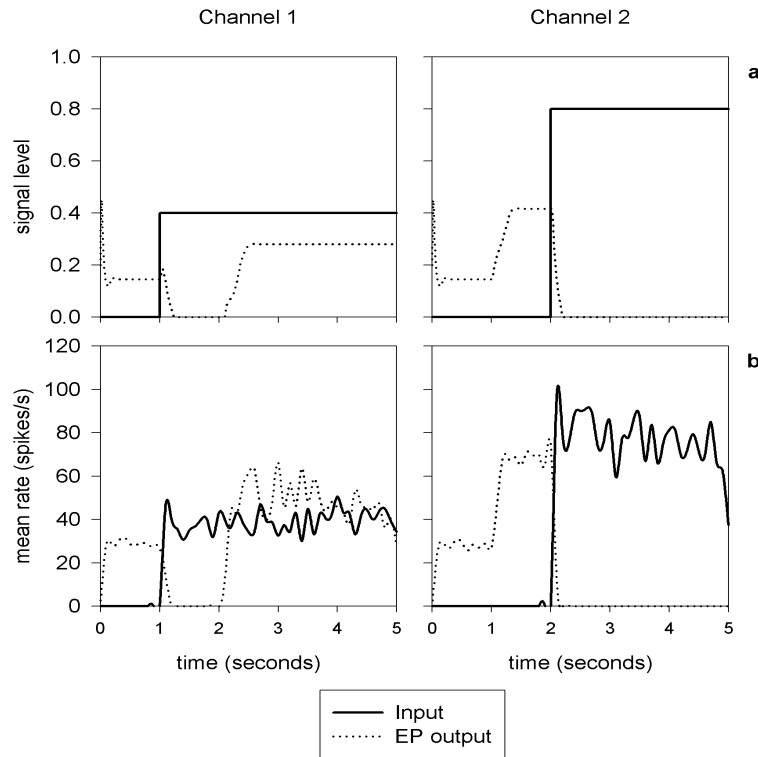


Figure 4.4: A comparison of the selection and switching abilities of the continuous-time (**a**) and spiking (**b**) TRN models. The models received equivalent inputs of 0.4 and 40 spikes/s to channel 1 at $t = 1$, followed by an input of 0.8 and 80 spikes/s to channel 2 at $t = 2$. Selection of channel 1 and switching to channel 2, as signalled by the changes in EP output, occurred in both models in approximately equivalent time-scales.

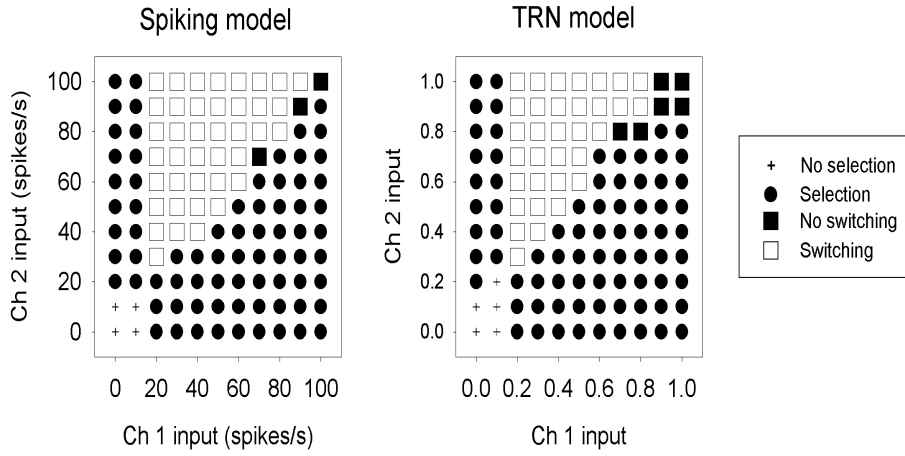


Figure 4.5: The selection and switching properties of the spiking extended model were similar to the continuous time TRN model. Low level selection in the two models occurred at equivalent saliences (20 spikes/s and 0.2).

in Figure 4.4 for the sensory input pairs ($S_1 = 0.4, S_2 = 0.8$) and ($S_1 = 40$ spikes/s, $S_2 = 80$ spikes/s), respectively. The summary plots for all input pairs in Figure 4.5 show that the output states of the spiking model (left-hand plot) were very similar to those of the continuous time TRN model (right-hand plot). Low salience selection and the initial case of switching occurred following equivalent salience inputs to both models. Furthermore, the spiking model showed a majority of single channel selection states, and many successful switching states. Thus, the spiking version of the extended model retained the basic selection and switching properties of the continuous time model, emphasising the validity of comparisons between the two model types. Moreover, the replication of the TRN model's results has established that the changes made to accommodate the spiking model neurons has not altered the ability of the basal ganglia to function as a switching mechanism.

Two modes of oscillatory behaviour

I turn now to the examination of the results for the full extended model (four complete sets of simulations from the experiment matrix). The first concern is the two active channels: the EP output of the third, non-active, channel will be examined in the subsequent section. Here, the

selection time is determined first, which is just the total period of the ON signal from $R(t)$, for each channel for any given input. These are plotted in Figure 4.6a as a function of S_{min} for each ϕS value. In both channels, for every ϕS , the selection time was a monotonically increasing function of S_{min} , and the ordering of ϕS was preserved throughout. Further, it appears that a difference of just 2 spikes/s between the inputs to the two channels at the lowest absolute salience level ($S_{min} = 20$) was sufficient for the channel with the higher input to show selection, albeit briefly.

The proportion of total selected time (combined from both channels) to non-selected time was also a monotonically increasing function of S_{min} and showed preservation of the order of ϕS (see Figure 4.6c). At higher ϕS and S_{min} selection occurred throughout almost all of the duration of the simulations, indicating that the degree of continual action selection is directly dependent on the absolute salience level of the competing actions. Further, the mean spike rate * for each channel, depicted in Figure 4.6, was a monotonically decreasing function of S_{min} . Taken together, these results illustrate how the basal ganglia output directly encoded the level of sensory input both in the firing rate of the output and proportion of time containing a selected action.

Of particular interest to us, given the underlying hypothesis that the basal ganglia output governs action selection, is the degree to which the ON signals from the two active channels overlapped (that is, how long both channel 1 and channel 2 EP outputs were simultaneously θ_S). For most of the input pair combinations, the output was strictly non-overlapping. Overlapping ON signals were only observed for $S_{min} = 65$, which is not surprising given that channel 2 was selected for most of the duration of the simulation at this level, and so the very short channel 1 selection periods were superimposed on this continuous selection. Figure 4.7 shows that these periods of overlap are at the lower limit of those discernible from $F(t)$, given that a single bin is 100ms in width, and that not all simulations with the same inputs had overlapping channel selections.

For all simulations, the periodicity of selection, as determined from $R(t)$, had a very low

*This is calculated directly from the spike trains by $\sum_{i=1}^n (N_i^s/T)/n$ where N_i^s is the total number of spikes for unit i , T is the duration of the simulation in seconds, and n is the number of units.

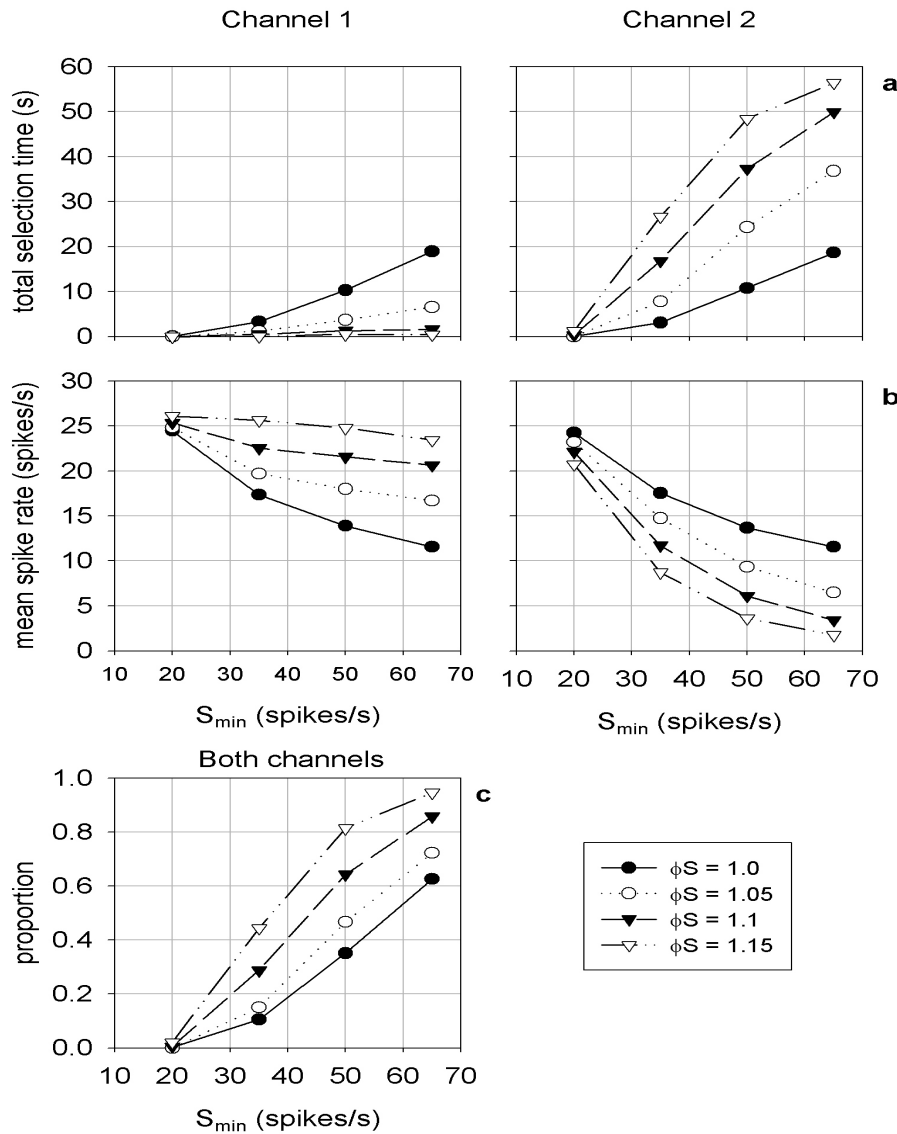


Figure 4.6: Summary statistics of four simulations of the extended model - all the values given are averaged over the simulation sets. **a** The total time spent selected for each channel was a monotonically increasing function of the input level, and was ordered according to ϕS . **b** Similarly, the mean spike rate maintained the ϕS order, and was a monotonically decreasing function of the input level. **c** The ratio of the total period of the simulation when either channel was selected to the total non-selected time.

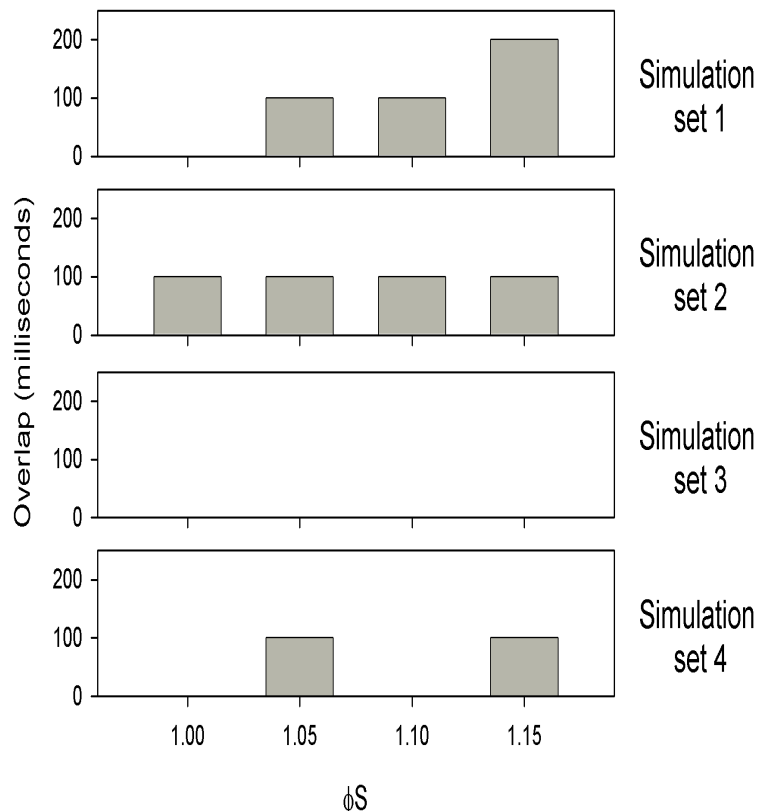


Figure 4.7: Length of time that channel 1 and channel 2 EP outputs were simultaneously below θ_S for all four simulations with $S_{min} = 65$ spikes/s from each of the four simulation sets. Channel selection overlap did not occur in all simulations and simulation sets, and was at the lowest detectable limit given that a single sample bin was 100ms.

frequency - consistently less than 1 Hz. The four sets of simulations also showed two distinct modes of oscillatory behaviour (illustrated in Figure 4.8). The periodicity showed a mono-modal distribution with increasing S_{min} for both channels and the majority of ϕS values in sets 1 and 3. For the other two sets, there was no such consistent relationship: for most ϕS the frequency of selection at $S_{min} = 65$ was greater than at $S_{min} = 50$. For all simulation sets, no periodicity of selection were observed in either channel for the lowest input level ($S_{min} = 20$) except when the inputs were most differentiated ($\phi S = 1.15$). A consideration of the maximum peaks in the $F(t)$ power spectra from set 3, shown in Figure 4.9, highlights the discrepancy between the detected frequencies of output oscillation and the periodicity of selection. Particularly noticeable is the oscillations in the output of channel 1 which, other than for $\phi S = 1$, were a monotonically increasing function of S_{min} after $S_{min} = 35$. The output oscillations of channel 2 were less than 1Hz for all simulations in which selection occurred, although they did not follow the patterning of the selection periodicity.

The mono-modal distribution of selection periodicity was correlated with the distribution of the number of bouts of selection (shown in Figure 4.9 for simulation set 3). The number of bouts in channel 2 was not a linear function of S_{min} for most ϕS due to the length of the selection periods - the greater the total selection time, the less bouts there can be in any period under consideration. Thus, the fall-off in the number of bouts of selection corresponded to the reduction in the periodicity of selection.

The non-active channel

I turn now to consider the third channel's EP output, which received no sensory input in each of the four sets of simulations. The first somewhat trivial result was that there was no selection of channel 3 in any simulation set. This exactly replicated the findings from the systems-level intrinsic and TRN models that a channel receiving no input (a non-active channel) showed no selection in its EP output (see Figure 2.3 for examples of channel 3 output in the higher level models). Of course, as there was no selection, no periodicity of selection needed to be determined.

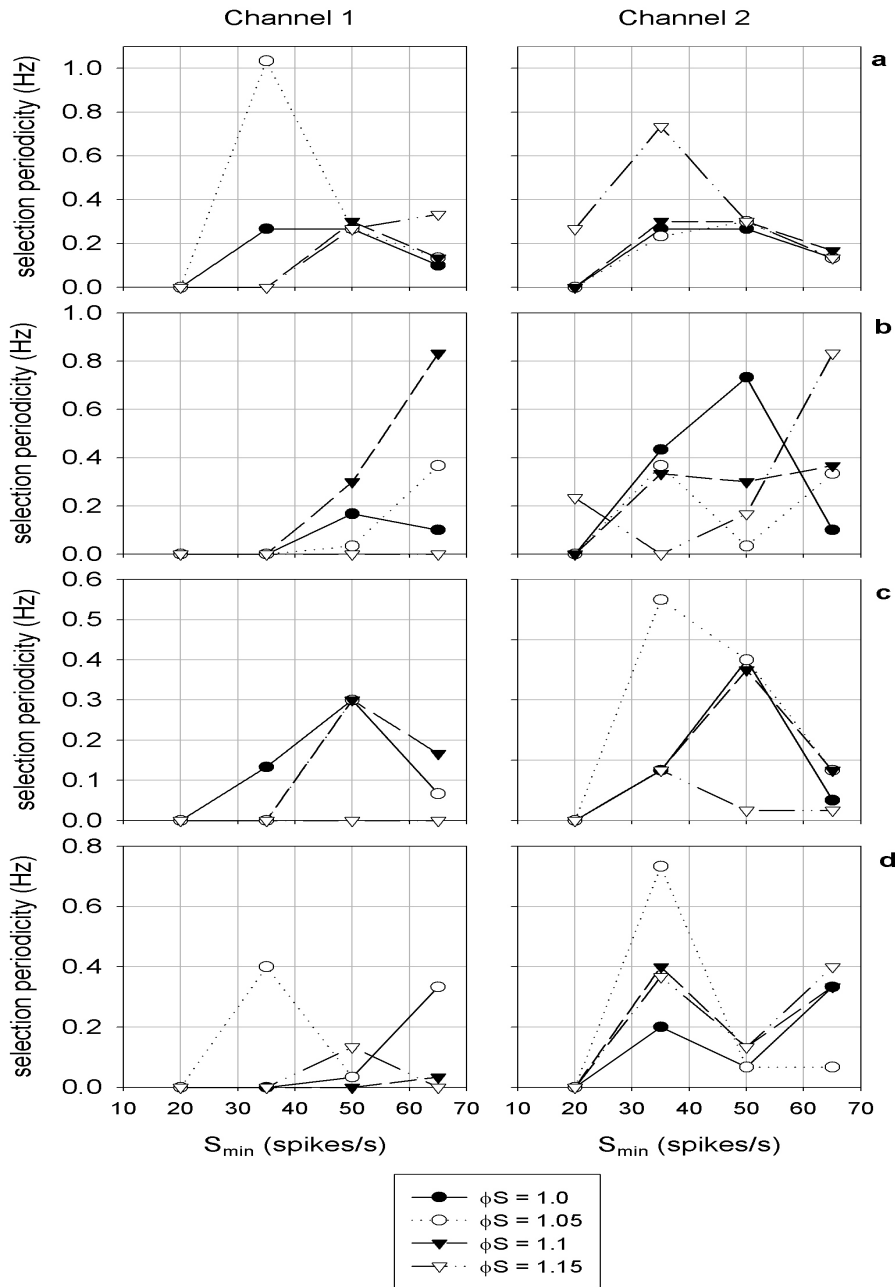


Figure 4.8: Frequencies of selection periodicity for all four simulations sets. There were two modes of selection periodicity observed in the four sets: a mono-modal distribution (**a, c** from sets 1 and 3), and a seemingly chaotic distribution (**b, d** from sets 2 and 4).

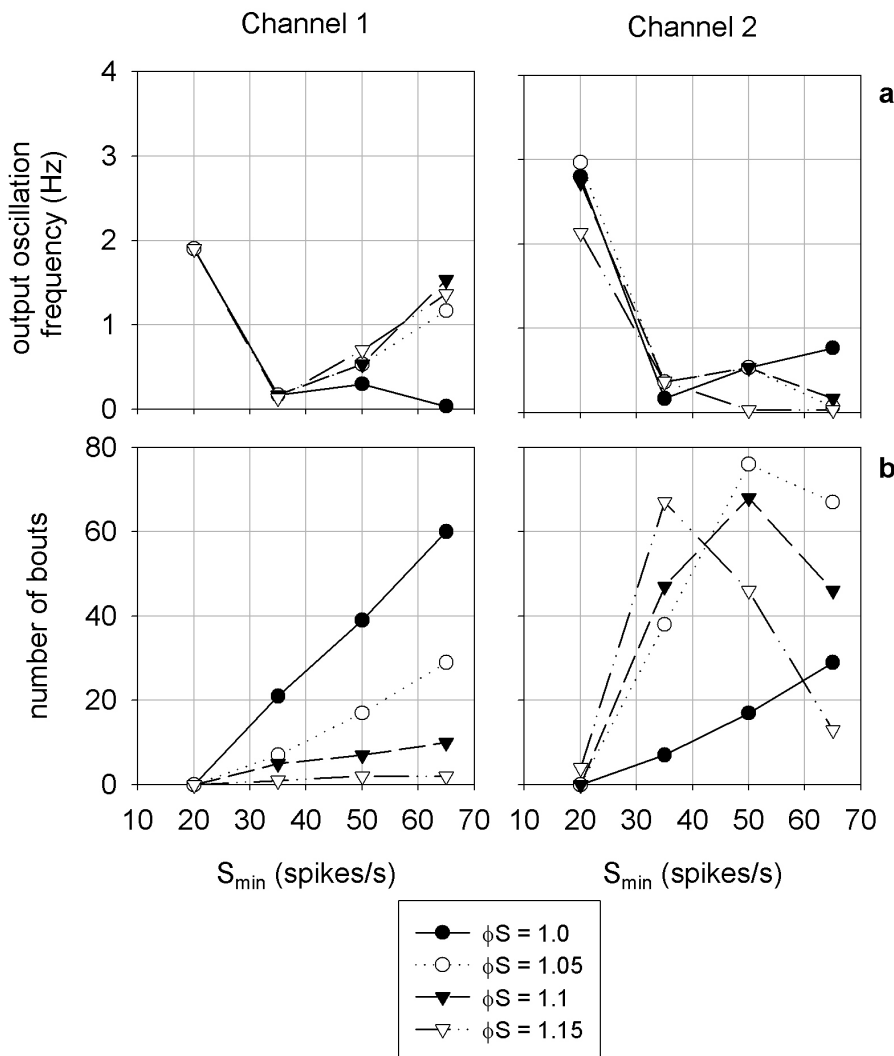


Figure 4.9: **a** Output oscillation frequencies and selection bouts from simulation set 3. The main frequency of oscillation in the EP output was not necessarily the periodicity of selection (compare with Figure 4.8c). **b** The mono-modal distribution was correlated with the number of bouts of selection observed - the decrease in the number of bouts in channel 2 corresponded to a decrease in selection periodicity (from set 3).

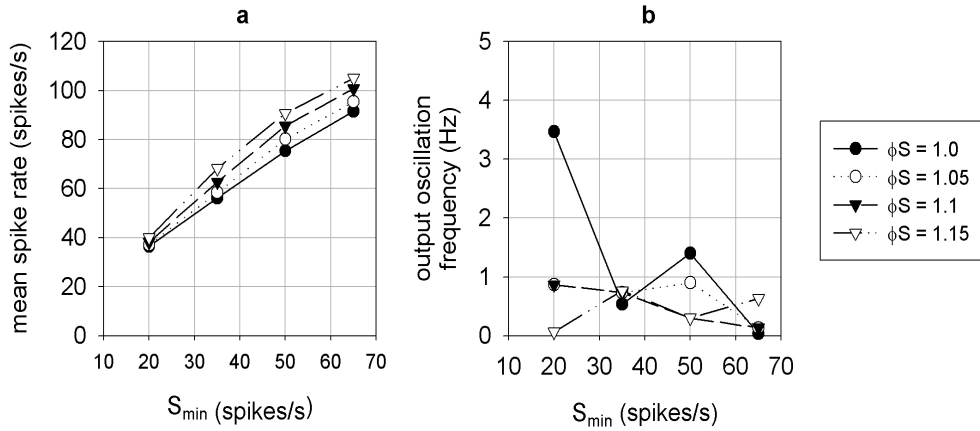


Figure 4.10: Mean spike rates and output oscillation frequencies of channel 3's EP output in the first simulation set. **a** The mean spike rate was a linearly increasing function of the input level. **b** EP output showed $\leq 1\text{Hz}$ oscillations for the majority of simulations in which selection occurred on the active channels

The mean spike rate and output oscillation frequency for every simulation in the first set are plotted in Figure 4.10. For every ϕS level, the mean spike rate was a linearly increasing function of the input level. This is diametrically opposite to the monotonic decrease in mean spike rate as a function of input level observed in both of the active channels (in the previous section). Therefore, the general increase in output emphasised the contrast between the active and non-active channels and, furthermore, the contrast between any selected channel and all non-active channels.

In contrast to the mean spike rate changes with input level, the non-active channel's EP output oscillation frequencies were similar to those seen in the active channels (compare Figure 4.9). For low input values the frequencies were spread across the whole detectable range (0-5Hz). With increasing input levels, the frequencies were mostly restricted to $\leq 1\text{Hz}$. The simulations in which this occurred also had selection of at least one active channel. Combining the results of this and the previous section it appears that, generally, the EP output oscillations in all channels are restricted in frequency when selection occurs. This suggests that selection of the active channels affects the output oscillation frequencies of the non-active channel. Furthermore, the

non-active channel is, by definition, receiving no input, and so its striatal D1 unit population has no output. Thus, the generation of the oscillations in the non-active channel's output cannot be dependent on striatal D1 unit input to EP.

4.3.2 Dopamine level changes

Following on from the successful simulations which generated outputs consistent with dopamine-related disorders in the higher-level basal ganglia models (see sections 1.4.2 and 2.5.3), the effect of changing dopamine levels on the oscillations in EP output was investigated. The experiment matrix was run twice on the extended model, once with no dopamine ($\lambda_e, \lambda_g = 0$), simulating a Parkinsonian-like condition, and once with high dopamine levels ($\lambda_e, \lambda_g = 0.8$).

The results for the no dopamine condition are summarised in Figure 4.11. Consistent with previous findings, the removal of dopamine prevented any selection from occurring in either channel, regardless of the input or ϕS value. Further, the relationship between input level and the mean spike rate was altered: mean spike rate became a monotonically increasing function of S_{min} , although the corresponding ordering of ϕS was maintained. This result suggests that the removal of dopamine inverts the effect that the EP's inputs have on its output.

Although the mean spike rate was a monotonically increasing function of input, the EP output oscillations output bore no obvious relation to input levels, and their frequencies covered the entire detectable range.

High dopamine levels caused the simultaneous and continuous selection of all active channels at all input levels (Figure 4.12). With the exception of the lowest input level, $S_{min} = 20$, the selection occurred for the entire duration of the stimuli. At the lowest input level, the time of selection was directly dependent on ϕS , and maintained the order of ϕ_s in both channels (again inverted in channel 1). This confirmed the simultaneous selection seen after increasing dopamine levels in the previous continuous-time models of basal ganglia (Humphries and Gurney, 2002; Gurney et al., 2001b).

Periodicity of selection was only detected for the simulations with the lowest input levels $S_{min} = 20$ because of the continuous selection of the EP channel outputs in all other simulations.

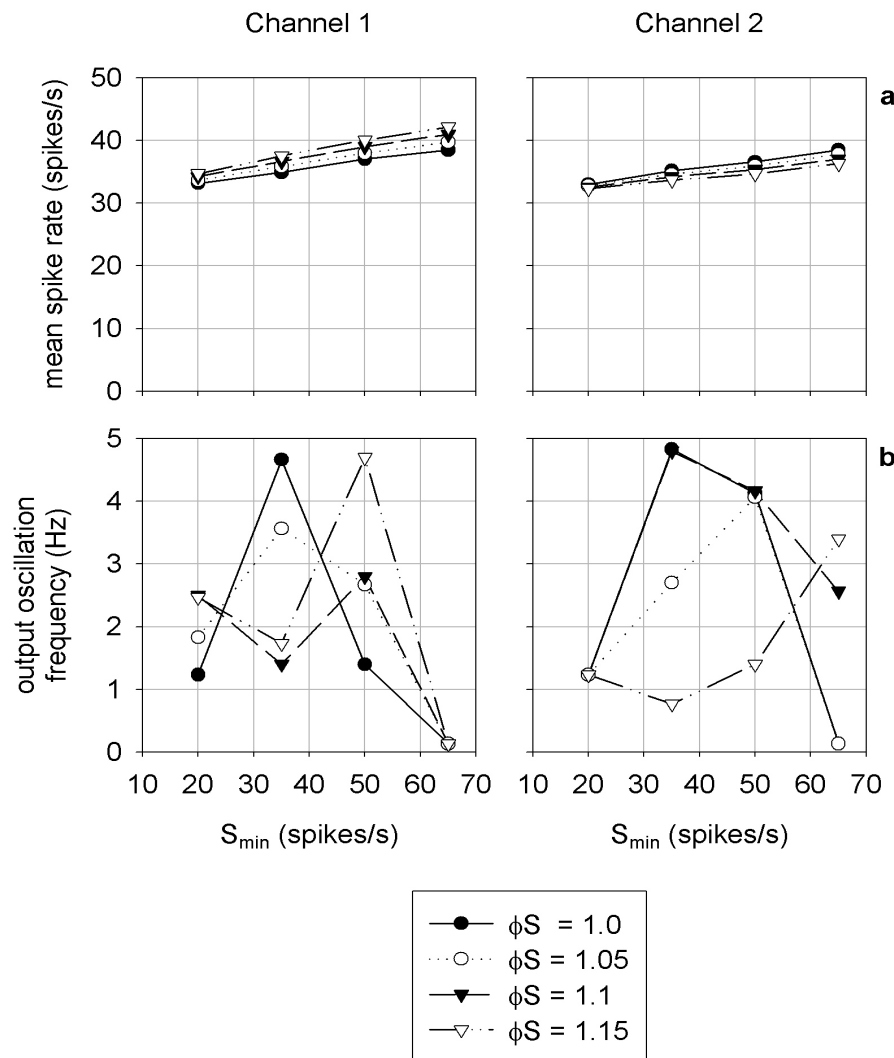


Figure 4.11: The removal of dopamine prevented selection and altered the input-output relations in terms of the mean spike rate (a - compare with Figure 4.6b) and the oscillations in EP output (b).

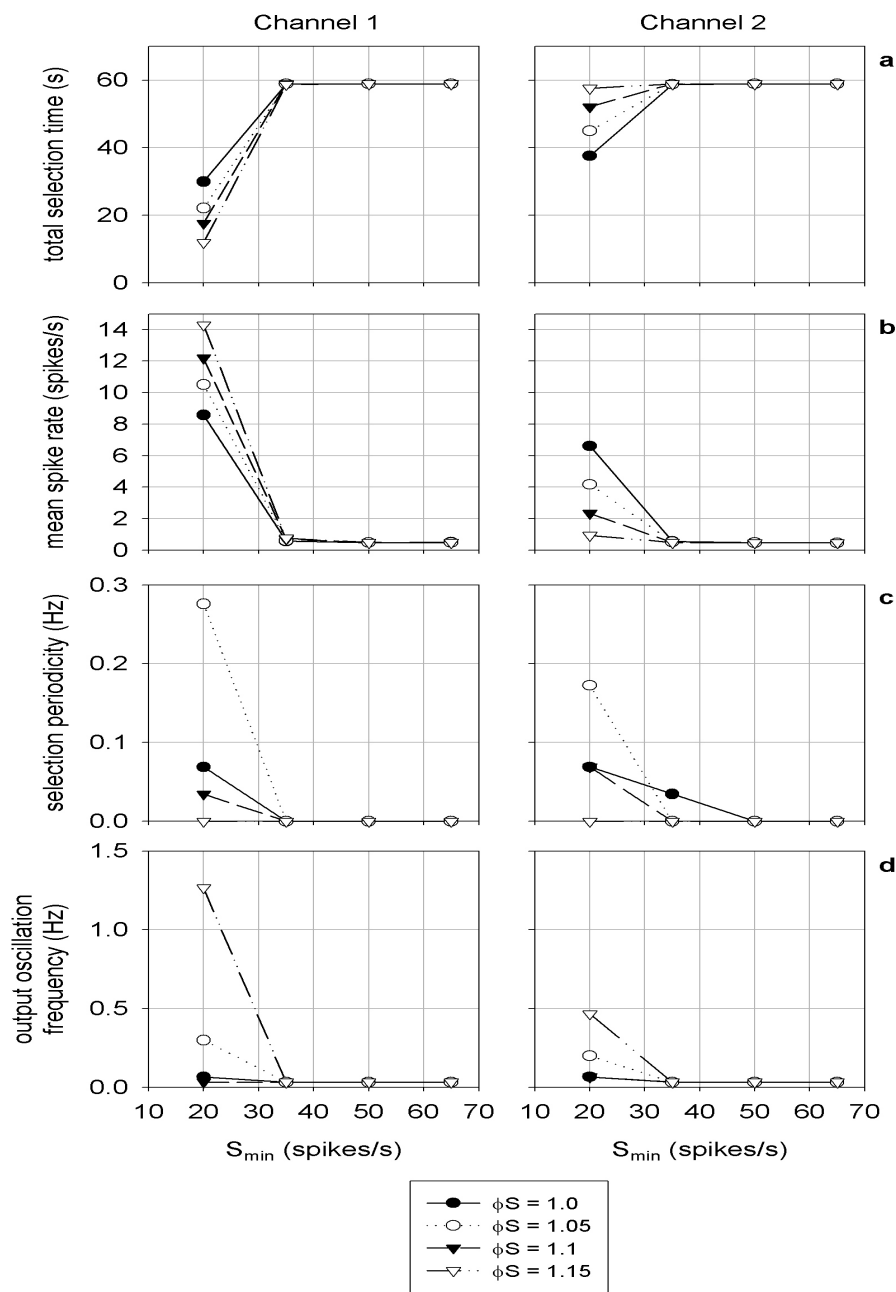


Figure 4.12: **a** Increasing dopamine levels led to the continuous and simultaneous selection of both channels following most inputs. **b** Correspondingly, the mean spike rate approached zero with increasing input levels. **c** Periodicities of selection were only detectable for the lowest input levels, where the selection was less than the total simulation duration. **d** The output oscillation frequencies corresponded to the very low mean spike rate.

However, the same outputs showed low frequency oscillations in the power spectra of $F(t)$ as there were sub θ_S oscillations, emphasising the importance and effectiveness of comparing the power spectrum peaks of $F(t)$ and $R(t)$ to elucidate the periodicity of selection.

4.3.3 The role of noise

Having established that oscillations in selection exist in the basal ganglia output of the extended model, I turned to the investigation of their underlying cause. Although extensive exploration of all possible oscillatory mechanisms within the model were beyond the scope of the current study, there was an obvious preliminary suggestion: that the oscillations were due to the noise component in the membrane equations (equation 4.7) because the continuous time models, which showed no oscillations with equivalent inputs, had no noise component. Thus, a full set of experiment matrix simulations was run on a completely noise-free extended model which had all of the I_{noise} currents set to zero in every structure. Furthermore, to ensure the complete removal of any source of noise, the sensory input was comprised of 16 fixed interval spike trains per channel so that each input in a channel was in exact synchrony with the other 15.

The most striking result, shown in Figure 4.13c, was that there was no periodicity of selection. The output oscillation frequency plots in Figure 4.13d show that the response to increasing S_{min} levels contained no discernible pattern for any ϕS level. Due to the lack of noise the $\phi S = 1$ outputs were identical for both channels and so have the same output oscillation frequencies.

The lack of selection periodicity is not surprising if one considers the selection time for each channel: where there was selection, it was for a small proportion of the total simulation time (see Figure 4.13a). Moreover, there was no selection of the lower frequency inputs and channel 1 showed no selection at all.

Somewhat paradoxically, the monotonic relationship between S_{min} and mean spike rate and its preserving of the order of ϕS , as found in the normal extended model, broke down following the removal of noise. Similar to the effect of removing dopamine reported in section 4.3.2, the noise-free model showed an inversion of the normal influence of the EP's afferent inputs, such that the output was not inversely related to the scalar value of the input, suggesting the

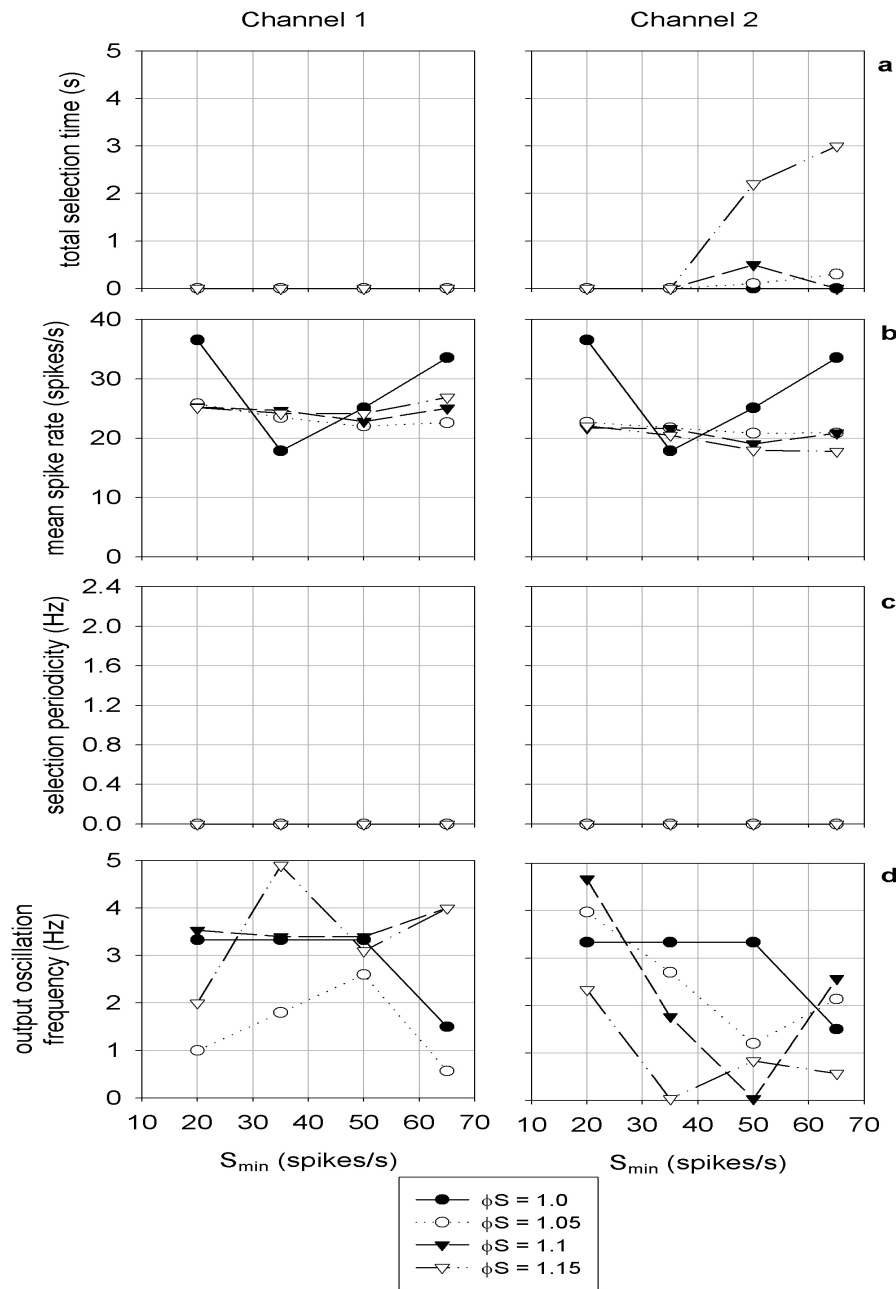


Figure 4.13: The effects of removing noise from the extended model. **a** Selection only occurred in channel 2, and then only at high input levels. **b** The mean spike rate showed no discernible correlation with the input level. **c** Periodicity of selection plotted against input level - no periodicity was detected. **d** Distribution of EP output oscillation frequency with respect to the input level.

domination of excitatory input (from STN) over the inhibitory input (from GP and the D1-type striatal neuron population).

To confirm that these results were dependent only on the complete removal of noise, two further sets of simulations were run which contained partial noise sources. The first set were run on a version of the extended which maintained the synchronised inputs, but was otherwise identical to the model tested in section 4.3.1 (i.e. with membrane noise reinstated). The second set was run on a model with all I_{noise} currents set to zero and again with fixed-interval inputs, but with the individual spike trains of the inputs starting at a random time within the first period (i.e. within 1/(spikes/s) ms) to ensure that all of the spike trains were not identical (thereby creating ‘phasic’ noise). Both of these sets of simulations showed some selection, though again for much shorter periods, and had detected selection periodicities, though only in channel 2 (not shown).

4.4 Discussion

The primary finding of this chapter is that, in a spiking-neuron based model of the basal ganglia and associated thalamocortical loop, closely matched sensory inputs cause the outputs of all active EP channels to oscillate and that this oscillation corresponds to alternations of selections both within and across channels. Further, these alternations of selection showed two modes of behaviour in the frequency domain: selection periodicity either had a mono-modal or a chaotic distribution with respect to the input level. Regardless of the mode, the selection periodicity was typically less than 1Hz. Thus, the outputs encoded slow oscillations in the ON/OFF signal, and the ON (selected) component did not significantly overlap across the active channels.

In terms of the requirements for a selection mechanism outlined in section 2.2.3, it is evident that the desired characteristic of persistence was lost following the most closely matched inputs: the EP outputs showed a form of ‘dithering’. The implications of this are discussed below (section 4.4.1). In contrast, clean switching was maintained as the active channels showed minimal levels of overlap between periods of selection.

The oscillations in EP output determined from the peak of the channel’s power spectrum did

not necessarily match the frequency of the selection periodicity. However, it was generally the case that the output oscillations were also restricted to the sub-1Hz range. This was also true of the non-active channel, which showed no selection. Thus, there is a clear distinction between the frequency of oscillations in the EP output and the specific periodicity of the selection.

The detectable frequency range was necessarily bounded by, first, the use of 100ms sample bins which gave an upper limit of 5 Hz and, second, the use of 59 seconds of simulated spike train data gave a lower limit of 0.034 Hz. Within these bounds it is not clear what factors determined the specific frequency of the selection periodicity or, where it differed, of the oscillations in EP output. The only definite influence was that of noise: the lack of consistent input rate-selection periodicity pattern across the four simulation sets could only have been due to the membrane noise component and randomly-generated sensory input interspike intervals. However, the noise only varied the selection periodicity within the 0-1 Hz range, and there is no indication of what set that range in the first place. Possibilities include the values of the time constants τ_m and τ_s which dictate how inputs to the model neuron integrate over time.

Comparing the EP output following closely matched inputs to the tonic EP output without stimuli showed that the existence of oscillations in the output were dependent on there being non-zero input and that they were not a native state of the network. Further, it was shown that the EP output of all channels reliably encodes the relative strength of channel input in the mean spike rate of the entire channel's output - for the active channels this was a monotonic inverse relation; for the non-active channels a positive, roughly linear relation. In the active channels, the total selection time of a channel and the proportion of simulation time during which selection occurred also reliably encoded the absolute level of sensory input to the network. These statistics were consistent across all four of the simulation sets and, therefore, it must be concluded that they cannot be used to uniquely identify the mode (mono-modal or chaotic) of selection periodicity.

Changes in dopamine level disrupted the input-output relationships of the extended model. Increasing or decreasing tonic dopamine led to the dissociation of the output oscillations from the input level. High dopamine levels led to the continuous and concurrent selection of both

channels for the entire post-stimulus onset period for most input levels. Moreover, the inversion of the input-mean spike rate relation following the removal of dopamine indicated that a lack of dopamine reduces the effectiveness of the striatal and GP inputs to the EP and allowed the STN to become the dominant determinant of EP output. However, some effect of the inhibitory input must have remained as the mean spike rate in EP's channel 2 was consistently less than that of channel 1 even though channel 2 had the same or higher input (S_{min}) in every simulation.

The removal of noise led to the model being unable to show selection following most inputs and to the considerable shortening of the total selection time for all selectable inputs. This resulted in the absence of any detected selection periodicity. Further, the monotonic, ϕS ordered, relationship between input level and mean spike rate broke down, and the output oscillations were chaotic with respect to the input. In addition, the two further sets of simulations with partial noise (one with membrane noise, one with phasic noise) did have some detected selection periodicities (though all the other results were similar to the completely noise-free simulations). From these combined results three important conclusions can be drawn. First, the presence of noise is essential for ensuring that the selection of an action occurs with low salience inputs and that the action is selected for a considerable period of time; this will be expanded upon below. Second, noise plays a seemingly paradoxical role in ensuring that a unit ensemble's output (i.e. a channel) is a coherent representation of the network input. Third, noise is essential for the occurrence of selection periodicity within a channel's output and, therefore, for the alternation of selection across channels.

Finally, all of the oscillatory phenomena observed may be dependent on the use of the more detailed spiking model. As discussed in the introduction, the previous continuous time basal ganglia models did not show any oscillatory activity in EP output following closely matched inputs. Further, because the basic selection and switching properties of the continuous time models were maintained in the spiking extended model, the existence of oscillatory output in the latter model did not occur due to changes in the basal ganglia's basic action selection functions.

However, I cannot discount the possibility that adding some form of suitably structured noise to a continuous-time model would result in similar low-frequency oscillations of selection. The noise would have to mimic the combination of the membrane noise component and the inter-spike interval noise present in the spiking TRN model: previous simulations (not reported here) have shown that the simple addition of a suitably-scaled Gaussian noise source to the units in the continuous-time TRN model is insufficient to cause selection oscillations.

Nevertheless, the primary aim of this chapter has been fulfilled by using the spiking model neuron to elucidate the exact nature of the spike trains underlying the mean firing rate output of the higher-level models. In addition, the maintenance of the selection and switching properties of the basal ganglia models when instantiated at a lower level of description provides further support for the hypothesis that the basal ganglia play a crucial role in action selection.

4.4.1 Behavioural consequences

The slow oscillations in the EP outputs of the active channels, corresponding to an ON/OFF signal to the thalamus and brainstem motor plant, and the clean switching between channels implies that closely matched saliences cause rapid alternations of behaviour. Such rapid switching characterises disorders such as ADHD and, therefore, a possible mechanism underlying these disorders could be a failure to sufficiently differentiate saliences.

The rapid alternations between selected channels, resulting from the most closely matched inputs, violate the requirement that a selected action should persist. Indeed, with equal salience inputs, the model appears to be ‘dithering’ between the choices of selected channel. The phenomenon of dithering has been observed in animal behaviour studies (Houston and Sumida, 1985) which could be taken as indicative of the imperfect *in vivo* performance of the neural action selection mechanism (whatever that may be). Thus, based on the hypothesis that the basal ganglia is a crucial action selection mechanism, it may be suggested that dithering may be the result of multiple competing actions with closely matched saliences causing rapid alternations of the selected channel in the basal ganglia output nuclei.

The behavioural significance of the EP outputs following the removal of noise from the

network is manifold: on one hand if, as we've just suggested, noise acts to regularise the model's response to a wide range of inputs then this would allow the behavioural result of a competing set of actions to become predictable, thus facilitating learning and automation of sequences of motor behaviours (Hikosaka, 1991; Hikosaka et al., 1999). In addition, the lack of selection with closely matched low salience actions suggests that noise is also essential for resolving low-level competitions so that an animal has an action to proceed with, as the alternative is to remain in a quiescent state, vulnerable to natural hazards.

The model's responses to dopamine level changes showed that significant oscillations in the output depended upon dopamine being present at 'normal' levels. Thus, any behaviours resulting from these oscillations would only be observable in animals with intact, healthy, dopamine systems. Moreover, the continuous, simultaneous selection and complete lack of selection following dopamine level increases and decreases, respectively, provided support for the hypothesis concerning the role of dopamine in action selection (see chapter 1). The breakdown in action selection ability following the removal of dopamine may underlie the difficulty in initiating movement in Parkinson's Disease (Bergman, Feingold, Nini, Raz, Slovin, Abeles, and Vaadia, 1998). Further, the inversion of the relationship between input level and mean spike rate observed with no dopamine suggests that the difficulty in initiating movement may be directly correlated with the urgency of that movement.

4.4.2 Methodological considerations

There are two main caveats concerning the interpretation of the model's results. First, the stimuli are continuously input to the model for 59 seconds at a fixed mean rate, which is probably not a realistic simulation of the *in vivo* sensory input to basal ganglia in a natural context: the mean rate would fluctuate with changes in the environment and, in any case, neurons would show adaptation to the stimulus after such a long presentation (Rieke, Warland, de Ruyter van Steveninck, and Bialek, 1999). Long continuous inputs were used to explore the properties of the extended model, and these properties (of selection periodicity, clean switching, and so on) would underlie any operation the basal ganglia performs in 'normal' circumstances.

Second, the use of a fixed θ_S value to determine the selection/non-selection distinction in EP channels' output may not be biologically realistic. A fixed value of θ_S was used to simplify the analysis of the complex data sets. However, it is reasonable to suppose that the actual value of θ_S is directly dependent on the strength of the command signal to the motor plant: a stronger signal is associated with higher θ_S , as it becomes easier to overcome the inhibition from EP. Conceivably, a sufficiently strong motor command signal could overcome the tonic EP output (the OFF signal), such as when voluntary movement is successfully initiated by a Parkinsonian patient.

There would only be a cortical input level dependent variability of θ_S if EP neurons' synaptic input to their brainstem targets is additive (i.e. the post-synaptic potentials sum linearly). If the EP neurons' input is multiplicative then the cortical input would be gated (similar to the dopaminergic synapses on striatal neurons - see equation 4.8), thus making the strength of that input irrelevant to the value of θ_S . Therefore, it would be prudent to carry out a comparative study of how the two different types of synaptic contact between EP units and brainstem structures would affect the output of brainstem units: firstly, between variable and fixed θ_S additive synapse models and, secondly, between these models and a fixed θ_S , multiplicative synapse model.

4.4.3 Conclusions

The slow oscillations of EP output observed in the computational model of the basal ganglia may underlie disorders that are characterised by rapid alternations of behaviour. I have established that the presence of noise is necessary for these alternations of selection to occur, though undoubtedly the structure of the basal ganglia circuitry is crucial too: this is the subject of ongoing work. Furthermore, we determined that noise plays a crucial role within the basal ganglia both in creating coherent responses to inputs (in terms of spike rate) and in allowing low salience actions to be selected.

The use of spiking model neurons fulfilled the primary aim of studying the form of spike trains underlying the mean firing rate outputs of higher level models. This success underscores

the importance of studying a neural circuit at multiple levels of description, and of using models at each of those levels of detail to determine functions and behaviours that are not evident *a priori* from an analysis of the connectivity. The greater detail obtainable by these relatively simple model units, compared to mean-firing rate output units, reinforces the case for their adoption in all large-scale models of neural circuits (Humphries and Gurney, 2001). I turn now to the question of whether the spiking model neuron can be adapted to accurately simulate neural circuit behaviour that is dependent on intra-cellular mechanisms, a domain normally restricted to multi-compartment models.

Chapter 5

STN-GP loop bursting

5.1 Introduction*

In the last chapter we saw that an ensemble of spiking model neurons could replace the single leaky-integrator neuron of the continuous-time models as the representation of a channel. Moreover, in doing so a more detailed study of the basal ganglia output was facilitated, resulting in the discovery of low frequency oscillations in channel selection following closely matched inputs. Thus, the conclusion was reached that this spiking model ‘mid-point’ in a model complexity spectrum between leaky-integrator and conductance-based compartmental models could successfully capture the dynamics of a complex neural circuit.

Continuing the exploration of the use of spiking models, the following question is posed: can the component neurons of the basal ganglia’s circuits be modelled at a lower level, incorporating some intrinsic membrane properties, yet retain the inherent simplicity of the phenomenological modelling approach? The increased computational requirements of the more complex model units limits the model network to a sub-circuit of the basal ganglia. Thus, the present chapter details an attempt to simulate the results of Plenz and Kitai’s (1999) STN-GP sub-circuit study: the gross anatomical connectivity of the circuit cultured by Plenz and Kitai is shown in Figure 5.1.

The work of Plenz and Kitai (1999) was based on single- and multi-unit recordings from

*This chapter is based on material previously presented in Humphries and Gurney (2001).

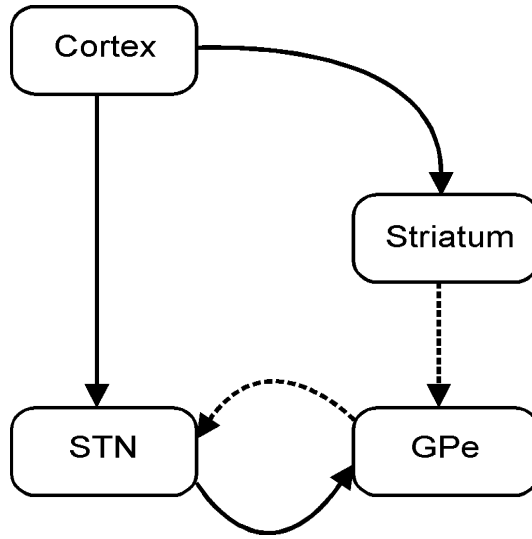


Figure 5.1: The basal ganglia circuit cultured by Plenz and Kitai (1999). Solid line: excitatory; Dashed line: inhibitory.

an *in vitro* organotypic culture obtained from neonatal rats. The STN-GP circuit showed synchronised spontaneous burst firing between STN neuron pairs and STN-GP neuron pairs at two main burst frequencies - 0.4 and 0.8Hz - in the complete culture (*cortex-intact* condition). Further, lesioning the cortex caused the bursting to occur predominantly at 0.8Hz (*cortex-disconnected* condition). Striatal lesions did not affect bursting frequency. This is not surprising as striatal neurons are generally silent unless driven by co-ordinated afferent input which shifts them from their DOWN-state to their firing-ready UP-state (Wickens and Wilson, 1998; Gerfen and Wilson, 1996). Therefore, the GP receives little or no inhibitory input from striatum and, hence, the striatum has no effect on the bursting in the STN-GP loop.

Plenz and Kitai concluded that the STN-GP circuit could act as a central pacemaker for the basal ganglia, controlling temporal aspects of processing. This suggests the hypothesis that the bursting is due to intrinsic properties of the STN-GP circuit which can be modulated by cortical input. In particular I make the hypothesis that the bursting behaviour observed by Plenz and Kitai was initiated by the Ca^{2+} current-based mechanism described by Beurrier, Congar, Bioulac, and Hammond (1999) . Under this assumption, the model was able to explain the mono-modal bursting without cortical input but was unable to replicate the diversity of

behaviour that occurred with cortical input. However, I then went on to incorporate the effects on the membrane potential due to the relative distribution of GP synapses over the surface of neurons in STN. This extra degree of realism gave the model the ability to show behaviour similar to that observed by Plenz and Kitai in their cultures with cortex intact.

Details of the Ca^{2+} current and synaptic distributions, together with their respective model counterparts, are given in the Methods. However the underlying methodology that allows their incorporation into the spiking neuron model is to continue in the spirit adopted in developing the basic model itself. That is, each further contribution to the membrane potential may be modelled using an additional functional component, explicitly crafted to capture the phenomenological time course of the corresponding potential component. Thus, at this level of modelling, the functional form of the membrane potential is not derived from more fundamental physical processes (such as ion channels).

The reader should note that the model discussed in this chapter does not explicitly address any questions about action selection. As there is no EP or SNr, there is no ‘output’ of the model which requires interpretation in behavioural terms. More importantly, there is no salience input - where there is input to the model it is simulating the background activity of cortical cells. The explicit focus of this chapter is on the development of the spiking class of model neurons within the framework of a basal ganglia sub-circuit. Any features of the STN-GP loop’s behaviour which pertain to action selection will of course be highlighted in the discussion - but more important is that this model is the first step in developing a full basal ganglia model at a yet lower level of description.

5.2 Method

5.2.1 Extending the model neuron

The basic equations used for the model neuron in this chapter are the same as those described in the previous chapter. Extensions to this model neuron, specific to this chapter, are detailed below. All that follows describes a model STN neuron; GP neurons are described by equations

of the form (4.6).

Modelling the Ca^{2+} mechanism

This section is based on the work of Beurrier et al. (1999) which explored bursting in STN neurons. The central finding of their study was that STN neurons could be made to burst-fire *in vitro* by the application of a small hyperpolarising current. The sudden increase in activity after a hyperpolarisation leads to the term ‘rebound’ burst firing for this phenomenon. Beurrier et al. attributed this counter-intuitive result to the following sequence of ion channel activity. The hyperpolarisation activates a Ca^{2+} current $I_{T/R}$ which depolarises the membrane until it crosses the activation threshold (from below) for the Ca^{2+} current I_L . Immediately after this $I_{T/R}$ deactivates. The I_L current is self-sustaining since it increases with the depolarisation of the membrane potential. The membrane potential then reaches a plateau phase where action potentials are continuously generated because the membrane potential is continuously above firing threshold. However, the high levels of intra-cellular Ca^{2+} now initiate a Ca^{2+} activated K^+ current I_K which acts to hyperpolarise the membrane. I_K is slightly larger than I_L resulting in a decrease in membrane potential and the diminution of the burst. Repolarisation occurs when the I_L deactivation threshold is passed (from above) and I_L rapidly deactivates. The cycle is then ready to begin again.

My model of this cycle of current activation and deactivation is based on a simple piecewise linear approximation $I_{Ca}(t)$ of the net current across the membrane. No attempt is made to model the detailed dynamics of each component current ($I_{T/R}, I_L, I_K$) nor their complex interaction. Thus, it is supposed that I_{Ca} is activated by the membrane potential hyperpolarising below a threshold θ_{Ca} . There is then an initial step pulse in I_{Ca} of duration t_1 and height α_{Ca} which models the rapid depolarisation to the start of the plateau phase caused by the Ca^{2+} T/R- and L-type currents. This is then followed by a slowly declining ramp (of duration t_2) which models the slow decrease of net current into the membrane via the combined action of

I_L and I_K . The pseudo-current I_{Ca} may be expressed formally by

$$I_{Ca} = \begin{cases} 0, & \text{if } u > \theta_{Ca}; \\ \alpha_{Ca}, & \text{if } u < \theta_{Ca} \& 0 < t < t_1; \\ -\alpha_{Ca}(t - t_1)/t_2 + \alpha_{Ca}, & \text{if } u < \theta_{Ca} \& t_1 < t < t_2; \end{cases} \quad (5.1)$$

where t is time since the beginning of period t_1 . Periods t_1 and t_2 have values commensurate with the fact that STN bursts can last several hundred milliseconds (Magill, Bolam, and Bevan, 2000; Plenz and Kitai, 1999).

The value for the triggering threshold θ_{Ca} was taken from Beurrier et al.'s study. They found that the hyperpolarisation of STN neurons from a mean resting potential of -41.3 mV to a mean of -51.0 mV was sufficient to cause burst firing. Thus, given that the resting potential of the spiking model neuron is 0 mV, θ_{Ca} was set to -10 mV. Therefore, if the membrane potential u fell below -10 mV then the sequence of current inputs described above would be initiated.

The level of α_{Ca} determines the intra-burst firing frequency: the larger α_{Ca} , the faster the neuron will fire during the burst. An initial value of $7.5\mu A$ for α_{Ca} was determined empirically by simulation of a single STN unit. A simulated hyperpolarising current was injected into the unit and the value of α_{Ca} was altered until the unit fired at between 80-100 spikes/s during the initial period of the burst. These target firing frequencies were determined from Plenz and Kitai's data for STN neurons bursting at 0.8Hz because these units were not receiving any input from cortex. The resulting STN firing pattern is shown in Figure 5.2. With the inclusion of I_{Ca} the membrane equation for STN (4.7) becomes, dropping (t) for brevity,

$$\tau_m \frac{du}{dt} = -u + R[I_{syn} + I_{spon} + I_{ref} + I_{Ca} + I_{noise}] \quad (5.2)$$

A Quasi-compartmental model

The patterns of synaptic contact on a STN neuron from each of its afferent inputs are not identical. Cortical axon terminals and STN axon collaterals synapse predominantly on the distal dendrites (Gerfen and Wilson, 1996). GP axon terminals, on the other hand, synapse on distal dendrites, proximal dendrites, and the soma in roughly equal proportions (with a slight preference for proximal dendrites) (Bevan et al., 1997; Gerfen and Wilson, 1996).

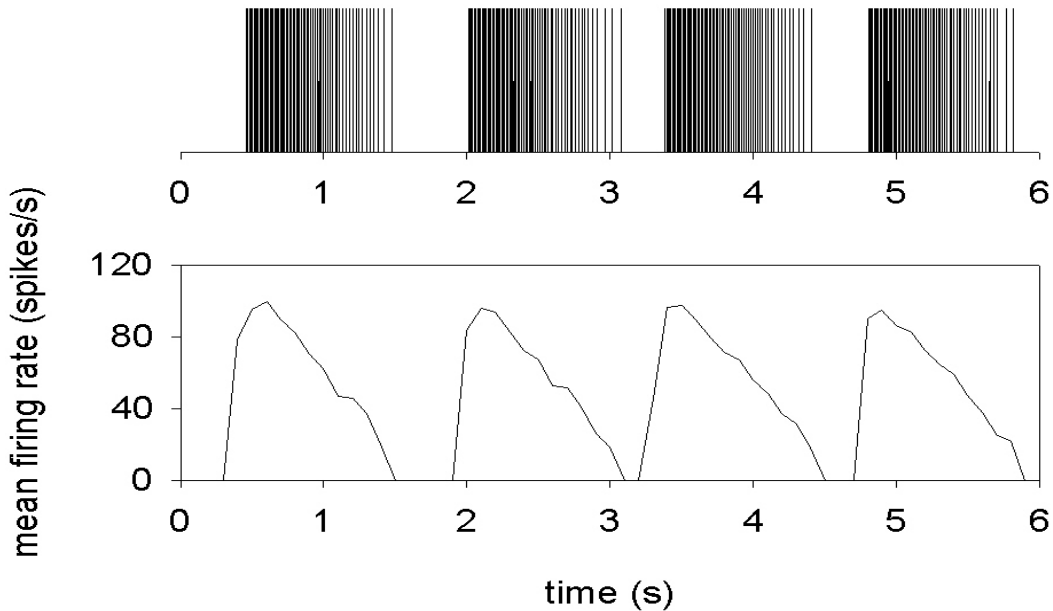


Figure 5.2: Top: spike train of an isolated simulated STN unit with the Ca^{2+} mechanism. The bursts show the stereotypical initial rapid firing period followed by a decay in rate as the Ca^{2+} current deactivates. Bottom: mean instantaneous firing rate plot for the unit, showing maximum firing rates between 80-100 spikes/s. Simulation parameters were: $t_1 = 200$; $t_2 = 1000$; $\alpha_{Ca} = 7.5$.

Synapses on distal dendrites are associated with the production of post-synaptic potentials that tend to combine additively (Borst and Egelhaaf, 1994) which is just the kind of post-synaptic potential interaction modelled by equation (4.3). However, inhibitory synapses on proximal dendrites and the soma often tend to have a multiplicative or ‘gating’ effect on distal synaptic input (Blomfield, 1974), often referred to as ‘shunting inhibition’. This means that they can substantially attenuate any post-synaptic potentials initiated on distal dendrites or even ‘veto’ their effect completely (Shepherd and Brayton, 1987). Hence, given the synaptic contact patterns described above, and the provision of inhibitory afferents to STN by GP, it seems possible that around 70% of GP synapses on a given STN neuron may exert a shunting inhibition effect on the cortical, STN axon collateral and (remaining) GP input.

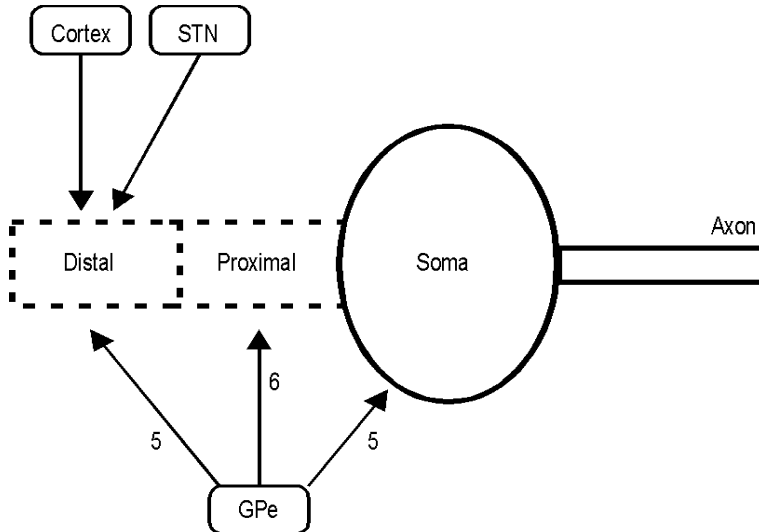


Figure 5.3: Schematic representation of a STN quasi-compartmental model neuron. Cortical and intra-nucleus STN axon collateral projections synapse predominantly on the distal dendrites. GP projections synapse on the distal and proximal dendrites and on the soma which make up 31%, 39% and 30%, respectively, of the GP synapses on a single STN neuron (Gerfen and Wilson, 1996). These values correspond to a 5:6:5 ratio of GP inputs to a single STN unit in the network.

One method of modelling the different synaptic contact patterns would be to create a full three compartment model neuron (Segev et al., 1989) with compartments for distal and proximal dendrites, and the soma. This would require modelling the temporal evolution of signals as they are transmitted across compartments, together with any inter-compartment attenuation. However, in keeping with my aim to retain the simplicity of the model neuron, the addition of synaptic input patterns is accomplished by assuming that these inter-compartmental features are of second order compared with the main arithmetical processing due to inhibitory signal gating near, and within, the cell soma. Therefore, the main arithmetic signal combinations are modelled in a single ‘compartment’ while respecting the spatially separated contributions to this processing described in Figure 5.3.

Let Γ_p be the set of GP afferents to an STN neuron that make contact with that neuron’s proximal dendritic compartment and let J_{prox} be the total additive synaptic current input from

GP on that compartment so that, from equation (4.3)

$$J_{prox}(t) = \sum_{j \in \Gamma_p} c_{gs}^- \sum_{t_j^{(f)} \in F^j} \alpha(t - t_j^{(f)}) \quad (5.3)$$

where c_{gs}^- is a measure of the synaptic strength (the scaling factor) between GP and STN. The maximum value any individual component of the sum in equation (5.3) can take is c_{gs}^-/τ_s , since $\alpha(s)$ is given by equation (4.4). If $J_{prox}^* = |\Gamma_p|c_{gs}^-/\tau_s$ then $J_{prox}(t) \leq J_{prox}^*$. Now put

$$h_{prox}(t) = 1 - \frac{J_{prox}(t)}{J_{prox}^*} \quad (5.4)$$

where $0 \leq h_{prox}(t) \leq 1$. When combined multiplicatively with other synaptic input, $h_{prox}(t)$ represents an inhibitory gating factor which attenuates that input.

A similar process may be used to model somatic inhibitory gating. Thus if Γ_s is the number of somatic afferents from GP, define

$$J_{soma}(t) = \sum_{j \in \Gamma_s} c_{gs}^- \sum_{t_j^{(f)} \in F^j} \alpha(t - t_j^{(f)}) \quad (5.5)$$

and if $J_{soma}^* = |\Gamma_s|c_{gs}^-/\tau_s$ then put

$$h_{soma}(t) = 1 - \frac{J_{soma}(t)}{J_{soma}^*} \quad (5.6)$$

Let I_{dist} be the current due to distal dendritic input where I_{dist} is of the form in equation (4.3) with contributions from GP and STN. The GP gating on proximal dendrites is assumed to attenuate I_{dist} so that the contribution from distal afferents becomes $h_{prox}(t)I_{dist}$. Further, somatic gating can affect, not only the proximal dendrites, but also I_{spon} which represents an intrinsic Na^+ current (Beurrier, Bioulac, and Hammond, 2000) and which is presumably effective at the soma. Thus, the membrane equation for STN neurons now becomes, again dropping (t) for brevity,

$$\tau_m \frac{du}{dt} = -u + R [(I_{dist}h_{prox} + I_{spon})h_{soma} + I_{ref} + I_{Ca} + I_{noise}] . \quad (5.7)$$

5.2.2 Network design

To maintain consistency with the models developed in the previous chapters, the channel architecture is retained in the model of the STN-GP loop. Due to the diffuseness of STN neuron

projections (Hazrati and Parent, 1992a; Hazrati and Parent, 1992b) every STN projects to every GP unit. The discrete channel scheme implies, however, that each GP units projects back only to every STN unit in the same channel. Further, as there is no salience input to the network, there is no distinction between active and non-active channels. Thus, the STN-GP model uses just two channels to facilitate study of the effect of cross-channel communication on the individual unit's outputs.

STN axon collaterals

The axon collateral connections between STN neurons are explicitly instantiated in the STN of the current model so as to incorporate all details which may contribute to the burst-firing phenomenon. Further, the smaller circuit and reduced number of channels allows the inclusion of connections which may otherwise have been prohibitive in terms of computing cost. Following the section on STN collaterals in chapter 3, the details of the axon collaterals are briefly reiterated and expanded here.

Fujimoto and Kita (1993) have provided indirect evidence for extensive axon collateralisation in the STN. Further, a recent study (Atherton et al., 2000) has demonstrated that a glutamate antagonist can influence STN neuron firing patterns in a slice preparation where all external inputs to STN have been removed, thereby implicating glutamatergic intra-nucleus collaterals. It has been estimated that every STN neuron is, at most, 2 synapses away from every other STN neuron via its intra-nuclear axon collaterals (Gillies and Willshaw, 1998). This implies that an STN neuron has direct synaptic contact, via its axon collaterals, with approximately 25% of all STN neurons. In the network, to model the intra-nucleus connections in STN, each unit is therefore randomly connected to 25% of all other STN units both within and between channels. Thus, the model's STN is massively interconnected.

Recent modelling work (Gillies et al., 2000) has indicated that an excitatory post-synaptic potential (EPSP) elicited by one STN neuron contacting another is likely to be small. Hence, a large number of coincident STN collateral induced EPSPs would be necessary for an STN neuron to depolarise sufficiently to release an action potential. In keeping with this data

the scaling factor c_{ss}^+ of the STN-STN connections in normally functioning networks is kept relatively small (about 10% of the magnitude of other weights - see Table 5.1)

Cortical input

Plenz and Kitai's (1999) data on bursting frequencies showed that the presence of one of their main burst frequencies (0.4Hz) was dependent on there being cortical innervation of STN. Since there is no sensory input *in vitro* this implies that the spontaneous output of cortex was sufficient to cause this change in behaviour. To model cortical input to the STN, each STN unit was innervated with 16 spike trains that represent spontaneous cortical firing. This number is consistent with the number of neurons in a basal ganglia channel and with the extensive cortical innervation of STN (Bevan et al., 1995). Each spike train was generated using a binomial distribution (using Bernoulli trials at each time step of the simulation) modified to take account of a cortical absolute refractory period; thus no two action potential spikes could be separated by less than 2ms. While random neural spike trains are believed to follow a Poisson distribution (Segundo, Stiber, and Vibert, 1995) it is also the case that the Poisson distribution approximates the Binomial distribution when the chance of a trial success is small and a large number of trials are conducted (Ross, 1985). This approximation holds in here since the mean firing rate of each cortical input to STN was set at 4 spikes/s.

5.2.3 Analysis of simulation data

The purpose of the analysis is to characterise the bursting behaviour of individual units and pairs of units: in particular, what units are bursting and, if they are, whether this bursting is phase locked with other units.

The starting point for the analysis of each set of simulation results was similar to that from the previous chapter. Inter-spike interval data were calculated from the spike train output of each unit. The reciprocal values of the inter-spike intervals were then sampled in 50ms bins to give the mean instantaneous firing rate plot (in spikes/s) for that unit. As this study is concerned with the output of individual units, the mean of these plots across a complete channel

set (the $F(t)$ from the previous chapter) was not calculated. The individual plot mean, or DC component, of each resulting signal was then subtracted before performing a power spectral density analysis. Each power spectral analysis used a Hanning window with width equal to half the number of bins (e.g. in a $T = 60$ second simulation with 50ms bins the Hanning window had a width of 600). The power spectra were high-pass filtered at 0.07Hz to remove window edge-effects. Each unit was then assigned a fundamental frequency f_0 which was the frequency associated with the largest power in the power spectrum.

Putatively, f_0 is the frequency of bursting, but determination of bursting status requires more work. The starting point for this analysis is the computation of the unit's autocorrelogram (after extraction of the DC component). The autocorrelogram always contains an oscillatory component that corresponds to f_0 and the depth of modulation of this component is an indication of the power present in the original signal at this frequency. Therefore, this feature is used to determine if a unit was bursting. To quantify this let the autocorrelogram functional form be denoted by $A(t)$. In all cases $A(t)$ is symmetric about $t = 0$ at which point it takes its maximum value. Let $\tau_0 = 1/f_0$ (the fundamental period of the unit). To be sure of inspecting a full period τ_0 , $A(t)$ is examined over the (half-open) interval $\Delta t = (0, 3\tau_0/2]$. Let $a_{max} = \max_{\Delta t}(A(t))$, $a_{min} = \min_{\Delta t}(A(t))$ and $d = |a_{max} - a_{min}|$. The quantity d is therefore a measure of the depth of modulation of the autocorrelogram at f_0 . Now fix a threshold ratio θ_a ; then the unit was deemed to be bursting if

$$d > \theta_a A(0) \quad (5.8)$$

The value of θ_a was chosen by ensuring that units showing unequivocal bursting in one of the simulations (by direct visual inspection of their mean instantaneous firing rate plots) were assigned the bursting status according to equation (5.8); this gave a value $\theta_a = 0.2$.

Candidate units for burst synchrony are drawn from all STN-STN, GP-GP and STN-GP pairs for which both units in the pair satisfy equation (5.8). To determine if a pair is synchronised (phase locked) a *synchrony index* S is computed as follows. Let f_0^1, f_0^2 be the fundamental frequencies of the two units. Express these as integral multiples n_0^1, n_0^2 of the smallest frequency expressible in the analysis (this is just the frequency step in the power spectrum which is, in

turn, fixed by the Hanning window size and the size of the inter-spike interval bins). Let N_{12} be the least common multiple of n_0^1 and n_0^2 . Then the signals are coincident every N_{12}/n_0^2 periods of signal 1 and N_{12}/n_0^1 periods of signal 2. High degrees of synchrony are therefore associated with small values of these quantities or, alternatively large values of their reciprocals. Therefore, S is defined to be the mean of these two latter quantities

$$S = \frac{n_0^1 + n_0^2}{2N_{12}} \quad (5.9)$$

where $0 < S \leq 1$. To clarify an understanding of this definition, consider the following two examples. First, identical signals constitute the case of maximal synchrony, which is consistent with their giving $S = 1$. Second, consider the case of two signals which differ slightly in frequency and for which $N_{12} = n_0^1 n_0^2 \approx n_0^{1^2}$. In this case, $S \approx 1/2n_0^1$ which tends to zero as n_0^1 becomes very large. This is consistent with the idea that two signals which have slightly differing frequencies are probably not causally related and should not therefore be considered as phase locked.

To explore phase angles in synchronous signal pairs the cross spectral density analysis of the pair is computed (after DC subtraction) to determine the common frequency of firing of both units, f_0^c , and its associated period τ_0^c . Next the cross-correlogram is computed (after DC subtraction) and its functional form denoted by $C(t)$. This function is, in general, not symmetric about zero and has a maximum value $C(t_{max})$ where (again in general) $t_{max} \neq 0$. t_{max} is the relative time displacement that the two signals have to undergo in order to find their largest overlap. This is now converted into a phase difference ϕ_{max} with respect to f_0^c according to

$$\phi_{max} = 360 \frac{t_{max}}{\tau_0^c} \quad (5.10)$$

All pairs that gave $\phi_{max} > \pm 360$ were excluded as the occurrence of phase angles greater than 360° implies a group of bursts in each signal which is not temporally coincident with its counterpart.

5.2.4 Implementation details

The equations for the membrane potentials of GP and STN units were solved in a discrete time simulation with a fixed time interval of 0.1ms. This was the largest interval commensurate with accurate solution over a wide range of conditions. For all the simulations described below, noise (the I_{noise} component) was sampled at each time-step from a Gaussian distribution ($\bar{x} = 0, \sigma^2 = 5$). The simulation was written in Matlab v5.2 (Mathworks).

5.3 Results

The parameters for all the simulations described below, and their normal values, are listed in Table 5.1. Weights for the connections were determined using the methods of section 4.2.4. Some of these parameters were not relevant to or were varied for some simulations. These are detailed in the appropriate cases. In every simulation the GP neurons were described by equation (4.6).

5.3.1 STN neuron-like bursting is not possible without the Ca^{2+} mechanism

One of the primary hypotheses of this chapter is that the Ca^{2+} mechanism described by Beurrier et al. (1999) was crucial in causing the bursting behaviour of STN neurons observed by Plenz and Kitai (1999). Thus, it would be expected that the STN-GP circuit as modelled here, but without the Ca^{2+} mechanism in place, would not be capable of showing neurophysiologically realistic bursting behaviour. This is not self-evident as it has been demonstrated that a simple central pattern generator circuit, consisting of two reciprocally linked excitatory units, can exhibit synchronised bursting behaviour when neither of the units is an endogenous burster (Rowat and Selverston, 1997). Bursting within this central pattern generator was dependent upon either the units having heterogeneous firing thresholds or on the units receiving significantly different amounts of injection current. In short, bursting was caused by a breaking of the symmetry between the two units.

Parameter	Description	Value
c_{ss}^+	scaling factor of the STN internal axon collaterals	0.1
c_{sg}^+	scaling factor of the STN \rightarrow GP connections	0.8
c_{gs}^-	scaling factor of the GP \rightarrow STN connections	-1
c_{cs}^+	scaling factor of the cortex \rightarrow STN connections	1
J_{prox}^*	maximum post-synaptic current due to proximal GP synapses	6
J_{soma}^*	maximum post-synaptic current due to somatic GP synapses	5
C	membrane capacitance	$2\mu F$
τ_m	membrane time constant	70ms
τ_s	synaptic time constant	3ms
θ	firing threshold	30mV
α_{Ca}	level of current input due to the Ca^{2+} mechanism	$7.5\mu A$
θ_{Ca}	the Ca^{2+} mechanism triggering threshold	-10mV
t_1	period of pulse component of Ca^{2+} current	200ms
t_2	period of ramp component of Ca^{2+} current	1000ms
I_{spon}	the current causing spontaneous firing	$0.8\mu A$

Table 5.1: Simulation parameter values and their descriptions

These findings are directly relevant to the network discussed here as the reciprocal excitatory connections between STN units set up just such a circuit in which two mutually excitatory units may be receiving different levels of input (from GP units and other STN axon collaterals). Furthermore, the noise introduced by the $I_{noise}(t)$ current is equivalent to a noisy threshold (Gerstner, 1999), so any two units will effectively have different firing thresholds at any particular time-step. Thus, any mutually connected pair of STN units may have their symmetry broken sufficiently to allow bursting to occur.

To test the possibility that STN units could be induced to burst without a Ca^{2+} mechanism three simulations were conducted using the STN-GP model in which STN units were described by equation (4.7) and in which c_{ss}^+ took the values of 0.1, 0.5 and 1. This was done to ascertain if any level of axon collateral connection strength could induce bursting. All other relevant parameters had the values shown in Table 5.1 and there was no external input to the network.

Figure 5.4 shows the mean instantaneous firing rate plot of an example STN from the simulation with $c_{ss}^+ = 0.1$. STN units from the other two simulations showed qualitatively the same results. The narrow peaks of mean firing rate coincided with pairs or triples of spikes which were close together in time.

The mean instantaneous firing rate plot and spike train for a typical STN bursting neuron from Plenz and Kitai's study are shown in Figure 5.4. A comparison of this data with the mean instantaneous firing rate plot and spike train from the example STN unit shows that these units were not bursting in the same manner as real STN neurons.

It seems, then, that it is not possible to induce STN neuron-like bursting in this network without the addition of the Ca^{2+} mechanism to the STN units. However, within the literature on thalamic neuron rebound bursting, authors have reported bursts that consist of as little as two spikes (Ulrich and Huguenard, 1997) and which have a normal range of 5-15 spikes (Kim and McCormick, 1998; Kim et al., 1997). Furthermore, authors rarely report the incidence of more than one burst. Their criteria for what constitutes a burst can, therefore, be characterised as: action potentials must occur closely in time, as few as two action potentials are enough to define a burst, and the absence of repeated occurrences of groups of action potentials does

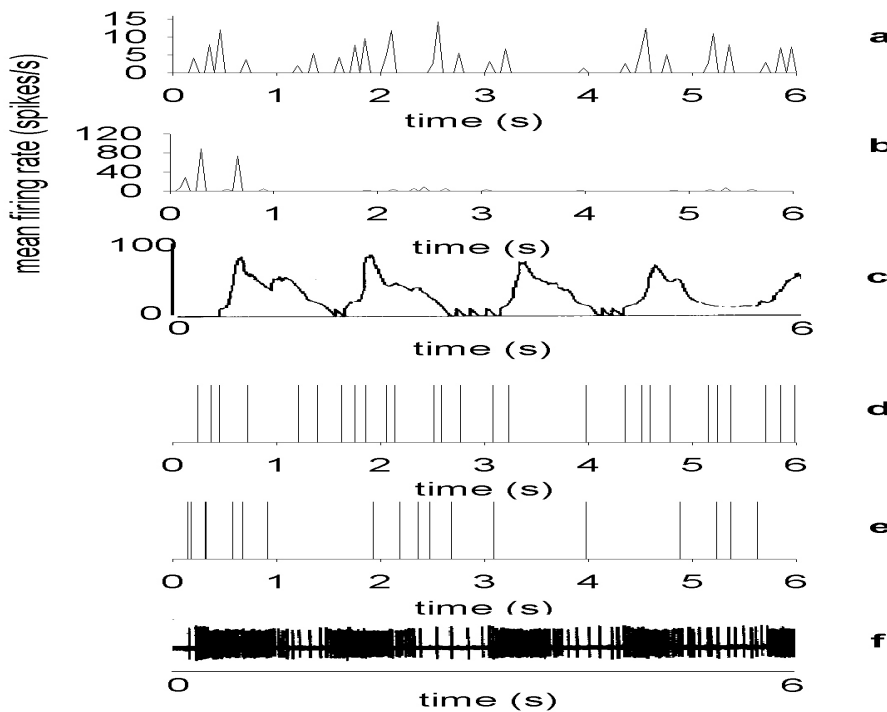


Figure 5.4: STN units could not burst-fire without the Ca^{2+} mechanism. **a-c** Mean instantaneous firing rate plots determined from the spike trains in **d-f**, respectively. **a** An example STN unit from a simulation with $c_{ss}^+ = 0.1$. It showed very short bursts of firing at an intra-burst maximum of 15 spikes/s. **b** Instantaneous firing rate plot of a spike train generated by a Poisson process. **c** A bursting STN neuron from Plenz and Kitai's (1999) study. **d** The spike train of the simulated STN unit. The close incidence of a few spikes, for example at $t = 2$ seconds, caused short bursts to appear in the mean instantaneous firing rate plot. **e** Spike train generated according to a Poisson process. **f** Spike train of the bursting STN neuron from Plenz and Kitai's study. It is clear that the simulated STN unit was not bursting in qualitatively the same way as the typical bursting STN neuron, but was similar to a randomly generated output. Figures reprinted by permission from Nature (400:677) copyright (1999) Macmillan Magazines Ltd.

not exclude a neuron from being classified as bursting. Similar criteria to these have been used for studies of bursting neurons in other areas of the mammalian brain (White, Lovinger, and Weight, 1989). Hence, according to these criteria, it is possible to interpret the mean instantaneous firing rate plot and spike train of the example STN unit as showing bursting.

However, the example STN unit's spike train is similar to a spike train obeying a Poisson distribution. This is illustrated by the train in Figure 5.4 which was generated according to a Poisson distribution. The corresponding mean instantaneous firing rate plot is also shown in Figure 5.4. Thus, even though it is possible to interpret the example STN unit's data as showing bursting, the similarity between this data and the data generated according to a Poisson distribution indicates that there is no underlying causal mechanism causing this bursting because it is indistinguishable from a randomly generated example.

5.3.2 The role of noise

Having shown that neurophysiologically realistic STN bursting was not possible without the Ca^{2+} mechanism it remained to be shown that the addition of this mechanism to the model neuron would cause bursting in STN units within a network. The networks simulated for this section used the model neuron described by equation (5.2) for all STN units, with the parameters from Table 5.1 (except where explicitly stated below). Again, there were no external inputs to the network.

Four experiments were carried out on the STN-GP model which explored the role played by the STN axon collaterals and the I_{noise} current. The first two experiments confirmed that the addition of the Ca^{2+} mechanism caused bursting to occur with or without STN axon collaterals. The no-noise investigation follows on from the testing of the extended spiking model in the last chapter: removing noise from that model showed that the oscillatory activity was dependent upon the presence of some form of noise. Here, experiments 3 and 4 investigated whether removing noise from the network prevents the bursting mechanism from triggering.

Experiment 1

A simulation of the STN-GP network without intra-nucleus axon collaterals within STN (a ‘collateral-free’ network, with $c_{ss}^+ = 0$) showed that units equipped with the Ca^{2+} mechanism were able to burst-fire when placed in a network. The burst detection algorithm found that all units burst and f_0 for all units was 0.67Hz, indicating that the network was bursting monomodally. In addition, the cross-spectral density analysis showed that the common frequency, f_0^c , between all bursting unit pairs was also 0.67Hz. The mean synchrony index S was 0.982. The breakdown of this value into its constituent mean scores from STN unit pairs (S_{ss}), GP unit pairs (S_{gg}), and STN-GP unit pairs (S_{sg}) was: $S_{ss} = 0.982$, $S_{gg} = 1$, $S_{sg} = 0.964$. These S scores show that the vast majority of units were completely phase-locked within STN and GP and across both nuclei.

Experiment 2

Three simulations, with c_{ss}^+ values of 0.1, 0.5 and 1, of the STN-GP model with STN intra-nucleus axon collaterals were run. The results were very similar to those of Experiment 1 for all c_{ss}^+ values: f_0 for every unit in each of the simulations was 0.67Hz and f_0^c for almost all bursting pairs was also 0.67Hz. The phase angle plots in Figure 5.5 show that the variation of ϕ_{max} was consistent in all three simulations and, therefore, did not change with increasing c_{ss}^+ .

This pair of experiments on the STN-GP model confirm that the bursting mechanism, which causes burst firing in the output of a hyperpolarised isolated STN unit (see section 5.2.1), also causes burst firing in STN units when they are placed in a network. Further, this bursting in STN output is successfully transmitted to the GP units, which burst fire in return. The occurrence of bursting, number of bursting units, and frequency of bursting were not dependent on the presence of STN axon collaterals.

Experiment 3

To investigate how the presence of noise affected the STN-GP model’s behaviour three simulations were run with the same parameters as those in Experiment 2, except that I_{noise} was

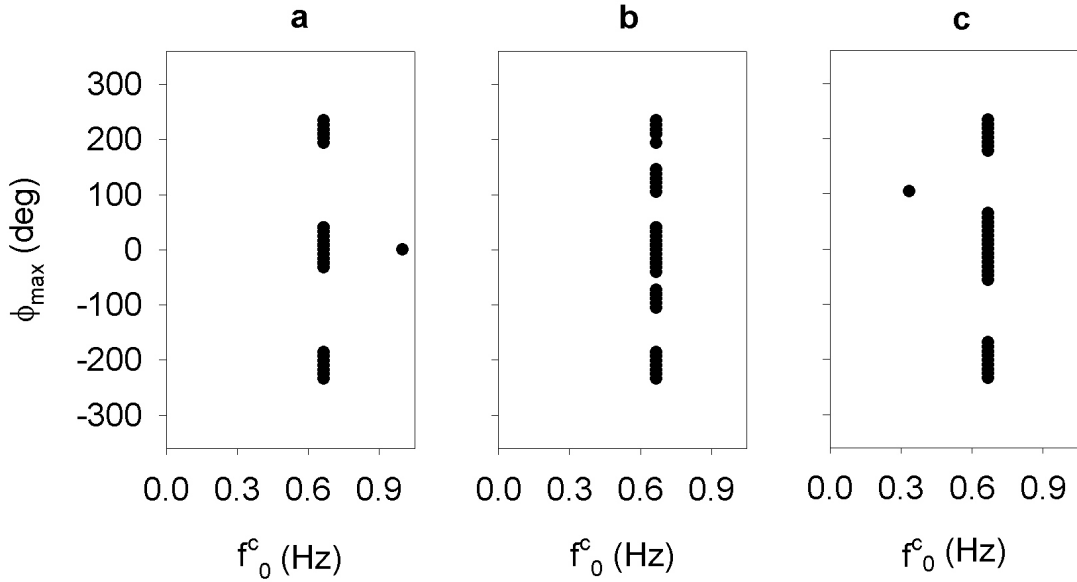


Figure 5.5: Phase-angle (ϕ_{max}) plots for STN unit pairs in three simulations of Experiment 2 with $c_{ss}^+ = 0.1$ (a), 0.5 (b), and 1 (c), respectively. Almost all units had a common frequency of firing at 0.67Hz, regardless of the level of c_{ss}^+ , and all had similarly wide ranges of ϕ_{max} indicating that most units were out-of-phase with each other.

set to zero. All three simulations showed burst firing in all units. Again, f_0 was 0.67Hz for all three values of c_{ss}^+ . The phase-angle plots for STN unit pairs are shown in Figure 5.6. It is immediately apparent that with increasing c_{ss}^+ came an increasingly diverse data set: the variation of ϕ_{max} increased going from $c_{ss}^+ = 0.1$ to $c_{ss}^+ = 0.5$, and at $c_{ss}^+ = 1$ a third f_0^c was observed. This is in direct contrast to the results of the equivalent simulations with noise, reported in Experiment 2, and suggests that noise acts to homogenise the behaviour of units in the network.

This suggestion is supported by the mean S scores from Experiments 2 and 3. These are broken down in Table 5.2 for all six simulations (three with noise, three without). The mean S scores show that STN-GP unit-pairs and STN unit-pairs became less phase-locked when noise was removed from the network. Therefore, the S scores show that removing noise reduces the level of synchrony in the STN-GP circuit (although the presence or absence of noise in the

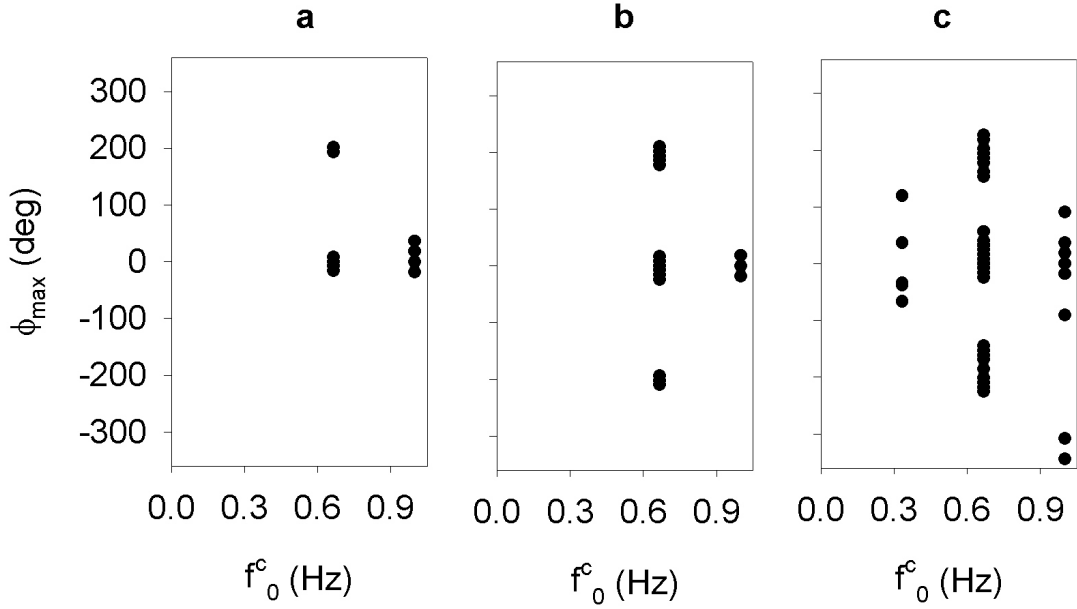


Figure 5.6: The phase-angle plots of STN bursting unit pairs for three simulations from Experiment 3, with $c_{ss}^+ = 0.1$ (**a**), 0.5 (**b**), and 1 (**c**), respectively. The phase-angle plots showed that increasing c_{ss}^+ caused a diversification of the data set: a wider range of ϕ_{max} and a third common frequency of firing between pairs of units.

network did not affect the degree of phase-locking in GP unit pairs).

Experiment 4

The final experiment in this section examined the effect of removing both the axon collaterals and noise from the model, given that removing them individually had no effect on the occurrence of bursting. A simulation of the collateral-free network used in Experiment 1 (i.e. with $c_{ss}^+ = 0$), but with I_{noise} set to zero, showed no firing in any unit. Clearly, the removal of noise meant that the membrane potential in STN units never reached θ . Thus, no STN output ensued with which to drive GP units. This, in turn, meant that there was no inhibition from GP to STN units with which to cause bursting.

To establish if a collateral-free network with no noise could ever burst fire two simulations were run of the same network with higher values of I_{spont} (3 and 5) than the default value in

$S_{unit-pair}$	c_{ss}^+						
		Noise			No noise		
		0.1	0.5	1	0.1	0.5	1
S_{ss}	0.964	1	1	1	0.757	0.898	0.789
S_{gg}	1	1	1	1	1	1	1
S_{sg}	1	1	1	1	0.931	0.931	0.931
$\bar{x}S$	0.979	1	1	1	0.896	0.943	0.907

Table 5.2: Mean S values from Experiments 2 (Noise) and 3 (No noise). Note how the S values for the no noise condition were much lower, particularly for STN, suggesting that the removal of noise reduced synchrony across the network.

Table 5.1. Increasing I_{spon} increases STN unit output and, therefore, would cause greater GP inhibitory feedback. This would, in turn, hyperpolarise the membrane of the STN units more than in the initial simulation with the default value of I_{spon} and, possibly, reach the level of θ_{Ca} .

All STN units in the two simulations had similar outputs: an initial burst was followed by persistent tonic firing. The bursting detection algorithm confirmed that no units in STN or GP were bursting in either simulation. This indicates that removing noise in a collateral-free network prevents the STN units from burst-firing, regardless of the level of input they provide to GP units.

5.3.3 Simulation of the basal ganglia pacemaker

Having established that the Ca^{2+} mechanism could cause burst firing of units in a network, it remained to be shown that the multi-frequency bursting observed by Plenz and Kitai could be simulated. The results of the previous section showed that the model neuron described by equation (5.2) was capable of mono-modal bursting, at 0.67Hz, when placed in a network. One of my primary hypotheses is that cortical input will modulate the intrinsic bursting properties of the STN-GP circuit and cause multiple frequency bursting. To test this hypothesis cortical

input was introduced, as described in Section 5.2.2, to the STN-GP model (with axon collaterals and noise) using the model neuron described by equation (5.2) for STN units. The parameters were set as shown in Table 5.1.

Results from a simulation of this network indicated that cortical input was not sufficient to cause multiple frequency bursting in the basic STN-GP model. The fundamental frequency f_0 for all units was 0.77Hz and, therefore, so too was the frequency of bursting (the bursting algorithm found that all units burst). No other frequencies were evident from the power or cross spectra.

As noted in the introduction, the failure of the basic STN-GP model to simulate the multi-modal bursting frequencies led to the development of the quasi-compartmental connection scheme. The following two experiments report the attempts to simulate Plenz and Kitai's data with the STN-GP model which used the quasi-compartmental STN model neuron, described by equation (5.7). The parameters used are those in Table 5.1.

Experiment 5

A simulation of 60 seconds duration was run without cortical input to attempt to repeat the mono-modal bursting already achieved by the network in Experiments 1 and 2. Figure 5.7 shows the mean power spectrum for all bursting units. From the power spectrum it is evident that the only frequency of any significance was 0.82 Hz. The burst detection algorithm found all units were bursting. Thus, without cortical input, STN and GP quasi-compartmental units burst fired at $\sim 0.8\text{Hz}$ which is in good agreement with the results observed by Plenz and Kitai (1999) in their cortex-disconnected condition.

The phase-angle plot in Figure 5.7 shows that STN unit pairs had a wide range of ϕ_{max} indicating that, although the majority were phase-locked ($S = 0.94$), they were normally out-of-phase with each other. Phase-locked GP unit pairs showed complete synchrony ($S = 1$) with $\phi_{max} = 0^\circ$ indicating that all units were completely in-phase. The homogeneous nature of the STN output can easily be seen in the pseudo-colour plot of all 32 STN units' outputs in Figure 5.8. All units burst with uniform regularity in very close temporal proximity. However,

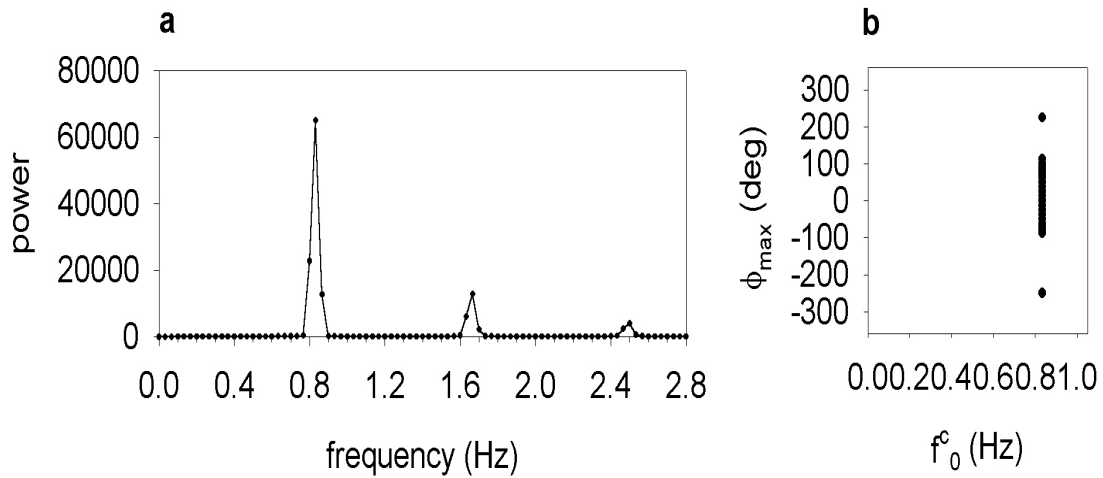


Figure 5.7: No cortical input gave one bursting frequency. **a** The mean power spectrum of all bursting units in a simulation of the network with quasi-compartmental model neurons (Experiment 5). The main frequency of bursting was 0.82Hz. **b** The phase-angle plot for STN unit pairs shows a wide range of ϕ_{max} indicating that most phase-locked units were out-of-phase with each other.

despite the similarities in the overall bursting behaviour of the units, there was a wide range of inter-burst periods and intra-burst firing frequency. This illustrates that, despite the lack of cortical output, the individual units did not have identical outputs.

Experiment 6

To investigate the effects of cortical input on the quasi-compartmental STN-GP model's behaviour, three simulations of 60 seconds duration were run, with cortical input as described in section 5.2.2. This was done to gather a large data set: it was evident from the first simulation that the data set was very rich and that a larger population of units was needed to satisfactorily establish the results. Hence, the total number of units in the results outlined below is 192 (96 STN and 96 GP units).

For the analysis of this data-set 100ms bins were used. Increasing the bin size acts as a

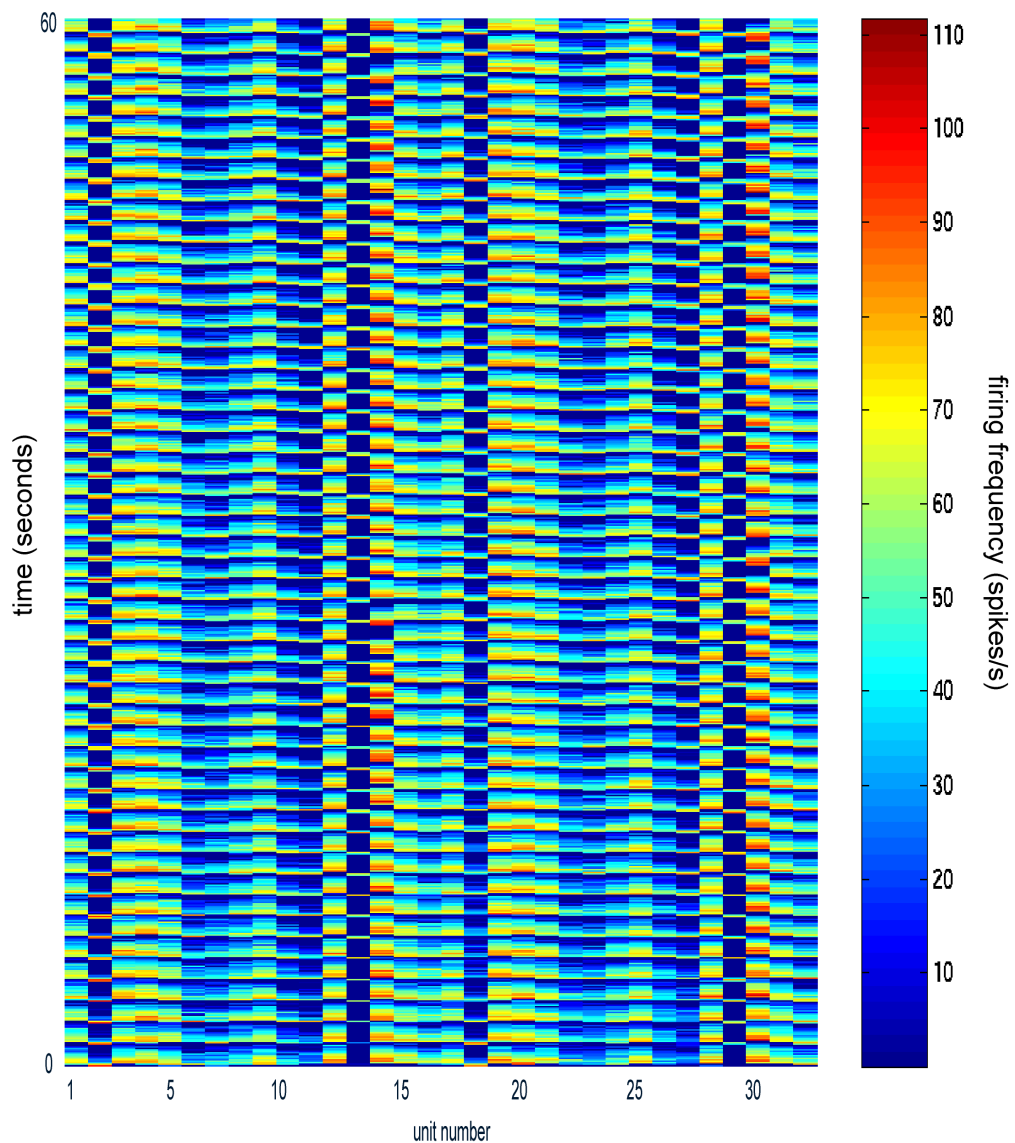


Figure 5.8: Pseudo-colour plot of the output of both STN channels in Experiment 5. Each block of colour is one 50ms bin from the unit's mean instantaneous firing rate plot. The output of STN is homogeneous in that all units burst at a uniform frequency for the duration of the simulation and the bursts occurred in rough synchrony. The main difference between units was in the length of inter-burst quiet periods and the maximum intra-burst frequency.

low-pass filter because the maximum frequency f_{max} that can be detected is determined by

$$\begin{aligned} n &= \frac{1}{s} \\ f_{max} &= \frac{n_b}{2} \end{aligned} \tag{5.11}$$

where s is bin size in seconds, and n_b is the number of bins in 1 second. Therefore, as bin size increases the maximum frequency that can be detected decreases: with 100ms bins, $n_b = 10$ and $f_{max} = 5$ Hz. The use of 100ms bins low-pass filtered the GP data, which was necessary because the power spectra of GP units showed a significant amount of power at high frequencies which obscured any low frequency bursting. To enable cross-nucleus analysis (crosscorrelograms, cross spectral density analyses and phase-angle plots) the STN data was also binned at 100ms. However, all the STN data was also binned at 50ms for comparison purposes and the within-nucleus analyses (power spectral density analyses, autocorrelograms, STN-STN phase-angles) were identical to those shown here.

Figure 5.9 shows the mean power spectrum for all bursting units. It reveals that bursting occurred at two main frequencies $f_{01} = 0.67$ Hz and $f_{02} = 0.83$ Hz. The largest peak was at f_{02} indicating that it was the dominant bursting frequency. The mean power spectrum from Plenz and Kitai(1999) is also shown in Figure 5.9. It clearly illustrates two peaks at ~ 0.4 and ~ 0.8 Hz, which they reported as the dominant bursting frequencies, and is qualitatively similar to the mean power spectrum derived from the simualtion's data.

The bursting algorithm returned 101/192 (101 out of 192 units tested) units as bursting (69/96 STN units, 32/96 GP units). Plenz and Kitai reported similar proportions of bursting neurons in these nuclei: 83/181 bursting STN neurons and 31/102 bursting GP neurons.

The mean cross-spectral density analysis of all bursting pairs (STN-STN, STN-GP and GP-GP) is shown in Figure 5.10. Again there were two main frequencies, $f_{01} = 0.63$ Hz and $f_{02} = 0.8$ Hz which were very close to those found in the mean power spectrum analysis. However, in contrast to the power spectrum, the lower frequency (f_{01}) dominated. Again, for comparison purposes, the mean power spectrum from Plenz and Kitai (1999) is shown in Figure 5.10: note that the greater power is at the lower peak in both spectrums.

Phase-angle plots of STN unit pairs and GP unit pairs are shown in Figure 5.11. The

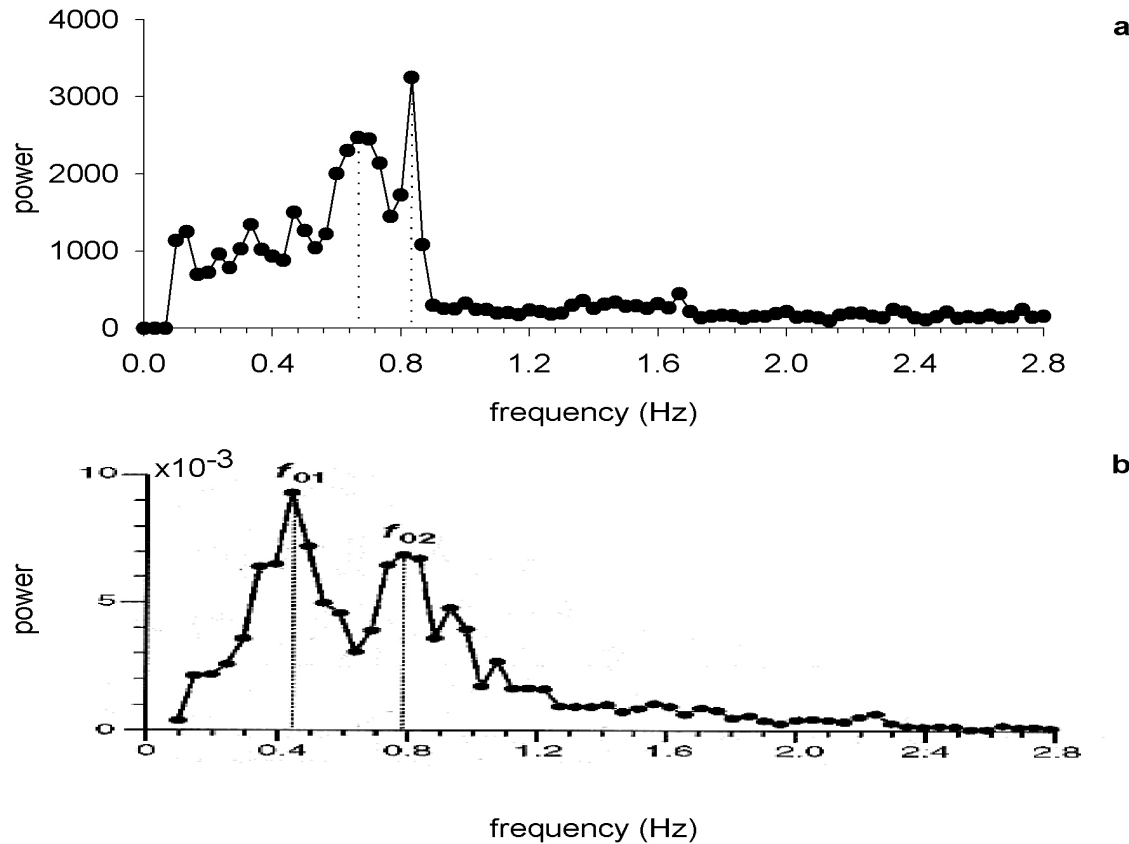


Figure 5.9: **a** Mean power spectrum of all bursting units from three simulations of the STN-GP network of quasi-compartmental units which received cortical input (Experiment 6). The dominant frequencies were 0.67Hz and 0.83Hz. **b** The equivalent mean power spectrum analysis from Plenz and Kitai's (1999) study showing two main frequencies of 0.4Hz and 0.8Hz. Figure reprinted by permission from Nature (400:677) copyright (1999) Macmillan Magazines Ltd.

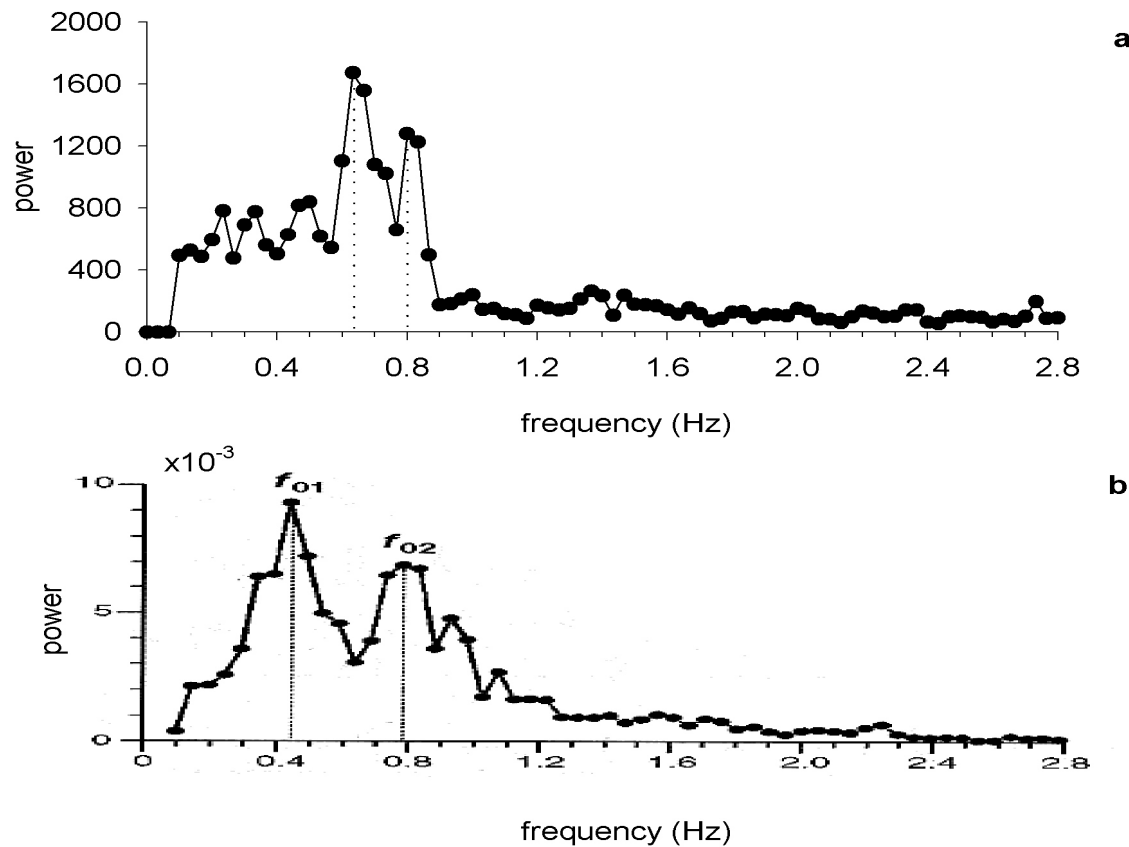


Figure 5.10: **a** The mean cross spectrum of all bursting unit pairs from the three simulations of the network with quasi-compartmental units and cortical input. The main peaks are at 0.8Hz and 0.63Hz. These were similar frequencies to the mean power spectrum in Figure 5.9a but the main power was at the lower frequency in this case. **b** The mean power spectrum from Plenz and Kitai's (1999) study showing the greatest power at the lowest peak (0.4Hz). Figure reprinted by permission from Nature (400:677) copyright (1999) Macmillan Magazines Ltd.

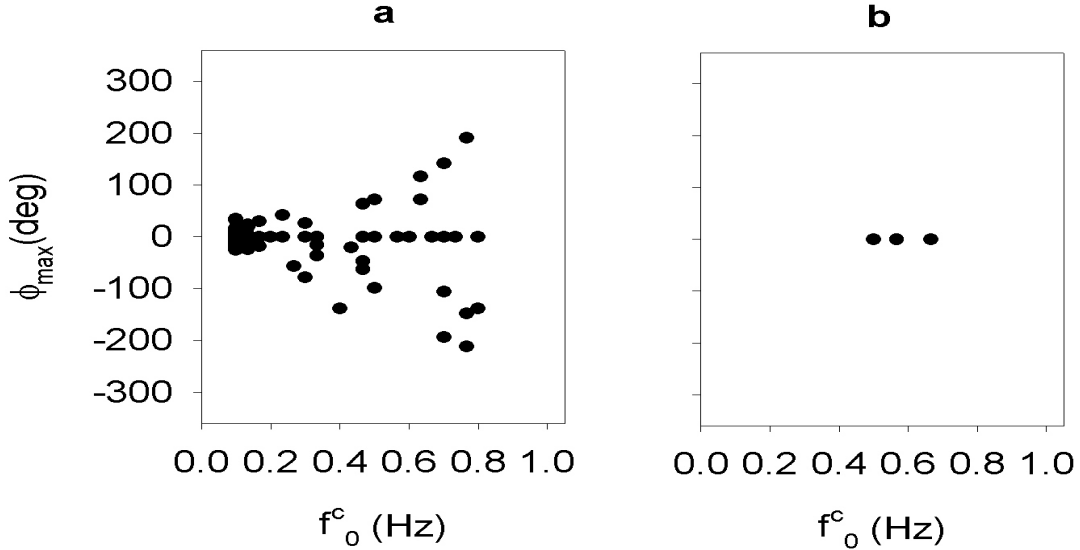


Figure 5.11: The phase-angle plots for all bursting STN(a) and GP(b) unit pairs from Experiment 6. STN unit pairs showed a wide range of ϕ_{max} : at low f_0^c the unit pairs were bursting in-phase; at higher f_0^c unit pairs were substantially more out of phase. The clustering of ϕ_{max} at zero indicates that all phase-locked GP units burst in phase.

phase-angle plot for the STN unit pairs clearly show that synchronised firing was not limited to a single f_0^c . STN unit pairs showed the closest phase of bursting when their common frequency, f_0^c , was low. This degree of phase diversified with increasing f_0^c so that the most out-of-phase pairs were those with $f_0^c = \sim 0.8\text{Hz}$. Phase-locked GP unit pairs were in complete synchrony at all f_0^c ($\phi_{max} = 0$). The mean S was 0.449 indicating that many unit pairs were not phase-locked. A comparison of the STN phase-angle plot with its equivalent from the no-cortical input network (in Figure 5.7) shows that the introduction of cortical input caused a substantial diversification of unit outputs.

The pseudo-colour plot of the mean instantaneous firing rate data for the first 32 STN units is shown in Figure 5.12. It clearly illustrates the diversification of unit outputs which occurred after the addition of cortical input (compare with Figure 5.8). The example mean instantaneous firing rate plots in Figure 5.13 further illustrate the range of STN unit behaviour: non-bursting units, which showed rapidly oscillating high frequency tonic firing, sporadically bursting units,

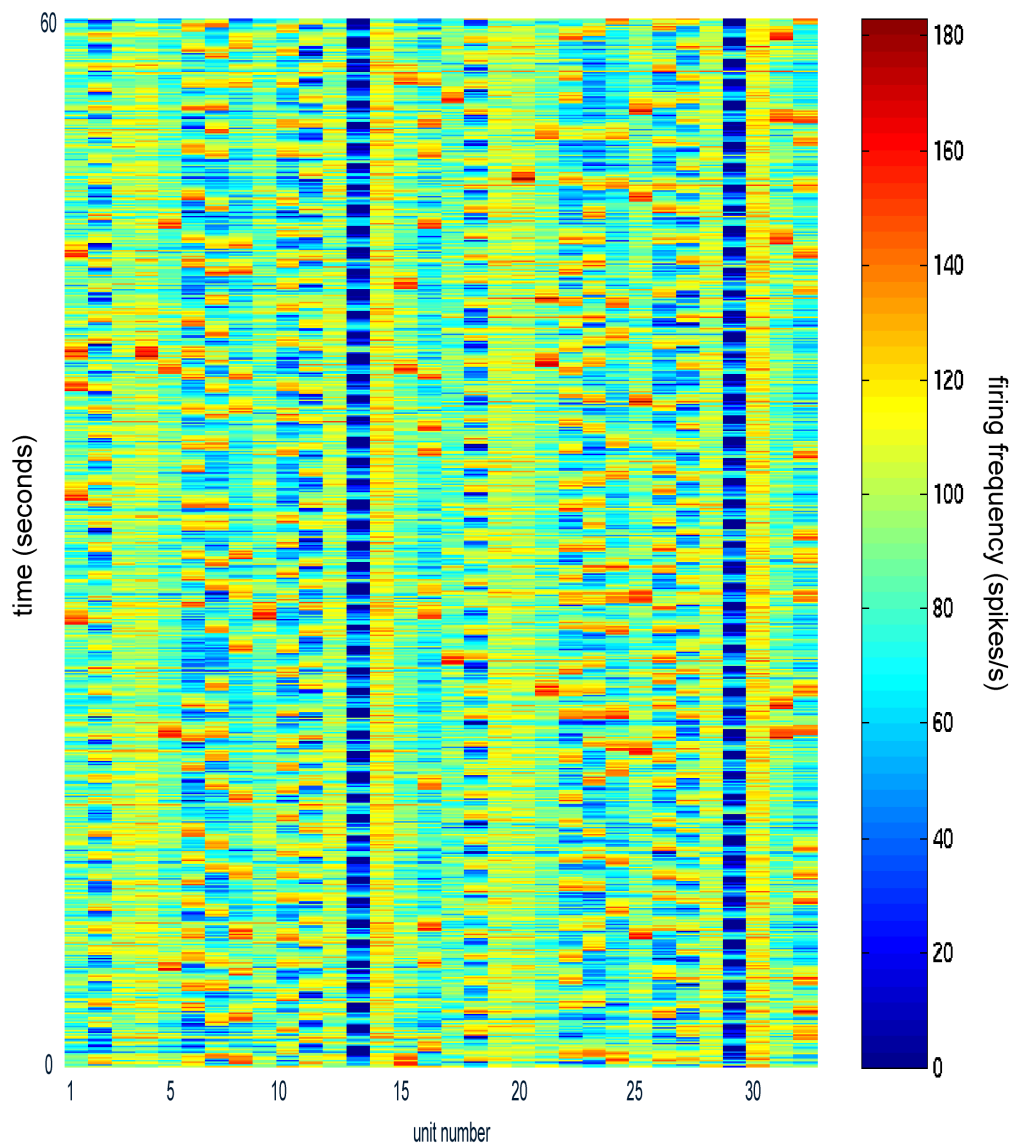


Figure 5.12: Pseudo-colour plot of the output of both STN channels in Experiment 6. Each block of colour is one 50ms bin from the unit's mean instantaneous firing rate plot. The output of STN is heterogeneous: unit outputs ranged between highly regular uniform bursting (unit 13) to noisy tonic firing with no bursts (unit 1).

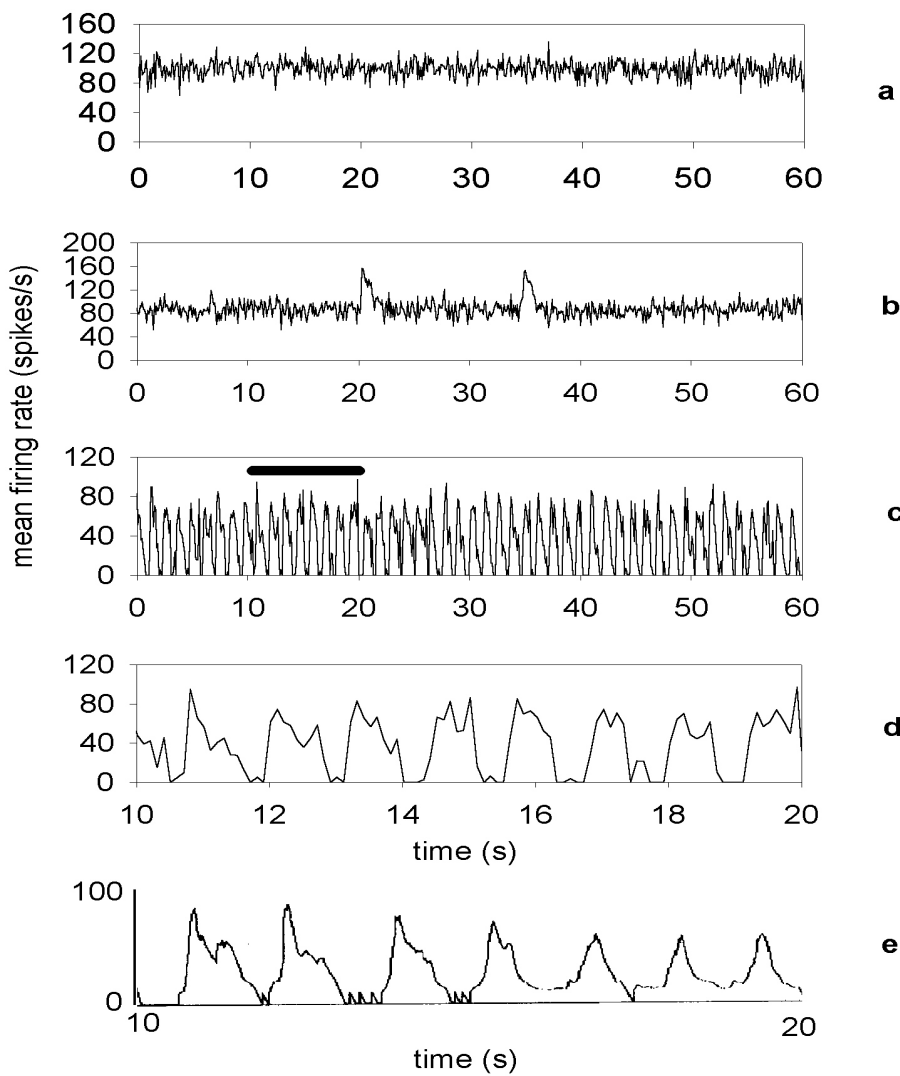


Figure 5.13: Example mean instantaneous firing rate plots from STN units showing noisy tonic firing (**a**), sporadic bursting (**b**) and regular 0.8Hz bursting (**c**). The heavy black bar indicates the section enlarged in **d**. An equivalent section from a 0.8Hz bursting STN neuron from Plenz and Kitai's study is shown in **e**. They both show a maximum intra-burst firing rate of 100Hz and occasional quiet inter-burst periods. Figures reprinted by permission from Nature (400:677) copyright (1999) Macmillan Magazines Ltd.

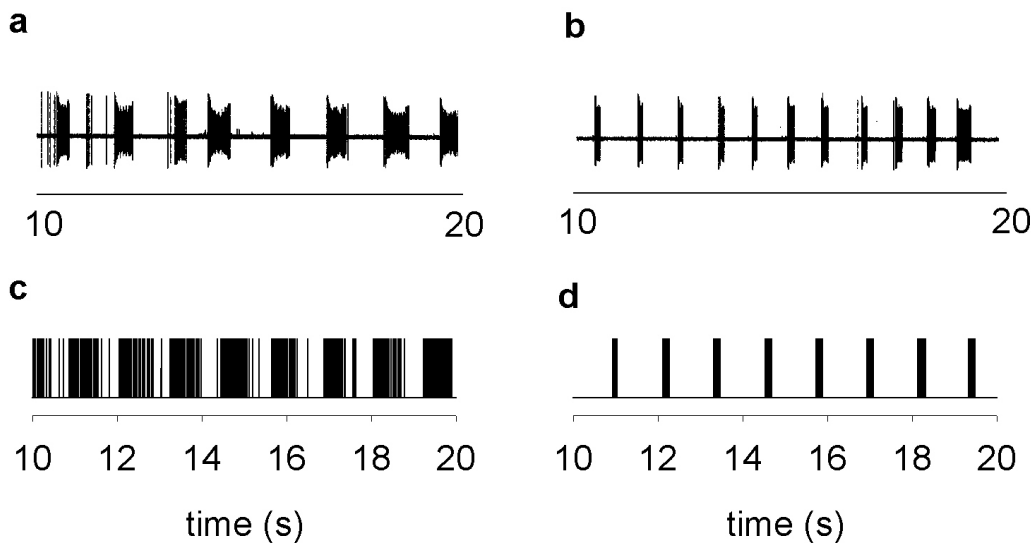


Figure 5.14: **a, b** Example STN neuron spike trains for the cortex-intact and cortex-disconnected conditions, respectively, from Plenz and Kitai's study. **c, d** Example STN unit spike trains from the corresponding network simulations with cortical input and without cortical input, respectively. The study data and simulation data are qualitatively similar. Figures reprinted by permission from Nature (400:677) copyright (1999) Macmillan Magazines Ltd.

and regularly bursting units. Figure 5.13 also shows mean instantaneous firing rate data, taken from Plenz and Kitai's study, for an STN neuron bursting at 0.8Hz. A comparison of this data with the a 0.8Hz bursting unit from the model shows that both had a maximum intra-burst firing rate of ~ 100 Hz and had alternating periods of quiet and low-level tonic firing between bursts.

Figure 5.14 shows example STN unit spike trains from the cortical and no-cortical input simulations and equivalent spike trains from Plenz and Kitai's study. The STN neuron spike train from a cortex-intact culture (a) shows long bursts with short inter-burst quiet periods often interrupted by occasional spikes. The STN neuron spike train from the cortex disconnected culture (b) shows very short bursts with long, completely silent, inter-burst periods. The example STN unit spike trains from the cortical and no-cortical input simulations (c and d respectively) show that my model neuron can emulate these real phenomenon very well.

5.3.4 Burst detection methods

The burst detection method introduced in this chapter (in Section 5.2.3) was based on the autocorrelogram of the unit's mean instantaneous firing rate, and was intended to identify significant levels of bursting in a unit's output. To test the validity of this method and to subject the data set from Experiment 6 to an alternative analysis, an alternative published burst detection method was tested (Kaneoke and Vitek, 1996), which has been used in some studies of the basal ganglia (Bevan et al., 1998; Walters, Ruskin, Allers, and Bergstrom, 2000).

Kaneoke and Vitek made a clear distinction between oscillatory and bursting neuron output, if only through their operational definitions: bursting output was any which matched the criteria below; oscillatory output was any which had a statistically significant peak in its autocorrelogram but did not fit the bursting criteria. Their burst detection was based on discharge density histograms, where discharge density is the number of spikes in a short interval. Briefly, the spike train is divided up into intervals of size t , and the number of spikes in each interval counted. The results are plotted in a frequency histogram. The period of t is normally determined by the reciprocal of the mean firing rate, although other values can be used as the numerator (e.g. 2/, 3/) to give a more detailed picture. To confirm bursting status, the histogram's distribution must be significantly different ($p < 0.05$) from a Poisson distribution of mean 1.0, using a Chi square test. Furthermore, the distribution must have a significant negative skew.

There were two minor problems with Kaneoke and Vitek's method. First, their paper consistently described the discharge density histogram of a bursting neuron's output as having a positive skew (i.e. to the left). This is in direct contradiction to the illustrative figures used in their paper, which clearly show a negative skew (i.e. to the right), and to the prototypical histograms generated here (see below). The check for skewness will, therefore, be for a significant negative skew. Second, the specific test for skewness they used is not recorded anywhere in their paper. I adopted the Fisher's cumulant test for skewness (Kanji, 1993), which is used throughout this section.

To illustrate how different forms of spike trains create different discharge density histograms,

and why the Chi square and skewness checks are essential, the distributions for regular tonic, irregular tonic, and burst firing units are shown in Figure 5.15.

The different forms of firing were created using a single model neuron: tonic firing was simulated using a model neuron, described by equation (4.7), which had I_{spon} set to $2\mu A$. This gave a tonic firing rate of approximately 25 spikes/s. An irregular spike train was created using the same model neuron, with I_{spon} set to $0.8\mu A$, and the variance of the Gaussian noise (I_{noise}) set to 2. Finally, burst firing was created using a model neuron described by equation (5.2). It was injected with hyperpolarising current (I_{spon} was set to $-0.8\mu A$) to repeatedly trigger the Ca^{2+} mechanism.

The top histogram shows that regular tonic firing gives a Gaussian distribution of discharge density. This is significantly different ($p < 0.01$) from a Poisson distribution (depicted by the line), but is not skewed. The centre histogram shows that irregular tonic firing gives a discharge density distribution which follows a Poisson distribution ($p > 0.05$). Therefore, neither of these two prototype spike trains were detected as bursting. The bottom histogram shows that burst firing creates a non-Poisson distribution ($p < 0.01$) which has a significant negative skew ($\alpha < 0.01$). Thus, these examples have demonstrated why both the Chi square and skewness checks are required to test for bursting in a spike train.

Having demonstrated that the burst detection method can successfully analyse pure spike trains of different forms, it remained to be seen if it could successfully analyse noisy spike trains from real data. The burst detection method was used on the experimental data from Experiment 6, using a t of $1/(\text{spikes/s})$. With this t value, there were 7/96 STN units bursting and 17/96 GP units bursting. These were much lower values than my burst detection method found (69/96 STN units, 32/96 GP units) and much smaller proportions than Plenz and Kitai found (83/181 bursting STN neurons and 31/102 bursting GP neurons). The analyses were run again using a larger value for t of $3/(\text{spikes/s})$ to get a wider range of possible discharge density values. Using this value, the detection method determined that 51/96 STN units were bursting but that no GP units were bursting at all.

There is a clear disagreement between the results of my burst detection method and the one

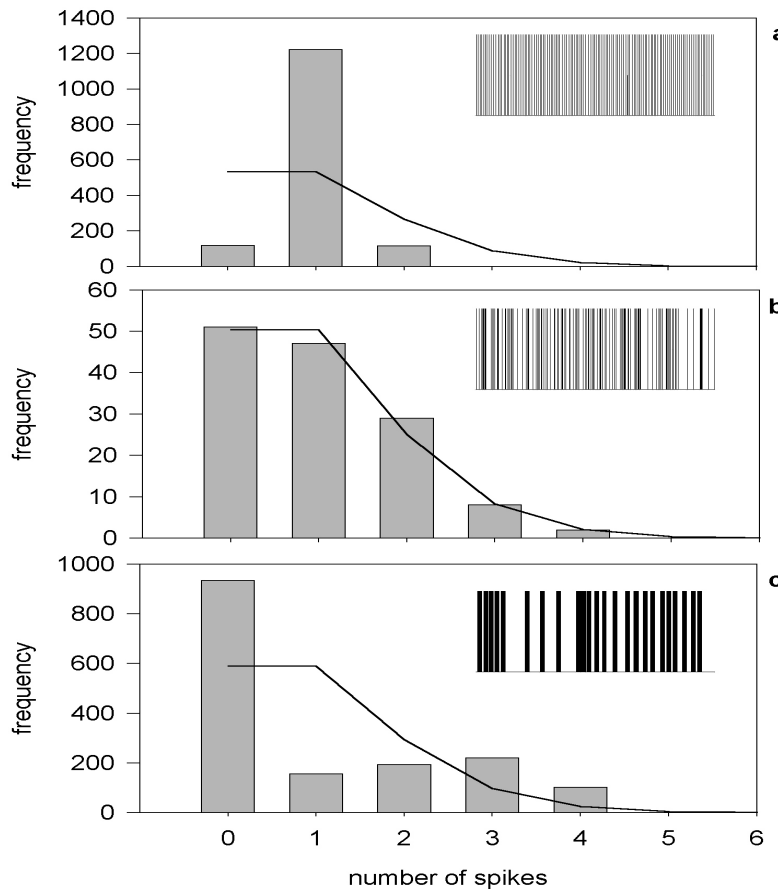


Figure 5.15: Discharge density frequency histograms illustrating the varying distributions for different underlying spike trains. The line illustrates the Poisson distribution. **a** Regular tonic firing gives a symmetric (Gaussian) distribution. **b** Irregular tonic firing gives a Poisson distribution. **c** Burst firing gives a negative skew. The insets show the spike train from which the histograms were generated.

proposed by Kaneoke and Vitek. Although there is no *a priori* reason for preferring one method over the other, I suggest here that Kaneoke and Vitek's method is flawed because it is unable to cope with burst firing imposed on noisy background firing. To illustrate this point, consider an example STN unit (unit 10) from the simulation data. Visual inspection of the pseudo-colour plot (Figure 5.12) column for unit 10, and its mean instantaneous firing rate plot (Figure 5.16, top), clearly shows that it is bursting. However, the discharge density histograms generated using Kaneoke and Vitek's methods for both t values (1/, 3/) were not significantly skewed (see Figure 5.16, bottom) and, therefore, the unit was deemed to be not bursting. This inability of Kaneoke and Vitek's detection method to successfully detect this bursting unit, even when using their recommended t value, leads one to a preference for the results of the burst detection method presented in this chapter. The implications for the failure of the published method will be dealt with in the discussion.

5.3.5 De-channelising the model

The use of a channel architecture in the STN-GP model was maintained for consistency with the Gurney et al. (2001a) model of basal ganglia functional anatomy (see chapter 1). However, it may be argued that the small size of this model makes the connection scheme imposed by the channels an unnecessary constraint. Thus, in this section, the effect of removing the channel constraints on the bursting activity of the quasi-compartmental STN-GP model is explored.

Removing the two channels left an homogeneous two layer network of 32 units per layer. The connection scheme between the two layers was generated thus: each STN unit contacted a number of GP units drawn from a Gaussian distribution of mean 25 and variance 5. This modelled the diffuse connections from STN to GP - capped by the limit of 32 connections from a single STN unit (which would therefore contact every GP unit). Similarly, a single GP unit contacted a number of STN units drawn from a Gaussian distribution of mean 16 and variance 5.

Two simulations were run using the dechannelised STN-GP model, one with and one without cortical input to STN units, again to simulate the two conditions in Plenz and Kitai's culture.

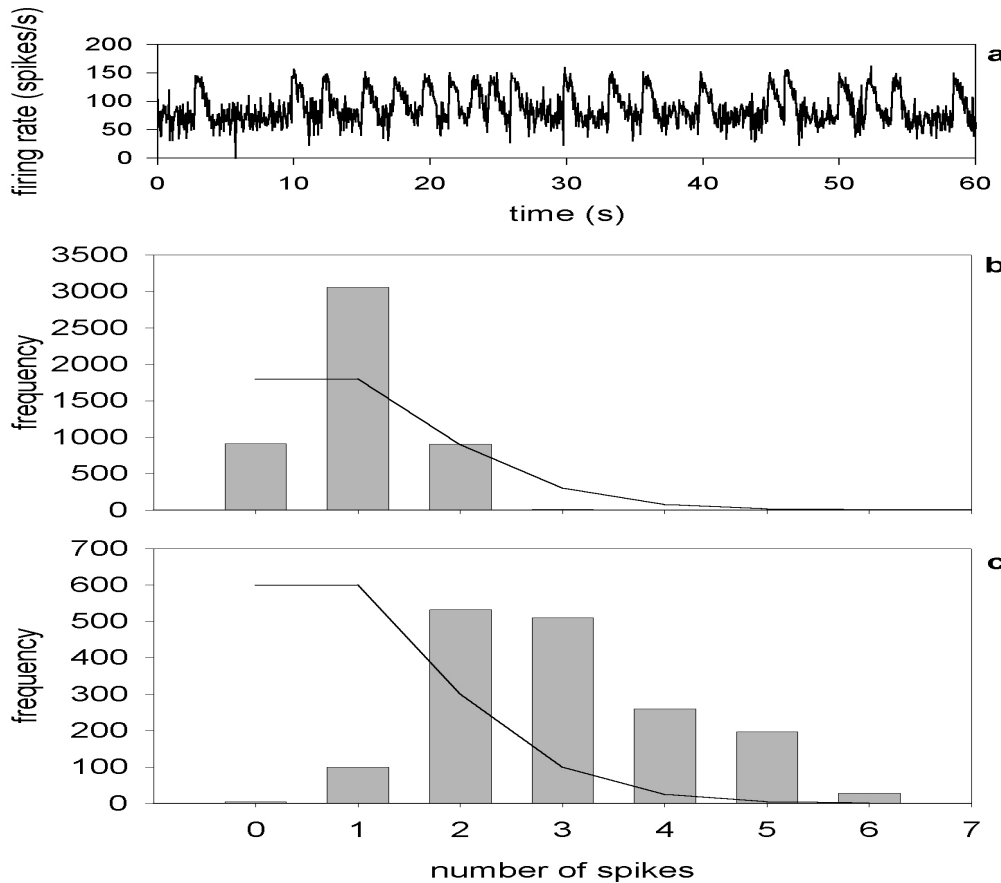


Figure 5.16: Kanoeke and Vitek's (1996) burst detection method does not successfully detect all bursting units. **a** the instantaneous firing rate plot of STN unit 10 from Experiment 6. It clearly shows noisy bursts superimposed on noisy tonic firing. Discharge density histograms for $t = 1/\text{(spikes/s)}$ (**b**) and $t = 3/\text{(spikes/s)}$ (**c**) are significantly different from a Poisson distribution (line), but they do not have a significant negative skew.

The burst detection method determined that all units in both structures burst without cortical input; with cortical input all STN units burst and 30 GP units burst. Figure 5.17 summarises the phase angles and mean power spectra for the STN units in the two simulations. With no cortical stimulation, STN unit pairs had phase angles clustered around zero but spread over a range of common firing frequencies. By contrast, the channel-based STN-GP model showed a single common firing frequency in the same condition (see Figure 5.7). The phase angles of STN unit pairs following cortical input were very similar to the channel-based model's results in this condition: the range of phase angles monotonically increased as a function of f_0^c .

The main result of removing the channels from the model was that the mono-modal/multi-modal bursting frequency distinction between the no-cortical/cortical input conditions was lost. The mean power spectra for the STN showed a distinct peak at $f_{01} = \sim 0.633\text{Hz}$ for the no-cortical input condition but showed no distinct peaks in the cortical input condition. Thus, while the no-input condition had a mono-modal bursting pattern, there was no clear mode for the input condition. Note also that there is a wider range of frequency values in the no-cortex condition than there was in its channel-based equivalent (compare Figure 5.7).

5.4 Discussion

5.4.1 Ca^{2+} mechanism is essential for bursting in simulation

The results from Section 5.3.1 showed that neurophysiologically realistic STN neuron bursting could not be achieved by the STN-GP network without the Ca^{2+} mechanism within the STN model neurons. Moreover, even though it was possible to interpret the STN model neuron outputs as bursting, according to criteria set out by researchers of thalamic neuron rebound bursting, this does not provide any support for Rowat and Selverston's (1997) findings (which were outlined in section 5.3.1). This was because the spike trains of the STN units were similar to those generated by a Poisson distribution and, therefore, there was no underlying mechanism causing this bursting. Instead, the probable source of the bursting observed was the noise component, I_{noise} , of the membrane equation: a short period of high-level, positive

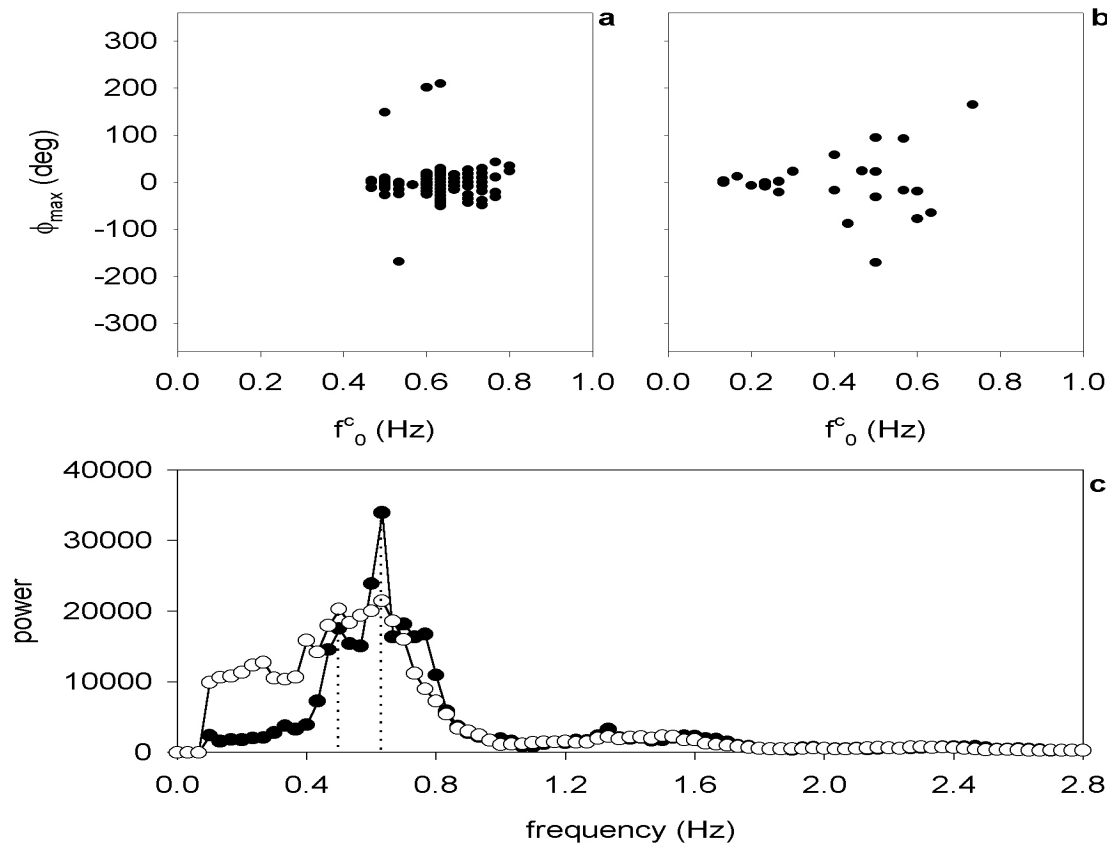


Figure 5.17: Removing channels from the STN-GP model retained bursting behaviour but lost the mono-modal/multi-modal bursting frequency distinction between cortical and no-cortical input conditions. **a** The phase angle plot of STN unit pairs in the no-cortex simulation shows that most pairs were closely synchronised. **b** The phase angles of STN unit pairs in the cortical-input simulation show a similar spread in angle and frequency range to the channel-based model. **c** The mean power spectra for STN units in the cortical (unfilled) and no-cortical input (filled) simulations. The no-cortical input simulation showed a single peak frequency of 0.633Hz, but the cortical-input simulation had no clear peaks.

noise would cause a few spikes to be fired consecutively at short intervals giving the appearance of ‘bursting’.

I cannot make the stronger conclusion that any modelled, *in vitro*, or *in vivo* STN-GP network can never burst without activation of the Ca^{2+} current cycle. Recent modelling work has demonstrated that burst-like output of STN and GP neurons can result simply from the correct balance of excitatory cortical input to STN neurons and inhibitory striatal input to the GP (Gillies, Willshaw, and Li, 2002). However, because Gillies et al.’s network was a model of the *in vivo* network, their results do not preclude the possibility that the Ca^{2+} current cycle is essential for STN bursting *in vitro* or in a dysfunctional basal ganglia. This possibility is supported by the modelling work of Terman and colleagues who demonstrated burst-like activity (which they term ‘episodic’ firing) in a model of an isolated STN-GP network which incorporated a hyperpolarisation activated Ca^{2+} current in the model STN units (Terman, Rubin, Yew, and Wilson, 2002). As their network had no external input other than direct current injection to the GP, it is approximately equivalent to the network modelled here, and is a good model of an *in vitro* study.

5.4.2 The effects of noise

One effect of noise on a model neuron’s output is clear: without noise all model neurons, with the same parameters, would give identical outputs. However, I have found that noise interacts with the extended spiking model neuron in a counter-intuitive manner.

In a noise-free network, with no STN axon collaterals, no units could be made to burst fire regardless of the level of I_{spon} . Hence, noise is essential for bursting in a collateral-free STN-GP circuit. By contrast, in a noise-free network with axon collaterals within the STN, burst firing still occurred. Furthermore, I also found that increasing c_{ss}^+ in a noise-free network caused unit outputs to diversify. An identical network, but with noise, showed a very homogeneous data set regardless of the value of c_{ss}^+ . The conclusion drawn from these results is that, paradoxically, the introduction of noise to the network acted to decrease the disorder of the network’s behaviour.

The ability of STN units to burst fire in a noise-free network was wholly dependent on

the presence of intra-nucleus axon collaterals. Because the collaterals from each STN unit are randomly connected to 25% of all other STN units each unit receives a different set of STN axon collateral inputs. Therefore, some STN units will receive greater excitation than others because they have a greater number of collateral inputs. Since all GP units receive input from every STN unit these would be driven harder in a network equipped with STN collaterals than in a collateral-free network. This, in turn, would cause greater GP firing which would be sufficient to hyperpolarise the STN units with less excitation and cause them to burst. Thus, the presence of axon collaterals introduces what may be termed ‘structural’ noise which may play the same role as the I_{noise} current component. The implications of the effects of noise reported in this and the previous chapter are further discussed in section 6.1.2.

5.4.3 Quasi-compartmental modelling

The use of Plenz and Kitai’s study

This chapter has focused on Plenz and Kitai’s study primarily because their data was used as a test-bed for the modelling approach: the phenomenological replication of each additional contribution to the membrane potential and a simple replication of synapse distribution. In this regard, their study was ideal because of the highly controlled nature of the culture which allowed a close comparison with a limited circuit model. Furthermore, the frequencies of bursting they observed are slow enough to be relevant at a behavioural level, which is of particular interest, given that the major theme of this work is the involvement of the basal ganglia in action selection.

Plenz and Kitai noted that their culture could be considered ‘Parkinsonian’, due to the lack of dopamine, but no comparisons between the network’s performance and Parkinsons patient or animal model data have been included here. I felt that such data was not relevant because the culture was not strictly in a Parkinsonian state for two important reasons. First, there is much neurophysiological evidence which suggests that the D2 dopamine receptors have an inhibitory effect on striatal neurons and the D2 equipped striatal neurons project predominantly to GP (Delgado et al., 2000; Hsu et al., 1995; Gerfen and Wilson, 1996). Therefore, under

Parkinsonian conditions, the lack of dopamine would increase the net inhibition of the GP neurons by the D2-type striatal neurons, leading to a reduction in the firing rate of GP neurons (Raz, Vaadia, Bergman, 2000). This could not occur in Plenz and Kitai's culture as cortical input was not sufficient to cause the striatal neurons to fire. Second, the main frequencies of oscillation/bursting found within a dopamine depleted basal ganglia are between 3-8 Hz (Bergman, Wichmann, Karmon, and DeLong, 1994; Bergman et al., 1998; Magnin, Morel, and Jeanmonod, 2000), which correspond to the frequency range of resting tremor in MPTP-treated primates and Parkinsonian patients. Nothing approaching these frequencies was found in the data from Plenz and Kitai's culture. Thus, it was felt that comparisons between the STN-GP model's performance and data from Parkinsonian patients and animal-models were inappropriate.

Qualitative simulation of Plenz and Kitai's data

The results from Experiments 5 and 6 have demonstrated that an STN-GP network, with quasi-compartmental model neurons within STN and with cortical input, showed bursting at two main frequencies ($\sim 0.67\text{Hz}$ and $\sim 0.83\text{Hz}$) in STN and GP units. The same network without cortical input had only one bursting frequency at 0.82Hz . This is qualitatively similar to the major result of Plenz and Kitai's study: there are two main frequencies of bursting with cortex-intact and only one with cortex-disconnected.

Other aspects of the simulation data also compared favourably with the equivalent data from Plenz and Kitai's paper. The spike trains and mean instantaneous firing rate plots from the simulation data all had qualitatively similar properties to their equivalents derived from the neurophysiological data. The quasi-compartmental model network also showed some features that were not studied by Plenz and Kitai. Most significantly I found that the addition of cortical input caused units to become less synchronised (in terms of the S values). Thus it is possible to form a prediction based on the model's results: subsequent neurophysiological studies or, possibly, a re-analysis of Plenz and Kitai's data will show that lesioning the cortex acts to increase the level of synchrony in the STN-GP circuit.

The diversification of unit behaviour with cortical input, such as the multiple frequencies of bursting, was observed in both the STN-GP model simulations and in Plenz and Kitai's study. It can be attributed to the 'driving' of a non-linear system, the STN-GP circuit, which is known to cause a bifurcation of these systems' modes of behaviour (Gaponov-Grekhov and Rabinovich, 1992): in the case of the STN-GP network cortical input caused a bifurcation of bursting frequencies.

There were, however, two main discrepancies between the model's frequency data and Plenz and Kitai's. First, it was found that the $\sim 0.83\text{Hz}$ frequency had the highest power spectrum peak in both cortical and no-cortical input cases. Their data showed that, with cortical input, the lowest of the two main frequencies (in their case 0.4Hz , in the model $\sim 0.67\text{Hz}$) was by far the most powerful. To determine the mean power spectrum (which they term the 'differential relative power spectrum'), from which they obtained their bursting frequencies, they averaged over power- and cross-spectral density analyses. I contend that this analysis possibly obscured the bursting frequencies of individual populations in the STN-GP circuit because cross-spectral density analyses show the relative power in each of the possible *shared* frequencies of both types of neuron. This is plausible as it was found that the mean cross-spectral density analysis of the model's cortical-input data clearly had the greater power at the lower main frequency (0.63Hz); see Figure 5.10. Thus, I would suggest that, without the inclusion of the paired-unit frequency data, their spectral analyses may have shown the 0.8Hz frequency as the dominant frequency in both cortex-intact and cortex-disconnected cases.

Second, the 0.4Hz and 0.8Hz peaks found in the cortex-intact condition had a ratio of 0.5, whereas the mean power spectrum peaks (0.67Hz and 0.83Hz) from the network's data had a ratio of 0.81. The possible significance of the frequency ratio was not discussed by Plenz and Kitai. However, it is possible, in principle, to obtain a mean power spectral density peak at 0.4Hz using the STN-GP network presented here. The data from Experiment 6 showed that the frequency of bursting for individual units ranged between 0.1 and 0.86 Hz with a small set of units bursting around 0.4Hz (6/101 bursting units). Further exploration of the model parameters or the use of alternate formalisms for some aspects of the quasi-compartmental

model (such as the shunting inhibition) may yield results with two main frequencies in a 0.5 ratio.

5.4.4 The factors determining bursting frequency

As the frequencies of bursting reported here are very close to those reported for the *in vitro* study, it is worth noting the factors which contribute to the determination of a model unit's bursting frequency. The detectable frequency range was limited by the analysis method and simulation's length, as noted in the previous chapter: the power spectrum is limited to a maximum of 5 Hz through the use of 100ms bins (10 Hz in sections 5.3.1 and 5.3.2 due to 50ms bins) and a minimum of 0.033 Hz due to the 60 seconds of simulated spike train data analysed.

More pertinently, two components of the model STN neuron have a direct influence over the rate of bursting. First, the Ca^{2+} time constants t_1 and t_2 ensured that the length of a burst from an isolated STN unit was roughly 1000ms in length. Thus, bursts from such a unit had a theoretical maximum frequency of approximately 1 Hz. Second, lowering the triggering threshold θ_{Ca} would decrease the bursting rate and vice versa.

While it may seem that both of these components had their values set to ensure that bursting occurred at the desired frequency of $\sim 0.8\text{Hz}$ in the cortex-disconnected condition, it must be remembered that their values were set according to reported data. Furthermore, while their contributions to an isolated STN unit could easily be determined, their contributions in the full network, particularly when there was input from cortex, were more complex and impossible to predict. For example, note from Figure 5.8 that the bursts in the cortex-disconnected condition varied considerably in length, and many were approximately 100ms in length. Thus, even if the parameters for the time course and triggering threshold had been set to give ideal results in an isolated unit, they may not have done so in a full network.

Moreover, it should also be noted that bursting at $\sim 0.8\text{Hz}$ in the full STN-GP network was dependent on the implementation of the quasi-compartmental synapse scheme and thus this was also crucial in determining the bursting frequency.

5.4.5 What is a ‘burst’?

The burst detection method created for use in this chapter was adequate for reliably identifying the bursting units in the STN-GP model. However, its main limitation was that it operated on data which I knew contained bursts *a priori* because they were engineered by the Ca²⁺ mechanism and so its sole function was to determine which of the units’ outputs contained significant levels of the triggered bursts. Thus, I make no attempt to claim that this method is suited to the general identification of bursts in spike trains.

In section 5.3.4 the alternative, general detection method of Kaneoke & Vitek (1996) was tested. Using prototypical data - regular, irregular, and bursting spike trains generated from an isolated STN unit - I explained the rationale behind their method and showed that it could uniquely identify the bursting unit. However, applying their method to the data set of Experiment 6 (generated by three runs of the complete quasi-compartmental STN-GP model with cortical input) resulted in the non-identification of the majority of bursting units. This was amply demonstrated by the instantaneous firing rate plot of the example unit in Figure 5.16. The plot showed clear bursting in the output of the neuron, but the discharge density histograms showed normal (non-skewed) distributions at both tested bin sizes. Thus, the conclusion was reached that the method of Kaneoke & Vitek was not reliable for detecting bursts in any given spike train data set.

Given that the burst-firing mode of a neuron is seen as both distinct from other output modes (tonic, oscillatory) and of great significance in information transmission (Sherman, 2001) a reliable method for determining burst status would be desirable. However, before any general method can be constructed, it is necessary to have a concrete answer to the question: what *is* a burst?

The exact nature of an action potential burst is often implicit in papers which describe ‘bursting’ neurons. This was emphasised in section 5.3.1 where I briefly elucidated the criteria used by researchers of thalamic rebound bursting: none of the papers cited in that section gave a clear definition of a burst. It seems that much research on bursting neurons relies on a shared intuitive idea of a ‘burst’. Thus, it is possible that these intuitive notions can be given

a concrete form.

It should be noted that Kaneoke and Vitek did give an explicit definition of a burst: they stated that a burst is “a period in which a significantly higher number of discharges occur compared to other periods in a spike train, while oscillation is defined as a pattern of neuronal activity in which discharges occur periodically” (Kaneoke & Vitek, 1996, p. 212). Both of these definitions appear weak. First, we have already seen that their detection method does not quite follow their definition of a burst: the model units it failed to detect clearly showed periods of significantly higher discharge levels (see Figure 5.16). Surprisingly, beyond this definition they do not explicitly discuss functional definitions of a burst in a neuron’s output anywhere in the paper. Rather, they have followed other authors of burst detection methods (Legéndy and Salcman, 1985) by defining a burst as anything that was detected by their method.

Second, defining oscillatory activity so loosely does not clearly separate it from bursting activity - one of the characteristic features of the STN-GP loop bursting is its regular periodicity. However, I do agree that a distinction must be made between bursting and oscillatory activity: results in this chapter have shown that bursts result from intra-cellular current mechanisms; in the previous chapter we saw that oscillatory activity resulted from a combination of membrane noise and the interaction of feedback loops in the complete network. Thus, a distinction between bursting and oscillatory activity is essential because of their separate underlying causal mechanisms and, in all probability, their different functional significance.

I shall proceed by first examining how the failure of Kaneoke and Vitek’s method to identify bursting units in the model’s data set may shed light on the definition of a burst. If one considers the prototypical bursting spike train of the isolated STN unit which their method successfully identified, it is striking that the inter-burst periods of the prototypical spike train are completely silent. Contrast this with the output of the example unit from Experiment 6: this unit showed relatively high levels of tonic firing between bursts, so that the bursts seemed to be superimposed on the background activity. It seems, then, that implicit in Kaneoke and Vitek’s definition of a burst was the requirement for near-silence between clusters of action potentials. Such an assumption may hold true for thalamic neuron bursting, as there tends

to be lower levels of background activity during burst firing than tonic firing (Swadlow and Gusev, 2001). However, this case cannot necessarily be extrapolated to other bursting neurons in the brain: the example mean instantaneous firing rate plot in Figure 5.13e, taken from Plenz and Kitai's study, shows that inter-burst periods in the output of STN neurons could often be noisy. Therefore, note that, for a sub-set of neuron types, bursts are typified by clusters of action potentials separated by periods of near-silence.

If the criterion of near-silence between bursts cannot be relied on to uniquely identify them in any spike train then further constraining criteria must be sought. A consideration of the previous chapter's results may prove useful: they showed oscillatory activity in the output of EP neurons. Most of the output occurred during the OFF periods, which contained constant fluctuations in firing rate, and did not have a consistent length. Moreover, the outputs of the afferent model neurons (not shown) that the oscillatory firing of the EP neurons tracks changes in their input. Thus, the maximum firing rate of an OFF period is rarely observed at its beginning.

Contrast this with the stereotyped pattern of firing rate changes within a 'burst' in a cell's output: the example mean instantaneous firing rate plots, from both the STN-GP model units and the neurons in Plenz and Kitai's culture (see e.g. Figures 5.2, 5.13), throughout this chapter have shown that bursts usually have their maximum firing rate when they are initiated and that the firing rate generally decreases over time, before abruptly falling to the background firing rate. Further, the period of a burst is dependent on the time course of specific underlying currents which ensures that the period is relatively constant for that cell. As shown in the pseudo-color plot in Figure 5.12, although the unit outputs varied considerably across the STN, the bursting shown by each individual unit had a consistent length and firing rate pattern.

The stereotyped period of a burst is important for solving the outstanding issue of how to distinguish a burst from a random grouping of action potentials. In section 5.3.1 we saw that the implicit criteria used by thalamic rebound bursting researchers could identify as bursts small clusters of action potentials in spike trains which were generated by, or similar to, a random process. What differentiates the thalamic rebound bursting from a random spike train

is the reliable response of a cluster of spikes in the output of the neuron following stimulation. However, this differentiation is of no use if the spike train data of a neuron is presented without knowledge of the specific afferent input which caused that output. With no causal knowledge, there is no immediate distinction between a short burst, with underlying causal mechanisms, and a random grouping caused by, for example, membrane noise. As just noted, the key to distinguishing between the two lies in the consistency of burst lengths for an individual cell. Therefore, the recurrence of bursts in a neuron's output could be used to distinguish between short bursts and random groupings of action potential: a bursting cell would repeatedly output bursts of a consistent size, whereas random groupings are unlikely to achieve the same level of consistency.

Let's summarise all of this into a definition: a burst is identified by a non-linear step in firing rate at the initiation of a burst, by a general decrease in firing rate during the course of the burst followed by a non-linear step to the background firing rate, by lower rates of firing between bursts, and by consistent repetitions of this pattern over similar time-courses throughout the cell's output. The first two criteria identify single bursts; the second two identify the cell's output as bursting. Together they can distinguish bursts from regular and irregular tonic, and oscillatory firing modes.

It remains the subject of future work to quantify this definition into a burst detection algorithm which can give consistent results with any spike train data. I emphasise again that the method used in this chapter was sufficient to determine the bursting status of the units in the model, and was more successful in doing so than a published method used in basal ganglia research.

5.4.6 The channel constraint

Removing the channel-based restrictions on GP output and changing the manner of STN unit's connections to GP did not stop the bursting activity in the network in either the cortex-intact or cortex-disconnected conditions. However, the unit outputs in the latter condition were not consistent with the data from the channel-based model or from Plenz and Kitai's study. There

where more frequencies of bursting, and no distinct power spectrum peaks for the cortex-intact condition, thus failing to simulate the main finding of the mono-modal/multi-modal bursting distinction between the two conditions. Further, the unit outputs in the dechannelised model were perhaps too uniform in both conditions in that all but two of the units were bursting whereas the channel-based model and the culture showed roughly similar proportions of bursting units.

The removal of channels thus prevented the STN-GP model from accurately simulating the results of Plenz and Kitai's study. This result provides evidence for the existence of a channel-based connection scheme between these two structures of the basal ganglia. Indeed, it is remarkable that the simple segregation of GP output can have such a dramatic effect on the output of units in the model.

5.4.7 Conclusions

In summary, the network containing the quasi-compartmental model neuron was able to confirm my hypothesis concerning Plenz and Kitai's (1999) study: that the Ca^{2+} mechanism, described by Beurrier et al. (1999), was the intrinsic property of the STN-GP circuit which initiated bursting, at a 'native' frequency of $\sim 0.8\text{Hz}$, and that cortical input modulated this bursting. To achieve this required a modelling approach that phenomenologically replicated each contribution to the membrane potential. Exploration of this neuron model showed that without the Ca^{2+} mechanism bursting could not occur, that noise can assist in the generation of bursting, and that it can act to homogenise unit outputs across a network. With the addition of the quasi-compartmental scheme of spatially separated synapses Plenz and Kitai's data was used to show that the simplified neuron model (as compared to true multi-compartment models) could successfully account for further aspects of the neurophysiological data.

Of course, some properties of the extended spiking model neurons introduced in this chapter remain to be explored. Two aspects are particularly interesting: First, the extent to which noise causes a homogeneity of unit behaviour in a network needs to be further investigated; the overall conclusions about the role of noise from the work in this and the preceding chapter are discussed

in section 6.1.2. Secondly, the extent to which synaptic processing (determined by the interplay of addition and shunting inhibition) may be captured by a quasi-compartmental model neuron remains to be established.

Finally, have we learnt anything further about the usefulness of the spiking model approach? The answer is, emphatically, yes. The use of simple phenomenological representations of a complicated interplay of currents and of a segregated synapse pattern in a spiking model neuron allowed a minimal network to display complex behaviours which accurately simulated those found in a real neural circuit. Thus, this neuron model has demonstrated the flexibility of the phenomenological approach while also emphasising the case for modelling at multiple levels of description.

Chapter 6

General Discussion

The initial discussion highlights what the studies have contributed to the three central themes of action selection, modelling levels, and the influence of noise and, furthermore, the general features that arise from considering the results of all the studies together. Following this, the general limitations of the work are discussed, considering both the underlying functional anatomy and the modelling approach. Finally, the prospects for future computational modelling and theoretical research on the basal ganglia are considered.

6.1 Thematic conclusions

6.1.1 Action selection

The starting point for the studies detailed in this work was the wish to explore further the basal ganglia in the context of the action selection hypothesis. More specifically, the computational model of intrinsic basal ganglia processing had shown that signal selection and switching was supported by this group of neural structures (Gurney et al., 2001a; Gurney et al., 2001b). To develop on this success, the intrinsic model was embedded into a full neural circuit, the thalamocortical loop which subserves motor functions, in order to study the effect that the circuit had on the basal ganglia output's selection properties.

The results of chapters 2, 3, and 4 show that the selection and switching properties of

basal ganglia output consistent with action selection were maintained across a wide range of models. First, when the intrinsic model was initially extended to form the continuous-time TRN model, the basal ganglia outputs showed improved low salience selection and showed properties that were in good agreement with our prior specified requirements of a selection mechanism. By decomposing the fully extended model into versions without the TRN and with alternate TRN designs, I was able to analyse the specific contributions of the extrinsic structures to the improvements in basal ganglia action selection capability. Thus, it was ascertained that the thalamocortical loop formed by the motor cortex and VL thalamus was able to amplify low saliences to a level sufficient for selection. Moreover, the TRN was responsible for the increase in signal level difference between the outputs of the selected and non-selected channels and for the suppression of responses to a wide-range of transient salience increases.

I reached the conclusion that the thalamocortical loop is thus an amplification circuit upon which the TRN acts directly as a gain control, and that the TRN acts indirectly via the thalamocortical loop to ‘clean-up’ basal ganglia output. Further, the improvements in the basal ganglia’s action selection ability were dependent on the precise design of the TRN-to-VL connections: of the two biologically plausible alternatives, the one containing the combination of between- and within-channel pathways was the superior. Thus, I advance this functional design as a plausible hypothesis for the organisational principles of the TRN and thalamic inter-connections at a lower level of detail than the current sector based demarcation of the TRN.

Second, when further basal ganglia intrinsic connections were added to the TRN model (in chapter 3), the selection and switching properties were maintained regardless of the connection type and strength. Of course, that is not to say that all changes led to improvements, but rather that none led to a catastrophic breakdown in the selection of inputs to the basal ganglia. While it could be argued that this did not occur due to the conservative parameter values used in these connections, we had already seen in chapter 2 that a small weight does not equate to a negligible influence on the overall behaviour of the model, in the context of the TRN within-channel connection. Indeed, this observation was repeatedly made throughout

chapter 3. Increasing parameter values for the new connections often resulted in a change in the mode of output behaviour where the simultaneous selection of two actions was abolished and the selection of a single action, the first to become available for selection, dominated for high saliences.

Where the introduction of new pathways did markedly attenuate the selection ability of the basal ganglia, the introduction of a second pathway or connection type reversed the effect of the first pathway e.g. the addition of striatal interneurons compensated for both of the EP-to-GP and the GP-to-striatum pathways (sections 3.6.1 and 3.6.2). It was noted that this pairing of antagonistic pathways may be an organisational feature repeated throughout the basal ganglia at various levels. The pairings act to ensure that action selection is able to continue smoothly, but the roles of the individual pathways remain unclear.

Finally, when the extended (TRN) model was instantiated at a lower level of description, using the spiking model neuron, the selection and switching properties were maintained. Most notable was the correspondence between the minimum levels of salience input required for selection to occur in the continuous-time and spiking models. Although the spike rates for the salience inputs to the spiking extended model were explicitly based on the 100:1 ratio (spiking:continuous-time) of the selection threshold values, this ratio was exactly maintained in the minimum salience level.

A reasonable expectation is that increasing the complexity of the basal ganglia model through all of the additions and alterations just outlined would have resulted in the breakdown of its selection and switching abilities. Therefore, it is genuinely surprising that the simple addition of a thalamocortical loop and TRN, *without* a search through the parameter space (see section 2.3.8), actually resulted in an improvement to the action selection capability of the model basal ganglia. It was also surprising that the same improvement was maintained when the spiking model neurons were instantiated: again there was no search through the parameter space (the scaling weights were taken directly from the continuous-time models) and, moreover, the fundamental calculations performed by the network were altered (see section 1.5). Thus, the basal ganglia's ability to select competing input signals was extremely robust,

which provides extensive evidence for the hypothesis that they play a crucial role in solving the action selection problem.

The primary result of chapter 4 was the discovery of robust oscillations in the basal ganglia output. At the time of writing, oscillatory behaviour of neurons in a normal basal ganglia has become a topic of intense research activity. This is in addition to the ongoing research into the oscillations within the basal ganglia which may underlie the limb tremor associated with Parkinson's Disease (Magnin et al., 2000; Raz et al., 2000; Pare et al., 1990). Walters and co-workers have demonstrated robust oscillations which have a multi-second period in the output of neurons within the GP, EP, and SNr (Walters et al., 2000; Ruskin, Bergstrom, Kaneoke, Patel, Twery, and Walters, 1999a; Ruskin, Bergstrom, and Walters, 1999b). I did not draw any direct comparisons between the data from the spiking extended model and their results because the oscillations they observed were consistently less than 0.1Hz (usually an order of magnitude slower) and the simulations reported here were not long enough for such slow oscillations to be detected reliably. Nevertheless, their results have shown that oscillations do exist in undiseased rat basal ganglia *in vivo*. Thus, their data support the results from the spiking extended model in that there is evidence both for the existence of oscillations in EP output in a normal basal ganglia and for the existence of multi-second period oscillations within the basal ganglia.

An important feature of the network studies in chapter 4, in terms of the action selection hypothesis, was that the oscillations corresponded to cleanly switching bouts of selection across channels. These rapid (on a behavioural time scale) alternations of selected actions may underlie disorders such as ADHD; in this case, the disorder would result from a breakdown in the ability to sufficiently differentiate saliences to ensure clean selection of a single channel. It was also noted that the rapid alternation of selection may also be consistent with the behavioural dithering.

The final result of chapter 4 pertinent to action selection was that the ability to select most inputs and the alternation between selected channels was lost following the removal of noise. This has wide reaching behavioural implications: it seems that, without neural noise, the selection of an action from a set of closely-matched actions (in terms of salience) is impossible if

the absolute salience level is relatively low. Thus, neural noise is necessary to force the selection of an action (or actions), to ensure that an animal is not left in a quiescent, vulnerable state.

Finally, there are four results from the last chapter which have an indirect bearing on the action selection hypothesis. First, the bursting behaviours observed in the circuit could be pertinent to the functions of the basal ganglia *in vivo* when it had been damaged in a specific way. The results of Plenz & Kitai's (1999) culture-based study and my computer-based simulation have recently been replicated *in vivo* as part of a study of oscillatory activity in the rat STN-GP network (Magill et al., 2001). Thus, bursts within the STN and GP are found *in vivo* that could plausibly cause bursting in the EP. This would create a pulsed ON/OFF signal to the basal ganglia's target structures, possibly resulting in short, repetitive bursts of behaviour.

Second, the adapted spiking model neuron accurately simulated the results of a culture-based electrophysiology study. This success lends validation to the spiking model neuron as an approximate model of a biological neuron. Thus, the oscillatory behaviour observed in the full basal ganglia circuit (chapter 4) becomes more plausible as an *in vivo* phenomenon.

Third, the removal of channels from the STN-GP model prevented the successful simulation of Plenz and Kitai's results. This provides strong evidence for the existence of a channel-based architecture in the basal ganglia, which is a crucial component of the proposed action selection mechanism.

Finally, expanding the model neuron to encompass more detailed membrane channel behaviours is the initial step in developing the basal ganglia models at a yet lower level of detail. As already noted, the maintenance of the basal ganglia's selection ability in a wide variety of models at two levels of description enforces the case for it playing a crucial role in action selection. If this could be maintained at a yet lower level of description, this could only provide more evidence in favour of the action selection hypothesis. In the section below, we see what the studies presented herein have shown about the utility of modelling at multiple levels of description.

6.1.2 The effects of noise and dopamine

Wherever possible, the effects of changing noise and dopamine levels within the models have been explored. The results of changing dopamine levels have interpretations that are more specific to the action selection hypothesis and, in particular, to the basal ganglia, so they shall be considered first. Following this, the more general influence of noise on the behaviour of the modelled neural circuits will be discussed, which leads into the final part of this section on the general meta-level lessons that can be learnt from the use of multiple modelling levels.

At the systems-level, changing dopamine levels in the intrinsic, TC, and TRN models consistently resulted in a breakdown of the basal ganglia's ability to act as a selection and switching mechanism. Increasing dopamine levels forced continuous selection of all active channels for most pairs of salience/sensory input levels. Removing dopamine prevented the selection of any channel, regardless of the salience/sensory input levels. As already noted, the latter result is consistent with the inability of Parkinsonian patients to initiate voluntary movements. These results were replicated in the spiking extended model, using a smaller set of input values: with increased dopamine, simultaneous selection always occurred; with no dopamine, no selection ever occurred. Thus, changing dopamine levels in the spiking extended model affected the oscillations in EP output, as there was no longer any periodicity of selection. Further, the oscillations in EP output, as determined directly from the power spectra, now covered the complete detectable frequency range at all input levels. It seemed, then, that changing dopamine levels resulted in a dissociation between input level and output frequency.

The depletion of dopamine also profoundly affected another input-output relation in the spiking extended model. The mean spike rate of the EP output became a roughly linear, increasing function of the input level following the removal of dopamine. In contrast, with normal levels of dopamine, the output spike rate was a monotonically decreasing function of the input level. This result, together with the absence of the same effect following an increase in dopamine, suggested that dopamine is responsible for the inverse mapping of the level of input salience in the striatum to the output rate of the EP channels. Thus, it seems that the removal of dopamine allows the STN input to become the dominant driving force of the EP units, but

the striatal and/or GP inputs must still have some effect as the coding of the difference in level between the channel inputs was maintained.

A similar effect was observed following the removal of noise (both completely and partially), in that the spike rate of the EP output was no longer a monotonically decreasing function of the input level. However, unlike the effect of dopamine removal, the encoding of the difference between the channel input levels was also lost. Further, without noise the EP output oscillations again covered the entire detectable frequency range, removing any semblance of an input level-output frequency relationship. This translated into a loss of selection at many input levels, as noted above. These results taken together suggest that the removal of noise causes the behaviour of the network, in terms of input-output encoding, to become chaotic.

This suggestion was given substantial weight by the results from chapter 5 which showed that removing noise from the STN-GP network also profoundly affected its behaviour. The increase in the range of phase-angles and common frequencies of bursting between pairs of STN units with increasing STN collateral weights only occurred after the removal of noise. There was also a marked decrease in temporal coincidence (synchrony index) between bursts from pairs of STN units. With noise, these parameters were consistent across STN collateral weight changes.

Thus, I make the general conclusion that neural noise acts to make the behaviour of a network of neurons coherent; that is, it ensures that the output of an ensemble of neurons in a structure within a neural circuit is an interpretable encoding of the input to some part of that circuit. This somewhat paradoxical conclusion, which can be summarised as ‘noise brings order’, is in good agreement with some recent theoretical discussions on the possible role of noise in neurons. Numerous authors have bemoaned the unreliability of neural output that neural noise causes: they often wish that repeated presentations of a stimulus would evoke the same spike train output (Ferster, 1996). However, two important roles for noise in neural networks have recently been advanced, both supported by the findings presented in chapters 4 and 5. First, more noise in the input to a neuron can result in less variable output (Cecchi, Sigman, Alonso, Martinez, Chialvo, and Magnasco, 2000), thus improving the reliability of the encoding

of the underlying signal. We saw in chapter 4 that, with neural noise, the mean spike rate of EP output was directly dependent on the input level: removing the noise removed this dependence. Further, in chapter 5 we saw that the presence of noise synchronised bursts. Second, neural noise can ensure that information contained within inputs that are sub-firing-threshold is not lost (Traynelis and Jaramillo, 1998). Just this role for noise was observed in chapter 4 in that the presence of noise allowed for the selection of low-level input signals.

6.1.3 Levels of modelling

I begin this section by posing an oft-asked question: what can we learn from computer simulations of a neural system that cannot be gleaned from considering the results of neurophysiological studies of that system? Some authors have suggested that simulations have two main functions: one is to act as a testing ground for theoretical analysis tools, thus facilitating the interpretation of the analysis when the tools are applied to complex data from real neural systems. The other is to utilise the controlled environment which a simulation presents to make predictions about a system (Amit, 1998). Absent from this list is a third function, one which is more pertinent to the posed question, and to which the studies presented here have made a significant contribution: simulations allow an understanding of the function of complex systems and the role of parameters within those systems, percepts which may be beyond the limits of human intuitive capability.

This point is well illustrated by considering the multiple mixed-type feedback loops contained within the extended (TRN) systems-level model. Even at this high level of modelling abstraction, the effect on the output of the basal ganglia by any given pair of inputs is impossible to predict based on a consideration of the model's connections. With the level of non-linear processing created by the mixed connection types and channel cross-talk between the STN-GP and TRN-VL pathways, a mathematical analysis of the systems properties, such as was done for the intrinsic model (Gurney et al., 2001b; Gurney et al., 1998b), becomes infeasible. Thus, the computer simulations of the extended model become an empirical investigation much like any neurophysiological study.

The utility of simulations in revealing the role of parameters within a complex neural system has also been well illustrated in this work, both for neural noise and connection weights. How noise affects the models has already been described at length, and will be further discussed below: it is sufficient to mention here that the counter-intuitive property of neural noise as an homogeniser of unit outputs could only have been revealed through analysis of the simulation results. As for connection weights, parts of the studies in chapters 2, 3, and 5 have demonstrated that connections with small weights may have a marked effect on basal ganglia output (for example, the removal of the TRN-within connection - see section 2.4.7). In particular, the minor studies in chapter 3 revealed that the addition of new intrinsic basal ganglia pathways could have a large effect on basal ganglia output regardless of the weight values: in fact, increasing the weights in some new connections resulted in a new mode of behaviour. Small weights are generally used in simulations when the projection to a structure is sparse (as in the GP-to-striatal D1 cell population projection), or the neuron population is of low volume compared to other cell types in the same structure (as with the striatal interneurons), or where the post-synaptic potential elicited by the synapse from that projection is known to be small (as with the STN neuron axon collaterals). All the projections which fall into these categories are often ignored by researchers when creating functional models due to their ‘minor’ status. However, we have seen from the studies in this work that this may be a dangerous omission to make as ‘minor’ pathways could have a disproportionate effect on a system’s behaviour.

There is a more specific question I can ask which is pertinent to the studies presented in this work: why should neural circuits be modelled and simulated at multiple levels of description? The investigation of the systems-level models in chapters 2 and 3 highlighted a primary reason: the behaviour of these models is easier to understand post hoc and the outputs require less work to analyse than the spiking-neuron models in the other two main chapters. For example, the impact of the TRN-VL connection design on basal ganglia output could be easily ascertained in the improvements it brought to general selection and switching performance, and I was also able to explain how it had this effect. Thus, systems-level modelling allows the researcher to clearly determine the gross effects on a network’s behaviour caused by an additional pathway

or parameter change, and to determine possible causal explanations for these effects.

By shifting the models under investigation to a lower level of description I have demonstrated the robustness of the basal ganglia as a selection mechanism: the selection and switching properties of the systems-level and spiking-neuron extended models were very similar. Thus, the first reason for modelling at multiple levels is that the replication of results in increasingly realistic systems adds weight to the hypothesis under study.

Further reasons for using multiple-level models concern the new features that can be studied at the lower levels. Primary among these is the ability to directly ascertain the spike trains which underlie the mean firing rate outputs of systems-level models. In chapter 4 this allowed me to show that closely-matched inputs to the extended model resulted in oscillations of selected actions, a phenomenon which was not observed at the systems-level.

Modelling at a lower level allowed the study of the effects of spatial segregation of afferent synaptic contact on a STN neuron (as reported in chapter 5). The adoption of this quasi-compartmental model was necessary to properly replicate the results of Plenz and Kitai's (1999) study. Moreover, it allowed observations of how the location of a synapse on a neuron may affect that neuron's output, which could not possibly be observed at the systems-level.

Finally, modelling at lower levels of details removes a layer of abstraction which may obscure the full appreciation of what the model has shown. Creating models which compute explicitly using spikes facilitates the understanding of the implications of the models results by non-modellers in the research field. As a corollary of this, the established analysis methods used by the neuroscientist on spike trains become available to the modeller as tools that can be applied to the outputs of their simulated neurons. Thus, the analysis of data from simulated models can become more standardised, and the important results of the model can be more widely disseminated and appreciated.

6.2 Issues and Directions

6.2.1 The trouble with dopamine

One of the most contentious issues about the reworking of the functional anatomy is the maintenance of the D1/D2 distinction in the selection and control pathways and, more specifically, the antagonistic influence of the two receptor types on their striatal neurons. As outlined in chapter 1, the current consensus in the neurophysiology literature concurs with the dual-pathway interpretation, but there are numerous dissenting voices. Some researchers have contended that the dopamine receptors may have the opposite effects on the striatal projection neurons to those they are normally ascribed. For example, a study of striatal activity levels in freely moving rats following selective blockade of D1 and D2 receptors showed that activity was attenuated following application of a D1 agonist (Kiyatkin and Rebec, 1999). However, there is little direct neurophysiological evidence to support the hypothesis that dopamine acts on D1 receptors to inhibit striatal neuron output *in vivo*. Thus, this possibility is discounted until new *in vivo* data becomes available.

There is also the possibility that D1 and D2 receptors are co-localised on a large proportion of striatal neurons and, therefore, that D2 receptors act to inhibit the facilitatory action of D1 receptors rather than inhibiting the other inputs to striatal neurons (Harsing and Zigmond, 1997). If this was the case then the strict D1/D2 pathway split would be wrong, although the net effects in the striatal neuron output of activating the two receptors would remain the same. As there are numerous lines of evidence for the co-localisation of D1 and D2 receptors (Aizman, Brismar, Uhlen, Zettergren, Levey, Forssberg, Greengard, and Aperia, 2000; and see references in Harsing and Zigmond, 1997) , this possibility cannot be ignored. Thus, the modelling of three populations of striatal neurons (D1, D2, D1 + D2), based on the dopamine receptor types, is the subject of future work.

Aside from the question of co-localisation, it should be noted that recent data has indicated the existence of striatal neurons which project to both the EP and (via collaterals) to the GP(Wu, Richard, and Parent, 2000) . This data has therefore shown that the assumption of

a clearly-defined selection/control pathway split may not be tenable. In response, a study was conducted by our research group in which this new anatomical connection was instantiated into the intrinsic model: this addition resulted not only in the maintenance of the selection ability of the model but also made single-channel selection more robust to dopamine level changes (Wood, Gurney, and Redgrave, 2001; Gurney, Wood, Humphries, Prescott, and Redgrave, 2001c). Thus, it has been shown that the model can accommodate changes to the strict selection/control pathway split. Therefore, instantiating the three populations of striatal neurons (which would violate the assumption of D1/D2 population correspondence with selection/control pathways) may not overtly damage the basal ganglia's action selection ability.

6.2.2 The lack of learning

A striking omission from all the models presented in this work is the ability to modify synaptic efficacy (the connection weights) during the course of the simulations. It is worth emphasising that the original continuous-time intrinsic model and all subsequent models were designed to study the signal flow through the basal ganglia at any given moment, to study the selection process that acts on the inputs to the basal ganglia whenever a competition for selection occurs. Therefore, synaptic modification was irrelevant because the time-scales I was interested in were too short for synaptic changes to have any significant effect.

However, the ability to modify synaptic efficacy during simulation would become essential if one wished to study the long-term course of action selection where, for example, a behaviour-evoking stimulus is repeated many times. That learning occurs within the basal ganglia is not controversial: many of the computational models briefly reviewed in chapter 1 contained synaptic weight modification as they were concerned with learning of various types (Brown et al., 1999; Suri and Schultz, 1998). Moreover, the basal ganglia, and dopamine in particular, are crucial to the learning phase of many conditioning tasks (Spanagel and Weiss, 1999; Redgrave, Prescott, and Gurney, 1999b; Suri and Schultz, 1998). Thus, studying the changes of the basal ganglia's action selection capability over a long time course would require the instantiation of modifiable connections weights.

We did, however, see the potential effects of changes in synaptic efficacy in various parts of this work, in particular the studies of chapter 3. There we saw that for some of the added pathways the exact pattern of basal ganglia output was dependent upon the strength of the additional connections. More precisely, higher connection strengths caused single channel selection to occur with high-level inputs rather than dual selection. Therefore, if these synaptic connections were modifiable in real neural tissue then basal ganglia output and, in turn, the animal's selection of actions would be directly dependent on past experience of these actions.

6.2.3 Phenomenological modelling

There are numerous possibilities for extending the properties of the spiking model neuron and for exploring their effects on network behaviours through parameter and connection type variation: two of the most interesting are considered here.

First, given that we can observe the effects of spike-timing on a network's behaviour and that the time-scales of the effects are of interest (cf the oscillatory basal ganglia output), it would be useful to model the inter-neuronal transmission delays. In any connection between two neurons, the time-course of the propagation of the action potential from the cell body to the axon terminals of the pre-synaptic neuron cannot be presumed 'instantaneous' and therefore of no importance to the calculations performed by the post-synaptic neuron. The transmission delays of the inter-nucleus connections within the basal ganglia may have a negligible effect on the overall behaviour of the intrinsic network as they are on the order of 2 to 5 milliseconds (Nakanishi, Kita, and Kitai, 1987, 1991; Wilson, Chang, and Kitai, 1982). As this is on a par with the time-course of the post-synaptic potentials elicited by spike arrivals, there is not a clear distinction for any basal ganglia structure of which order the pre-synaptic spikes arrived from other basal ganglia structures.

However, it is well known that the transmission delay from cortex to striatum is significantly slower than the delay from cortex to the subthalamic nucleus and that both delays are an order of magnitude greater than those of the intrinsic basal ganglia connections (Mink and Thach, 1993). The rapid cortico-subthalamic transmission has led to the idea that the subthalamic

nucleus acts to reset basal ganglia output before the cortical input to striatum can affect the output of the basal ganglia (Gillies and Willshaw, 1998). Thus, implementing these transmission delays would allow study of this hypothesised reset mechanism. Further, and more pertinent to the work presented here, the introduction of transmission delays to the extended basal ganglia model may affect the oscillatory basal ganglia output observed following closely-matched inputs.

Second, the STN-GP loop model needs to be integrated into full extended model. The presumption that the bursting behaviour could only be observed in a diseased basal ganglia needs to be explicitly demonstrated (Wichmann and DeLong, 1999). Thus, under normal conditions, the burst firing of the STN-GP loop should not be observed when it is integrated into the extended model. In addition, if the original culture was indeed a model of a ‘Parkinsonian’ state, as claimed by the authors (Plenz and Kitai, 1999), then the burst firing should be observed following dopamine depletion in the model.

As already noted, a recent *in vivo* rat study has demonstrated that bursting does occur in this loop following a 6-OHDA lesion of striatum. However, this study did not observe a mono-modal/multi-modal burst frequency distinction between the cortex-disconnected and cortex-intact conditions. Thus, integration of the STN-GP loop model into the extended model would allow the exploration of why the multi-modal output does not occur in a complete circuit.

The integration of the STN-GP model is the first step in using the extended spiking model as a framework into which more detailed neuron models can be slotted once their properties have been explored in isolation. Currently, a detailed model of the striatal neuron is being developed which can be tested in the extended model.

6.2.4 Conclusion

To conclude, the work presented here has successfully contributed significant results to each of the three main themes identified in chapter 1. First, the utility of modelling neural circuits at multiple levels of description has been amply demonstrated. Second, the surprising results of the noise-free simulations in chapters 4 and 5 have led to the general proposal that noise acts to unify a neural network’s behaviour. Finally, and most importantly, this work constitutes a

substantial body of evidence in favour of the hypothesis that the basal ganglia plays a crucial role in action selection.

Bibliography

- Adams, N. C., Lozsádi, D. A., and Guillory, R. W. (1997). Complexities in the thalamocortical and corticothalamic pathways. *European Journal of Neuroscience*, 9:204–209.
- Aizman, O., Brismar, H., Uhlen, P., Zettergren, E. Levey, A. I., Forssberg, H., Greengard, P., and Aperia, A. (2000). Anatomical and physiological evidence for d1 and d2 dopamine receptor colocalization in neostriatal neurons. *Nature Neuroscience*, 3:226–230.
- Albin, R. L., Young, A. B., and Penney, J. B. (1989). The functional anatomy of basal ganglia disorders. *Trends in Neurosciences*, 12:366–375.
- Albin, R. L., Young, A. B., and Penney, J. B. (1995). The functional anatomy of basal ganglia disorders. *Trends in Neurosciences*, 18:63–64.
- Amit, D. J. (1998). Simulation in neurobiology: theory or experiment? *Trends in Neurosciences*, 21:231–237.
- Amos, A. (2000). A computational model of information processing in the frontal cortex and basal ganglia. *Journal of Cognitive Neuroscience*, 12:505–519.
- Ando, N., Izawa, Y., and Shinoda, Y. (1995). Relative contributions of thalamic reticular nucleus neurons and intrinsic interneurons to inhibition of thalamic motor neurons projecting to motor cortex. *Journal of Neurophysiology*, 73:2470–2485.
- Asanuma, C. (1994). GABAergic and pallidal terminals in the thalamic reticular nucleus of squirrel monkeys. *Experimental Brain Research*, 101:439–451.

- Atherton, J. F., Gillies, A. J., and Arbuthnott, G. W. (2000). Evidence for the presence of glutamatergic interconnections between neurones in the rat subthalamic nucleus. *European Journal of Neuroscience*, 12(supp. 11):62.20.
- Beiser, D. G. and Houk, J. C. (1998). Model of cortical-based ganglionic processing: Encoding the serial order of sensory events. *Journal of Neurophysiology*, 79:3168–3188.
- Bergman, H., Feingold, A., Nini, A., Raz, A., Slovin, H., Abeles, M., and Vaadia, E. (1998). Physiological aspects of information processing in the basal ganglia of normal and parkinsonian primates. *Trends in Neurosciences*, 21(1):32–38.
- Bergman, H., Wichmann, T., Karmon, B., and DeLong, M. R. (1994). The primate subthalamic nucleus. II. Neuronal activity in the MPTP model of parkinsonism. *Journal of Neurophysiology*, 72:507–520.
- Berns, G. S. and Sejnowski, T. J. (1995). How the basal ganglia make decisions. In Damasio, A., Damasio, H., and Christen, Y., editors, *The neurobiology of decision making*. Berlin: Springer-Verlag.
- Beurrier, C., Bioulac, B., and Hammond, C. (2000). Slowly inactivating sodium current (I_{NaP}) underlies single-spike activity in rat subthalamic neurons. *Journal of Neurophysiology*, 83:1951–1957.
- Beurrier, C., Congar, P., Bioulac, M., and Hammond, C. (1999). Subthalamic nucleus neurons switch from single spike-activity to burst-firing mode. *Journal of Neuroscience*, 19(2):599–609.
- Bevan, M. D., Booth, P. A. C., Eaton, S. A., and Bolam, J. P. (1998). Selective innervation of neostriatal interneurons by a subclass of neuron in the globus pallidus of the rat. *The Journal of Neuroscience*, 18(22):9438–9452.
- Bevan, M. D., Clarke, N. P., and Bolam, J. P. (1997). Synaptic integration of functionally diverse pallidal information in the entopeduncular nucleus and subthalamic nucleus in the rat. *Journal of Neuroscience*, 17(1):308–324.

- Bevan, M. D., Francis, C. M., and Bolam, J. P. (1995). The glutamate-enriched cortical and thalamic input to neurons in the subthalamic nucleus of the rat: Convergence with GABA-positive terminals. *Journal of Comparative Neurology*, 361:491–511.
- Blomfield, S. (1974). Arithmetical operations performed by nerve cells. *Brain Research*, 69:115–124.
- Blumberg, B. (1994). Action selection in Hamsterdam: Lessons from ethology. In Cliff, D., Husbands, P., Meyer, J.-A., and Wilson, S. W., editors, *From animals to animats 3: Proceedings of the Third International Conference on Simulation of Adaptive Behavior*, pages 22–29. Cambridge MA: MIT Press.
- Borst, A. and Egelhaaf, M. (1994). Dendritic processing of synaptic information by sensory interneurons. *Trends in Neuroscience*, 17:257–263.
- Brown, J., Bullock, D., and Grossberg, S. (1999). How the basal ganglia use parallel excitatory and inhibitory learning pathways to selectively respond to unexpected rewarding cues. *Journal of Neuroscience*, 19:10502–10511.
- Brown, L. L. and Sharp, F. R. (1995). Metabolic mapping of rat striatum: somatotopic organization of sensorimotor activity. *Brain Research*, 686:207–222.
- Brown, L. L., Smith, D. M., and Goldbloom, L. M. (1998). Organizing principles of cortical integration in the rat neostriatum: Corticostriate map of the body surface is an ordered lattice of curved laminae and radial points. *Journal of Comparative Neurology*, 392:468–488.
- Brown, P. and Marsden, C. D. (1998). What do the basal ganglia do? *The Lancet*, 351:1801–1804.
- Calvin, W. H. and Stevens, C. F. (1967). Synaptic noise as a source of variability in the interval between action potentials. *Science*, 155:842–844.

- Cecchi, G. A., Sigman, M., Alonso, J.-M., Martinez, L., Chialvo, D. R., and Magnasco, M. O. (2000). Noise in neurons is message dependent. *Proceedings of the National Academy of Sciences USA*, 97:5557–5561.
- Centonze, D., Gubellini, P., Bernardi, G., and Calabresi, P. (1999). Permissive role of interneurons in corticostriatal synaptic plasticity. *Brain Research Reviews*, 31:1–5.
- Chevalier, G. and Deniau, J. M. (1990). Disinhibition as a basic process in the expression of striatal function. *Trends in Neurosciences*, 13:277–280.
- Cicirata, F., Angaut, P., Serapide, M. F., and Panto, M. R. (1990). Functional organization of the direct and indirect projection via the reticularis thalami nuclear complex from the motor cortex to the thalamic nucleus ventralis lateralis. *Experimental Brain Research*, 79:325–337.
- Contreras-Vidal, J. L. and Stelmach, G. E. (1995). A neural model of basal ganglia-thalamocortical relations in normal and parkinsonian movement. *Biological Cybernetics*, 73:467–476.
- Cornwall, J., Cooper, J. D., and Phillipson, O. T. (1990). Projections to the rostral reticular thalamic nucleus in the rat. *Experimental Brain Research*, 80:157–171.
- Crick, F. (1984). Function of the thalamic reticular complex: The searchlight hypothesis. *Proceedings of the National Academy of Science USA*, 81:4586–4590.
- Delgado, A., Sierra, A., Querejeta, E., Valdiosera, R. F., and Aceves, J. (2000). Inhibitory control of the GABAergic transmission in the rat neostriatum by D2 dopamine receptors. *Neuroscience*, 95:1043–1048.
- Denny-Brown, D. (1962). *The basal ganglia and their relation to disorders of movement*. Oxford: OUP.
- Diamond, M. E. (1995). Somatosensory thalamus of the rat. In Jones, E. G. and Diamond,

- I. T., editors, *Cerebral cortex*, volume 11, chapter 4, pages 189–219. New York: Plenum Press.
- Farkas, T., Kis, Z., Toldi, J., and Wolff, J.-R. (1999). Activation of the primary motor cortex by somatosensory stimulation in adult rats is mediated mainly by associational connections from the somatosensory cortex. *Neuroscience*, 90:353–361.
- Ferster, D. (1996). Is neural noise just a nuisance? *Science*, 273:1812.
- Flaherty, A. W. and Graybiel, A. M. (1994). Input-output organization of the sensorimotor striatum in the squirrel monkey. *Journal of Neuroscience*, 14:599–610.
- Floresco, S. B., Braaksma, D. N., and Phillips, A. G. (1999). Thalamic-cortical-striatal circuitry subserves working memory during delayed responding on a radial arm maze. *Journal of Neuroscience*, 19(24):11061–11071.
- Friedberg, M. H., Lee, S. M., and Ebner, F. F. (1999). Modulation of receptive field properties of thalamic somatosensory neurons by the depth of anesthesia. *Journal of Neurophysiology*, 81:2243–2252.
- Fujimoto, K. and Kita, H. (1993). Response characteristics of subthalamic neurons to the stimulation of the sensorimotor cortex in the rat. *Brain Research*, 609:185–192.
- Gandia, J. A., De Las Heras, S., García, M., and Giménez-Amaya, J. M. (1993). Afferent projections to the reticular thalamic nucleus from the globus pallidus and the substantia nigra in the rat. *Brain Research Bulletin*, 32:351–358.
- Gaponov-Grekhov, A. V. and Rabinovich, M. I. (1992). *Non-linearities in action*. Berlin: Springer-Verlag.
- Gerfen, C., Engber, T., Mahan, L., Susel, Z., Chase, T., Monsma, F., and Sibley, D. (1990). D1 and D2 dopamine receptor-regulated gene expression of striatonigral and striatopallidal neurons. *Science*, 250:1429–1432.

- Gerfen, C. and Wilson, C. (1996). The basal ganglia. In Swanson, L., Bjorklund, A., and Hokfelt, T., editors, *Handbook of chemical neuroanatomy. Vol 12: Integrated systems of the CNS. Part III*, pages 371–468. Amsterdam: Elsevier.
- Gerstner, W. (1999). Spiking neurons. In Maass, W. and Bishop, C. M., editors, *Pulsed neural networks*, pages 3–53. Cambridge MA: MIT Press.
- Gillies, A., Atherton, J., Arbuthnott, G., and Willshaw, D. (2000). Glutamatergic interactions between subthalamic nucleus projection neurons. *European Journal of Neuroscience*, 12(supp. 11):226.03.
- Gillies, A., Willshaw, D., and Li, Z. (2002). Subthalamic-pallidal interactions are critical in determining normal and abnormal functioning of the basal ganglia. *Proceedings of the Royal Society of London B*, 269(1491):545–551.
- Gillies, A. J. and Willshaw, D. J. (1998). A massively connected subthalamic nucleus leads to the generation of widespread pulses. *Proceedings of the Royal Society of London-B*, 265:2101–2109.
- Gonon, F. (1997). Prolonged and extrasynaptic excitatory action of dopamine mediated by D1 receptors in the rat striatum *in vivo*. *Journal of Neuroscience*, 17:5972–5978.
- Greenberg, N. (2001). The past and future of the basal ganglia. In Cory, G. and Gardner, R., editors, *The neuroethology of Paul MacLean: Frontiers and convergences*. Praeger, in press.
- Grillner, S., Georgopoulos, A., and Jordan, L. (1997). *Selection and initiation of motor behavior*. Cambridge, MA: MIT Press.
- Guillery, R. W., Feig, S. L., and Lozsádi, D. A. (1998). Paying attention to the thalamic reticular nucleus. *Trends in Neuroscience*, 21(1):28–32.
- Gulley, J. M., Kuwajima, M., Mayhill, E., and Rebec, G. V. (1999). Behavior-related changes in the activity of substantia nigra pars reticulata neurons in freely moving rats. *Brain Research*, 845:68–76.

Gurney, K., Prescott, T., and Redgrave, P. (1998a). A model of intrinsic processing in the basal ganglia. In *Proceedings of the 2nd Int. Conf. on cognitive and neural systems*. Boston University.

Gurney, K., Prescott, T. J., and Redgrave, P. (2001a). A computational model of action selection in the basal ganglia I: A new functional anatomy. *Biological Cybernetics*, 85:401–410.

Gurney, K., Prescott, T. J., and Redgrave, P. (2001b). A computational model of action selection in the basal ganglia II: Analysis and simulation of behaviour. *Biological Cybernetics*, 85:411–423.

Gurney, K., Redgrave, P., and Prescott, A. (1998b). Analysis and simulation of a model of intrinsic processing in the basal ganglia. Technical Report AIVRU 131, Dept. Psychology University of Sheffield.

Gurney, K., Wood, R., Humphries, M., Prescott, T. J., and Redgrave, P. (2001c). A computationally based reformulation of basal ganglia functional architecture can incorporate direct pathway connections to globus pallidus. *Neuroscience*, page submitted.

Hall, R. D. and Lindholm, E. P. (1974). Organisation of motor and somatosensory neocortex in the albino rat. *Brain Research*, 66:23–38.

Harsing, L. G., J. and Zigmond, M. J. (1997). Influence of dopamine on GABA release in striatum: evidence for D1-D2 interactions and non-synaptic influences. *Neuroscience*, 77:419–429.

Hazrati, L.-N. and Parent, A. (1991). Projection from the external pallidum to the reticular thalamic nucleus in the squirrel monkey. *Brain Research*, 550:142–146.

Hazrati, L.-N. and Parent, A. (1992a). Convergence of subthalamic and striatal efferents at pallidal level in primates: an anterograde-labeling study with biocytin and PHA-L. *Brain Research*, 569:336–340.

- Hazrati, L.-N. and Parent, A. (1992b). Differential patterns of arborization of striatal and subthalamic fibers in the two pallidal segments in primates. *Brain Research*, 598:311–315.
- Hazrati, L.-N., Parent, A., Mitchell, S., and Haber, S. N. (1990). Evidence for interconnections between the two segments of the globus pallidus in primates: a PHA-L anterograde tracing study. *Brain Research*, 533:171–175.
- Hernández-López, S., Bargas, J., Surmeier, D. J., Reyes, A., and Galarraga, E. (1997). D1 receptor activation enhances evoked discharge in neostriatal medium spiny neurons by modulating an L-type Ca^{2+} conductance. *Journal of Neuroscience*, 17(9):3334–3342.
- Hikosaka, O. (1991). Basal ganglia - possible role in motor coordination and learning. *Current Opinion in Neurobiology*, 1:638–643.
- Hikosaka, O., Nakahara, H., Rand, M. S., Sakai, K., Lu, X., Nakamura, K., Miyachi, S., and Doya, K. (1999). Parallel neural networks for learning sequential procedures. *Trends in Neuroscience*, 22:464–471.
- Hikosaka, O. and Wurtz, R. H. (1989). The basal ganglia. In Wurtz and Goldberg, editors, *The neurobiology of saccadic eye movements*, pages 257–281. Amsterdam: Elsevier.
- Hinde, R. (1966). *Animal Behaviour*. McGraw-Hill.
- Hoogland, P. V., Welker, E., and Van der Loos, H. (1987). Organisation of the projections from barrel cortex to thalamus in mice studied with phaseolus vulgaris-leucoagglutinin and HRP. *Experimental Brain Research*, 68:73–87.
- Hoover, J. E. and Strick, P. L. (1993). Multiple output channels in the basal ganglia. *Science*, 259:819–821.
- Hoover, J. E. and Strick, P. L. (1999). The organization of cerebellar and basal ganglia outputs to primary motor cortex as revealed by retrograde transneuronal transport of herpes simplex virus type 1. *Journal of Neuroscience*, 19(4):1446–1463.

- Houston, A. and Sumida, B. (1985). A positive feedback model for switching between two activities. *Animal Behaviour*, 33:315–25.
- Hsu, K.-S., Huang, C.-C., Yang, C.-H., and Gean, P.-W. (1995). Presynaptic D2 dopaminergic receptors mediate inhibition of excitatory synaptic transmission in the rat neostriatum. *Brain Research*, 690:264–268.
- Humphries, M. D. and Gurney, K. N. (2001). A pulsed neural network model of bursting in the basal ganglia. *Neural Networks*, 14:845–863.
- Humphries, M. D. and Gurney, K. N. (2002). The role of intra-thalamic and thalamocortical circuits in action selection. *Network: Computation in Neural Systems*, 13:131–156.
- Humphrys, M. (1996). *Action selection methods using reinforcement learning*. PhD thesis, University of Cambridge.
- Ilinsky, I. A., Toga, A. W., and Kultas-Ilinsky, K. (1993). Anatomical organisation of internal neuronal circuits in the motor thalamus. In Minciucchi, D., Molinari, M., Macchi, G., and Jones, E. G., editors, *Thalamic networks for relay and modulation*, chapter 14, pages 155–164. Oxford: Pergamon Press.
- Ilinsky, I. A., Ambardekar, A. V., and Kultas-Ilinsky, K. (1999). Organization of projections from the anterior pole of the nucleus reticularis thalami (NRT) to subdivisions of the motor thalamus: Light and electron microscopic studies in the rhesus monkey. *Journal of Comparative Neurology*, 409:369–384.
- Izraeli, R. and Porter, L. L. (1995). Vibrissal motor cortex in the rat: Connections with the barrel field. *Experimental Brain Research*, 104:41–54.
- Jacobson, S. and Trojanowski, J. Q. (1975). Corticothalamic neurons and thalamocortical terminal fields: An investigation in rat using horseradish peroxidase and autoradiography. *Brain Research*, 85:385–401.

- Jaeger, P., Hitoshi, K., and Wilson, C. J. (1994). Surround inhibition among projection neurons is weak or nonexistent in the rat neostriatum. *Journal of Neurophysiology*, 72(5):2555–2558.
- Jahanshahi, M. and Frith, C. D. (1998). Willed action and its impairments. *Cognitive Neuropsychology*, 15:483–533.
- Joel, D. and Weiner, I. (1997). The connections of the primate subthalamic nucleus: indirect pathways and the open-interconnected scheme of basal gangli-thalamocortical circuitry. *Brain Research Reviews*, 23:62–78.
- Jones, E. G. (1985). *The thalamus*. New York: Plenum Press.
- Kaneoke, Y. and Vitek, J. L. (1996). Burst and oscillation as disparate neuronal properties. *Journal of Neuroscience Methods*, 68:211–223.
- Kanji, G. K. (1993). *100 statistical tests*. London: Sage.
- Kawaguchi, Y., Wilson, C. J., Augood, S. J., and Emson, P. C. (1995). Striatal interneurones: Chemical, physiological and morphological characterization. *Trends in Neurosciences*, 18:527–535.
- Kelley, A. E., Domesick, V. B., and Nauta, W. J. H. (1982). The amygdalostriatal projection in the rat—an anatomical study by anterograde and retrograde tracing methods. *Neuroscience*, 7(7):615–630.
- Kha, H. T., Finkelstein, D. I., Pow, D. V., Lawrence, A. J., and Horne, M. K. (2000). Study of projections from the entopeduncular nucleus to the thalamus of the rat. *Journal of Comparative Neurology*, 426:366–377.
- Kim, U. and McCormick, D. A. (1998). The functional influence of burst and tonic firing mode on synaptic interactions in the thalamus. *Journal of Neuroscience*, 18(22):9500–9516.
- Kim, U., Sanchez-Vives, M. V., and McCormick, D. A. (1997). Functional dynamics of the GABAergic inhibition in the thalamus. *Science*, 278:130–134.

- Kita, H. and Kitai, S. T. (1991). Intracellular study of rat globus pallidus neurons: membrane properties and responses to neostriatal, subthalamic and nigral stimulation. *Brain Research*, 564:296–305.
- Kita, H., Tokuno, H., and Nambu, A. (1999). Monkey globus pallidus neurons projecting to the neostriatum. *NeuroReport*, 10:1467–1472.
- Kiyatkin, E. A. and Rebec, G. V. (1999). Striatal neuronal activity and responsiveness to dopamine and glutamate after selective blockade of d1 and d2 dopamine receptors in freely moving rats. *Journal of Neuroscience*, 19(9):3594–3609.
- Kolmac, C. I. and Mitrofanis, J. (1998). Patterns of brainstem projections to the thalamic reticular nucleus. *Journal of Comparative Neurology*, 396:531–543.
- Koós, T. and Tepper, J. M. (1999). Inhibitory control of neostriatal projection neurons by gabaergic interneurons. *Nature Neuroscience*, 2(5):467–472.
- Kropotov, J. D. and Etlinger, S. C. (1999). Selection of actions in the basal ganglia thalamocortical circuits: review and model. *International Journal of Psychophysiology*, 31:197–217.
- Kultas-Ilinsky, K., Yi, H. A., and Ilinsky, I. A. (1995). Nucleus reticularis thalami input to the anterior thalamic nuclei in the monkey: a light and electron microscopic study. *Neuroscience Letters*, 186:25–28.
- Kupfermann, I. and Weiss, K. R. (2001). Motor program selection in simple model systems. *Current Opinion in Neurobiology*, 11:673–677.
- LeDoux, J. (1995a). Emotion: Clues from the brain. *Annual Review of Psychology*, 46:209–235.
- LeDoux, J. (1995b). *The emotional brain*. New York: Simon & Schuster.
- Legéndy, C. R. and Salcman, M. (1985). Bursts and recurrence of bursts in the spike trains of spontaneously active striate cortex neurons. *Journal of Neurophysiology*, 53:926–939.

- Lévesque, M., Charara, A., Gagnon, S., Parent, A., and Deschênes, M. (1996). Corticostriatal projections from layer v cells in rat are collaterals of long-range corticofugal axons. *Brain Research*, 709:311–315.
- Lozsádi, D. A. (1994). Organization of cortical afferents to the rostral, limbic sector of the rat thalamic reticular nucleus. *Journal of Comparative Neurology*, 341:520–533.
- Maass, W. (1997). Networks of spiking neurons: The third generation of neural network models. *Neural Networks*, 10:1659–1671.
- MacLean, P. (1978). Effects of lesions of globus pallidus on species-typical display behaviour of squirrel monkeys. *Brain Research*, 149:175–196.
- Magill, P. J., Bolam, J. P., and Bevan, M. D. (2000). Relationship of activity in the subthalamic nucleus-globus pallidus network to cortical electroencephalogram. *Journal of Neuroscience*, 20:820–833.
- Magill, P. J., Bolam, J. P., and Bevan, M. D. (2001). Dopamine regulates the impact of the cerebral cortex on the subthalamic nucleus-globus pallidus network. *Neuroscience*, 106:313–330.
- Magnin, M., Morel, A., and Jeanmonod, D. (2000). Single-unit analysis of the pallidum, thalamus and subthalamic nucleus in parkinsonian patients. *Neuroscience*, 96:549–564.
- Manwani, A. and Koch, C. (1999). Detecting and estimating signals in noisy cable structures, I: Neuronal noise sources. *Neural Computation*, 11:1797–1829.
- Marin, O., Smeets, W. J. A. J., and González, A. (1998). Evolution of the basal ganglia in tetrapods: a new perspective based on recent studies in amphibians. *Trends in Neuroscience*, 21:487–494.
- Marsden, C. D. and Obeso, J. A. (1994). The function of the basal ganglia and the paradox of stereotaxic surgery in Parkinson's disease. *Brain*, 117:877–897.

- Matarić, M. J. (1998). Behavior-based robotics as a tool for synthesis of artificial behaviour and analysis of natural behavior. *Trends in Cognitive Sciences*, 2:82–87.
- Mengual, E., de la Heras, S., Erro, E., Lanciego, J. L., and Giménez-Amaya, J. M. (1999). Thalamic interaction between the input and output systems of the basal ganglia. *Journal of Chemical Neuroanatomy*, 16:187–200.
- Mink, J. W. (1996). The basal ganglia: Focused selection and inhibition of competing motor programs. *Progress in Neurobiology*, 50:381–425.
- Mink, J. W. and Thach, W. T. (1993). Basal ganglia intrinsic circuits and their role in behavior. *Current Opinion in Neurobiology*, 3:950–957.
- Missale, C., Nash, S., Robinson, S., Jaber, M., and Caron, M. (1998). Dopamine receptors: from structure to function. *Physiological Review*, 78(1):189–225.
- Miyashita, E., Keller, A., and Asanuma, H. (1994). Input-output organisation of the rat vibrissal motor cortex. *Experimental Brain Research*, 99:223–232.
- Montes-Gonzalez, F., Prescott, T. J., Gurney, K., Humphries, M., and Redgrave, P. (2001). An embodied model of action selection mechanisms in the vertebrate brain. In Meyer, J.-A., Berthoz, A., Floreano, D., Roitblat, H., and Wilson, S. W., editors, *From animals to animats 6: Proceedings of the sixth international conference on simulation of adaptive behaviour*, pages 157–166. Cambridge, MA: MIT Press.
- Morari, M., Marti, M., Sbrenna, S., Fuxe, K., Bianchi, C., and Beani, L. (1998). Reciprocal dopamine-glutamate modulation of release in the basal ganglia. *Neurochemistry International*, 33:383–397.
- Nakanishi, H., Kita, H., and Kitai, S. T. (1987). Intracellular study of rat substantia nigra pars reticulata neurons in an in vitro slice preparation: electrical membrane properties and response characteristics to subthalamic stimulation. *Brain Research*, 437:45–55.

- Nakanishi, H., Kita, H., and Kitai, S. T. (1991). Intracellular study of rat entopeduncular nucleus neurons in an in vitro slice preparation: response to subthalamic stimulation. *Brain Research*, 549:285–291.
- Newman, J., Baars, B. J., and Cho, S.-B. (1997). A neural global workspace model for conscious attention. *Neural Networks*, 10(7):1196–1206.
- Ni, Z.-G., Bouali-Benazzouz, R., Gao, D.-M., Benabid, A.-L., and Benazzouz, A. (2001). Time-course of changes in firing rates and firing patterns of subthalamic nucleus neuronal activity after 6-OHDA-induced dopamine depletion in rats. *Brain Research*, 899:142–147.
- Onla-or, S. and Winstein, C. J. (2001). Function of the ‘direct’ and ‘indirect’ pathways of the basal ganglia motor loop: evidence from reciprocal aiming movements in Parkinson’s disease. *Cognitive Brain Research*, 10:329–332.
- Pare, D., Curro’Dossi, R., and Steriade, M. (1990). Neuronal basis of the parkinsonian resting tremor: A hypothesis and its implications for treatment. *Neuroscience*, 35:217–226.
- Paré, D., Hazrati, L.-N., Parent, A., and Steriade, M. (1990). Substantia nigra pars reticulata projects to the reticular thalamic nucleus of the cat: a morphological and electrophysiological study. *Brain Research*, 535:139–146.
- Parent, A. and Cicchetti, F. (1998). The current model of basal ganglia organisation under scrutiny. *Movement Disorders*, 13(2):199–202.
- Parent, A., Lévesque, M., and Parent, M. (2001). A re-evaluation of the current model of the basal ganglia. *Parkinsonism and Related Disorders*, 7:193–198.
- Pinault, D. and Deschênes, M. (1998). Anatomical evidence for a mechanism of lateral inhibition in the rat thalamus. *European Journal of Neuroscience*, 10:3462–3469.
- Plenz, D. and Kitai, S. T. (1999). A basal ganglia pacemaker formed by the subthalamic nucleus and external globus pallidus. *Nature*, 400:677–682.

- Poirier, L. J. and Sourkes, T. L. (1965). Influence of the substantia nigra on the catecholamine content of the striatum. *Brain*, 88:181–192.
- Prescott, T. (2001). The evolution of action selection. In Holland, O. and McFarland, D., editors, *The whole iguana*. Cambridge MA: MIT Press, to appear.
- Prescott, T., Redgrave, P., and Gurney, K. (1999). Layered control architectures in robots and vertebrates. *Adaptive Behavior*, 7:99–127.
- Press, W. H., Flannery, B. P., Teukolsky, S. A., and Vetterling, W. T. (1989). *Numerical recipes in C*. Cambridge: Cambridge University Press.
- Price, J. L. (1995). Thalamus. In Paxinos, G., editor, *The rat nervous system*, chapter 24, pages 629–648. New York: Academic Press, 2nd edition.
- Rajakumar, N., Elisevich, K., and Flumerfelt, B. A. (1994). The pallidostriatal projection in the rat: a recurrent inhibitory loop? *Brain Research*, 651:332–336.
- Raz, A., Vaadia, E., and Bergman, H. (2000). Firing patterns and correlations of spontaneous discharge of pallidal neurons in the normal and the tremulous 1-methyl-4-phenyl-1,2,3,6-tetrahydropyridine vervet model of parkinsonism. *Journal of Neuroscience*, 20:8559–8571.
- Redgrave, P., Prescott, T. J., and Gurney, K. (1999a). The basal ganglia: A vertebrate solution to the selection problem? *Neuroscience*, 89(4):1009–1023.
- Redgrave, P., Prescott, T. J., and Gurney, K. (1999b). Is the short-latency dopamine response too short to signal reward error? *Trends in Neuroscience*, 22:146–151.
- Reiner, A., Medina, L., and Veenman, C. L. (1998). Structural and functional evolution of the basal ganglia in vertebrates. *Brain Research Reviews*, 28:235–285.
- Rieke, F., Warland, D., de Ruyter van Steveninck, R., and Bialek, W. (1999). *Spikes: Exploring the neural code*. Cambridge MA: MIT Press.
- Roe, D. L. (1999). The discovery of dopamine's physiological importance. *Brain Research Bulletin*, 50:375–376.

- Ross, S. M. (1985). *Introduction to probability models*. Orlando: Academic Press, 3rd edition.
- Rowat, P. F. and Selverston, A. I. (1997). Synchronous bursting can arise from mutual excitation, even when individual cells are not endogenous bursters. *Journal of Computational Neuroscience*, 4:129–139.
- Ruskin, D. N., Bergstrom, D. A., Kaneoke, Y., Patel, B. N., Twery, M. J., and Walters, J. R. (1999a). Multisecond oscillations in firing rate in the basal ganglia: Robust modulation by dopamine receptor activation and anesthesia. *Journal of Neurophysiology*, 81:2046–2055.
- Ruskin, D. N., Bergstrom, D. A., and Walters, J. R. (1999b). Multisecond oscillations in firing rate in the globus pallidus: Synergistic modulation by D1 and D2 dopamine receptors. *Journal of Pharmacology and Experimental Therapeutics*, 290:1493–1501.
- Sawyer, S. F., Martone, M. E., and Groves, P. M. (1991). A GABA immunocytochemical study of rat motor thalamus: Light and electron microscopic observations. *Neuroscience*, 42:103–124.
- Seeman, P. (1987). Dopamine receptors and the dopamine hypothesis of schizophrenia. *Synapse*, 1:133–152.
- Seeman, P., Ulpian, C., Bergeron, C., Riederer, P., Jellinger, K., Gabriel, E., Reynolds, G. P., and Tourtellotte, W. W. (1984). Bimodal distribution of dopamine receptor densities in brains of schizophrenics. *Science*, 225:728–731.
- Segev, I., Fleshman, J. W., and Burke, R. E. (1989). Compartmental models of complex neurons. In Koch, C. and Segev, I., editors, *Methods in neuronal modeling*, pages 63–96. Cambridge MA: MIT Press.
- Segundo, J. P., Stiber, M., and Vibert, J.-F. (1995). Synaptic coding of spike trains. In Arbib, M. A., editor, *The handbook of brain theory and neural networks*, pages 953–956. Cambridge MA: MIT Press.

- Shepherd, G. M. and Brayton, R. K. (1987). Logic operations are properties of computer-simulated interaction between excitable dendritic spines. *Neuroscience*, 21:151–165.
- Sherman, S. M. (2001). A wake-up call from the thalamus. *Nature Neuroscience*, 4:344–346.
- Shosaku, A., Kayama, Y., and Sumitomo, I. (1984). Somatotopic organization in the rat thalamic reticular nucleus. *Brain Research*, 311:57–63.
- Snaith, S. and Holland, O. (1990). An investigation of two mediation strategies suitable for behavioural control in animals and animats. In *From animals to animats: Proceedings of the First International Conference on Simulation of Adaptive Behaviour*, pages 255–262. Cambridge, MA: MIT Press.
- Softky, W. and Koch, C. (1995). Single-cell models. In Arbib, M. A., editor, *The handbook of brain theory and neural networks*, pages 879–884. Cambridge MA: MIT Press.
- Sourkes, T. L. (2000). How dopamine was recognised as a neurotransmitter: a personal view. *Parkinsonism and Related Disorders*, 6:63–67.
- Spanagel, R. and Weiss, F. (1999). The dopamine hypothesis of reward: past and current status. *Trends in Neurosciences*, 22:521–527.
- Sumitomo, I. and Iwama, K. (1987). Neuronal organisation of the rat thalamus for processing information of vibrissal movements. *Brain Research*, 415:389–392.
- Suri, R. and Schultz, W. (1998). Learning of sequential movements by neural network model with dopamine-like reinforcement signal. *Experimental Brain Research*, 121:350–354.
- Swadlow, H. A. and Gusev, A. G. (2001). The impact of ‘bursting’ thalamic impulses at a neocortical synapse. *Nature Neuroscience*, 4:402–408.
- Swanson, J., Castellanos, F., Murias, M., LaHoste, G., and Kennedy, J. (1998). Cognitive neuroscience of attention deficit hyperactive disorder. *Current Opinion in Neurobiology*, 8:263–271.

- Tai, Y., Yi, H., Ilinsky, I. A., and Kultas-Ilinsky, K. (1995). Nucleus reticularis thalami connections with the mediodorsal thalamic nucleus: A light and electron microscopic study in the monkey. *Brain Research Bulletin*, 38:475–488.
- Takada, M., Tokuno, H., Ikai, Y., and Mizuno, N. (1994). Direct projections from the entopeduncular nucleus to the lower brainstem in the rat. *The Journal of Comparative Neurology*, 342:409–429.
- Taylor, N. R. and Taylor, J. G. (2000). Hard-wired models of working memory and temporal sequence storage and generation. *Neural Networks*, 13(2):201–224.
- Terman, D., Rubin, J. E., Yew, A. C., and Wilson, C. J. (2002). Activity patterns in a model for the subthalamopallidal network of the basal ganglia. *Journal of Neuroscience*, 22(7):2963–76.
- Traynelis, S. F. and Jaramillo, F. (1998). Getting the most of noise in the central nervous system. *Trends in Neurosciences*, 21:137–145.
- Tunstall, M. J., Oorschot, D. E., Kean, A., and Wickens, J. R. (2002). Inhibitory interactions between spiny projection neurons in the rat striatum. *Journal of Neurophysiology*, 88(3):1263–1269.
- Turner, R. S. and DeLong, M. R. (2000). Corticostriatal activity in primary motor cortex of the macaque. *Journal of Neuroscience*, 20:7096–7108.
- Ulrich, D. and Huguenard, J. R. (1997). GABAa-receptor-mediated rebound burst firing and burst shunting in the thalamus. *Journal of Neurophysiology*, 78:1748–1751.
- Umemiya, M. and Raymond, L. A. (1997). Dopaminergic modulation of excitatory postsynaptic currents in rat neostriatal neurons. *Journal of Neurophysiology*, 78:1248–1255.
- Uno, M., Ozawa, N., and Yoshida, M. (1978). The mode of pallido-thalamic transmission investigated with intracellular recording from cat thalamus. *Experimental Brain Research*, 33:493–507.

- Walters, J. R., Ruskin, D. N., Allers, K. A., and Bergstrom, D. A. (2000). Pre- and postsynaptic aspects of dopamine mediated transmission. *Trends in Neuroscience*, 23(Suppl.):S41–S47.
- Weese, G. D., Phillips, J. M., and Brown, V. J. (1999). Attentional orienting is impaired by unilateral lesions of the thalamic reticular nucleus in the rat. *Journal of Neuroscience*, 19(22):10135–10139.
- Whishaw, I. Q. (1990). The decorticate rat. In Kolb, B. and Tees, R. C., editors, *The cerebral cortex of the rat*, pages 239–267. Cambridge MA: MIT press.
- White, E. L. (1989). *Cortical circuits: synaptic organization of the cerebral cortex*. Boston: Birkhauser.
- White, G., Lovinger, D. M., and Weight, F. F. (1989). Transient low-threshold Ca^{2+} current triggers burst firing through an after-depolarizing potential in an adult mammalian neuron. *Proceedings of the National Academy of Sciences U.S.A.*, 86:6802–6806.
- Wichmann, H., Bergman, H., and DeLong, M. (1994). The primate subthalamic nucleus. I. Functional properties in intact animals. *Journal of Neurophysiology*, 72:494–506.
- Wichmann, T. and DeLong, M. R. (1999). Oscillations in the basal ganglia. *Nature*, 400:621–622.
- Wickens, B. G. and Wilson, C. J. (1998). Regulation of action-potential firing in spiny neurons of the rat neostriatum in vivo. *Journal of Neurophysiology*, 79:2358–2364.
- Wilson, C. J., Chang, H. T., and Kitai, S. T. (1982). Origins of postsynaptic potentials evoked in identified rat neostriatal neurons by stimulation in substantia nigra. *Experimental Brain Research*, 45:157–167.
- Wilson, C. J., Chang, H. T., and Kitai, S. T. (1983). Disfacilitation and long-lasting inhibition of neostriatal neurons in the rat. *Experimental Brain Research*, 51:227–235.

- Wood, R., Gurney, K., and Redgrave, P. (2001). Direct pathway connections to globus pallidus in a computational model of the basal ganglia. In *British Neuroscience Association Abstracts*, volume 16, page p79.
- Wu, Y., Richard, S., and Parent, A. (2000). The organization of the striatal output system: a single cell juxtacellular labeling study in the rat. *Neuroscience Research*, 38:49–62.
- Zarzecki, P. (1991). The distribution of corticocortical, thalamocortical, and callosal inputs on identified motor cortex output neurons: mechanisms for their selective recruitment. *Somatosensory & Motor Research*, 8(4):313–325.